Metabolic changes as biomarkers for prediction of malignant transformation of skin precancerous lesions

Léa Dousset

THÈSE PRÉSENTÉE

POUR OBTENIR LE GRADE DE

DOCTEUR

DE L'UNIVERSITÉ DE BORDEAUX

ÉCOLE DOCTORALE

SCIENCES DE LA VIE ET DE LA SANTÉ Spécialité Biologie Cellulaire et Physiopathologie

Présentée et soutenue publiquement le 10 Novembre 2022 par

Léa DOUSSET

Metabolic and immune features as predictive biomarkers of risk stratification of skin carcinoma

Sous la direction de : Hamid Rezvani

Soutenue le 10/11/2022

Membres du jury

Mme Nicole BASSET-SEGUIN	PU-PHem	Université de Paris	Présidente
Mr Kiarash KHOSROTEHRANI	PU-PH	Université du Queensland	Rapporteur
Mr Yves DELNESTE	DR	Université d'Angers	Rapporteur
Mme Fatima MECHTA-GRIGORIOU	DR	Université de Paris	Examinateur
Mme Marie BEYLOT-BARRY	PU-PH	Université de Bordeaux	Invitée
Mr Hamid REZVANI	DR	Université de Bordeaux	Directeur

Étude des changements métaboliques comme biomarqueurs prédictifs de la transformation maligne des lésions précancéreuses de la peau

Résumé

Les carcinomes épidermoïdes cutanés (CEC) sont en constante augmentation du fait des habitudes d'exposition solaire et du vieillissement de la population. Le CEC est un modèle de carcinogenèse en plusieurs étapes : de la lésion précancéreuse, la kératose actinique (KA) au CEC *in situ* puis infiltrant jusqu'au stade métastatique. Bien que sa prise en charge initiale ne présente pas d'enjeu thérapeutique (exérèse chirurgicale), plus de 4% de ces CEC récidiveront sous la forme de métastases, avec des conséquences dramatiques en termes de morbi-mortalité (mortalité de 1.5%).

Notre équipe a récemment découvert que des modifications métaboliques spécifiques précédaient la formation des CEC. Nos données indiquent que : 1) les voies de biosynthèse de la pyrimidine et de la purine sont up-régulées dans les différents stades de la carcinogenèse induite par les UVB et que : 2) l'activation de l'enzyme DHODH (4ème étape dans la synthèse de la pyrimidine) située sur la membrane mitochondriale, est essentielle à la biosynthèse des nucléotides et à la génération d'énergie lors cette respiration mitochondriale. Ce « nœud » métabolique reliant les acides nucléiques à la respiration pourrait constituer une cible d'intérêt stratégique.

En conséquence, la première partie de ma thèse à consister en la caractérisation du profil métabolique des CEC, aux différents stades de la carcinogenèse, puis d'étudier l'effet de l'inhibition de l'enzyme DHODH en fonction des profils métaboliques.

Grâce à l'étude translationnelle Mitoskin (étude prospective monocentrique au CHU de Bordeaux) en analysant par la protéomique les différents voies impliquées dans le métabolisme énergétique (glycolyse, phosphorylation oxydative, cycle de Krebs, beta oxydation des acides gras) nous avons classé les patients par leurs score métabolique en 3 sous-groupes avec un score métabolique haut, intermédiaire et faible où toutes les protéines impliquées dans les différentes voies du métabolisme sont abaissées. Nous avons ensuite sélectionné plusieurs lignées CEC en fonction de leur profil métabolique et les avons

xénogreffées chez la souris NSG : la croissance tumorale s'est avérée différente en fonction des profils ainsi que le potentiel métastatique. L'administration du Leflunomide (LFN), inhibiteur de l'enzyme, a inhibé la croissance tumorale des lignées « faible » et « intermédiaire » exprimant de façon plus importante l'enzyme. A l'inverse, en surexprimant l'enzyme DHODH dans la lignée cellulaire résistantes au LFN (lignées avec score métabolique haut), nous avons réversé la résistance au traitement et rendu les tumeurs sensibles au LFN.

La deuxième partie de mon projet a consisté en la caractérisation des différentes populations immunitaires constituant les CEC agressifs localement avancés en les comparant à une lésion précancéreuse présente sur un même patient, grâce au séquençage de l'ARN en cellule unique (Single Cell RNA Sequencing, ScRNA-Seq) et à la transcriptomique spatiale. Après tri des cellules immunitaires CD45+, j'ai pu identifier 19 clusters immunitaires, dont certains clusters étaient sous-représentés (notamment les lymphocytes B et les cellules plasmacytoïdes) ou apparaissaient lors du passage à la forme tumorale, notamment 2 clusters semblant spécifiques à la forme tumorale : macrophagique et lymphocytaire.

En conclusion, mon travail de thèse a exploré les voies du métabolisme des CEC aux différents stades de la carcinogenèse et pu mettre en évidence qu'il existait 3 signatures métaboliques pouvant être utilisé comme biomarqueurs. Cibler DHODH en fonction des différents profils métaboliques semble être une alternative intéressante en cas d'impasse thérapeutique. Enfin, le travail sur la caractérisation des sous-populations immunitaires pourrait ouvrir la voie à de nouvelles cibles thérapeutiques.

Mots clés : carcinogénèse, carcinome épidermoïde, métabolisme, DHODH, mitochondrie, dimère de pyrimidine

Metabolic and immune features as predictive biomarkers of risk stratification of skin carcinoma

Abstract:

Cutaneous squamous cell carcinomas (cSCCs) are one of the most frequent malignancies worldwide, with substantial associated morbidity and cost. A better understanding of the molecular changes involved in the transformation of this UVB-induced precancerous lesions (actinic keratosis (AK)) to localized tumors and then to metastasis will aid in early detection, development of biomarkers and future targeted treatment strategies. Here we aimed at characterizing the molecular and metabolic features of cSCC at different stages of carcinogenesis and their immunologic landscapes in order to uncover clinically relevant biomarkers predicting the cSCC evolution risk. Our previous work showed that metabolic reprogramming occurs at an early stage of carcinogenesis during cSCC progression through the activation of DHODH. Dihydroorotate dehydrogenase (DHODH) is the rate-limiting enzyme in the uridine monophosphate (UMP) biosynthetic pathway and mostly located in the inner membrane of mitochondria, catalyzing the transformation of dihydroorotate to orotate. It has emerged as a new therapeutic target in a wide spectrum of malignancies as *de novo* pyrimidine synthesis is extensively used in rapidly proliferative cancer cell lines.

To investigate metabolic heterogeneity in cutaneous squamous cell carcinoma (cSCC), 60 samples from patients with various stages of cSCC ranging from precancerous actinic keratosis to metastatic cSCC were subjected to proteomic analysis. Three subgroups with low-, medium- and high- metabolic were detected in all stages of carcinogenesis. To examine the functional impact of the detected metabolic heterogeneities on tumor features and their responses to treatment, human cSCC cell lines with different metabolic activities were transplanted subcutaneously into mice. Evaluation of tumor growth revealed that cell lines had different aggressiveness and metastatic potential according to their metabolic profile. Interestingly, the restraining effect of DHODH inhibition (with leflunomide, LFN) on tumor growth and metastatic potency also depended on metabolic profiles of the cells. We found that the expression level of DHODH was also different between cell lines and can be a predict

marker for the sensitivity to DHODH inhibition. DHODH overexpression in refractory cell lines to LFN rendered them sensitive to DHODH inhibition.

To explore immunologic landscapes of cSCC at different stages of carcinogenesis, single cell RNA sequencing (scRNAseq) was applied on a premalignant and an aggressive sample of cSCC from 4 patients. We uncovered several immune cell subsets depleted in cSCC compared to AK, particularly B cells and plasma cells, and a specific cluster of macrophages and T cells enriched in the tumor compared to AK. We also performed spatial transcriptomic using GeoMx DSP and found that a metabolic rewiring of immune cells when tumoral formation is occurring.

To conclude, our data suggest that metabolic and immune features of cSCC could be used as pertinent biomarkers for stratification of cSCC. Targeting DHODH through disruption of the pyrimidine biosynthesis is a potential therapeutic target in a subgroup of cSCC with a particular metabolic profile and that DHODH expression level can be used as a predicted biomarker of response to DHODH inhibition-based metabolic therapy.

Key words:
carcinogenesis, squamous cell carcinoma, metabolism, DHODH, mitochondria, pyrimidine dimer

BoRdeaux Institute of onCology (BRIC) – Inserm UMR1312

Team 5 - *Translational Research on Oncodermatology and Orphean skin diseases* (TRIO2) - Université de Bordeaux,

146 rue Léo Saignat, 33076 BORDEAUX

Remerciements

A mon directeur de thèse

Monsieur le Docteur Hamid Rezvani,

Directeur de recherche, Équipe 5 "Translational Research on Oncodermatology and Orphean skin diseases (TRIO2), INSERM U1312-BoRdeaux Institute of onCology (BRIC)

Hamid, merci de m'avoir fait l'honneur de diriger cette thèse. Un paragraphe n'est pas suffisant pour exprimer ma gratitude et ma sincère reconnaissance sur ces années passées à tes côtés, depuis mon master2 (2015 déjà). Merci pour ta bienveillance et ton écoute. Une page se tourne avec cette thèse, j'ai hâte de poursuivre et de continuer ce que nous avons commencé.

Aux membres du jury

Mes rapporteurs

Monsieur le Professeur Kiarash Khosrotehrani,

Directeur de recherche et professeur des universités, MD PhD FACD, Experimental Dermatology Group, head of the Dermatology Department, Diamantina Institute, Queensland

Cher professeur, merci d'avoir accepté de juger ce travail. Merci pour votre disponibilité. Et votre expertise. Votre parcours professionnel est un exemple pour nous tous. C'est pour moi un grand honneur de venir dans votre équipe après cette thèse.

Monsieur le Docteur Yves Delneste,

Directeur de recherche, Équipe 04 Immunité Innée et Cancer, UMR Inserm 1307 et CNRS 6075, Université d'Angers

Vous m'avez fait l'honneur d'accepter d'être le rapporteur de cette thèse et je vous en remercie. Votre expertise nous sera très précieuse. Veuillez trouver ici l'expression de mon profond respect.

A Madame le Professeur Marie Beylot-Barry,

Professeur des Universités, Praticien Hospitalier, Chef du service de Dermatologie ; Hôpital Saint-André, CHU de Bordeaux, Co-dir. Equipe Translational Research on Oncodermatology and Orphean skin diseases (TRIO2) BoRdeaux Institute of onCology (BRIC) - UMR 1312 INSERM/Université de Bordeaux

Vous m'avez fait un grand honneur en acceptant de me confier Mitoskin. Votre rigueur et votre encadrement pédagogique m'ont accompagnée tout au long de mon parcours de clinicienne et je vous en suis très reconnaissante. Vous êtes pour moi une grande source de motivation et un modèle.

Aux examinateurs

Madame le Professeur Nicole Basset-Seguin,

Professeur émérite des Universités, Praticien Hospitalier, AP-HP, Service de Dermatologie, Hôpital Saint-Louis, Équipe Inserm U976 « Immunologie Humaine, Pathophysiologie, Immunothérapie », Université Paris Cité.

Je vous remercie de me faire l'honneur de juger ce travail. Votre expertise dans le domaine des carcinomes nous sera d'une grande aide pour améliorer ce travail. J'espère que nous aurons l'occasion de poursuivre notre collaboration et de mener à bien notre travail sur les basocellulaires ano-génitaux.

Madame le Docteur Fatima Mechta-Grigoriou,

Directeur de recherche "Stress and Cancer", Scientific Director of Canceropole Ile de France, Coordinator of the Breast Cancer Scientific and Medical Program, Institut Curie - Inserm U830

Je vous remercie de me faire l'honneur de juger ce travail. Votre expertise dans le domaine des carcinomes nous sera d'une grande aide pour améliorer ce travail.

Monsieur le Professeur Taïeb,

Professeur émérite des Universités, ancien Praticien Hospitalier, Services de Dermatologie Adulte et Pédiatrique, Centre de Référence pour les Maladies Rares de la Peau, Hôpital Saint André, Bordeaux

Mr Taïeb, c'est avec émotion et gratitude que je me remémore votre bienveillance et votre accompagnement précieux durant ces années d'internat, de clinicat ou de thèse d'université. Outre votre impressionnant savoir, vous avez été et êtes toujours une grande source de motivation pour moi. Merci de m'avoir accueillie dans votre laboratoire de recherche. Par ces mots je vous témoigne ma plus haute considération et ma plus sincère reconnaissance.

A l'équipe Dermato, ancien U1035 et nouveau Trio2,

Pauline Michon : *Pauline, avoir travaillé en duo avec toi pendant ces 3 ans aura permis à ce beau projet de grandir et de se développer. Un grand et sincère merci pour ton travail et ta présence à mes côtés, notamment lors de nos interminables journées animalières. Je te souhaite tout le meilleur pour la suite.*

François Moisan : *François, grâce à toi, ma thèse a pu prendre un nouveau versant avec la transcriptomique spatiale, merci de ton écoute et de ta bienveillance. Travailler à tes côtés et pas seulement sur mon projet a toujours été un plaisir ; plus que te parrainer dans le futur j'espère que nous pourrons développer de nouveaux projets ensemble.*

Muriel Cario-André : *Muriel, merci de ton écoute et soutien. Ton bureau est une position stratégique avec le déshydratateur, il manquera au futur BRIC ;-) J'ai hâte de poursuivre ce que nous avons commencé sur les encapsulations d'anticorps.*

Walid Mafhouf et Elodie Muzotte : *un grand merci à vous 2 pour votre travail et aide quotidienne.*

Giulia Guzzo : *Giulia, ti scrivo in italiano perché è la tua lingua madre, ma volevo ringraziarti sinceramente per il tuo preziosissimo aiuto e il tuo orecchio gentile, per non parlare della correzione delle bozze! Non ho dubbi che ci terremo in contatto.*

Pierre et Nadine Thiebaud, Jérome Rambert, Sandrine Fédou, Joudi El Mir, Sandra Oucherif, Corinne Faucheux, pour tous les staffs, discussions et conseils.

Et également un grand merci à **l'équipe d'Immuno-Dermato** avec qui travailler a été (et sera) toujours un plaisir : Julien Séneschal et Katia Boniface, Laure Migayron, Ribal Mehri, Denis Thiolat, Claire Drullion, Christina Martins, Clément Jacquemin.

A toute l'équipe Trio2,

Merci pour votre écoute, bienveillance (et patience) lors de nos staffs. Hâte de vous retrouver dans le nouveau bâtiment.

Fanny Beltzung : un grand merci pour ton œil anapath et ta précieuse disponibilité.

A Benoît Rousseau et à toute son équipe,

Benoît Rousseau : mes sincères remerciements pour ton implication dans mon projet, tes précieux conseils, ta compréhension, et toutes nos discussions échangées tout au long de ces journées passées à tes côtés. L'univers clos de l'animalerie ne l'était plus grâce à toi. Ta capacité de travail (sans manger) est impressionnante !

Merci à Julien Izotte, Léa Morat Charrot, Mélanie Estiez, Geoffroy Saillol et Guy Aventin pour leur aide et travail.

A Maya Saleh et à toute son équipe,

Pr Maya Saleh : un grand merci pour votre expertise et conseils. J'espère que nous aurons encore l'occasion de collaborer sur de nouveaux projets.

Julie Giraud et Domitille Chalopin : plus qu'un plaisir, travailler à vos côtés m'a permis de beaucoup apprendre et je ne parle pas au passé. J'ai hâte de finaliser ce travail avec vous.

Gaël Galli, Éloïse Ramel, Sébastian Lillo: merci pour votre aide dans votre unité, sur la paillasse et à l'animalerie.

A Macha Nikolski et à son équipe,

Domitille Chalopin: Domitille travailler à tes côtés est extrêmement enrichissant, tu arrives à rendre simple la bioinfo. Merci encore pour toute ton aide et de m'avoir fait rencontrer Vitalina.

Vitalina Bashynska: so great to have you at the end of my thesis. Thank you from the bottom of my heart for all your work, we have not yet finished, and I can't wait to take the next step.

Macha Nikolski : un grand merci pour votre expertise et conseils. J'espère que nous aurons encore l'occasion de collaborer sur de nouveaux projets.

A Rodrigue Rossignol et Nivea Amoedo, et toute l'équipe de Cellomet

Nivea et Rodrigue : merci l'aide précieuse, les conseils (scientifiques et familial ;-)) et la bonne humeur, en espérant pouvoir valoriser très prochainement notre travail par une belle publication.

A Xavier Gauthereau et à la plateforme de cytométrie TBM Core

A Stéphane Claverol et la plateforme de protéomique, notamment Anne-Marie Lomenech

A Béatrice Vergier et à l'équipe d'anatomopathologie, notamment Olivier Augereau, et au CRB Cancer.

A Alban Bessede et l'équipe d'Immusmol, notamment Jean-Philippe Guegan et Christophe Rey,

A tous les patients inclus dans Mitoskin

A toute l'équipe dermato de Saint-André, en particulier :

Christine Alfaro, Marie-Lou Capela.
Vincent Orlandini, Jean-Michel Amici, Olivier Cogrel, Paul Cirotteau.
Emilie Gérard, Caroline Dutriaux, Anne Pham-Ledard, Sorilla Prey, Océane Ducharme
Aux secrétaires, infirmières et aide-soignantes, sans lesquel(le)s je n'aurai pas pu travailler.

Aux équipes de chirurgie plastique et maxillo-faciale du CFXM, en particulier :

Mathieu Bondaz, Vincent Pinsolle, Antoine Héron, Antoine Dannepond, et toutes les infirmières et aide-soignantes du bloc opératoire pour leur accueil et gentillesse.

A mes proches :

***A mes parents** : merci de m'avoir aidé à arriver jusque-là. Je vous aime.*

***A ma sœur, Eva** : merci, je t'aime.*

***A mes grand-mères** : toujours à mes côtés, aimantes et bienveillantes.*

A Dominique et Philippe : mes beaux-parents adorés. Merci d'être toujours là pour moi et merci pour vos précieux conseils.

***A mes amis de toujours** : Nicolas, Julia, Manon, Gui et Guillaume, Clément, Pauline, Michael, Maria, Laura, Aurélie, Rachel et Gabi.*

***A Guillaume** :* mon amour.

***A Amé**.*

Merci à l'Institut National de la Santé et de la Recherche Médicale et au CHU de Bordeaux pour avoir financé mes 3 années de thèse.

Merci à la fondation SILAB-Jean Paufique, au Groupe de Cancérologie Cutanée d'avoir soutenu personnellement mon projet de recherche, et à la Société Française de Dermatologie, à La Ligue Contre le Cancer et à L'Institut National du Cancer pour les financements accordés aux projets durant cette thèse.

TABLE OF CONTENTS

FIGURE LIST

TABLE LIST

LIST OF ABBREVIATIONS

2-DG: 2-Deoxy-D-glucose
5-HT2A: Receptor 5-hydroxytryptamine 2A
6-4 PP : 6-4 photoproduits
ADP : Adénosine diphosphate
dADP: désoxyadénosine diphosphate
AMP : Adénosine Monophosphate
AMPK: AMP-activated protein kinase
ARH: aryl hydrocarbon receptor
ATM: Ataxia Telangiectasia Mutated
ATP: Adénosine Triphosphate
BER : réparation par excision de base
CDK1-2: cyclin-dependent kinases
CDKN2A: cyclin dependent kinase inhibitor 2A
CDP: Cytosine diphosphate
CEC: Carcinome épidermoïde cutané
Chk1: Checkpoint kinase 1
Chk2 : Checkpoint kinase 2
CMH : Complexe Majeur d'Histocompatibilité
CMP : Cytosine monophosphate
CPD : dimères cyclobutylique de pyrimidine
CTP: Cytosine Triphosphate
CXCL5/12: C-X-C motif chemokine ligand 5/12
CXCR4: C-X-C motif chemokine receptor
DDB1/DDB2: DNA damage-binding protein 1/2
DDR: DNA Damage Response
DHO: dihydroorotate
DHODH: Dihydroorotate dehydrogenenase
EGFR: Epidermal growth receptor
ERCC1: Excision repair cross- complementation group 1
ERK: Extracellular signal-regulated kinases **ETC**: Electron Transport Chain
FADD: Fas Associates Death Domain
FADH: flavine adénine dinucléotide
ptor 3 **FICZ**: 6-formylindolo[3,2-b]carbazole
GDP: Guanosine diphosphate
dGDP: désoxyguanosine diphosphate
GLS: Glutaminase
GLUT: Glucose transporter
GMP: Guanosine monophosphate
GTP: Guanosine triphosphate
HK2: Hexokinase 2
HIF-1α: Hypoxia-inducible factor-1 alpha
H-RAS: HRas Proto-Oncogene, GTPase
MAPK: Mitogen-activated protein kinases
MCR1: MelanoCortin 1 Receptor
MCT: Monocarboxylate transporters
MDM2: Mouse double minute 2 homolog
MEK: Mitogen-activated protein kinase kinase
MFN 1/2: Mitofusin 1 et 2

MITF:Microphtalmia-associated Transcription Factor
mTOR : Mechanistic target of rapamycin
NADH: nicotinamide adénine dinucléotide
NADPH: Nicotinamide adénine dinucléotide phosphate
NER: Nucleotide excision repair
NSCLC: Non-Small Cell Lung Cancer
NOTCH1/2: Notch Receptor 1/2
NOX: NADPH oxidases
NRAS: Neuroblastoma RAS viral oncogene homolog
OGG1: 8-oxoguanine glycosylase
OPA1: Optic Atrophy protéine 1
OSM: Oncostatine M
OXPHOS: Oxidative phosphorylation
PCNA: proliferating cell nuclear antigen
PD-1: Programmed cell death 1
PD-L1/2: Programmed death-ligand 1/2
PFK1: phosphofructokinase-1
PHGDH: Phosphoglycerate dehydrogenase
RIP1/3: receptor-interacting protein 1
ROS: Reactive oxygen species
RPA : Replication Protein A
Sp1: Sp1 Transcription Factor
TNF α: tumour necrosis factor a
TPI-1: Triosephosphate Isomerase 1
TRP1: tyrosinase-related protein
TRP2/DCT: tyrosinase-related protein 2
UDP: Uridine diphosphate
UMP: Uridine monophosphate
UTP: Uridine triphosphate
UHRF-2: Ubiquitin-like with PHD and ring finger domains 1
USF-1 : ubiquitous bHLH-LZ transcription factor
UVRAG : UV radiation resistance-associated gene protein
XMP : Xanthosine monophosphate
XP : Xeroderma Pigmentosum
XRCC1 : X-ray repair cross-complementing protein 1

INTRODUCTION

Chapter I

Cutaneous Squamous Cell Carcinoma

Cutaneous squamous cell carcinoma (cSCC) is the second most frequent form of skin cancer after basal cell carcinoma (BCC) (Lomas, Leonardi-Bee, & Bath-Hextall, 2012). Its incidence continues to rise because of population ageing and UV exposure.

I.1.a Epidemiology

Precise incidence rates are difficult to evaluate as cSCC is not included in many cancer registries. Indeed, common primary cSCC have very good prognosis when they are treated early and correctly, so the costs of tracking cSCC incidence and outcomes have been considered too high. Thus the incidence of cSCC and deaths resulting from it is not known and may be underestimated (Karia, Han, & Schmults, 2013b). A population-based study in Minnesota compared the periods from years 1976-1984 with years 2000-2010 and revealed an increase of cSCC incidence from 62 to163 cases per 100,000 person/year with a disproportionate increase of cSCC relatively to BCC (Muzic et al., 2017). In Australia, where incidence of keratinocytes cancers (KCs) is the highest in the world, it is estimated that 300/100000 people were affected in 2018 (Bray et al., 2018). Moreover, several factors, like age, male sex and low altitude, have been linked to an increase incidence of cSCC as well as a previous history of KCs (Pandeya, Olsen, & Whiteman, 2017). Pandeya et al showed that KCs incidence was eight times as high among people with a prior history of excisions as among those without.

International incidence data are presented in Table 1 (Deady, Sharp, & Comber, 2014; Karia, Han, & Schmults, 2013a; Pandeya et al., 2017; Robsahm, Helsing, & Veierød, 2015; Venables et al., 2019)

Table 1. International incidence for cSCC. Adapted from Stratigos et al, 2020.

Country	Time period	Age standardized incidence (per 100000 PY)	Reference
Australia		270	Pandeya et al
Queensland		467	
Tasmania		175	
United Kingdom	2013-2015	77 in men 34.1 in women	Venables ZC et al

Ireland	1994-2011	66.1 in men 30.6 in women	Deady S et al
Norway	2008-2011	20 in men 15 in women	Robsahm TE et al
USA	2012	In northern latitudes: 46.3-134.5 in men 15.7-42.9 in women In southern latitudes: 233.2-497.1 in men 83.3-180.5 in women	Karia PS et al
Japan	2007-2016	Increased from 14.7 to 51.6 in people aged 80 years or more	Umezono Y et al

The public health burden of cSCC may be underestimated because of poor ascertainment by cancer registries. In Australia, it remains one of the most costly cancer mainly because of the multiplicity of new lesions after diagnosis of cSCC (Gordon et al., 2022). Gordon et al, estimated Australasian-wide direct costs for newly diagnosed patients with KCs at AU$824.0 millions (versus AU$397.9 millions for melanoma).

I.1.b Tumour staging and prognostic factors

The majority of cSCC are curable when they are treated early, with 5-years survival rate of greater than 90% (Brougham, Dennett, Cameron, & Tan, 2012).

Tumour staging of cSCC is based on the American Joint Committee on Cancer (AJCC) classification, 8th ed. (Amin et al., 2017), which additionally considers tumour thickness (Brantsch et al., 2008a), perineural infiltration diameter, and tumour invasion depth (Karia, Han, & Schmults, 2013c) (Table 2). The AJCC 8th classification was developed for head and neck cSCC which are the most frequent locations for cSCC (80-90%) (Alam & Ratner, 2001) so may not be relevant for all cSCC. Alternatively, the Brigham and Women's Hospital (BWH) classification has also been proposed as a simpler and more intuitive classification system for localized stage disease. The BWH system may be a better predictor of regional nodal relapse or disease-related mortality than AJCC 8th ed. (Ruiz, Karia, Besaw, & Schmults, 2019),

although no differences have been observed for immunosuppressed patients (Blechman, Carucci, & Stevenson, 2019).

Table 2. Summary of tumour classification systems AJCC 8th edition and BWH

AJCC-8 Classification		BWH Classification	
	Primary tumour (T)		
T1	Tumour < 2 cm in greatest dimension	**T1**	0 high-risk factors [b]
T2	Tumour ≥ 2 cm and <4 cm in greatest dimension	**T2a**	1 high-risk factor
T3	Tumour ≥ 4 cm in greatest dimension or minor bone erosion or PNI or deep invasion [a]	**T2b**	2–3 high-risk factors
T4a	Tumour with gross cortical bone/marrow invasion	**T3**	4 high-risk factors or bone invasion
T4b	Tumour with axial skeleton invasion including foraminal involvement and vertebral foramen involvement to the epidural space		
	Regional lymph nodes (N)		
Nx	Regional lymph nodes cannot be assessed		
N1	Metastasis in a single ipsilateral lymph node ≤3 cm in greatest dimension and ENE (−)		
N2a	Metastasis in a single ipsilateral lymph node >3 cm and ≤6 cm in greatest dimension and ENE (−)		
N2b	Metastasis in multiple ipsilateral nodes all ≤6 cm in greatest dimension and ENE (−)		
N2c	Metastasis in bilateral or contralateral lymph node(s), all ≤6 cm in greatest dimension and ENE (−)		
N3a	Metastasis in a lymph node >6 cm in greatest dimension and ENE (−)		
N3b	Metastasis in any lymph node(s) and ENE (+)		
	Distant metastasis (M)		
M0	No distant metastasis		
M1	Distant metastasis		

AJCC, American Joint Committee on cancer; BWH, Brigham and Women's Hospital; ENE, extranodal extension; PNI, perineural invasion. [a] Deep invasion is defined as invasion beyond the subcutaneous fat or >6mm. [b] Risk factors include tumours diameter 2 cm or larger, poorly differentiated histology, perineural invasion, and invasion beyond the subcutaneous fat (excluding bone, which automatically upgrades to T3). Adapted from Garcia-Foncillas et al, 2022.

Recurrence

The rate of recurrence was reported to be 4.6% in a large single-center study of more than 900 patients with cSCC followed for approximately 10 years; 3.7% for nodal disease and 2.1% for disease-specific death (Schmults, Karia, Carter, Han, & Qureshi, 2013b). The rate of local recurrence was 3% in a prospective study of 615 patients with surgically resected cSCC, with a 4% rate of metastases, after a median follow up of 43 months (Brantsch et al., 2008b).

Risk stratification

Current prognostic factors for recurrence are based on local staging, location, depth and pathological features. The NCCN guidelines establish low- and high-risk features for cSCC (Table 3) (Schmults et al., 2021). High-risk features are observed in approximately 5% of all cSCC and include locally advanced disease (stages T3-4), nodal involvement, perineural invasion (PNI), local and regional recurrence, or immunosuppression (Porceddu et al., 2018).

Table 3. Clinical and pathological features for risk stratification of cSCC. Adapted from Garcia-Foncillas et al, 2022.

	Low-Risk cSCC	High-Risk cSCC
Clinical history and parameters		
• Location/size	Area L < 20 mm Area M < 10 mm	Area L ≥ 20 mm Area M ≥ 10 mm Area H
• Borders	Well-defined	Poorly defined
• Primary vs. recurrent	Primary	Recurrent
• Immunosuppression	-	+
• Prior RT or chronic inflammatory process	-	+
• Rapidly growing tumour	-	+
• Neurologic symptoms	-	+
Pathology		
• Degree of differentiation	Well or moderately defined	Poorly defined
• Subtypes		
• Acantholytic (adenoid), adenosquamous, desmoplastic, or metaplastic (carcinosarcomatous) subtypes	-	+
• Depth: thickness or level of invasion	≤6 mm, no invasion beyond subcutaneous fat	>6 mm or invasion of subcutaneous fat
• Perineural, lymphatic, or vascular involvement	-	+

PNI is a well-known high-risk factor for local or distant relapse that affects 5% of patients, mostly in cSCC (Carter, Johnson, Chua, Karia, & Schmults, 2013). In a systematic review, patients with clinical PNI (CPNI) showed a significantly increased risk of local recurrence (37% vs. 17%) and disease-specific death (27% vs. 6%) compared with patients with incidental PNI (IPNI), whereas nodal and distant metastasis were similar regardless of PNI classification. Moreover, CPNI had significantly poorer mean 5-year recurrence-free survival (61% vs. 76%) and disease-specific survival (70% vs. 88%) than IPNI patients (Karia, Morgan, Ruiz, & Schmults, 2017).

Immunosuppression

Immunosuppression in patients with cSCC may include human immunodeficiency virus (HIV) infection, solid organ transplant, hematopoietic stem cell transplant, or chronic lymphocytic leukemia (CLL) (Xu et al., 2018). Several studies have shown worse outcomes for cSCC in immunosuppressed patients compared to immunocompetent patients (Basset Seguin et al., 2019; Dusendang et al., 2022; Lindelöf, Sigurgeirsson, Gäbel, & Stern, 2000; Omland, Gniadecki, Hædersdal, Helweg-Larsen, & Omland, 2016; Tokez et al., 2022).

Metastatic potential

Data on nationwide incidence and disease-specific survival rates of metastatic cSCC are lacking. The most recent European data on metastatic risk came from a recent study by Tokez et al (Tokez et al., 2022) estimating a metastasis rate of 1.9% in the Dutch population, diagnosed within a 1.5 years from the primary cSCC. The risk factors were age (adjusted hazard ratio [aHR] 1.03, 95% CI 1.02-1.05), male sex (aHR 1.7, 95% CI 1.3-2.3) and immunosuppression (aHR [organ transplant recipient] 5.0, 95% CI 2.5-10.0; aHR [hematologic malignancy] 2.7, 95% CI 1.6-4.6). The five-year disease specific survival was 79.1%. Other studies reported a metastasis incidence from 1.5% to 5.2% (Brantsch et al., 2008b; Brougham et al., 2012; Knuutila, Riihilä, Kurki, Nissinen, & Kähäri, 2020; Mourouzis et al., 2009; Nelson & Ashton, 2017; Schmults, Karia, Carter, Han, & Qureshi, 2013a; Venables et al., 2019)

Even if the classification allows the identification of cSCC that will recur, a recent German study has shown that **among 190 advanced cSCC patients**, **58% had a primary with a low T stage (T in situ, T1 and T2)**, pointing out the need of identification of new risk factors (Hillen et al., 2018).

I.1.c Etiopathogenesis and emerging biomarkers

Beside ultraviolet radiation (UVR) exposure (sun exposure and use of tanning beds (Morris, Luke, & Perna, 2018)), which is by far the most important causal factor for cSCC, some others have been implicated such as immunosuppression, HPV subtypes (Chahoud et al., 2016; Conforti, Paolini, Venuti, Dianzani, & Zalaudek, 2019) and smoking (Dusingize et al., 2017; Pirie et al., 2018).

The main carcinogen for cSCC development is UVR exposure. While most cSCCs will arise in the context of AKs and in patients with chronic photoaging, the rate of transformation of clinically evident AKs into cSCC is very low, at least in a few years period of follow-up (less than 1/1000 per year during a 5-year follow up) (Dotto & Rustgi, 2016; Marks, Rennie, & Selwood, 1988; Werner et al., 2013). Available evidence indicates that incidence rates are consistently highest in fair-skinned populations in geographic locations with high ambient UV exposure; are higher among men than women; increase markedly with age (80% occur in people over 60), probably because of the driving role of cumulative sun exposure, which increases with age.

Markedly increased rates of cSCC have been reported in organ transplant patients (Garrett et al., 2017) and in patients with chronic lymphocytic leukemia (CLL) (Brewer et al., 2015) or HIV (Omland et al., 2018). Risk was increased by 9 to 18-fold in Danish and US hematopoietic stem cell transplant recipients compared with the general population (Omland et al., 2016; Wu et al., 2019). In a US cohort, HIV patients with CD4 count<200 cells/mL had a 2.2 times increased risk compared to HIV-uninfected individuals for subsequent cSCC after a first cSCC (Asgari, Ray, Quesenberry, Katz, & Silverberg, 2017).

Photosensitizing thiazide antihypertensives have been recently associated with the risk of cSCC development (George et al., 2021; Pedersen et al., 2018; Su, Habel, Achacoso, Friedman, & Asgari, 2018), however causality has not been substantiated. A meta-analysis by Gandini et al. reported no association between thiazide diuretics and cSCC (Gandini et al., 2018). While a positive association was reported in the meta-analysis of Tang et al., there was no association noted between thiazide use and cSCC risk when only studies that had accounted for sun exposure were included (Tang et al., 2018).

Molecular pathogenesis

cSCC presents the highest number of mutations of any other tumours, up to 5 times that of lung cancer or 4 times that of melanoma (Pickering et al., 2014). By accumulating these mutations, an area of the skin can -usually in response to UV light damage-progress through increased levels of dysplasia to become a cSCC. In fact, areas of photo-exposed skin share many of the same frequently mutated genes (Figure 1) (Hussein, 2005). Although there is a large range of tumour mutational burden (TMB) in cSCC, the median TMB is the highest compared with other tumour types. Exome sequencing in the cSCC has revealed approximately 1300 nucleotide somatic variations per exome. This observation has led to the hypothesis that

constant damage to basal keratinocytes by UV radiation may be responsible for multiple cSCC mutational events (Durinck et al., 2011)(Figure 1).

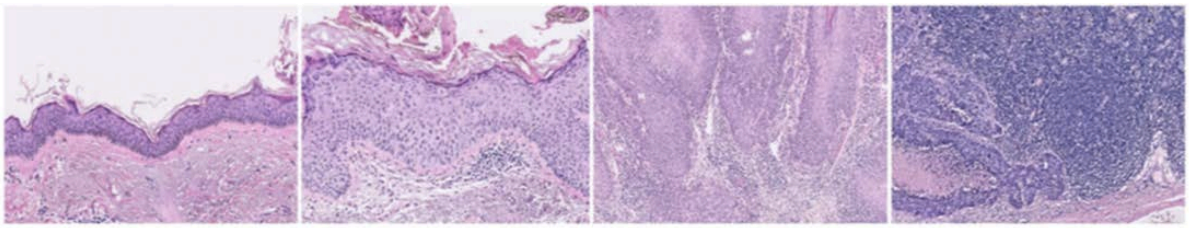

Photo-exposed skin	Dysplasia	Squamous carcinoma	Metastatic carcinoma
Frequently mutated genes			
TP53, NOTCH1, NOTHC2, CDKN2A, HRAS, KNSTRN, CARD11	TP53, NOTCH1, NOTHC2, CDKN2A, HRAS, KNSTRN, CARD11	TP53, NOTCH1, NOTHC2, PIK3CA, CDKN2A, CCND1, HRAS, EGFR, AJUBA, FBXW7, KMT2C, ERBB4, CASP8, PTCH1, FAT1, NF1, PARD3, TERT, RASA1, TP300, KMT2D, PTEN, BRCA2, CARD11	TP53, NOTCH1, NOTHC2, PIK3CA, CDKN2A, HRAS, EGFR, KRAS, BRAF, FGFR3, KIT, ERBB4, MTOR, EZH2, HGF, CARD11
Differential expression of miRNA			
		Overexpression of let-7a, miR365, miR9, miR21, miR135b, miR424, miR766, miR31, miR223	Overexpression of miR4286, miR200e-3p, miR148a-3p
		Inhibition of miR125b, miR34, miR124, miR483, miR193/365a, miR378, miR145, miR140-3p, miR30a, miR125a, let-7b, let-7c, let-7f, let-7g, miR99a, miR100, miR101, miR143	Inhibition of miR1915-3p, miR205-5p, *miR4516, miR150-5p*
Cytogenetic alterations			
		Gain of 3q, 7, 8q, 9, 9q, 11q, 14, 20 Loss of 2q, 3p, 4, 5q, 8p, 9p, 11, 13, 17p, 18, 19, 21 Alelic gain of 3q, 8q, 11q Isocromosomes 3q, 8q, 9q Microdeletions 9p23, 9q21, 3p14	Gain of 3q, 7, 8q, 9, 9q, 11q, 14, 20 Loss of 2q, 3p, 4, 5q, 8p, 9p, 11, 13, 17p, 18, 19, 21 Microdeletions 9p23, 9q21
Epigenetic changes			
Methylation of DAPK1	Methylation of DAPK1	Methylation of DCDH13, CDKN2A	Hypermethylation of 9p23, TFAP2C, ASCL2 Hypomethylation of ACTG2

Figure 1. Histology and molecular pathology of photo-exposed skin, dysplasia, squamous carcinoma and metastasis (García-Foncillas et al., 2022). Median tumor mutational burden in cSCC is the highest compared with other tumor types, with approximately 1300 nucleotide somatic variations per exome identified by exome sequencing, explaining that constant damage by UV radiation to basal keratinocytes may be responsible for multiple cSCC mutational events.

The most frequent mutations in cSCC are associated with UV and affect TP53 and NOTCH signaling pathway genes (Pickering et al., 2014). Activating mutations on genes of the RAS family, mainly HRAS, have been identified in up to 9% of cSCC (Durinck et al., 2011). Less frequently, alterations in STAT3, PIK3CA, KIT, RIPK4 and RAS1 have also been described (Lui et al., 2014). Li et al performed targeted sequencing on 29 lymph node metastases arising from cSCC and found that C>T mutations were the dominant substitution, and TP53, CDKN2A and NOTCH1 were altered in 50% samples (Y. Y. Li et al., 2015). CDKN2A seems to be associated with tumour aggressiveness (Küsters-Vandevelde et al., 2010). Another recent study looked at the genetic alterations between patient-matched cSCC primary tumors and lymph node metastases (Lobl, Clarey, Higgins, Sutton, & Wysong, 2022). ALK was discovered to be a potential driver mutation of metastasis, with ALK mutations co-

occurring with ERBB2 mutations, suggesting a possible mechanism through the MAPK/ERK signaling pathway.

Normal-looking skin on photo-exposed areas and precancerous lesion

Martincorena et al showed that even normal-looking skin in cSCC areas carries UV signature mutations in common cSCC driver genes such as TP53 and NOTCH1 (Martincorena & Campbell, 2015). It illustrates that normal-looking surface skin harbors oncogenic driver mutations and is already undergoing early stages of carcinogenesis. In cSCC, transformation process begins long before cancer is developed, or morphological changes can be detected. It mostly arises in sun exposed sites (head, neck, upper-limb extremities, dorsum of the hands). The presence of actinic keratosis (AK) seems to be more a predictor of development of cSCC rather than a precursor lesion as the rate of transformation is described as low (Werner et al., 2013). However, little is known about the reason why only some AK will persist at the same stage, while others will regress, and a few will give rise to cSCC.

In an intraepithelial UV-induced damage (known as cancerization field), the earliest presentation of AK is altered cornification of the skin, which can be felt (scaly hyperkeratotic plaque) rather than seen, and inflammation. The cytological atypia, present initially at the basal layer of the AK, can extend upwards involving progressively all the epidermis (Fernandez Figueras, 2017).

AK classification

Clinically AK may be graded using the "Olsen scale", a three-point grading system based on thickness of hyperkeratosis, with higher grades indicating more severe lesions (Jansen et al., 2019; Olsen et al., 1991). Olsen grade I reflects slightly palpable AK, more easily felt than seen; grade II reflects moderately thick AK, easy to see and feel; and grade III reflects very thick AK. Looking at the histological classification, AKs have traditionally being categorized as AK I if focal atypia of basal keratinocytes involves only the lower third of the epidermis, AK II if atypia affects the two lower thirds of the epidermis and AK III if the atypical cells extend to the upper layers (Röwert-Huber et al., 2007).

From AK to cSCC: is it possible to predict which AKs will progress?

Ahmady S et al showed that in patients with severe AK (Olsen grade III), the risk of cSCC was 20.9%, and the risk was especially high (33.5%) in patients with severe AK who needed

additional treatment after a first treatment (imiquimod, fluorouracil, methyl aminolevulinate photodynamic therapy, or ingenol mebutate gel) (Ahmady et al., 2022). Nevertheless, according to Schmitz et al, clinical classifications do not correlate accurately with histology and so it is not possible to predict which AKs will progress, regardless "low" or "high" risk classified AKs. What is known is the estimated annual risk of progression from AK to cSCC for an individual lesion is low (0.53%), the cumulative risk for a patient with multiple AKs lesions is high (Figure 2).

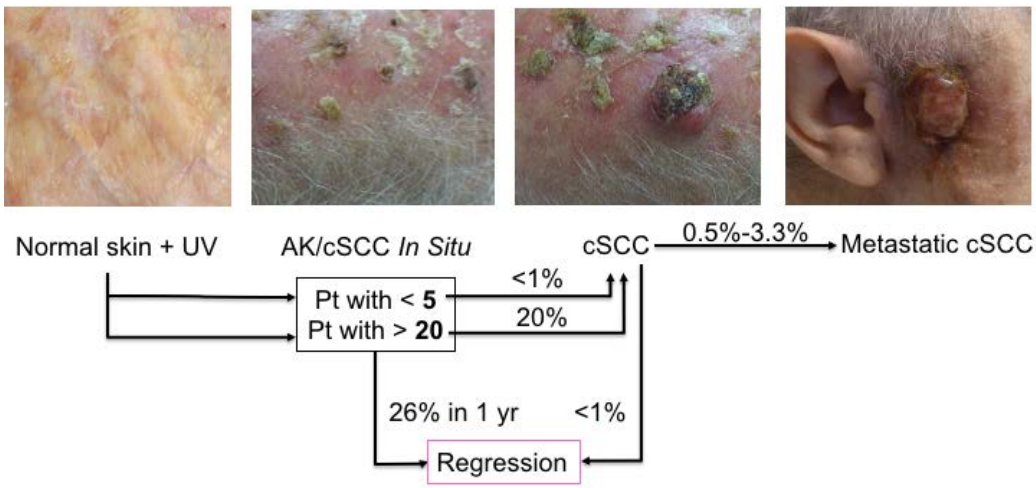

Figure 2. Actinic keratosis fate. Probability that human cutaneous neoplastic lesions will progress to invasive carcinoma. The likelihood of AKs in patients with fewer than 5 or more than 20 lesions progressing to cSCC is shown.
Abbreviations: Pt, patients; cSCC, cutaneous squamous cell carcinoma; UV, ultraviolet; yr, year.

I.1.d DNA Damage and Response to UV

UV radiation is the major etiologic agent in the development of skin cancers. UV-induced DNA damages have a great diversity due to the multiple interactions of radiations with the genome. Such damages may be the result of a direct absorption of photons by DNA bases or of an indirect effect related to the production of free radicals induced by UV irradiation. The main DNA damages are shown in Figure 3. UV-induced DNA damage sets in motion a highly complex well-coordinated series of responses whereby DNA damage and stalled replication forks can be detected.

Alterations of Nucleotide Bases

Damage to bases is the result of direct effect of radiation and/or the attack of free radicals to the DNA(Rastogi, Richa, Kumar, Tyagi, & Sinha, 2010). The most common direct damages

include the formation of CPDs (Cyclobutane Pyrimidine Dimers) and 6-4 PPs (Pyrimidine-Pyrimidone (6-4) Photoproducts) (Figure 3).

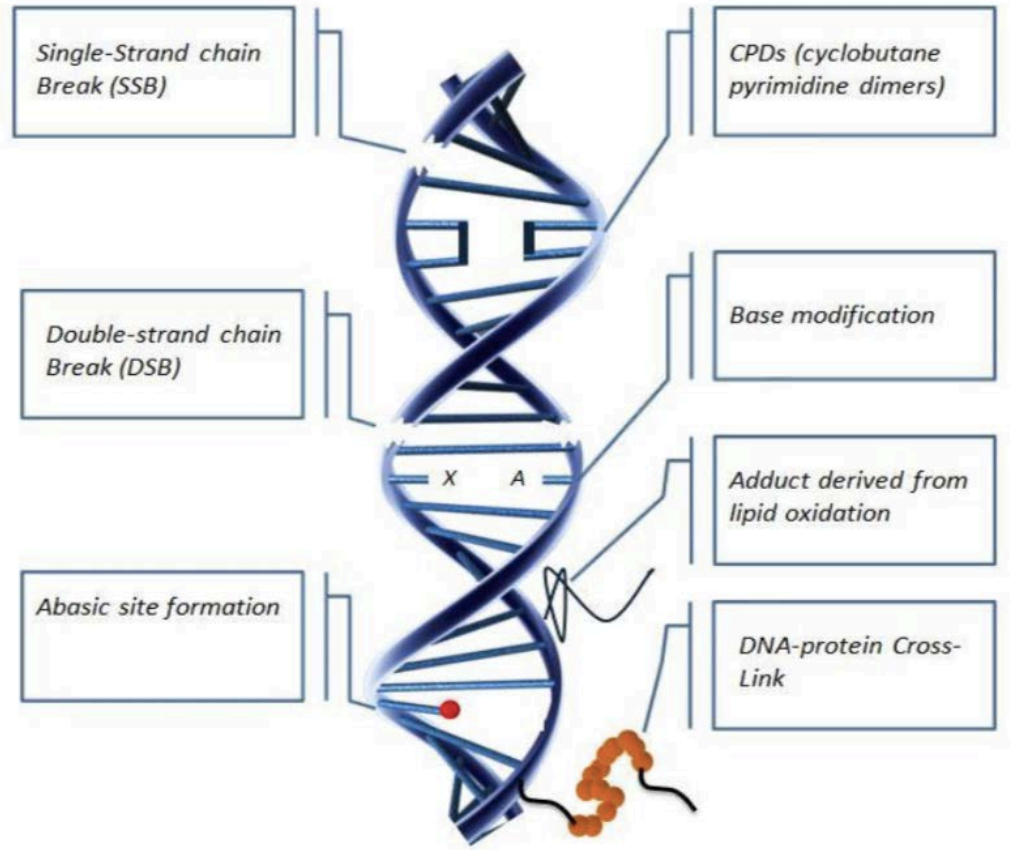

Figure 3. Major UV-induced DNA damages. Adapted from Hosseini et al, 2015. UV-induced DNA damages have a great diversity due to the multiple interactions of radiations with the genome.

It has been shown that the 6-4 PP is 5 to 10 times less prevalent than CPD, although it is repaired more effectively (Tornaletti & Pfeifer, 1996). One of the most abundant oxidative modifications of DNA bases is the C-8 hydroxylation of guanine which produce 7,8-hydro-8-oxodeoxyguanosine (8-oxo-dG). This modification is frequently considered as the marker of oxidative DNA damage. In addition, loss of bases can also be occurred by irradiation (Rastogi et al., 2010).

Nucleotide Excision Repair (NER)

To prevent the genotoxic effect of UV radiation and ensure the genomic integrity, two major well-conserved repair mechanisms, namely photoreactivation and nucleotide excision repair (NER), have been developed in different organisms (Figure 4). In the former system, a specialized enzyme known as "DNA photolyase" bind specifically to CPDs (CPD photolyase) or 6-4PPs (6-4PP photolyase) and breaks the cyclobutane ring of the dimer by using the energy

of visible/blue light (Essen & Klar, 2006; Kim, Sancar, & Heelis, 1992). Photolyases are evolutionary old proteins found in many species from bacteria to nonplacental mammals.

Nucleotides excision repair (NER) is probably one of the most important repair processes as it is effective in removing bulky lesions which cause structural DNA distortions. These lesions are induced by ultraviolet light, ionizing radiation, mutagens, chemical carcinogens and certain therapeutic substances (D'orazio, Jarrett, Amaro-Ortiz, & Scott, 2013). This process applies to various adducts such as CPD, 6-4 PP, thymine glycols and other certain base modifications, adducts psoralen-thymine, cisplatin-guanine, mitomycin-guanine and interstrand cross-links. There are twenty different proteins involved in the process (Berens & Molinier, 2020). The main genes implicated in NER were discovered following the identification of genes related to hereditary diseases such as xeroderma pigmentosum (XP), trichothiodystrophy (TTD) and Cockayne syndrome in humans (Frit et al., 2002).

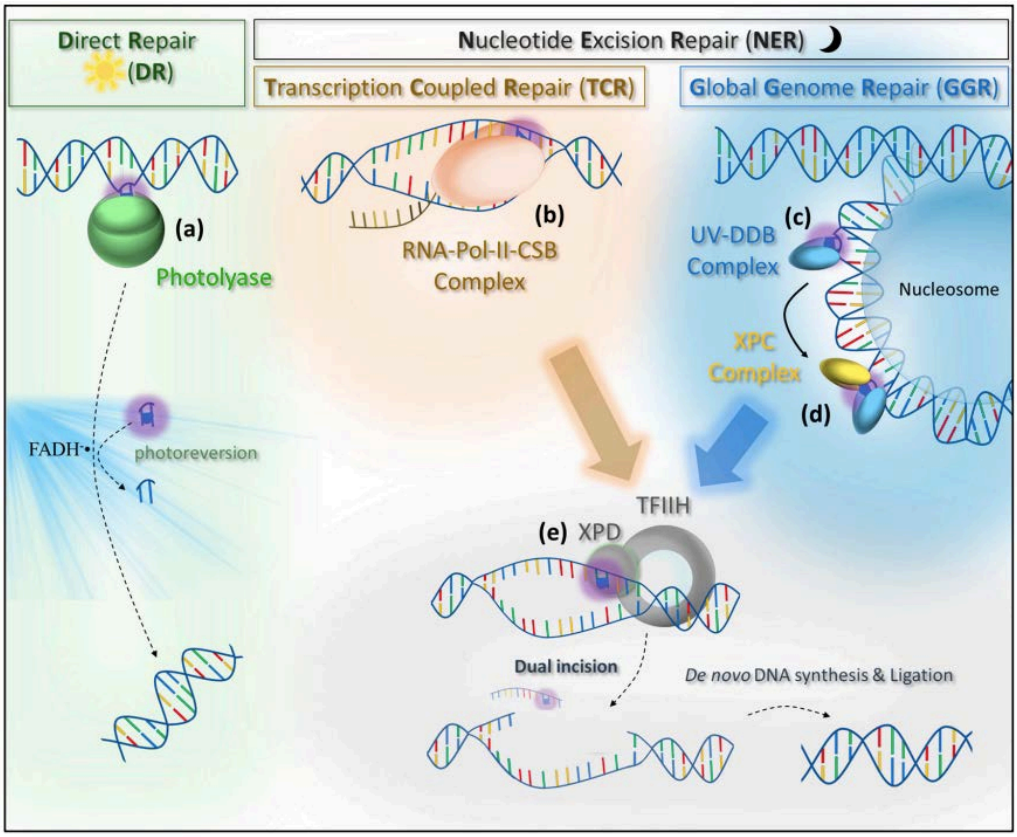

Figure 4. Photolesion recognition and repair pathways. Adapted from To Berens et al, 2020. a) The direct repair pathway (light repair) relies on specific photolyases, which either recognize CPD or 6-4PP. The photolyase interne flavin adenine dinucleotide (FAD) cofactor, excited by blue light, catalyzes photoreversion to restore the initial undamaged sequence. **(b)** The transcription coupled repair (TC-NER) pathway is specific to transcribed genomic regions and depends on the RNA Pol II–CSB (RNA Polymerase II-Cockayne Syndrome protein B) complex for the recognition step. RNA Pol II stalls and arrests at the damage site. **(c)** The global

genome repair (GG-NER) pathway primarily recognizes the photolesion by the damage sensor complex UV–DDB on non-transcribed part of genome. **(d)** Once bound to the damage, UV–DDB recruits the Rad4/XPC complex for a second recognition step. The stalled RNA Pol II–CSB and The Rad4/XPC complex recruit the TFIIH (Transcription Factor II H) protein complex. **(e)** The damaged DNA region is excised by a dual incision process, and the gap is filled by de novo DNA synthesis and nick ligation (Berens & Molinier, 2020).

There are two different sub-pathways for NER: global genome repair (GG-NER) which is independent of transcription and transcription-coupled repair (TC-NER) (Figure 4) (Feuerhahn & Egly, 2008). Both repair processes are done in the five following steps: recognition of the lesion, separation of double helix at the lesion site, incision at both sides of the lesion, excision of the lesion, reparative DNA synthesis (resynthesis) for filling the gap and ligation. The major difference between GG-NER and TC-NER is the lesion recognition step. In GG-NER, poly- ubiquitination of XPC by XPE (UV-DDB) seems to stimulate the binding of XPC-RAD23B complexes to the damaged DNA and initiate GG-NER (Rastogi et al., 2010). In TC-NER, damage is recognized by a stalled RNA polymerase II at a DNA lesion in transcriptionally active regions upon its interaction with CSB (ERCC6) and CSA (ERCC8) proteins (Singh, Compe, Le May, & Egly, 2015). The UV-stimulated scaffold protein A (UVSSA) forms a complex with ubiquitin-specific protease 7 (USP7) which removes ubiquitin and stabilizes the ERCC6–RNA Pol II complex. RNA Pol II which is stalled on the DNA template is then displaced to provide access to NER factors in order to remove the transcription-stalling damage.

Damage recognition for both GG-NER and TC-NER pathways is followed by recruitment of TFIIH (including XPB, XPD, p8/TTDA and several other subunits) via interaction with either XPC or the arrested transcription apparatus. Unwinding the DNA helix is then triggered by TFIIH complex, XPG, XPA and replication protein A (RPA). The DNA around the damage is then incised by XPF-ERCC1 and XPG leading to the release of the oligonucleotide segment containing the damaged base(s). The resulted gap is then filled by a DNA polymerase (ε or δ) in presence of PCNA (Proliferating Cell Nuclear Antigen) and Replication Factor C (RFC). The 3’ nick is finally closed by DNA ligase (Hosseini, Ezzedine, Taieb, & Rezvani, 2015).

I.1.e Treatment

Surgical excision

Surgical excision is the first-line treatment for cSCC patients, regardless of age and anatomical location (Stratigos et al., 2020). The surgical margins are adapted: for low risk lesions, clinical practice guidelines recommend performing an excision with 4–6 mm margins and 10mm for high risk lesions when feasible (Stratigos et al., 2020)

Local treatment

Based on the risk stratification if surgery is not feasible, or if cSCC is in situ, local approaches may be considered to treat the tumour and the field cancerization.

Photodynamic therapy consists of a 2-step method that involves the topical application of a photosensitizer, such as methyl aminolevulinate, followed by an incubation period with light irradiation. Alternatively, a topical therapy with imiquimod up to 5% or 5-fluorouracil may be also applied (Jansen et al., 2019).

Role of Radiotherapy

Radiotherapy (RT) may be used:

-in first line in patients unable to undergo surgical resection or decline surgery

-in adjuvant settings when: (a) close or positive margins are not amenable to re-resection, (b) relapse after prior margin-free surgery, (c) stage T3–T4, (d) when PNI are present. In patients with regional node metastasis, adjuvant RT after therapeutic lymphadenectomy is also strongly recommended (Likhacheva et al., 2020).

Systemic Treatment

Immune checkpoint inhibitors

Immune checkpoint inhibitors (ICIs) have changed the therapeutic landscape of locally advanced and metastatic cSCC.

Currently, anti-programmed cell death-1 (anti-PD-1) antibodies constitute the first-line systemic treatment for metastatic or locally advanced cSCC in which curative surgery or RT are not feasible.

The anti-PD-1 cemiplimab is the first approved by the FDA as a first line agent in patients with locally advanced or metastatic cSCC who are not candidates for curative surgery or curative

radiation. It has demonstrated efficacy (overall response rate (ORR) 46.1%) and long-term durable response with very effective disease control (disease control rate: 72.5%) in patients with advanced and metastatic cSCC (Migden et al., 2018; Rischin et al., 2021). Recently improvement has also been shown in neoadjuvant settings (Gross et al., 2022), with pathological complete response in 51% of patients.

Targeted therapy

Epidermal growth factor receptor (EGFR) expression is present in 90% of cSCC tumours, with overexpression in 35% and it is a risk factor of poor outcome (Cañueto et al., 2017). Data evaluating the cetuximab alone, an anti-EGFR monoclonal antibody, are limited but a French phase-2 trial prospectively evaluated cetuximab as 1rst-line monotherapy on 36 advanced cSCC and this study showed an objective response rate (ORR) of 28%, and an overall disease-control rate of 69% (Maubec et al., 2011)

Chemotherapy

Chemotherapy is commonly used mostly as palliative treatment, but its safety profile limits its use most of the time. No chemotherapeutic agents have been specifically approved, but platinum, 5-fluorouracil, anthracycline or bleomycine alone or in combination are frequently used (Chapalain et al., 2020; Nakamura, Okuyama, Saida, & Uhara, 2013).

Conclusion

Although prognosis of cSCC is generally excellent, there is a subset of patient that carries a markedly elevated risk of nodal metastasis and death. This tumor subset is termed “high-risk cSCC”. But even if its risk factors and its associated outcomes have recently been better identified, there is an unmet need for the identification of new risk factors.

References

Ahmady, S., Jansen, M. H. E., Nelemans, P. J., Kessels, J. P. H. M., Arits, A. H. M. M., De Rooij, M. J. M., … Mosterd, K. (2022). Risk of Invasive Cutaneous Squamous Cell Carcinoma After Different Treatments for Actinic Keratosis: A Secondary Analysis of a Randomized Clinical Trial. *JAMA Dermatology*, *158*(6), 634–640. https://doi.org/10.1001/JAMADERMATOL.2022.1034

Alam, M., & Ratner, D. (2001). Cutaneous squamous-cell carcinoma. *The New England Journal of Medicine*, *344*(13), 975–983. https://doi.org/10.1056/NEJM200103293441306

Alfarouk, K. O., Verduzco, D., Rauch, C., Muddathir, A. K., Bashir, A. H. H., Elhassan, G. O., … Harguindey, S. (2014). Erratum: Glycolysis, tumor metabolism, cancer growth and dissemination. A new pH-based etiopathogenic perspective and therapeutic approach to an old cancer question. *Oncoscience*, *2*(4), 317. https://doi.org/10.18632/ONCOSCIENCE.158

Amin, M. B., Greene, F. L., Edge, S. B., Compton, C. C., Gershenwald, J. E., Brookland, R. K., … Winchester, D. P. (2017). The Eighth Edition AJCC Cancer Staging Manual: Continuing to build a bridge from a population-based to a more "personalized" approach to cancer staging. *CA: A Cancer Journal for Clinicians*, *67*(2), 93–99. https://doi.org/10.3322/CAAC.21388

Amoedo, N. D., Sarlak, S., Obre, E., Esteves, P., Bégueret, H., Kieffer, Y., … Rossignol, R. (2021). Targeting the mitochondrial trifunctional protein restrains tumor growth in oxidative lung carcinomas. *Journal of Clinical Investigation*. https://doi.org/10.1172/JCI133081

Amuthan, G., Biswas, G., Ananadatheerthavarada, H. K., Vijayasarathy, C., Shephard, H. M., & Avadhani, N. G. (2002). Mitochondrial stress-induced calcium signaling, phenotypic changes and invasive behavior in human lung carcinoma A549 cells. *Oncogene*, *21*(51), 7839–7849. https://doi.org/10.1038/SJ.ONC.1205983

Andrejeva, G., & Rathmell, J. C. (2017). Similarities and Distinctions of Cancer and Immune Metabolism in Inflammation and Tumors. *Cell Metabolism*, *26*(1), 49–70. https://doi.org/10.1016/J.CMET.2017.06.004

Asgari, M. M., Ray, G. T., Quesenberry, C. P., Katz, K. A., & Silverberg, M. J. (2017). Association of Multiple Primary Skin Cancers With Human Immunodeficiency Virus Infection, CD4 Count, and Viral Load. *JAMA Dermatology*, *153*(9), 892–896. https://doi.org/10.1001/JAMADERMATOL.2017.1716

Basset Seguin, N., Malvehy, J., Nadal, F., Creancier, L., Rauly-Lestienne, I., Beauchamp, R., … Ulianov, L. (2019). Risk behaviour and patient preferences for an improved non-melanoma skin cancer prevention modality for organ-transplanted patients; a European, multi-country, online patient community study. *European Journal of Dermatology : EJD*. https://doi.org/10.1684/ejd.2019.3639

Baysal, B. E., Ferrell, R. E., Willett-Brozick, J. E., Lawrence, E. C., Myssiorek, D., Bosch, A., … Devlin, B. (2000). Mutations in SDHD, a mitochondrial complex II gene, in hereditary paraganglioma. *Science (New York, N.Y.)*, *287*(5454), 848–851. https://doi.org/10.1126/SCIENCE.287.5454.848

Bensaad, K., & Vousden, K. H. (2007). p53: new roles in metabolism. *Trends in Cell Biology*, *17*(6), 286–291. https://doi.org/10.1016/J.TCB.2007.04.004

Berens, P. J. T., & Molinier, J. (2020). Formation and Recognition of UV-Induced DNA Damage within Genome Complexity. *International Journal of Molecular Sciences*, *21*(18), 1–23. https://doi.org/10.3390/IJMS21186689

Blechman, A. B., Carucci, J. A., & Stevenson, M. L. (2019). Stratification of Poor Outcomes for Cutaneous Squamous Cell Carcinoma in Immunosuppressed Patients Using the

American Joint Committee on Cancer Eighth Edition and Brigham and Women's Hospital Staging Systems. *Dermatologic Surgery : Official Publication for American Society for Dermatologic Surgery [et Al.]*, *45*(9), 1117–1124. https://doi.org/10.1097/DSS.0000000000001774

Boulton, D. P., & Caino, M. C. (2022). Mitochondrial Fission and Fusion in Tumor Progression to Metastasis. *Frontiers in Cell and Developmental Biology*, *10*. https://doi.org/10.3389/FCELL.2022.849962

Brandon, M., Baldi, P., & Wallace, D. C. (2006). Mitochondrial mutations in cancer. *Oncogene*, *25*(34), 4647–4662. https://doi.org/10.1038/SJ.ONC.1209607

Brantsch, K. D., Meisner, C., Schönfisch, B., Trilling, B., Wehner-Caroli, J., Röcken, M., & Breuninger, H. (2008a). Analysis of risk factors determining prognosis of cutaneous squamous-cell carcinoma: a prospective study. *The Lancet. Oncology*, *9*(8), 713–720. https://doi.org/10.1016/S1470-2045(08)70178-5

Brantsch, K. D., Meisner, C., Schönfisch, B., Trilling, B., Wehner-Caroli, J., Röcken, M., & Breuninger, H. (2008b). Analysis of risk factors determining prognosis of cutaneous squamous-cell carcinoma: a prospective study. *The Lancet Oncology*, *9*(8), 713–720. https://doi.org/10.1016/S1470-2045(08)70178-5

Branzei, D., & Foiani, M. (2008). Regulation of DNA repair throughout the cell cycle. *Nature Reviews. Molecular Cell Biology*, *9*(4), 297–308. https://doi.org/10.1038/NRM2351

Bray, F., Ferlay, J., Soerjomataram, I., Siegel, R. L., Torre, L. A., & Jemal, A. (2018). Global cancer statistics 2018: GLOBOCAN estimates of incidence and mortality worldwide for 36 cancers in 185 countries. *CA: A Cancer Journal for Clinicians*, *68*(6), 394–424. https://doi.org/10.3322/CAAC.21492

Brewer, J. D., Shanafelt, T. D., Khezri, F., Sosa Seda, I. M., Zubair, A. S., Baum, C. L., … Otley, C. C. (2015). Increased incidence and recurrence rates of nonmelanoma skin cancer in patients with non-Hodgkin lymphoma: a Rochester Epidemiology Project population-based study in Minnesota. *Journal of the American Academy of Dermatology*, *72*(2), 302–309. https://doi.org/10.1016/J.JAAD.2014.10.028

Brougham, N. D. L. S., Dennett, E. R., Cameron, R., & Tan, S. T. (2012). The incidence of metastasis from cutaneous squamous cell carcinoma and the impact of its risk factors. *Journal of Surgical Oncology*, *106*(7), 811–815. https://doi.org/10.1002/JSO.23155

Brown, K. K., Spinelli, J. B., Asara, J. M., & Toker, A. (2017). Adaptive reprogramming of De novo pyrimidine synthesis is a metabolic vulnerability in triple-negative breast cancer. *Cancer Discovery*. https://doi.org/10.1158/2159-8290.CD-16-0611

Cañueto, J., Cardeñoso, E., García, J. L., Santos-Briz, Castellanos-Martín, A., Fernández-López, E., … Román-Curto, C. (2017). Epidermal growth factor receptor expression is associated with poor outcome in cutaneous squamous cell carcinoma. *The British Journal of Dermatology*, *176*(5), 1279–1287. https://doi.org/10.1111/BJD.14936

Caro, P., Kishan, A. U., Norberg, E., Stanley, I. A., Chapuy, B., Ficarro, S. B., … Danial, N. N. (2012). Metabolic signatures uncover distinct targets in molecular subsets of diffuse large B cell lymphoma. *Cancer Cell*, *22*(4), 547–560. https://doi.org/10.1016/J.CCR.2012.08.014

Carter, J. B., Johnson, M. M., Chua, T. L., Karia, P. S., & Schmults, C. D. (2013). Outcomes of primary cutaneous squamous cell carcinoma with perineural invasion: an 11-year cohort study. *JAMA Dermatology*, *149*(1), 35–42. https://doi.org/10.1001/JAMADERMATOL.2013.746

Chahoud, J., Semaan, A., Chen, Y., Cao, M., Rieber, A. G., Rady, P., & Tyring, S. K. (2016). Association Between β-Genus Human Papillomavirus and Cutaneous Squamous Cell Carcinoma in Immunocompetent Individuals-A Meta-analysis. *JAMA Dermatology*, *152*(12), 1354–1364. https://doi.org/10.1001/JAMADERMATOL.2015.4530

Chapalain, M., Baroudjian, B., Dupont, A., Lhote, R., Lambert, J., Bagot, M., … Basset-Seguin, N. (2020). Stage IV cutaneous squamous cell carcinoma: treatment outcomes in a series of 42 patients. *Journal of the European Academy of Dermatology and Venereology : JEADV*, *34*(6), 1202–1209. https://doi.org/10.1111/JDV.16007

Chiche, J., Brahimi-Horn, M. C., & Pouysségur, J. (2010). Tumour hypoxia induces a metabolic shift causing acidosis: a common feature in cancer. *Journal of Cellular and Molecular Medicine*, *14*(4), 771–794. https://doi.org/10.1111/J.1582-4934.2009.00994.X

Christian, S., Merz, C., Evans, L., Gradl, S., Seidel, H., Friberg, A., … Janzer, A. (2019). The novel dihydroorotate dehydrogenase (DHODH) inhibitor BAY 2402234 triggers differentiation and is effective in the treatment of myeloid malignancies. *Leukemia*, *33*(10), 2403–2415. https://doi.org/10.1038/s41375-019-0461-5

Condeelis, J., & Pollard, J. W. (2006). Macrophages: obligate partners for tumor cell migration, invasion, and metastasis. *Cell*, *124*(2), 263–266. https://doi.org/10.1016/J.CELL.2006.01.007

Conforti, C., Paolini, F., Venuti, A., Dianzani, C., & Zalaudek, I. (2019). The detection rate of human papillomavirus in well-differentiated squamous cell carcinoma and keratoacanthoma: is there new evidence for a viral pathogenesis of keratoacanthoma? *The British Journal of Dermatology*, *181*(6), 1309–1311. https://doi.org/10.1111/BJD.18212

D'orazio, J., Jarrett, S., Amaro-Ortiz, A., & Scott, T. (2013). UV Radiation and the Skin. *Int. J. Mol. Sci*, *14*, 12222–12248. https://doi.org/10.3390/ijms140612222

Dang, C. V., Lewis, B. C., Dolde, C., Dang, G., & Shim, H. (1997). Oncogenes in tumor metabolism, tumorigenesis, and apoptosis. *Journal of Bioenergetics and Biomembranes*, *29*(4), 345–354. https://doi.org/10.1023/A:1022446730452

de Martel, C., & Franceschi, S. (2009). Infections and cancer: established associations and new hypotheses. *Critical Reviews in Oncology/Hematology*, *70*(3), 183–194. https://doi.org/10.1016/J.CRITREVONC.2008.07.021

De Visser, K. E., Eichten, A., & Coussens, L. M. (2006). Paradoxical roles of the immune system during cancer development. *Nature Reviews. Cancer*, *6*(1), 24–37. https://doi.org/10.1038/NRC1782

Deady, S., Sharp, L., & Comber, H. (2014). Increasing skin cancer incidence in young, affluent, urban populations: a challenge for prevention. *The British Journal of Dermatology*, *171*(2), 324–331. https://doi.org/10.1111/BJD.12988

Denicola, G. M., Karreth, F. A., Humpton, T. J., Gopinathan, A., Wei, C., Frese, K., … Tuveson, D. A. (2011). Oncogene-induced Nrf2 transcription promotes ROS detoxification and tumorigenesis. *Nature*, *475*(7354), 106–110. https://doi.org/10.1038/NATURE10189

Dhup, S., Kumar Dadhich, R., Ettore Porporato, P., & Sonveaux, P. (2012). Multiple biological activities of lactic acid in cancer: influences on tumor growth, angiogenesis and metastasis. *Current Pharmaceutical Design*, *18*(10), 1319–1330. https://doi.org/10.2174/138161212799504902

Dotto, G. P., & Rustgi, A. K. (2016). Squamous Cell Cancers: A Unified Perspective on Biology and Genetics. *Cancer Cell*, *29*(5), 622–637. https://doi.org/10.1016/J.CCELL.2016.04.004

Durinck, S., Ho, C., Wang, N. J., Liao, W., Jakkula, L. R., Collisson, E. A., … Cho, R. J. (2011). Temporal dissection of tumorigenesis in primary cancers. *Cancer Discovery*, *1*(2), 137–143. https://doi.org/10.1158/2159-8290.CD-11-0028

Dusendang, J. R., Carlson, E., Lee, D. S., Marwaha, S., Madani, S., Alexeeff, S. E., … Herrinton, L. J. (2022). Cohort and nested case-control study of cutaneous squamous cell carcinoma in solid organ transplant recipients, by medication. *Journal of the American*

Academy of Dermatology, *86*(3), 598–606. https://doi.org/10.1016/J.JAAD.2021.07.065
Dusingize, J. C., Olsen, C. M., Pandeya, N. P., Subramaniam, P., Thompson, B. S., Neale, R. E., … Whiteman, D. C. (2017). Cigarette Smoking and the Risks of Basal Cell Carcinoma and Squamous Cell Carcinoma. *The Journal of Investigative Dermatology*, *137*(8), 1700–1708. https://doi.org/10.1016/J.JID.2017.03.027
Ecker, J., & Liebisch, G. (2014). Application of stable isotopes to investigate the metabolism of fatty acids, glycerophospholipid and sphingolipid species. *Progress in Lipid Research*, *54*(1), 14–31. https://doi.org/10.1016/J.PLIPRES.2014.01.002
Essen, L. O., & Klar, T. (2006). Light-driven DNA repair by photolyases. *Cellular and Molecular Life Sciences : CMLS*, *63*(11), 1266–1277. https://doi.org/10.1007/S00018-005-5447-Y
Feng, Y., Ye, Z., Song, F., He, Y., & Liu, J. (2022). The Role of TAMs in Tumor Microenvironment and New Research Progress. *Stem Cells International*, *2022*, 1–11. https://doi.org/10.1155/2022/5775696
Fernandez Figueras, M. T. (2017). From actinic keratosis to squamous cell carcinoma: pathophysiology revisited. *Journal of the European Academy of Dermatology and Venereology : JEADV*, *31 Suppl 2*, 5–7. https://doi.org/10.1111/JDV.14151
Feuerhahn, S., & Egly, J. M. (2008). Tools to study DNA repair: what's in the box? *Trends in Genetics : TIG*, *24*(9), 467–474. https://doi.org/10.1016/J.TIG.2008.07.003
Frit, P., Kwon, K., Coin, F., Auriol, J. érôme, Dubaele, S., Salles, B., & Egly, J. M. (2002). Transcriptional Activators Stimulate DNA Repair. *Molecular Cell*, *10*(6), 1391–1401. https://doi.org/10.1016/S1097-2765(02)00732-3
Galluzzi, L., Kepp, O., Heiden, M. G. V., & Kroemer, G. (2013). Metabolic targets for cancer therapy. *Nature Reviews. Drug Discovery*, *12*(11), 829–846. https://doi.org/10.1038/NRD4145
Gandini, S., Palli, D., Spadola, G., Bendinelli, B., Cocorocchio, E., Stanganelli, I., … Caini, S. (2018). Anti-hypertensive drugs and skin cancer risk: a review of the literature and meta-analysis. *Critical Reviews in Oncology/Hematology*, *122*, 1–9. https://doi.org/10.1016/J.CRITREVONC.2017.12.003
García-Foncillas, J., Tejera-Vaquerizo, A., Sanmartín, O., Rojo, F., Mestre, J., Martín, S., … Mesía, R. (2022). Update on Management Recommendations for Advanced Cutaneous Squamous Cell Carcinoma. *Cancers*, *14*(3). https://doi.org/10.3390/CANCERS14030629
Garrett, G. L., Blanc, P. D., Boscardin, J., Lloyd, A. A., Ahmed, R. L., Anthony, T., … Arron, S. T. (2017). Incidence of and Risk Factors for Skin Cancer in Organ Transplant Recipients in the United States. *JAMA Dermatology*, *153*(3), 296–303. https://doi.org/10.1001/JAMADERMATOL.2016.4920
Geltink, R. I. K., Kyle, R. L., & Pearce, E. L. (2018). Unraveling the Complex Interplay Between T Cell Metabolism and Function. *Annual Review of Immunology*, *36*, 461–488. https://doi.org/10.1146/ANNUREV-IMMUNOL-042617-053019
Gentric, G., Kieffer, Y., Mieulet, V., Goundiam, O., Bonneau, C., Nemati, F., … Mechta-Grigoriou, F. (2019). PML-Regulated Mitochondrial Metabolism Enhances Chemosensitivity in Human Ovarian Cancers. *Cell Metabolism*. https://doi.org/10.1016/j.cmet.2018.09.002
George, E. A., Baranwal, N., Kang, J. H., Qureshi, A. A., Drucker, A. M., & Cho, E. (2021). Photosensitizing Medications and Skin Cancer: A Comprehensive Review. *Cancers*, *13*(10). https://doi.org/10.3390/CANCERS13102344
Gordon, L. G., Leung, W., Johns, R., McNoe, B., Lindsay, D., Merollini, K. M. D., … Whiteman, D. C. (2022). Estimated Healthcare Costs of Melanoma and Keratinocyte Skin Cancers in Australia and Aotearoa New Zealand in 2021. *International Journal of*

Environmental Research and Public Health, *19*(6). https://doi.org/10.3390/IJERPH19063178
Gottlieb, E., & Tomlinson, I. P. M. (2005). Mitochondrial tumour suppressors: a genetic and biochemical update. *Nature Reviews. Cancer*, *5*(11), 857–866. https://doi.org/10.1038/NRC1737
Grande, S., Palma, A., Ricci-Vitiani, L., Luciani, A. M., Buccarelli, M., Biffoni, M., … Rosi, A. (2018). Metabolic Heterogeneity Evidenced by MRS among Patient-Derived Glioblastoma Multiforme Stem-Like Cells Accounts for Cell Clustering and Different Responses to Drugs. *Stem Cells International*, *2018*. https://doi.org/10.1155/2018/3292704
Gross, N. D., Miller, D. M., Khushalani, N. I., Divi, V., Ruiz, E. S., Lipson, E. J., … Rischin, D. (2022). Neoadjuvant Cemiplimab for Stage II to IV Cutaneous Squamous-Cell Carcinoma. *The New England Journal of Medicine*. https://doi.org/10.1056/NEJMOA2209813
Guerra, C., Schuhmacher, A. J., Cañamero, M., Grippo, P. J., Verdaguer, L., Pérez-Gallego, L., … Barbacid, M. (2007). Chronic pancreatitis is essential for induction of pancreatic ductal adenocarcinoma by K-Ras oncogenes in adult mice. *Cancer Cell*, *11*(3), 291–302. https://doi.org/10.1016/J.CCR.2007.01.012
Hanahan, D., & Weinberg, R. A. (2011). Hallmarks of cancer: the next generation. *Cell*, *144*(5), 646–674. https://doi.org/10.1016/J.CELL.2011.02.013
Harbottle, A., & Birch-Machin, M. A. (2006). Real-time PCR analysis of a 3895 bp mitochondrial DNA deletion in nonmelanoma skin cancer and its use as a quantitative marker for sunlight exposure in human skin. *British Journal of Cancer*, *94*(12), 1887–1893. https://doi.org/10.1038/SJ.BJC.6603178
Heiden, M. G. V., Cantley, L. C., & Thompson, C. B. (2009). Understanding the warburg effect: The metabolic requirements of cell proliferation. *Science*. https://doi.org/10.1126/science.1160809
Hensley, C. T., Faubert, B., Yuan, Q., Lev-Cohain, N., Jin, E., Kim, J., … DeBerardinis, R. J. (2016). Metabolic Heterogeneity in Human Lung Tumors. *Cell*. https://doi.org/10.1016/j.cell.2015.12.034
Hillen, U., Leiter, U., Haase, S., Kaufmann, R., Becker, J., Gutzmer, R., … Livingstone, E. (2018). Advanced cutaneous squamous cell carcinoma: A retrospective analysis of patient profiles and treatment patterns-Results of a non-interventional study of the DeCOG. *European Journal of Cancer (Oxford, England : 1990)*, *96*, 34–43. https://doi.org/10.1016/J.EJCA.2018.01.075
Hosseini, M., Dousset, L., Mahfouf, W., Serrano-Sanchez, M., Redonnet-Vernhet, I., Mesli, S., … Rezvani, H. R. (2018). Energy Metabolism Rewiring Precedes UVB-Induced Primary Skin Tumor Formation. *Cell Reports*, *23*(12), 3621–3634. https://doi.org/10.1016/j.celrep.2018.05.060
Hosseini, M., Ezzedine, K., Taieb, A., & Rezvani, H. R. (2015). Oxidative and energy metabolism as potential clues for clinical heterogeneity in nucleotide excision repair disorders. *The Journal of Investigative Dermatology*, *135*(2), 341–351. https://doi.org/10.1038/JID.2014.365
Hsu, P. P., & Sabatini, D. M. (2008). Cancer cell metabolism: Warburg and beyond. *Cell*, *134*(5), 703–707. https://doi.org/10.1016/J.CELL.2008.08.021
Hu, S., Balakrishnan, A., Bok, R. A., Anderton, B., Larson, P. E. Z., Nelson, S. J., … Goga, A. (2011). 13C-pyruvate imaging reveals alterations in glycolysis that precede c-Myc-induced tumor formation and regression. *Cell Metabolism*, *14*(1), 131–142. https://doi.org/10.1016/J.CMET.2011.04.012
Hussein, M. R. (2005). Ultraviolet radiation and skin cancer: molecular mechanisms. *Journal*

of Cutaneous Pathology, *32*(3), 191–205. https://doi.org/10.1111/J.0303-6987.2005.00281.X

Jansen, M. H. E., Kessels, J. P. H. M., Nelemans, P. J., Kouloubis, N., Arits, A. H. M. M., van Pelt, H. P. A., … Mosterd, K. (2019). Randomized Trial of Four Treatment Approaches for Actinic Keratosis. *The New England Journal of Medicine*, *380*(10), 935–946. https://doi.org/10.1056/NEJMOA1811850

Jia, S., Liu, Z., Zhang, S., Liu, P., Zhang, L., Lee, S. H., … Zhao, J. J. (2008). Essential roles of PI(3)K-p110beta in cell growth, metabolism and tumorigenesis. *Nature*, *454*(7205), 776–779. https://doi.org/10.1038/NATURE07091

Jin, H., Wang, S., Zaal, E. A., Wang, C., Wu, H., Bosma, A., … Bernards, R. (2020). A powerful drug combination strategy targeting glutamine addiction for the treatment of human liver cancer. *ELife*, *9*, 1–20. https://doi.org/10.7554/ELIFE.56749

Jose, C., Bellance, N., & Rossignol, R. (2011). Choosing between glycolysis and oxidative phosphorylation: a tumor's dilemma? *Biochimica et Biophysica Acta*, *1807*(6), 552–561. https://doi.org/10.1016/J.BBABIO.2010.10.012

Karia, P. S., Han, J., & Schmults, C. D. (2013a). Cutaneous squamous cell carcinoma: estimated incidence of disease, nodal metastasis, and deaths from disease in the United States, 2012. *Journal of the American Academy of Dermatology*, *68*(6), 957–966. https://doi.org/10.1016/J.JAAD.2012.11.037

Karia, P. S., Han, J., & Schmults, C. D. (2013b). Cutaneous squamous cell carcinoma: Estimated incidence of disease, nodal metastasis, and deaths from disease in the United States, 2012. *Journal of the American Academy of Dermatology*, *68*(6), 957–966. https://doi.org/10.1016/j.jaad.2012.11.037

Karia, P. S., Han, J., & Schmults, C. D. (2013c). Cutaneous squamous cell carcinoma: Estimated incidence of disease, nodal metastasis, and deaths from disease in the United States, 2012. *Journal of the American Academy of Dermatology*, *68*(6), 957–966. https://doi.org/10.1016/j.jaad.2012.11.037

Karia, P. S., Morgan, F. C., Ruiz, E. S., & Schmults, C. D. (2017). Clinical and Incidental Perineural Invasion of Cutaneous Squamous Cell Carcinoma: A Systematic Review and Pooled Analysis of Outcomes Data. *JAMA Dermatology*, *153*(8), 781–788. https://doi.org/10.1001/JAMADERMATOL.2017.1680

Kim, S. T., Sancar, A., & Heelis, P. F. (1992). Energy transfer (deazaflavin-->FADH2) and electron transfer (FADH2-->T T) kinetics in Anacystis nidulans photolyase. *Biochemistry*, *31*(45), 11244–11248. https://doi.org/10.1021/BI00160A040

Kitamura, S., Yanagi, T., Imafuku, K., Hata, H., Abe, R., & Shimizu, H. (2017). Drp1 regulates mitochondrial morphology and cell proliferation in cutaneous squamous cell carcinoma. *Journal of Dermatological Science*, *88*(3), 298–307. https://doi.org/10.1016/J.JDERMSCI.2017.08.004

Knuutila, J. S., Riihilä, P., Kurki, S., Nissinen, L., & Kähäri, V. M. (2020). Risk Factors and Prognosis for Metastatic Cutaneous Squamous Cell Carcinoma: A Cohort Study. *Acta Dermato-Venereologica*, *100*(16), 1–9. https://doi.org/10.2340/00015555-3628

Koundinya, M., Sudhalter, J., Courjaud, A., Lionne, B., Touyer, G., Bonnet, L., … Morris, A. (2018). Dependence on the Pyrimidine Biosynthetic Enzyme DHODH Is a Synthetic Lethal Vulnerability in Mutant KRAS-Driven Cancers. *Cell Chemical Biology*, *25*(6), 705-717.e11. https://doi.org/10.1016/J.CHEMBIOL.2018.03.005

Krawczyk, C. M., Holowka, T., Sun, J., Blagih, J., Amiel, E., DeBerardinis, R. J., … Pearce, E. J. (2010). Toll-like receptor-induced changes in glycolytic metabolism regulate dendritic cell activation. *Blood*, *115*(23), 4742–4749. https://doi.org/10.1182/BLOOD-2009-10-249540

Krishnan, K. J., & Birch-Machin, M. A. (2006). The incidence of both tandem duplications

and the common deletion in mtDNA from three distinct categories of sun-exposed human skin and in prolonged culture of fibroblasts. *The Journal of Investigative Dermatology*, *126*(2), 408–415. https://doi.org/10.1038/SJ.JID.5700099

Krishnan, K. J., Harbottle, A., & Birch-Machin, M. A. (2004). The use of a 3895 bp mitochondrial DNA deletion as a marker for sunlight exposure in human skin. *The Journal of Investigative Dermatology*, *123*(6), 1020–1024. https://doi.org/10.1111/J.0022-202X.2004.23457.X

Küsters-Vandevelde, H. V. N., Leeuwen, A. Van, Verdijk, M. A. J., De Koning, M. N. C., Quint, W. G. V., Melchers, W. J. G., … Blokx, W. A. M. (2010). CDKN2A but not TP53 mutations nor HPV presence predict poor outcome in metastatic squamous cell carcinoma of the skin. *International Journal of Cancer*, *126*(9), 2123–2132. https://doi.org/10.1002/IJC.24871

Lanz, J., Bouwes Bavinck, J. N., Westhuis, M., Quint, K. D., Harwood, C. A., Nasir, S., … Hofbauer, G. F. L. (2019). Aggressive Squamous Cell Carcinoma in Organ Transplant Recipients. *JAMA Dermatology*, *155*(1), 66–71. https://doi.org/10.1001/JAMADERMATOL.2018.4406

Li, L., Ng, S. R., Colón, C. I., Drapkin, B. J., Hsu, P. P., Li, Z., … Jacks, T. (2019). Identification of DHODH as a therapeutic target in small cell lung cancer. *Science Translational Medicine*, *11*(517). https://doi.org/10.1126/scitranslmed.aaw7852

Li, Y. Y., Hanna, G. J., Laga, A. C., Haddad, R. I., Lorch, J. H., & Hammerman, P. S. (2015). Genomic analysis of metastatic cutaneous squamous cell carcinoma. *Clinical Cancer Research*. https://doi.org/10.1158/1078-0432.CCR-14-1773

Likhacheva, A., Awan, M., Barker, C. A., Bhatnagar, A., Bradfield, L., Brady, M. S., … Devlin, P. M. (2020). Definitive and Postoperative Radiation Therapy for Basal and Squamous Cell Cancers of the Skin: Executive Summary of an American Society for Radiation Oncology Clinical Practice Guideline. *Practical Radiation Oncology*, *10*(1), 8–20. https://doi.org/10.1016/J.PRRO.2019.10.014

Lindelöf, B., Sigurgeirsson, B., Gäbel, H., & Stern, R. S. (2000). Incidence of skin cancer in 5356 patients following organ transplantation. *British Journal of Dermatology*, *143*(3), 513–519. https://doi.org/10.1111/J.1365-2133.2000.03703.X

Lobl, M. B., Clarey, D. D., Higgins, S., Sutton, A., & Wysong, A. (2022). Sequencing of Cutaneous Squamous Cell Carcinoma Primary Tumors and Patient-Matched Metastases Reveals ALK as a Potential Driver in Metastases and Low Mutational Concordance in Immunocompromised Patients. *JID Innovations : Skin Science from Molecules to Population Health*, *2*(4), 100122. https://doi.org/10.1016/J.XJIDI.2022.100122

Lomas, A., Leonardi-Bee, J., & Bath-Hextall, F. (2012). A systematic review of worldwide incidence of nonmelanoma skin cancer. *The British Journal of Dermatology*, *166*(5), 1069–1080. https://doi.org/10.1111/J.1365-2133.2012.10830.X

Lui, V. W. Y., Peyser, N. D., Ng, P. K. S., Hritz, J., Zeng, Y., Lu, Y., … Grandis, J. R. (2014). Frequent mutation of receptor protein tyrosine phosphatases provides a mechanism for STAT3 hyperactivation in head and neck cancer. *Proceedings of the National Academy of Sciences of the United States of America*, *111*(3), 1114–1119. https://doi.org/10.1073/PNAS.1319551111

Mantovani, A., Allavena, P., Sica, A., & Balkwill, F. (2008). Cancer-related inflammation. *Nature*, *454*(7203), 436–444. https://doi.org/10.1038/NATURE07205

Mantovani, A., Marchesi, F., Malesci, A., Laghi, L., & Allavena, P. (2017). Tumour-associated macrophages as treatment targets in oncology. *Nature Reviews. Clinical Oncology*, *14*(7), 399–416. https://doi.org/10.1038/NRCLINONC.2016.217

Marks, R., Rennie, G., & Selwood, T. S. (1988). MALIGNANT TRANSFORMATION OF SOLAR KERATOSES TO SQUAMOUS CELL CARCINOMA. *The Lancet*, *331*(8589),

795–797. https://doi.org/10.1016/S0140-6736(88)91658-3
Martincorena, I., & Campbell, P. J. (2015, September 25). Somatic mutation in cancer and normal cells. *Science*. American Association for the Advancement of Science. https://doi.org/10.1126/science.aab4082
Martínez-Reyes, I., Cardona, L. R., Kong, H., Vasan, K., McElroy, G. S., Werner, M., … Chandel, N. S. (2020). Mitochondrial ubiquinol oxidation is necessary for tumour growth. *Nature*, *585*(7824), 288–292. https://doi.org/10.1038/S41586-020-2475-6
Maubec, E., Petrow, P., Scheer-Senyarich, I., Duvillard, P., Lacroix, L., Gelly, J., … Avril, M. F. (2011). Phase II study of cetuximab as first-line single-drug therapy in patients with unresectable squamous cell carcinoma of the skin. *Journal of Clinical Oncology : Official Journal of the American Society of Clinical Oncology*, *29*(25), 3419–3426. https://doi.org/10.1200/JCO.2010.34.1735
Michalek, R. D., Gerriets, V. A., Jacobs, S. R., Macintyre, A. N., MacIver, N. J., Mason, E. F., … Rathmell, J. C. (2011). Cutting edge: distinct glycolytic and lipid oxidative metabolic programs are essential for effector and regulatory CD4+ T cell subsets. *Journal of Immunology (Baltimore, Md. : 1950)*, *186*(6), 3299–3303. https://doi.org/10.4049/JIMMUNOL.1003613
Migden, M. R., Rischin, D., Schmults, C. D., Guminski, A., Hauschild, A., Lewis, K. D., … Fury, M. G. (2018). PD-1 blockade with cemiplimab in advanced cutaneous squamous-cell carcinoma. *New England Journal of Medicine*, *379*(4), 341–351. https://doi.org/10.1056/NEJMoa1805131
Moreno-Sánchez, R., Rodríguez-Enríquez, S., Marín-Hernández, A., & Saavedra, E. (2007). Energy metabolism in tumor cells. *The FEBS Journal*, *274*(6), 1393–1418. https://doi.org/10.1111/J.1742-4658.2007.05686.X
Morris, K. L., Luke, M. C., & Perna, F. M. (2018). Prevalence of Skin Cancer Examination Among Users of Indoor Tanning Beds. *JAMA Dermatology*, *154*(7), 840–842. https://doi.org/10.1001/JAMADERMATOL.2018.1118
Mota, J. M., Leite, C. A., Souza, L. E., Melo, P. H., Nascimento, D. C., De-Deus-Wagatsuma, V. M., … Rego, E. M. (2016). Post-Sepsis State Induces Tumor-Associated Macrophage Accumulation through CXCR4/CXCL12 and Favors Tumor Progression in Mice. *Cancer Immunology Research*, *4*(4), 312–322. https://doi.org/10.1158/2326-6066.CIR-15-0170
Mourouzis, C., Boynton, A., Grant, J., Umar, T., Wilson, A., Macpheson, D., & Pratt, C. (2009). Cutaneous head and neck SCCs and risk of nodal metastasis - UK experience. *Journal of Cranio-Maxillo-Facial Surgery : Official Publication of the European Association for Cranio-Maxillo-Facial Surgery*, *37*(8), 443–447. https://doi.org/10.1016/J.JCMS.2009.07.007
Muzic, J. G., Schmitt, A. R., Wright, A. C., Alniemi, D. T., Zubair, A. S., Olazagasti Lourido, J. M., … Baum, C. L. (2017). Incidence and Trends of Basal Cell Carcinoma and Cutaneous Squamous Cell Carcinoma: A Population-Based Study in Olmsted County, Minnesota, 2000 to 2010. *Mayo Clinic Proceedings*, *92*(6), 890–898. https://doi.org/10.1016/j.mayocp.2017.02.015
Nakamura, K., Okuyama, R., Saida, T., & Uhara, H. (2013). Platinum and anthracycline therapy for advanced cutaneous squamous cell carcinoma. *International Journal of Clinical Oncology*, *18*(3), 506–509. https://doi.org/10.1007/S10147-012-0411-Y
Nelson, T. G., & Ashton, R. E. (2017). Low incidence of metastasis and recurrence from cutaneous squamous cell carcinoma found in a UK population: Do we need to adjust our thinking on this rare but potentially fatal event? *Journal of Surgical Oncology*, *116*(6), 783–788. https://doi.org/10.1002/JSO.24707
O'Neill, L. A. J., Kishton, R. J., & Rathmell, J. (2016). A guide to immunometabolism for

immunologists. *Nature Reviews Immunology 2016 16:9*, *16*(9), 553–565. https://doi.org/10.1038/nri.2016.70

O'Sullivan, D. (2019). The metabolic spectrum of memory T cells. *Immunology and Cell Biology*, *97*(7), 636–646. https://doi.org/10.1111/IMCB.12274

Olsen, E. A., Lisa Abernethy, M., Kulp-Shorten, C., Callen, J. P., Glazer, S. D., Huntley, A., … Wolf, J. E. (1991). A double-blind, vehicle-controlled study evaluating masoprocol cream in the treatment of actinic keratoses on the head and neck. *Journal of the American Academy of Dermatology*, *24*(5 Pt 1), 738–743. https://doi.org/10.1016/0190-9622(91)70113-G

Omland, S. H., Ahlström, M. G., Gerstoft, J., Pedersen, G., Mohey, R., Pedersen, C., … Omland, L. H. (2018). Risk of skin cancer in patients with HIV: A Danish nationwide cohort study. *Journal of the American Academy of Dermatology*, *79*(4), 689–695. https://doi.org/10.1016/J.JAAD.2018.03.024

Omland, S. H., Gniadecki, R., Hædersdal, M., Helweg-Larsen, J., & Omland, L. H. (2016). Skin Cancer Risk in Hematopoietic Stem-Cell Transplant Recipients Compared With Background Population and Renal Transplant Recipients: A Population-Based Cohort Study. *JAMA Dermatology*, *152*(2), 177–183. https://doi.org/10.1001/jamadermatol.2015.3902

Orth, M., & Schapira, A. H. V. (2001). Mitochondria and degenerative disorders. *American Journal of Medical Genetics*, *106*(1), 27–36. https://doi.org/10.1002/AJMG.1425

Pandeya, N., Olsen, C. M., & Whiteman, D. C. (2017). The incidence and multiplicity rates of keratinocyte cancers in Australia. *Medical Journal of Australia*, *207*(8), 339–343. https://doi.org/10.5694/mja17.00284

Panieri, E., & Santoro, M. M. (2016). ROS homeostasis and metabolism: a dangerous liason in cancer cells. *Cell Death & Disease*, *7*(6). https://doi.org/10.1038/CDDIS.2016.105

Pavlova, N. N., & Thompson, C. B. (2016). The Emerging Hallmarks of Cancer Metabolism. *Cell Metabolism*, *23*(1), 27–47. https://doi.org/10.1016/J.CMET.2015.12.006

Pe, K. C. S., Saetung, R., Yodsurang, V., Chaotham, C., Suppipat, K., Chanvorachote, P., & Tawinwung, S. (2022). Triple-negative breast cancer influences a mixed M1/M2 macrophage phenotype associated with tumor aggressiveness. *PloS One*, *17*(8), e0273044. https://doi.org/10.1371/JOURNAL.PONE.0273044

Pedersen, S. A., Gaist, D., Schmidt, S. A. J., Hölmich, L. R., Friis, S., & Pottegård, A. (2018). Hydrochlorothiazide use and risk of nonmelanoma skin cancer: A nationwide case-control study from Denmark. *Journal of the American Academy of Dermatology*, *78*(4), 673-681.e9. https://doi.org/10.1016/J.JAAD.2017.11.042

Peppicelli, S., Bianchini, F., & Calorini, L. (2014). Extracellular acidity, a "reappreciated" trait of tumor environment driving malignancy: perspectives in diagnosis and therapy. *Cancer Metastasis Reviews*, *33*(2–3), 823–832. https://doi.org/10.1007/S10555-014-9506-4

Petros, J. A., Baumann, A. K., Ruiz-Pesini, E., Amin, M. B., Sun, C. Q., Hall, J., … Wallace, D. C. (2005). mtDNA mutations increase tumorigenicity in prostate cancer. *Proceedings of the National Academy of Sciences of the United States of America*, *102*(3), 719–724. https://doi.org/10.1073/PNAS.0408894102

Pickering, C. R., Zhou, J. H., Lee, J. J., Drummond, J. A., Peng, S. A., Saade, R. E., … Frederick, M. J. (2014). Mutational landscape of aggressive cutaneous squamous cell carcinoma. *Clinical Cancer Research*. https://doi.org/10.1158/1078-0432.CCR-14-1768

Pirie, K., Beral, V., Heath, A. K., Green, J., Reeves, G. K., Peto, R., … Green, A. C. (2018). Heterogeneous relationships of squamous and basal cell carcinomas of the skin with smoking: the UK Million Women Study and meta-analysis of prospective studies. *British Journal of Cancer*, *119*(1), 114–120. https://doi.org/10.1038/S41416-018-0105-Y

Porceddu, S. V., Bressel, M., Poulsen, M. G., Stoneley, A., Veness, M. J., Kenny, L. M., … Rischin, D. (2018). Postoperative Concurrent Chemoradiotherapy Versus Postoperative Radiotherapy in High-Risk Cutaneous Squamous Cell Carcinoma of the Head and Neck: The Randomized Phase III TROG 05.01 Trial. *Journal of Clinical Oncology : Official Journal of the American Society of Clinical Oncology*, *36*(13), 1275–1283. https://doi.org/10.1200/JCO.2017.77.0941

Porporato, P. E., Payen, V. L., Pérez-Escuredo, J., De Saedeleer, C. J., Danhier, P., Copetti, T., … Sonveaux, P. (2014). A mitochondrial switch promotes tumor metastasis. *Cell Reports*, *8*(3), 754–766. https://doi.org/10.1016/J.CELREP.2014.06.043

Pospisilova, J., Vit, O., Lorkova, L., Klanova, M., Zivny, J., Klener, P., & Petrak, J. (2013). Resistance to TRAIL in mantle cell lymphoma cells is associated with the decreased expression of purine metabolism enzymes. *International Journal of Molecular Medicine*, *31*(5), 1273–1279. https://doi.org/10.3892/IJMM.2013.1302

Powers, J. M., Murphy, G., Ralph, N., O'Gorman, S. M., & Murphy, J. E. J. (2016). Mitochondrial DNA deletion percentage in sun exposed and non sun exposed skin. *Journal of Photochemistry and Photobiology. B, Biology*, *165*, 277–282. https://doi.org/10.1016/J.JPHOTOBIOL.2016.10.030

Rastogi, R. P., Richa, Kumar, A., Tyagi, M. B., & Sinha, R. P. (2010). Molecular mechanisms of ultraviolet radiation-induced DNA damage and repair. *Journal of Nucleic Acids*, *2010*. https://doi.org/10.4061/2010/592980

Rawls, J., Knecht, W., Diekert, K., Lill, R., & Löffler, M. (2000). Requirements for the mitochondrial import and localization of dihydroorotate dehydrogenase. *European Journal of Biochemistry*, *267*(7), 2079–2087. https://doi.org/10.1046/J.1432-1327.2000.01213.X

Rezvani, H. R., Kim, A. L., Rossignol, R., Ali, N., Daly, M., Mahfouf, W., … Bickers, D. R. (2011). XPC silencing in normal human keratinocytes triggers metabolic alterations that drive the formation of squamous cell carcinomas. *Journal of Clinical Investigation*. https://doi.org/10.1172/JCI40087

Rich, P. R. (2003). The molecular machinery of Keilin's respiratory chain. *Biochemical Society Transactions*, *31*(Pt 6), 1095–1105. https://doi.org/10.1042/BST0311095

Rischin, D., Khushalani, N. I., Schmults, C. D., Guminski, A., Chang, A. L. S., Lewis, K. D., … Migden, M. R. (2021). Integrated analysis of a phase 2 study of cemiplimab in advanced cutaneous squamous cell carcinoma: extended follow-up of outcomes and quality of life analysis. *Journal for Immunotherapy of Cancer*, *9*(8). https://doi.org/10.1136/JITC-2021-002757

Robsahm, T. E., Helsing, P., & Veierød, M. B. (2015). Cutaneous squamous cell carcinoma in Norway 1963-2011: increasing incidence and stable mortality. *Cancer Medicine*, *4*(3), 472–480. https://doi.org/10.1002/CAM4.404

Rodier, F., Coppé, J. P., Patil, C. K., Hoeijmakers, W. A. M., Muñoz, D. P., Raza, S. R., … Campisi, J. (2009). Persistent DNA damage signalling triggers senescence-associated inflammatory cytokine secretion. *Nature Cell Biology*, *11*(8), 973–979. https://doi.org/10.1038/NCB1909

Röwert-Huber, J., Patel, M. J., Forschner, T., Ulrich, C., Eberle, J., Kerl, H., … Stockfleth, E. (2007). Actinic keratosis is an early in situ squamous cell carcinoma: a proposal for reclassification. *The British Journal of Dermatology*, *156 Suppl 3*(SUPPL. 3), 8–12. https://doi.org/10.1111/J.1365-2133.2007.07860.X

Ruiz, E. S., Karia, P. S., Besaw, R., & Schmults, C. D. (2019). Performance of the American Joint Committee on Cancer Staging Manual, 8th Edition vs the Brigham and Women's Hospital Tumor Classification System for Cutaneous Squamous Cell Carcinoma. *JAMA Dermatology*, *155*(7), 819–825. https://doi.org/10.1001/JAMADERMATOL.2019.0032

Russell, O., & Turnbull, D. (2014). Mitochondrial DNA disease-molecular insights and potential routes to a cure. *Experimental Cell Research*, *325*(1), 38–43. https://doi.org/10.1016/J.YEXCR.2014.03.012

Schmults, C. D., Blitzblau, R., Aasi, S. Z., Alam, M., Andersen, J. S., Baumann, B. C., … Nguyen, M. Q. (2021). NCCN Guidelines® Insights: Squamous Cell Skin Cancer, Version 1.2022. *Journal of the National Comprehensive Cancer Network : JNCCN*, *19*(12), 1382–1394. https://doi.org/10.6004/JNCCN.2021.0059

Schmults, C. D., Karia, P. S., Carter, J. B., Han, J., & Qureshi, A. A. (2013a). Factors predictive of recurrence and death from cutaneous squamous cell carcinoma: a 10-year, single-institution cohort study. *JAMA Dermatology*, *149*(5), 541–547. https://doi.org/10.1001/JAMADERMATOL.2013.2139

Schmults, C. D., Karia, P. S., Carter, J. B., Han, J., & Qureshi, A. A. (2013b). Factors predictive of recurrence and death from cutaneous squamous cell carcinoma: A 10-year, single-institution cohort study. *JAMA Dermatology*, *149*(5), 541–547. https://doi.org/10.1001/jamadermatol.2013.2139

Shao, E. X., Khosrotehrani, K., Campbell, S., Isbel, N., & Green, A. (2022). Pathways from Diagnosis to Death from Keratinocyte Cancer in Kidney Transplant Recipients. *Dermatology (Basel, Switzerland)*. https://doi.org/10.1159/000524120

Singh, A., Compe, E., Le May, N., & Egly, J. M. (2015). TFIIH subunit alterations causing xeroderma pigmentosum and trichothiodystrophy specifically disturb several steps during transcription. *American Journal of Human Genetics*, *96*(2), 194–207. https://doi.org/10.1016/J.AJHG.2014.12.012

Smolková, K., Plecitá-Hlavatá, L., Bellance, N., Benard, G., Rossignol, R., & Ježek, P. (2011). Waves of gene regulation suppress and then restore oxidative phosphorylation in cancer cells. *International Journal of Biochemistry and Cell Biology*. https://doi.org/10.1016/j.biocel.2010.05.003

Sparmann, A., & Bar-Sagi, D. (2004). Ras-induced interleukin-8 expression plays a critical role in tumor growth and angiogenesis. *Cancer Cell*, *6*(5), 447–458. https://doi.org/10.1016/j.ccr.2004.09.028

Speiser, D. E., Ho, P. C., & Verdeil, G. (2016). Regulatory circuits of T cell function in cancer. *Nature Reviews. Immunology*, *16*(10), 599–611. https://doi.org/10.1038/NRI.2016.80

Stratigos, A. J., Garbe, C., Dessinioti, C., Lebbe, C., Bataille, V., Bastholt, L., … Grob, J. J. (2020). European interdisciplinary guideline on invasive squamous cell carcinoma of the skin: Part 2. Treatment. *European Journal of Cancer*, *128*, 83–102. https://doi.org/10.1016/j.ejca.2020.01.008

Su, K. A., Habel, L. A., Achacoso, N. S., Friedman, G. D., & Asgari, M. M. (2018). Photosensitizing antihypertensive drug use and risk of cutaneous squamous cell carcinoma. *The British Journal of Dermatology*, *179*(5), 1088–1094. https://doi.org/10.1111/BJD.16713

Sykes, D. B., Kfoury, Y. S., Mercier, F. E., Wawer, M. J., Law, J. M., Haynes, M. K., … Scadden, D. T. (2016). Inhibition of Dihydroorotate Dehydrogenase Overcomes Differentiation Blockade in Acute Myeloid Leukemia. *Cell*. https://doi.org/10.1016/j.cell.2016.08.057

Tang, H., Fu, S., Zhai, S., Song, Y., Asgari, M. M., & Han, J. (2018). Use of antihypertensive drugs and risk of keratinocyte carcinoma: A meta-analysis of observational studies. *Pharmacoepidemiology and Drug Safety*, *27*(3), 279–288. https://doi.org/10.1002/PDS.4384

Tannahill, G. M., Curtis, A. M., Adamik, J., Palsson-Mcdermott, E. M., McGettrick, A. F., Goel, G., … O'Neill, L. A. J. (2013). Succinate is an inflammatory signal that induces

IL-1β through HIF-1α. *Nature*, *496*(7444), 238–242. https://doi.org/10.1038/NATURE11986

Tokez, S., Wakkee, M., Kan, W., Venables, Z. C., Mooyaart, A. L., Louwman, M., … Hollestein, L. M. (2022). Cumulative incidence and disease-specific survival of metastatic cutaneous squamous cell carcinoma: A nationwide cancer registry study. *Journal of the American Academy of Dermatology*, *86*(2), 331–338. https://doi.org/10.1016/J.JAAD.2021.09.067

Tomlinson, I. P. M., Alam, N. A., Rowan, A. J., Barclay, E., Jaeger, E. E. M., Kelsell, D., … Aaltonen, L. A. (2002). Germline mutations in FH predispose to dominantly inherited uterine fibroids, skin leiomyomata and papillary renal cell cancer. *Nature Genetics*, *30*(4), 406–410. https://doi.org/10.1038/NG849

Tornaletti, S., & Pfeifer, G. P. (1996). UV damage and repair mechanisms in mammalian cells. *BioEssays : News and Reviews in Molecular, Cellular and Developmental Biology*, *18*(3), 221–228. https://doi.org/10.1002/BIES.950180309

Van Kuilenburg, A. B. P., Van Lenthe, H., Löffler, M., & Van Gennip, A. H. (2004). Analysis of pyrimidine synthesis "de novo" intermediates in urine and dried urine filter-paper strips with HPLC-electrospray tandem mass spectrometry. *Clinical Chemistry*, *50*(11), 2117–2124. https://doi.org/10.1373/CLINCHEM.2004.038869

Vasan, K., Werner, M., & Chandel, N. S. (2020). Mitochondrial Metabolism as a Target for Cancer Therapy. *Cell Metabolism*, *32*(3), 341–352. https://doi.org/10.1016/J.CMET.2020.06.019

Venables, Z. C., Autier, P., Nijsten, T., Wong, K. F., Langan, S. M., Rous, B., … Leigh, I. M. (2019). Nationwide Incidence of Metastatic Cutaneous Squamous Cell Carcinoma in England. *JAMA Dermatology*, *155*(3), 298–306. https://doi.org/10.1001/jamadermatol.2018.4219

Vercellino, I., & Sazanov, L. A. (2022). The assembly, regulation and function of the mitochondrial respiratory chain. *Nature Reviews. Molecular Cell Biology*, *23*(2), 141–161. https://doi.org/10.1038/S41580-021-00415-0

Vyas, S., Zaganjor, E., & Haigis, M. C. (2016). Mitochondria and Cancer. *Cell*, *166*(3), 555–566. https://doi.org/10.1016/J.CELL.2016.07.002

Wang, C., Lin, Y., Zhu, H., Zhou, Y., Mao, F., Huang, X., … Li, C. (2022). The Prognostic and Clinical Value of Tumor-Associated Macrophages in Patients With Breast Cancer: A Systematic Review and Meta-Analysis. *Frontiers in Oncology*, *12*. https://doi.org/10.3389/FONC.2022.905846

Wang, W., Cui, J., Ma, H., Lu, W., & Huang, J. (2021). Targeting Pyrimidine Metabolism in the Era of Precision Cancer Medicine. *Frontiers in Oncology*, *11*. https://doi.org/10.3389/FONC.2021.684961

Wang, X., Yang, K., Wu, Q., Kim, L. J. Y., Morton, A. R., Gimple, R. C., … Rich, J. N. (2019). Targeting pyrimidine synthesis accentuates molecular therapy response in glioblastoma stem cells. *Science Translational Medicine*, *11*(504). https://doi.org/10.1126/scitranslmed.aau4972

Wang, Z. C., Wang, X. M., Jiao, B. H., Jin, Y. X., Miao, M. Y., Zhu, K. J., & Ni, Q. G. (2003). Detection of mitochondrial DNA deletion by a modified PCR method in a 60Co radiation-exposed patient. *IUBMB Life*, *55*(3), 133–137. https://doi.org/10.1080/1521654031000110181

Warburg, O. (1956). On the origin of cancer cells. *Science (New York, N.Y.)*, *123*(3191), 309–314. https://doi.org/10.1126/SCIENCE.123.3191.309

Ward, P. S., & Thompson, C. B. (2012a). Metabolic reprogramming: a cancer hallmark even warburg did not anticipate. *Cancer Cell*, *21*(3), 297–308. https://doi.org/10.1016/J.CCR.2012.02.014

Ward, P. S., & Thompson, C. B. (2012b). Metabolic Reprogramming: A Cancer Hallmark Even Warburg Did Not Anticipate. *Cancer Cell*. https://doi.org/10.1016/j.ccr.2012.02.014

Watmough, N. J., & Frerman, F. E. (2010). The electron transfer flavoprotein: ubiquinone oxidoreductases. *Biochimica et Biophysica Acta*, *1797*(12), 1910–1916. https://doi.org/10.1016/J.BBABIO.2010.10.007

Weinberg, S. E., & Chandel, N. S. (2015). Targeting mitochondria metabolism for cancer therapy. *Nature Chemical Biology*, *11*(1), 9–15. https://doi.org/10.1038/NCHEMBIO.1712

Werner, R. N., Sammain, A., Erdmann, R., Hartmann, V., Stockfleth, E., & Nast, A. (2013). The natural history of actinic keratosis: a systematic review. *The British Journal of Dermatology*, *169*(3), 502–518. https://doi.org/10.1111/BJD.12420

Whitaker-Menezes, D., Martinez-Outschoorn, U. E., Flomenberg, N., Birbe, R. C., Witkiewicz, A. K., Howell, A., … Sotgia, F. (2011). Hyperactivation of oxidative mitochondrial metabolism in epithelial cancer cells in situ: visualizing the therapeutic effects of metformin in tumor tissue. *Cell Cycle (Georgetown, Tex.)*, *10*(23), 4047–4064. https://doi.org/10.4161/CC.10.23.18151

White, R. M., Cech, J., Ratanasirintrawoot, S., Lin, C. Y., Rahl, P. B., Burke, C. J., … Zon, L. I. (2011). DHODH modulates transcriptional elongation in the neural crest and melanoma. *Nature*, *471*(7339), 518–522. https://doi.org/10.1038/nature09882

Wise, D. R., Deberardinis, R. J., Mancuso, A., Sayed, N., Zhang, X. Y., Pfeiffer, H. K., … Thompson, C. B. (2008). Myc regulates a transcriptional program that stimulates mitochondrial glutaminolysis and leads to glutamine addiction. *Proceedings of the National Academy of Sciences of the United States of America*, *105*(48), 18782–18787. https://doi.org/10.1073/PNAS.0810199105

Wu, P. A., Stern, R. S., Huang, V., Liu, K. X., Chen, C. (Amy), Tzachanis, D., … Ho, V. T. (2019). Reduced-Intensity Conditioning Regimens, Prior Chronic Lymphocytic Leukemia, and Graft-Versus-Host Disease Are Associated with Higher Rates of Skin Cancer after Allogeneic Hematopoietic Stem Cell Transplantation. *The Journal of Investigative Dermatology*, *139*(3), 591–599. https://doi.org/10.1016/J.JID.2018.08.025

Xiao, Y., Wang, Z., Zhao, M., Deng, Y., Yang, M., Su, G., … Fan, R. (2022). Single-Cell Transcriptomics Revealed Subtype-Specific Tumor Immune Microenvironments in Human Glioblastomas. *Frontiers in Immunology*, *13*. https://doi.org/10.3389/FIMMU.2022.914236

Xiao, Z., Dai, Z., & Locasale, J. W. (2019). Metabolic landscape of the tumor microenvironment at single cell resolution. *Nature Communications*, *10*(1). https://doi.org/10.1038/S41467-019-11738-0

Xu, M. J., Lazar, A. A., Garsa, A. A., Arron, S. T., Ryan, W. R., El-Sayed, I. H., … Yom, S. S. (2018). Major prognostic factors for recurrence and survival independent of the American Joint Committee on Cancer eighth edition staging system in patients with cutaneous squamous cell carcinoma treated with multimodality therapy. *Head & Neck*, *40*(7), 1406–1414. https://doi.org/10.1002/HED.25114

Yeung, S. J., Pan, J., & Lee, M. H. (2008). Roles of p53, MYC and HIF-1 in regulating glycolysis - the seventh hallmark of cancer. *Cellular and Molecular Life Sciences : CMLS*, *65*(24), 3981–3999. https://doi.org/10.1007/S00018-008-8224-X

Zhang, Z., Gao, Z., Rajthala, S., Sapkota, D., Dongre, H., Parajuli, H., … Liang, X. (2020). Metabolic reprogramming of normal oral fibroblasts correlated with increased glycolytic metabolism of oral squamous cell carcinoma and precedes their activation into carcinoma associated fibroblasts. *Cellular and Molecular Life Sciences : CMLS*, *77*(6), 1115–1133. https://doi.org/10.1007/S00018-019-03209-Y

Chapter II

Energy Metabolism

II.1 Cellular Energy Metabolism

Our body obtain/acquire energy through food consumption and a series of biochemical reactions is required to make the nutrients accessible to the cells. Indeed, metabolism is a set of life-sustaining chemical reactions which convert food in energy and also in macromolecules (the building blocks) to sustain cell proliferation; it is also responsible of the removal of toxic metabolic by products. Biological molecules (nutrients) first are degraded and then re-synthesized during these processes (Figure 5).

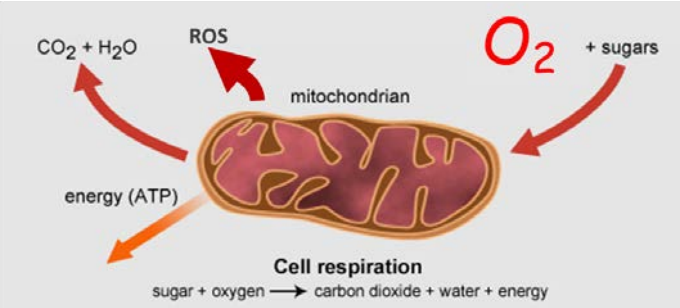

Figure 5. Energy metabolism simply means consumption of sugar and oxygen for producing energy as the main product and reactive oxygen species ROS) and CO2 as by-product.

Metabolism is divided into two groups of biochemical reactions: catabolism and anabolism. Catabolism consists of all enzymatic reactions which break down macromolecules and produce energy (Figure 6). Indeed, the catabolism of 1 gram of carbohydrates, proteins and lipids releases 4.1, 5.3 and 9.3 kcal, respectively. Anabolism is composed of processes in which cells consume energy in order to produce macromolecules including carbohydrates, proteins, lipids and nucleic acids.

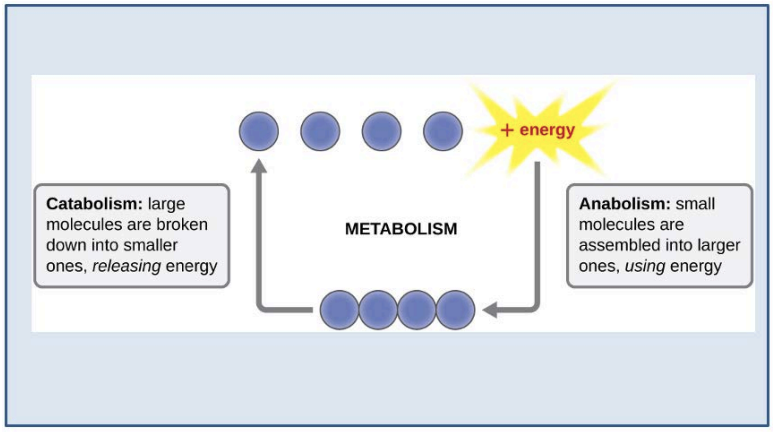

Figure 6. Catabolism and anabolism principles. Anabolism creates molecules the body needs for functionality and it uses energy in the process. Catabolism, on the other hand, breaks down complex molecules and releases energy which is available for the body to use.

Accumulating evidence indicates that malignant transformation is associated with changes that affect several branches of metabolism to support, on the one hand, the energy demands of cancer cells and, on the other, the anaplerotic reactions that are ultimately required for the generation of sufficient building blocks (i.e., nucleic acids, proteins, and membranes) (Galluzzi, Kepp, Heiden, & Kroemer, 2013; Hanahan & Weinberg, 2011).

Compartmentalization of Metabolic Pathways

A metabolic pathway is composed of a series of chemical reactions catalyzed by different enzymes. Different metabolic pathways in the cells have common features and undergo general principles of regulation. In eukaryotic cells, metabolic pathways are compartmentalized. This compartmentalization, which plays an important role in sustenance of eukaryotic cell, is important for following reasons: 1) to separate quite heterogeneous cellular environments and to optimize the course of chemical reactions by concentrating the required components to a confined space within the cell, and 2) to protect the cell itself from lytic enzymes, that are confined in lysosomes to prevent autodegradation. Metabolic roles of different cell organelles are described in Table 4.

Table 4. Compartmentalization of Metabolic Pathways.

Compartment	Metabolic pathways
Cell membrane	Transport
Nucleus	DNA replication, Transcription
Ribosomes	Protein synthesis
Rough Endoplasmic Reticulum	Protein synthesis, Protein processing, Glycosylation, Phospholipid synthesis
Smooth Endoplasmic Reticulum	Synthesis of fatty acids, Lipids, Phospholipids, Steroids
Golgi	Protein synthesis, Protein processing, Polysaccharide synthesis
Cytosol	Glycolysis, Gluconeogenesis, Pentose phosphate pathway, Fatty acid synthesis, Amino acid metabolism, Tetrapyrrol and steroid synthesis, Glycogen synthesis
Peroxysomes	Oxidative reactions, β-oxidation,
Mitochondria	TCA cycle, Oxidative phosphorylation, β-oxidation, Initiation of gluconeogenesis, Amino acid metabolism, Tetrapyrrol and steroid synthesis, Urea cycle
Lysosome	Degradation of macromolecules, Storage of nutrients

In order to produce energy, eukaryotic cells use three major catabolic pathways including glycolysis (**in cytosol**), Krebs cycle/ TCA (**in mitochondria**) and lipid ß-oxidation (Figure 7).

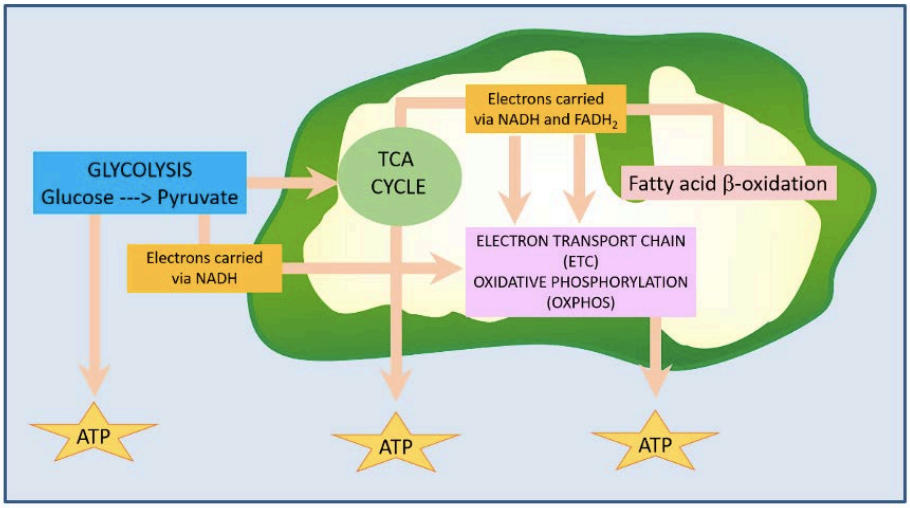

Figure 7. Different metabolic pathways to product ATP. ATP can be produced directly by glycolysis or indirectly through transport electron from the energy precursors from the glycolysis, TCA cycle and fatty acid ß-oxidation into electron transport chain (ETC) and producing energy via mechanism called oxidative phosphorylation.

The balance between these pathways is crucial for eukaryotic cell life, while, on the contrary, their imbalance has been reported in a wide range of cancers (Galluzzi et al., 2013).
Thereafter, many factors including nutrients, environmental and oxidative stress, calorie restriction and toxic agents could influence compartmentalization and energy metabolism.

II.1.a Glycolysis

Glycolysis relies on two steps known as energy-investment and energy-pay off respectively. Meanwhile, glucose is considered as the main substrate for producing energy in this process. Subsequent to the entry of glucose into the cell via specific glucose transporters (GLUT), glucose is converted into glucose-6-phosphate (G6P) by hexokinase through a phosphorylation reaction (Figure 8). Depending on cell demands, two different metabolic fates could occur to G6P either by passing on glycolysis or entering pentose phosphate pathway which produces essential monosaccharides for the synthesis of nucleotides and NADPH that provided reducing equivalents and protects against ROS toxicity.
In glycolysis, glucose-6-phosphate (G6P) is converted to fructose-6-phosphate (F6P) by an isomerase (GPI) activity. Then, fructose-1,6 bisphosphate is produced via phosphorylation of

F6P by phosphofructokinase (PFK). Thereafter, fructose-1,6-bisphosphate would be converted into two three-carbon units called glyceraldehyde-3-phosphate (G3P) by lyase activity of fructose biphosphate aldolase. Subsequently, G3P is oxidized to 1,3-bisphosphoglycerate (1,3-BPG) by activity of an oxidoreductase enzyme. This reaction reduces two molecules of NAD^+ using hydrogen in order to produce one NADH + H^+ for each G3P. In the next step, through a transferase enzyme, phosphate group of 1,3PG is transferred to ADP to form ATP and 3-phosphoglycerate (3-PG). Then a mutase enzyme converts 3-PG to 2-PG and a lyase enzyme forms a phosphoenolpyruvate (PEP) from 2-PG afterwards. In the final step, PEP becomes dephosphorylated by the activity of pyruvate kinase in order to produce a molecule of pyruvate. This happens at the presence of one ADP which gives rise to the formation of an ATP molecule (Figure 8).

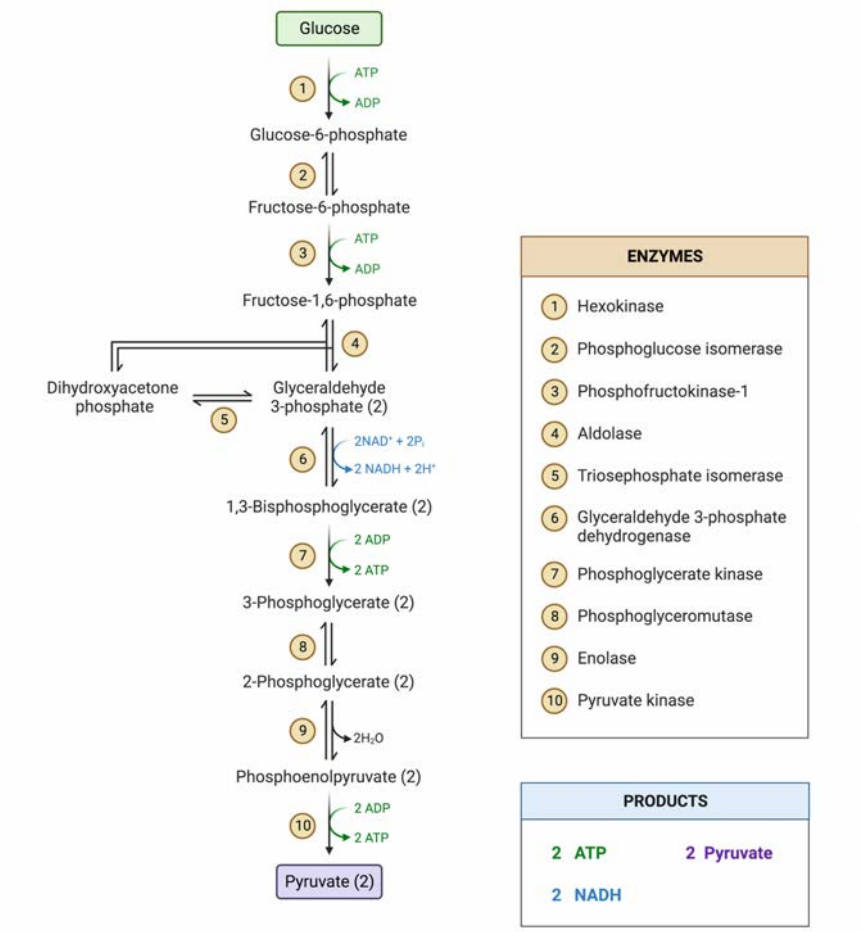

Figure 8. Glycolysis Pathway. Created with Biorender.

All these reactions occur in cell cytoplasm and finally produce two molecules of ATP as well as 2 NADH from NAD^+ cofactor. In the presence of oxygen, NAD^+ is renewed during the transfer of electrons to the respiratory chain while in hypoxia, NAD^+ can be quickly regenerated by reduction of pyruvate to lactate. This way of ATP production which occurs in the absence

of oxygen is called anaerobic glycolysis. Pyruvate is considered as a key intersection in cell metabolic pathways due to the great potential in producing necessary cell macromolecules including carbohydrates (gluconeogenesis), fatty acids, amino acids and ethanol. In normoxia, pyruvate is transported into mitochondria through mitochondrial pyruvate carrier and monocarboxylate transporters (MCTs). Thereafter, pyruvate undergoes oxidative decarboxylation by an enzymatic complex called pyruvate dehydrogenase (PDH) in order to form acetyl CoA. Acetyl-CoA then enters into citric acid cycle, also called TCA or Krebs cycle, and generates NADH and $FADH_2$ which will be ultimately give up their hydrogen to the respiratory chain and renewed oxidized equivalents (NAD^+ and FAD).

Another way of producing acetyl-CoA is through β-oxidation of fatty acids. Acyl-CoA is synthesized from fatty acids by acyl-CoA synthetase at the outer mitochondrial membrane. A shuttle system allows the entry of acyl-CoA to the mitochondria and the formation of acetyl-CoA. Decarboxylation of acetyl-CoA in Krebs cycle is done through eight successive reactions which produce 3 NADH, 1 $FADH_2$, 1 GTP (which is converted into ATP) and two molecules of CO_2. Final oxidation of NADH and $FADH_2$ in oxidative phosphorylation chain (OXPHOS) results in the formation of 3 and 2 molecules of ATP, respectively.

II.1.b Krebs Cycle, Electron Transport and Oxidative Phosphorylation

Beside glycolysis and its role in production of a part of energy from glucose or glucagon, tremendous amount of energy is produced by mitochondria. Due to the critical role of this dynamic organelle in energy production, it is the so-called powerhouse of the cell. Mitochondria are involved in several cellular processes including signaling, cell differentiation, cell death, cell cycle and cell growth as well as synthesis of amino acids, lipids, iron sulfur clusters and also ion homeostasis and thermogenesis.

Oxygen consumption by mitochondria accounts for 90% of cellular oxygen consumption, of which 80% is involved in ATP synthesis (Rich, 2003).

A growing body of evidence shows that mitochondrial morphology plays an important role in its function. In fact, under normal conditions, mitochondria appear as a single large interconnected membrane-bound tubular network within a cell. Alterations or defects in mitochondrial ultrastructure could affect its morphology and functionality afterwards.

Frequencies of fusion and fission events could control the length, size, shape and number of mitochondria and are fundamental to maintain a physiologically healthy pool of mitochondria. Fusion divides the organelle while fission links two separate mitochondria. Following an unbalanced fusion/ fission event, the length, size, shape and number of mitochondria would change. It has been reported that dysregulated fission and fusion also promote tumor progression (Boulton & Caino, 2022).

i. Overview of Krebs Cycle

Hans Krebs, pioneer German biochemist identified two major biochemical pathways of the cell, urea cycle and the tricarboxylic acid cycle (TCA). TCA is also called Krebs cycle in honor of the scientist.

The majority of the acetyl-CoA that enters the Krebs cycle comes from pyruvate. Oxidative decarboxylation of pyruvate converts it into acetyl-CoA by the activity of pyruvate dehydrogenase (PDH). This enzyme can be inhibited following its phosphorylation by pyruvate dehydrogenase kinase (PDK). Dichloroacetate (DCA) is used as the inhibitor of pyruvate dehydrogenase kinase activity. This inhibition induces more PDH activity leading to an increase in mitochondrial metabolism.

The first specific reaction of the cycle is catalyzed by citrate synthase (CS) combining acetyl-CoA with oxaloacetate to produce citrate (Figure 9). This reaction is accompanied by reduction of NAD^+ and production of a molecule of CO_2. This enzyme is highly regulated by NADH. Citrate is also exported out of the mitochondria via its specific transporter (SLC25A1) for the synthesis of fatty acids and amino acids in the cytosol.

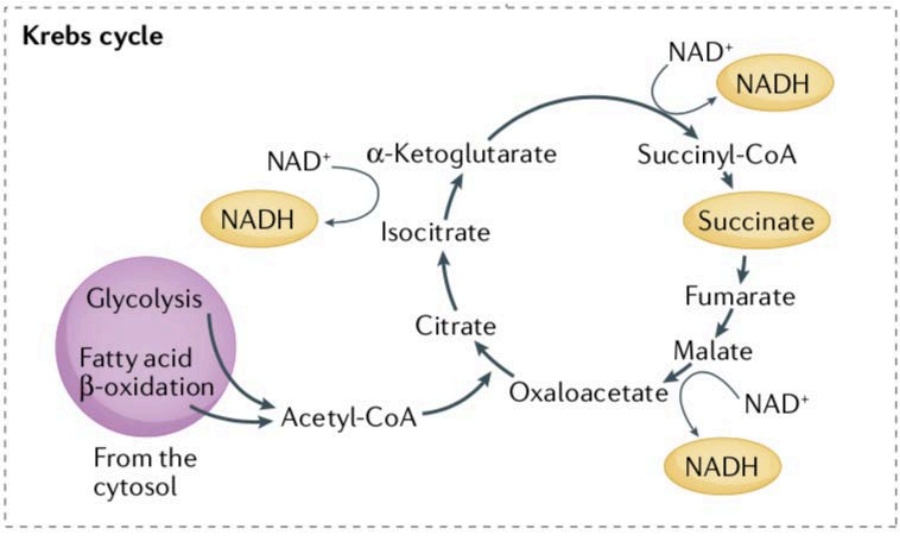

Figure 9. Krebs cycle (Vercellino & Sazanov, 2022)

In the Krebs cycle, aconitase catalyzes the synthesis of isocitrate from citrate. Isocitrate then undergoes oxidative decarboxylation catalyzed by isocitrate dehydrogenase allowing the formation of α-ketoglutarate. At the same time, NADH is synthesized by reduction of NAD^+ and is transferred to the electron transport chain. Thus, isocitrate dehydrogenase (IDH) is the first enzyme which connects the cycle to the oxidative respiratory chain (OXPHOS).

There are three isoforms of isocitrate dehydrogenase (IDH). IDH1 is the cytosolic isoform and the two others, IDH2 and IDH3 are mitochondrial isoforms of the enzyme. While IDH2 uses NADPH for functioning, IDH3 operates with NADH.

Alpha-ketoglutarate plays an important role in reactions catalyzed by amino-transferases. Indeed, α -ketoglutarate may also be synthesized from glutamine which then converts to glutamate. Deamination of glutamate forms α-ketoglutarate. Alpha-ketoglutarate dehydrogenase converts α-ketoglutarate to succinyl-CoA with reduction of NAD^+ to NADH. Then, succinyl- CoA synthetase by transforming succinyl-CoA to succinate allows the production of a molecule of GTP. Succinate dehydrogenase would oxidize succinate to fumarate thereafter by synthesizing a molecule of $FADH_2$. This enzyme provides the necessary $FADH_2$ for the respiratory chain at the level of complex II. Succinate dehydrogenase, or complex II, is bound to the inner membrane of the mitochondria and is the only enzyme of TCA cycle involved in respiratory chain. Thereafter, fumarate hydratase (FH) enables the synthesis of malate from fumarate and the last step of the TCA cycle is the conversion of malate to oxaloacetate which is catalyzed by malate dehydrogenase. This reaction is coupled with NAD+ reduction (Figure 9 and 10).

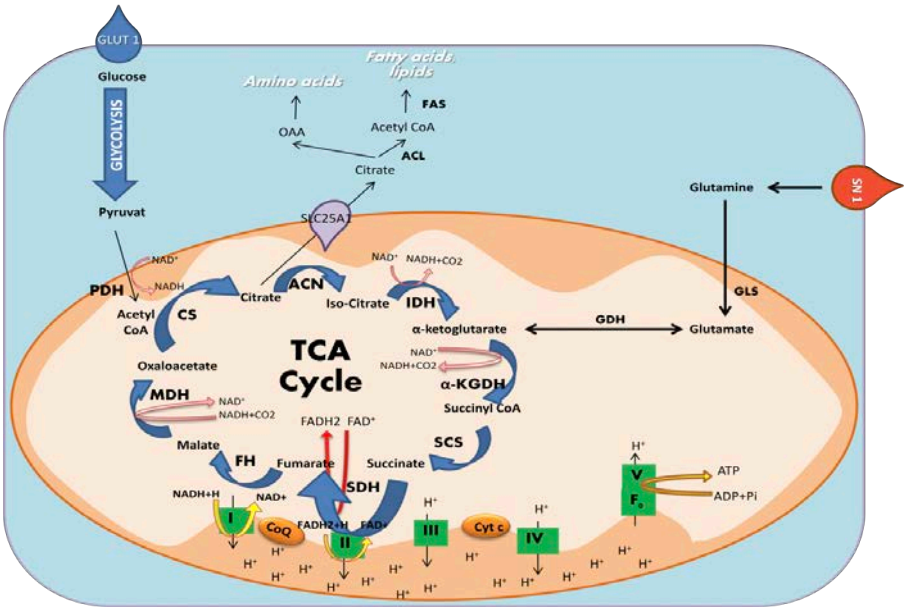

Figure 10. Mitochondria and oxidative phosphorylation chain (from Hosseini et al, 2018).

Mutations in SDH gene have been found in paragangliomas of the head and neck (Baysal et al., 2000). Moreover, mutations of FH have also been identified in the uterus, breast and kidney cancers (Tomlinson et al., 2002). These mutations lead to the stabilization of the transcriptional factor HIF-1α that induces the subsequent up-regulation of its downstream target genes, involved in hypoxia response, vascularization and glycolysis. In fact, SDH and FH mutations-mediated accumulation of succinate or fumarate, inhibits the activity of prolyl-hydroxylase (the enzyme responsible for HIF-1α hydroxylation and its subsequent degradation) which in turn exerts effects on transcription of HIF-1α (Dhup, Kumar Dadhich, Ettore Porporato, & Sonveaux, 2012).

ii. Mitochondrial Composition

Mitochondrial structure is enclosed by two membranes. The outer membrane separates the organelle from cytosol and the inner membrane is folded to form the cristae, providing a large amount of surface area for chemical reactions and optimize mitochondrial respiration and energy production (Figure 11). Main macromolecules found in mitochondria are nucleic acids, lipids, and proteins which number of mitochondria vary from one tissue to another depending on the energy demand and the physiological functions of the tissue. Lipids can be imported into the mitochondria or generated within the organelle and end up in the composition of the inner and outer membranes.

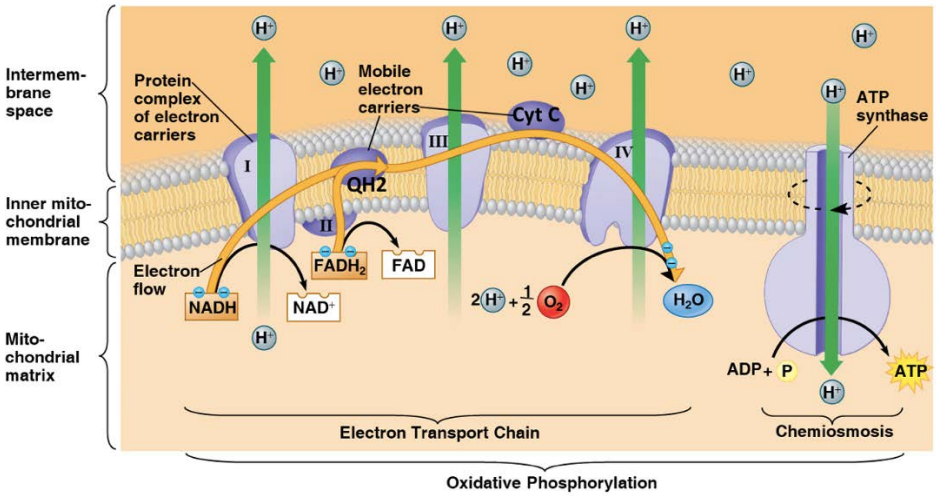

Figure 11. The mammalian mitochondrial electron transport chain consists of four enzyme complexes that are located in the mitochondrial inner membrane: complexes I, II, III and IV. Adapted from Hosseini et al, 2015. Complexes I and II transfer reducing equivalents from NADH and succinate, respectively, to complex III via the ubiquinone pool (CoQ, also named as Q or QH2, depending on its oxidation state), and complex III further transfers these equivalents to complex IV via cytochrome c.

Mitochondrial outer membrane is a lipid bilayer composed of about 50% proteins and 50% fat. It is permeable to small molecules of less than 10 kDa (pyruvate, fatty acids, and nucleotides) which cross the membrane through several proteins, such as the "voltage-dependent anion channel" VDAC, that are pore-forming membrane proteins. Small and uncharged molecules can passively diffuse through these pores; while proteins or other larger molecules require specific translocases in order to cross the outer mitochondrial membrane. Therefore, the outer membrane has no membrane potential due to its porosity. Mitochondrial proteins encoded by the nuclear DNA have an addressing sequence allowing them to enter mitochondria via an import system called TOM (Translocase of Outer Membrane) and TIM (Translocase of Inner Membrane). The inner mitochondrial membrane (IMM) has two features that differentiate it from all the other biological membranes: it is formed by up to 80% of proteins and it contains the phospholipid cardiolipin. Due to its particular lipid composition, this membrane is impermeable to ions, therefore transport of molecules requires the presence of TOM and TIM carriers. The IMM constitutes a tight diffusion membrane to all the other ions and larger molecules. As a consequence, the IMM has an electrochemical membrane potential.

Mitochondria have their own DNA which is transmitted to the daughter cells separately from nuclear DNA. As this DNA is not protected by histone proteins, rate of mutations is approximately 10 to 20 times more than nuclear DNA (Z. C. Wang et al., 2003). Unlike nuclear DNA, which is inherited from both parents, mitochondrial DNA (mtDNA) inheritance is just maternal.

Mitochondrial DNA is typically organized as a double strand circular structure with an approximate length of 16,806 bp containing 37 genes. These genes code for two ribosomal RNAs, 22 transfer RNAs and 13 polypeptides. In addition, there are approximately 1500 nuclear-encoded mitochondrial proteins which are all essential for physiological function of normal mitochondria. In each human cell, there are approximately 10-1000 mitochondria each containing 10^3-10^4 copies of mtDNA.

iii. Electron Transport Chain (ETC)

The primary determinant of the function of the electron transport chain (ETC) is the ADP:ATP ratio, reflecting the metabolic needs of the cell in terms of ATP consumption (energy requirements) in a certain moment. Electrons released during oxidative reactions are transferred to the ETC which include a series of electron donors and acceptors. NADH and $FADH_2$ are the

electron donors and molecular oxygen is the final electron acceptor. Electrons enter into ETC through complex I and II and are transferred to ubiquinone during the oxidation of NADH or $FADH_2$ (Figure 11).

Glycerol 3-phosphate dehydrogenase and electron transfer flavoprotein can also transfer electrons to ubiquinone and participate in the oxidative phosphorylation. This electron transfer is coupled with the extrusion of protons to the inter-membrane space using active pumps by respiratory chain complexes I, III and IV, to produce a proton gradient (chemical gradient) and a transmembrane charge (electrical gradient) as well. The translocation of protons from the matrix to the IMM generates an electrochemical gradient of protons that will be then used by ATP synthase (Complex V) to produce ATP from (Figure 12). The proton gradient is however essential not only for production of ATP but also indispensable to import proteins into the inner membrane and mitochondrial matrix.

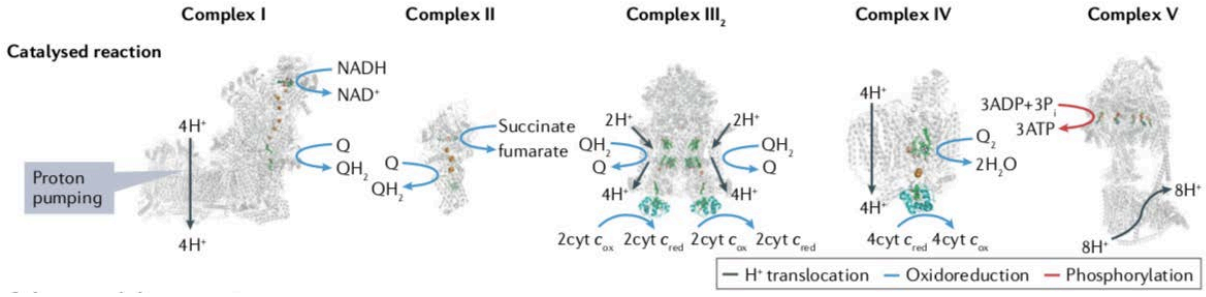

Figure 12. Structural properties of the electron transport chain (ETC). Adapted from Vercellino et al, 2022. Atomic models of complexes. H^+ indicates protons, Q is the oxidized form of quinone, QH_2 is the reduced form of quinone. The ETC components utilize the energy from nutritive substances in the form of the reducing equivalents in NADH and succinate, coming mainly from the Krebs cycle.

Complex I/ NADH Ubiquinone Oxidoreductase

Complex I or NADH-coenzyme Q reductase is a protein complex responsible for transferring electrons from NADH to ubiquinone. Complex I is the largest complex of the electron transport system with 45 subunits and a total size of ≃1000 kDa (Vercellino & Sazanov, 2022).

Complex II/ Succinate-Coenzyme Q Reductase

Succinate-coenzyme Q reductase transfers electrons from $FADH_2$ to ubiquinone. This enzyme complex is part of the Krebs cycle and is located into the mitochondrial inner membrane. It consists of four subunits which are encoded by the nuclear DNA. Complex II is responsible for oxidation of succinate to fumarate in the mitochondrial matrix and this oxidation is coupled to reduction of ubiquinone to ubiquinol in the inter-membrane space, but it doesn't contribute to the transmembrane proton gradient.

Complex I and II are the main entry points of electrons to ETC. However, there are other ways for electrons to enter. These include the transfer flavoprotein oxidoreductase ubiquinone-electrons and glycerol-3-phosphate dehydrogenase (Watmough & Frerman, 2010). Therefore, these enzymes reduce ubiquinone (CoQ) which acts as an electron-carrier between complexes II and III. It picks up reducing equivalents from Complexes I and II and transfers them to complex III.

Defect in human complex II has been correlated with neurodegenerative disorders such as Friedreich ataxia (Orth & Schapira, 2001) or paragangliomas (Baysal et al., 2000).

Complex III/ Coenzyme Q-Cytochrome c Reductase

Complex III also known as cytochrome bc1 complex participates in both electron transfer from CoQ (mitochondrial ubiquinone) to cytochrome c and also contributes to the proton gradient development. Indeed, two protons are transferred into the intermembrane space for each oxidized ubiquinol. Complex III is a dimer made up of two monomers, each consisting of 11 subunits of which only one subunit (cytochrome b) is encoded by mtDNA.

Recent work demonstrates that oxidation of ubiquinol back to ubiquinone has an essential role for the involvement of the ETC in tumor growth (Martínez-Reyes et al., 2020). Mitochondrial complex I and II donate electrons to ubiquinone (CoQ) generating ubiquinol. Mitochondrial complex III oxidizes ubiquinol back to ubiquinone, which allows complexes I and II to continue functioning and regenerate NAD+ and FAD. Ubiquinone is also used as an electron acceptor by dihydroorotate dehydrogenase (DHODH), an enzyme required for *de novo* pyrimidine synthesis (Figure 13). Martinez-Reyes et al showed impaired tumour growth in cancer cells that lack mitochondrial complex III (Martínez-Reyes et al., 2020).

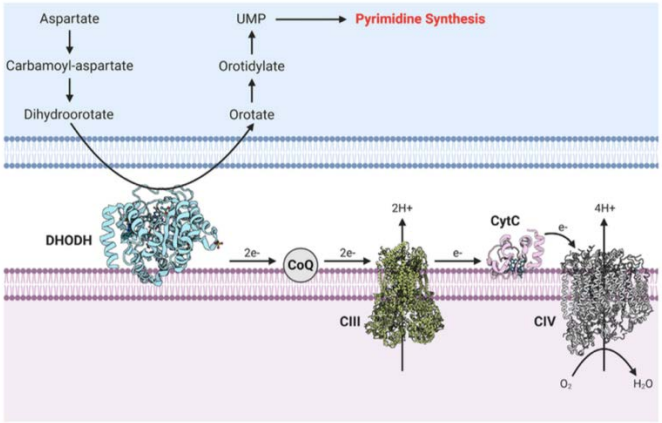

Figure 13. DHODH donates two electrons to mitochondrial ubiquinone (CoQ) within the ETC. Adapted from Vasan et al, 2020. This enzyme converts dihydroorotate to orotate in the intermembrane space.

Complex IV/ Cytochrome c oxidase

Cytochrome c oxidase is the last enzyme in ETC which transfers electrons to the oxygen as the final electron acceptor. In mammals, cytochrome c oxidase (COX) consists of 13 subunits of which three are encoded by mtDNA (Table 5). The reduction of O_2 to H_2O catalyzed by Complex IV requires four electrons. Complex IV is also interesting for its possible capacity to work in a second respiratory control mechanism with the proton-motive force. This mechanism is based on the allosteric inhibition (independent of mitochondrial membrane potential) of COX by ATP binding. Indeed, when ATP/ADP ratio is high, ATP can bind to the subunit IV leading to inhibition of complex IV and adjustment of the energy production to its physiological demand.

Complex V/ATP synthase

Complex V uses the proton-motive force in order to generate ATP from ADP. This step is known as the final step in oxidative phosphorylation (OXPHOS). Complex V can be divided into two main parts: F_1 and F_O. F_1 carries the catabolic center of ATPase complex and is involved in the transport of hydrogen ions. The catalytic mechanism involves conformational changes in F_1 which carries the nucleotide binding sites, producing ATP from ADP and inorganic orthophosphate (Pi). Protons previously transferred by complexes I, III and IV are present in greater amounts in the intermembrane space and therefore tend to go back into the mitochondrial matrix. In this way, protons move moves back into the matrix and the energy released is used by ATP synthase to convert ADP and Pi to ATP (Stock et al. 2000; Nakamoto et al. 2009).

Table 5. Overview of mitochondrial structure and inhibitors.

Complex	**I**	**II**	**III**	**IV**	**V**
Nuclear DNA subunits	39	4	10	10	14
Mitochondrial DNA subunits	ND1 ND2 ND3 ND4 ND5 ND6 ND4L		Cytochrome b	Cytochrome oxidase I, Cytochrome oxidase II, Cytochrome oxidase III	ATPase 6, ATPase 8

Enzyme	NADH-CoQ reductase	Succinate-CoQ reductase	CoQ-cytochrome C reductase	Cytochrome C oxidase	ATP synthase
Inhibitors	Rotenone, Amytal	TTFA, malonate	Antimycin A	Cuanide, Carbon monoxide, Azide	Oligomycine

II. 1.c Fatty Acid Metabolism

i. Fatty Acid Synthesis

Fatty acid synthesis generally occurs in the cytosol of liver cells and adipose tissues. Acetyl- CoA which is known as the major substrate of fatty acid biosynthesis is produced from pyruvate, acetate, amino acid catabolism and citrate degradation. Excess of citrate level triggers fatty acid synthesis whereas palmitoyl-CoA represses this process.

The initiation of this pathway starts with the carboxylation of acetyl-CoA to malonyl-CoA (Figure 14). Acetyl-CoA originates from different sources such as glycolysis, amino acid degradation or citrate. Mitochondrial membranes are not permeable to acetyl-CoA, therefore in order to export it into the cytosol, oxaloacetate and acetyl-CoA react together to form citrate which will leave the mitochondria through the SLC25A1 transporter. Once in the cytosol, ATP citrate lyase will catalyze the inverse reaction to separate acetyl-CoA from oxaloacetate.

The protein complex Fatty acids synthase (FAS) gathers all the reactions necessary for the synthesis of fatty acids. This series of reactions leads to the formation of butyryl-ACP. At this stage, butyryl-ACP can enter the fatty acid elongation phase by going through all the steps of the fatty acid synthesis cycle. The elongation will stop after 7 to 8 cycles by the release of the 16 or 18 carbon acyl residues of the FAS complex leading to a palmitate molecule (Ecker & Liebisch, 2014).

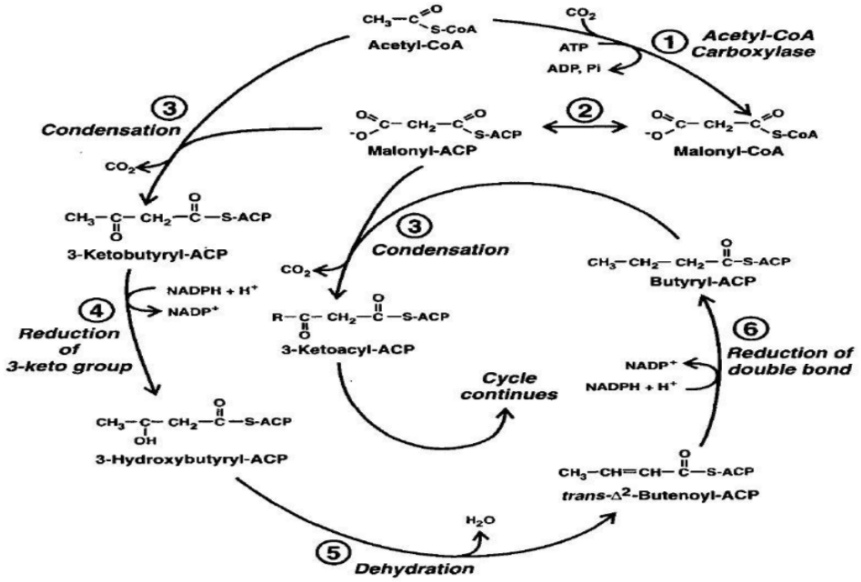

Figure 14. De novo fatty acid biosynthesis. Adapted from Ohlrogge and Browse, 1995.

ii. Fatty Acid β-Oxidation

In addition to glucose, β-oxidation of fatty acids is also a source of energy production. Fatty acid β-Oxidation is a multistep process which breaks down fatty acids for energy production. This process occurs in mitochondria and it's strictly linked to ETC (Figure 15). The products of this degradation are acetyl-CoA used by the Krebs cycle and NADH and FADH2 which will be used by the mitochondrial respiratory chain. Initially, an acyl-CoA will be formed from free fatty acids by acyl-CoA synthetase. In order to cross the mitochondrial membrane, acyl-CoA is converted to acyl-carnitine from carnitine by carnitine-acyl- transferase I (CPT1). CPT1 is located at the outer membrane of the mitochondria. Acyl-carnitine at the intermembrane space is then transferred to the mitochondrial matrix by carnitine acylcarnitine translocase (CACT). Carnitine acyl transferase II (CPT2) at the mitochondrial inner membrane will intervene and reconvert acyl-carnitine to acyl-CoA. The β-oxidation is a sequence of 4 steps allowing the formation of acetyl-CoA from acyl-CoA.

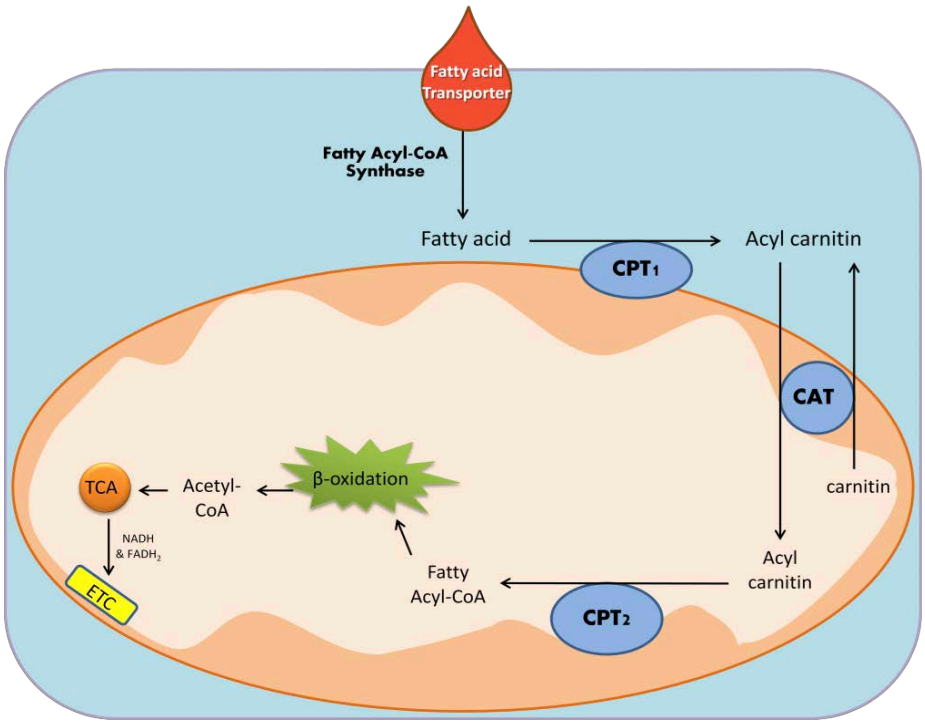

Figure 15. Overview of fatty acids β-oxidation. Adapted from Hosseini et al, 2018. This is multistep process by which fatty acids are broken down by various tissues to produce energy. Fatty acids primarily enter a cell via fatty acid protein transporters on the cell surface.

II.1.d Nucleotide Synthesis

Nucleotides are composed of a pentose whose 5 carbons come from glucose, of one or more phosphates esterifying the 5' carbon of the pentose and of a nitrogenous base linked to the 1' carbon (Figure 16). There are two groups:

- purines: Adenine and Guanine

- pyrimidines: Cytosine, Uracile and Thymine

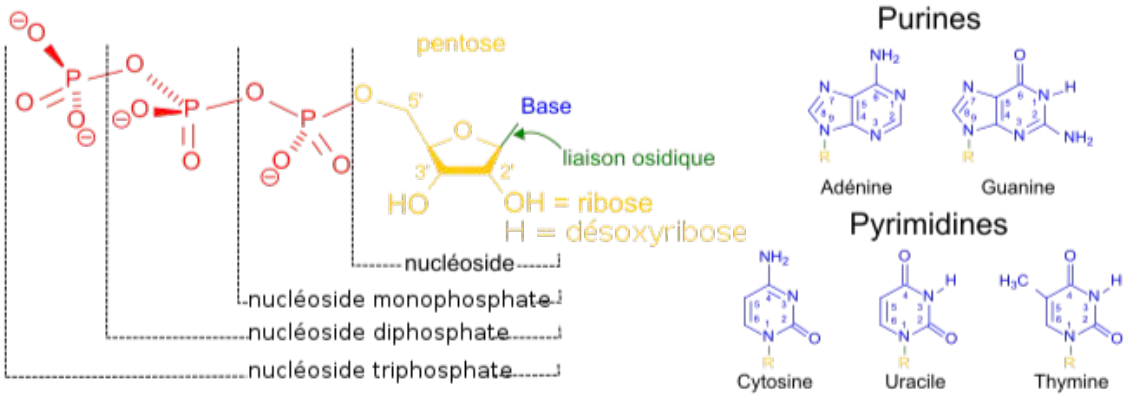

Figure 16. Nucleotides composition.

Synthesis of nucleotides is conducted in several steps requiring a large amount of energy. Of note, the ribose sugar (as the central metabolite of the pentose phosphate pathway) with a phosphate group is called 5-phosphoribosyl-1-pyrophosphate (PRPP) and is an essential step in purine and pyrimidine synthesis. ATP by giving two molecules of phosphate to ribose 5-phosphate transforms it to PRPP which is an intermediate in biosynthesis of purines, pyrimidines, NAD, histidine and tryptophan.

i. Purine Synthesis

Purine synthesis begins with adding glutamine-derived ammonia to PRPP. The first reaction is catalyzed by pyrophosphate amido-transferase which is activated by PRPP. This enzyme catalyzes the reaction of PRPP with glutamine and water to produce 5'-phosphoribosylamine, glutamate and pyrophosphate. Finally, phosphoribosylamine converts into Inosine-5'- monophosphate or IMP (Figure 17). IMP is the precursor of guanine and adenine. Other notable purines include hypoxanthine, xanthine, theobromine, caffeine, uric acid and isoguanine. The entire process of purine synthesis requires 5 molecules of ATP.

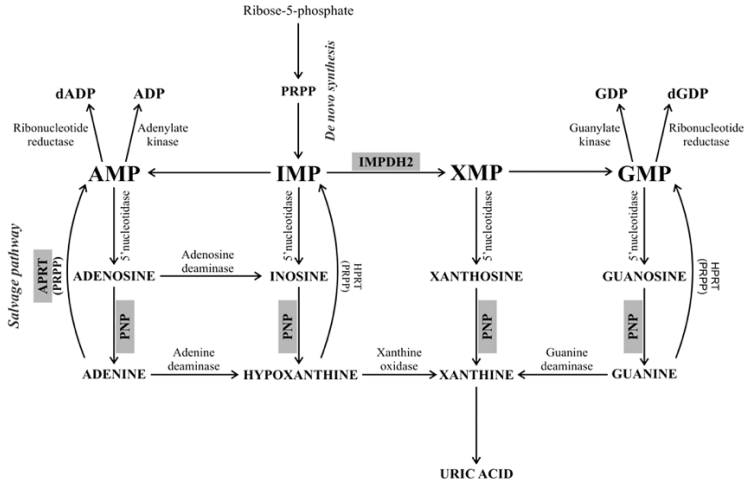

Figure 17. Purine *de novo* biosynthesis (Pospisilova et al., 2013)**.**

ii. Pyrimidine Synthesis

Pyrimidines can be synthesized by the *de novo* synthesis pathway or the salvage pathway by the contribution of circulating pyrimidines present in the bloodstream. In physiological conditions, the salvage pathway is the main source of pyrimidine, while the de novo pathway being solicited only when the cells have a high proliferative potential (tumor cells). The salvage pathway works with pyrimidines from intracellular recycling or from an extracellular pool. Several amino acids provide carbon and nitrogen atoms for pyrimidine

synthesis: aspartate provides carbon in C4, C5 and C6 and nitrogen in N1 and glutamine provides nitrogen in N3 (W. Wang, Cui, Ma, Lu, & Huang, 2021).

The first step of this process is the formation of carbamoyl phosphate by carbamoyl-phosphate synthetase-II activity. Then carbamylphosphate is converted to carbamoyl aspartic acid by the activity of aspartic transcarbamylase. In the next step, carbamoyl aspartic is dehydrated to dihydroorotate by dihydroorotase. Carbamoyl phosphate synthetase II, aspartic transcarbamylase and dihydroorotase are coded by the same enzyme called CAD.

Then dihydroorotate converts to orotate within the mitochondria by dihydroorotate dehydrogenase (DHODH). At this step, ribose-5-phosphate is joined to N-1 of orotate giving orotidine-5'-monophosphate (OMP). In this reaction, the donor of ribose phosphate is PRPP and the enzyme is orotate phosphoribosyl transferase. Decarboxylation of OMP by OMP-decarboxylase gives UMP. Phosphorylation of UMP consequently generates UDP which is the precursor of thymidine and cytosine (Figure 17).

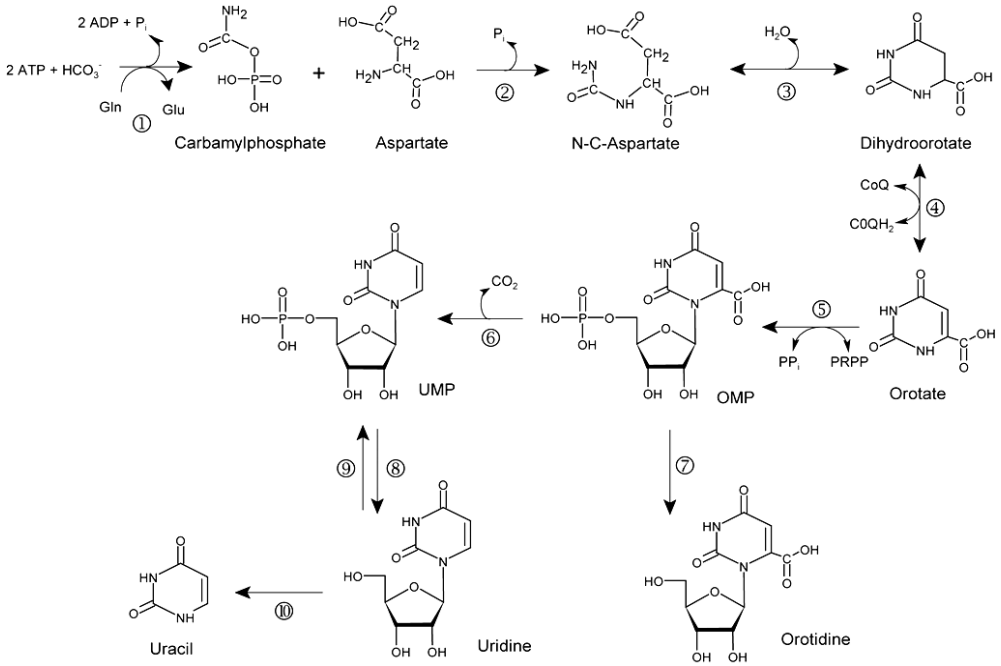

Figure 17. Pyrimidine *de novo* biosynthesis.

1) carbamylphosphate synthetase; 2) aspartate transcarbamylase; 3) dihydroorotase; 1+2+3) CAD; 4) dihydroorotate dehydrogenase; 5) orotate phosphoribosyltransferase; 6) orotidine 5′-monophosphate decarboxylase; 5+6) UMP synthase; 7) orotidine 5′-monophosphate phosphohydrolase; 8) pyrimidine 5′-nucleotidase; 9) uridine kinase; 10) uridine phosphorylase (Van Kuilenburg, Van Lenthe, Löffler, & Van Gennip, 2004)

iii. DHODH enzyme

The mitochondrial ETC is intrinsically coupled to pyrimidine nucleotide generation by sustaining DHODH activity (Figure 18). DHODH catalyzes the fourth enzymatic step, the ubiquinone-mediated oxidation of dihydroorotate to orotate, in de novo pyrimidine

biosynthesis. It is found to be located on the outer surface of the inner mitochondrial membrane (Rawls, Knecht, Diekert, Lill, & Löffler, 2000). A recent study demonstrates the availability of ubiquinone to receive electrons from dihydroorotate, which is only compromised when mitochondrial complex III is inhibited, is a key factor for the maintenance of de novo pyrimidine synthesis (Martínez-Reyes et al., 2020). Thus, DHODH activity is dependent on mitochondrial complex III function but does not contribute to the ETC's role in oxidative phosphorylation or the TCA cycle. DHODH inhibition has demonstrated efficacy in blocking tumor growth in different pre-clinical mouse models of cancer, including highly aggressive small-cell lung cancer (SCLC), acute myeloid leukemia (AML), triple-negative breast cancer, and Kras-driven cancers (Brown, Spinelli, Asara, & Toker, 2017; Christian et al., 2019; Koundinya et al., 2018; L. Li et al., 2019; Sykes et al., 2016; X. Wang et al., 2019; White et al., 2011).

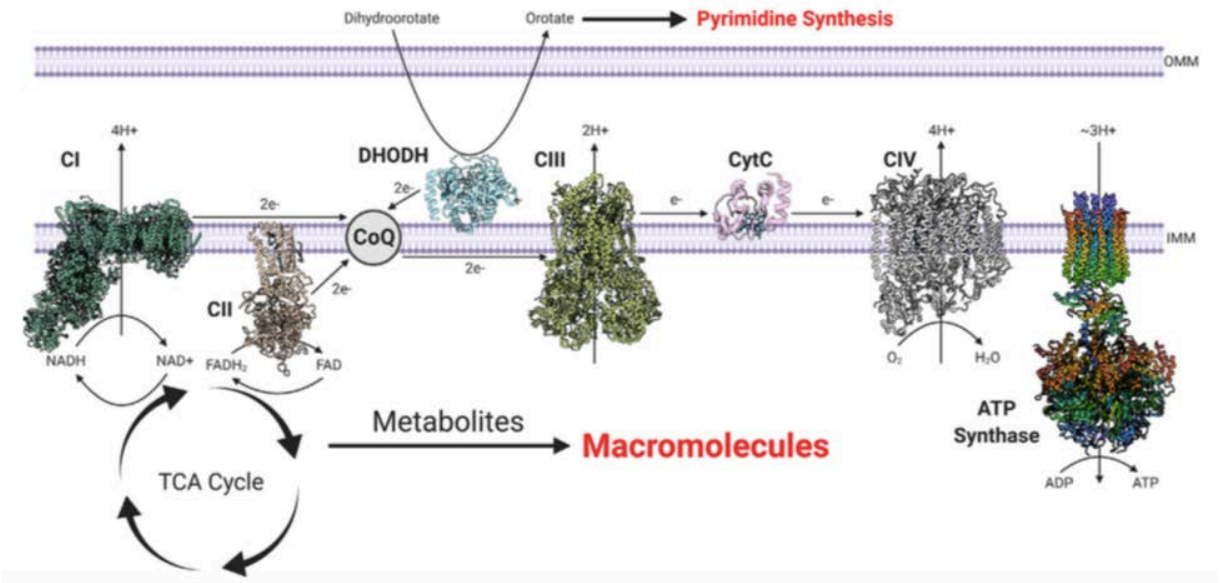

Figure 18. DHODH donates electrons to mitochondrial ubiquinone (CoQ) during the conversion of dihydroorotate to orotate (Vasan, Werner, & Chandel, 2020)**.** The five complexes of the ETC serve to produce the majority of ATP utilized by cancer cells as well as oxidize NADH and FADH2 to NAD+ and FAD, respectively. This allows for the TCA cycle to continue functioning, producing metabolites that support macromolecule synthesis.

II.2. Energy Metabolism and Cancer

II.2.a Energy Metabolism in Cancer

Cancer cells upregulate both glycolysis and TCA cycle metabolism in order to provide the substrates required for synthesis of macromolecules such as lipids and nucleotides that are required to sustain rapid cell proliferation (Figure 19). Multiple substrates feed into these biosynthetic pathways, thus providing cancer cells with metabolic flexibility to support tumor growth (Hanahan & Weinberg, 2011).

Mitochondrial metabolism supports tumor anabolism by providing key metabolites for macromolecule synthesis and by generating oncometabolites (fumarate, succinate, aspartate and D-2-hydroxyglutarate) to maintain the cancer phenotype.

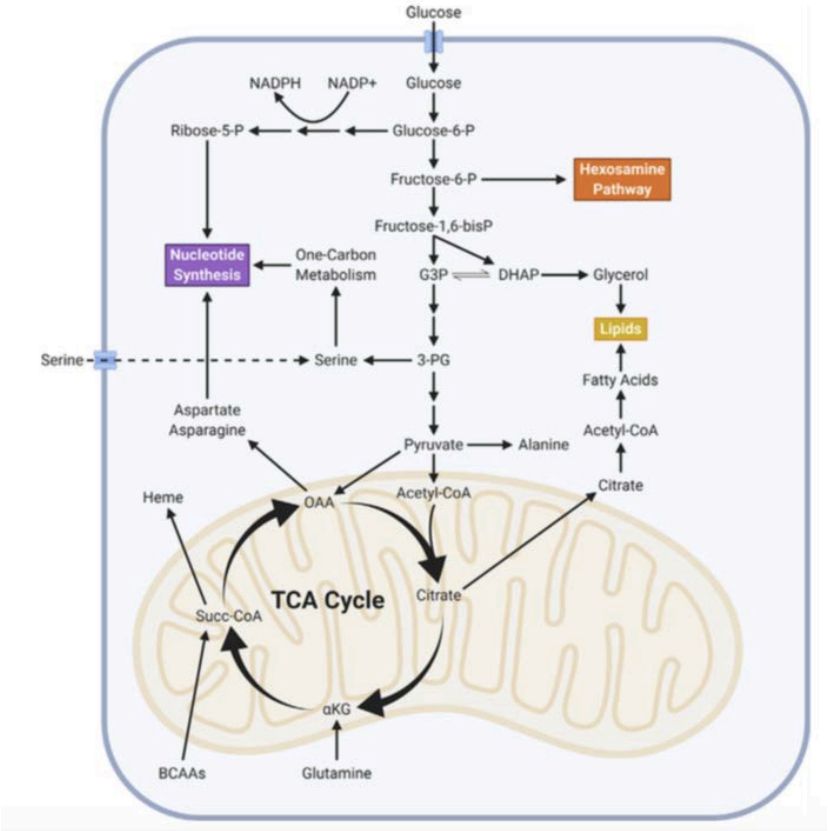

Figure 19. Metabolism Supports Macromolecules Synthesis for Growth (Vasan et al., 2020)**.** Cancer cells upregulate both glycolysis and TCA cycle metabolism in order to provide the substrates required for synthesis of macromolecules such as lipids and nucleotides that are required for cell proliferation. Multiple substrates feed into these biosynthetic pathways, thus providing can- cer cells with metabolic flexibility to support tumor growth.

During an oxidative stress, ROS are highly reactive and therefore toxic for cellular macromolecules, but nevertheless, at low concentrations, ROS act as intracellular signaling agents, regulating metabolic pathways. Increased levels of ROS are often found in cancer cells due to increased metabolic activities and altered antioxidant capacities. Mitochondria are involved in the regulation of cell death, through the release of cytochrome c (apoptosis and necrosis)(Rich, 2003). DNA mutations that affect mitochondria have been associated to cancer development, like SDH and FDH mutations in renal cell cancer and paraganglioma (Baysal et al., 2000; Tomlinson et al., 2002) or mutations in complex I subunits for hepatocarcinoma and prostate cancer(Orth & Schapira, 2001). A high mitochondrial turnover rate (fission and fusion) is characteristic of many cancer cells. Indeed, DRP1(fission protein) has been reported (Kitamura et al., 2017) to be overexpressed in cSCCs.

II.2.b Metabolic Flexibility

Metabolic flexibility is the ability of cells to modify their metabolic circuits by activating compensatory or alternative non-canonical pathways to maintain their energy homeostasis and other needs. Any disruption in this process leads to a variety of disorders such as cancer or metabolic diseases. The first to describe metabolic alterations in malignant cells was Otto Warburg in the 1920s (Warburg, 1956). He reported that malignant cells have an increased utilization of glucose via glycolysis in order to produce ATP despite the presence of oxygen: this phenomenon is called aerobic glycolysis or the “Warburg Effect”. Moreover, Warburg described an increased rate of lactate production as well assuming that cancer occurs when the mitochondrial oxidative metabolism is altered (Figure 20). The Warburg effect is the basis for tumor imaging by FDG-PET, which is used regularly in clinics.

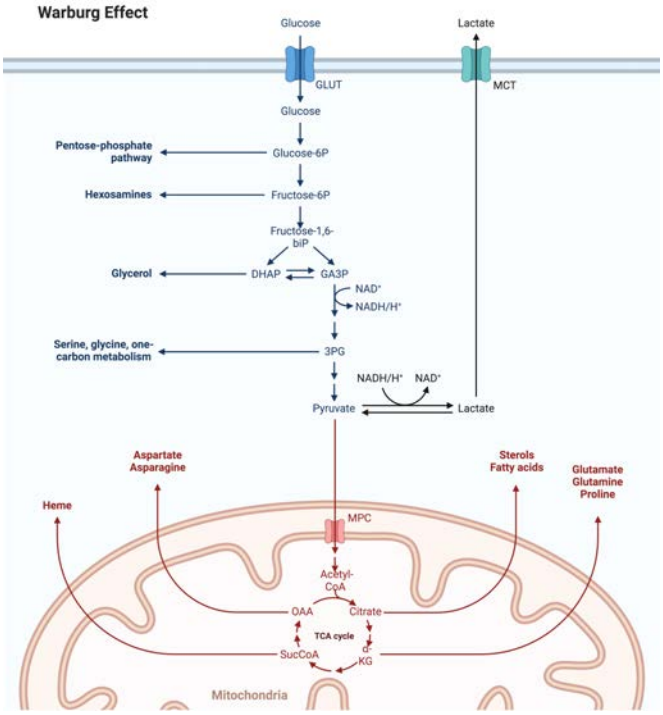

Figure 20. The Warburg effects. Adapted from DeBerardinis et al, 2020, created with Biorender. Cancer cells use essentially glucose as fuel, through glycolysis, in order to meet their energy and biomass needs to insure their cell proliferation.

Reprogramming of the metabolic network is now considered to be a hallmark of neoplastic transformation (Hanahan & Weinberg, 2011). Accumulating evidence indicates that malignant transformation is associated with changes that affect several branches of metabolism to support, on the one hand, the energy demands of cancer cells and, on the other, the anaplerotic reactions that are ultimately required for the generation of sufficient building blocks (i.e., nucleic acids, proteins, and membranes) (Galluzzi et al., 2013; Smolková et al., 2011; Ward & Thompson, 2012a). However, altered expressions of metabolic genes are very heterogeneous across different tumor types in that there is no uniform metabolic variation associated with all tumors (Hu et al., 2011). Indeed, since the seminal studies of Otto Warburg one century ago, biochemical research on cancer cell metabolism has revealed the highly metabolic plasticity of cancer cells. A large number of metabolic profiles have been discovered, from the highly glycolytic phenotype repeatedly observed on fast-growing cell lines (Heiden, Cantley, & Thompson, 2009; Ward & Thompson, 2012b) to the completely opposite profile characterized by a higher dependency on OXPHOS, as found in metastasis (Porporato et al., 2014) or a subclass of diffuse B cell lymphomas (Caro et al., 2012). In brief, to sustain their anaplerotic reactions and their energy demands cancer cells undergo metabolic reprogramming through various mechanisms including the deviation of glycolysis, Krebs cycle truncation, and

OXPHOS redirection toward lipid and protein synthesis (Jose, Bellance, & Rossignol, 2011; Pavlova & Thompson, 2016).

i. Cancers Relying on Glycolysis

In cancers relying on the Warburg effect, the expression of enzymes involved in glycolysis such as HK2 and PFK1, increases via the activation of certain oncogenes such as HIF-1α and c-Myc (Dang, Lewis, Dolde, Dang, & Shim, 1997). HIF-1α is mainly functional under hypoxic conditions while c-Myc promotes the expression of glycolytic genes under normoxic conditions. Their coordination thus stimulates glycolysis providing the necessary resources to the tumor cell to proliferate rapidly. Although ATP production by glycolysis is rapid, it is much less efficient than oxidative phosphorylation (2 glycolytic ATP *versus* 36 mitochondrial ATP). To compensate for this low production, the cell increases the synthesis of glucose transporters in order to transport more glucose into the cell and stimulate glycolysis (Hsu & Sabatini, 2008).

ii. Cancers Relying on OXPHOS

In contrast to the Warburg effect, some cancers show a stimulation of the activity of different respiratory chain complexes (especially complexes I and IV) and of oxidative phosphorylation (Moreno-Sánchez, Rodríguez-Enríquez, Marín-Hernández, & Saavedra, 2007; Weinberg & Chandel, 2015). For example overexpression of OXPHOS genes has been observed in breast cancer tumours and that causes an increase in their oxidative mitochondrial capacity (Whitaker-Menezes et al., 2011).

iii. Addiction to Some Metabolites

Through activation of oncogenes or loss of tumor suppressor genes, tumor cells may become dependent on certain amino acids such as serine or glutamine. Glutamine is an amino acid present in large quantities in the blood and an increase in its consumption is observed in cells with c-Myc oncogene activation (Wise et al., 2008). Glutaminolysis is a process by which cells convert glutamine into TCA cycle metabolites, through the activity of multiple enzymes. Myc activation stimulates glutaminolysis and contributes to the cell's dependence on glutamine, for their survival and proliferation. Indeed, glutaminolysis inhibition may be a potential in hepatocarcinoma (Jin et al., 2020).

II.2.c Factors Affecting the Energy Metabolism in Cancer Cells.

Several factors are able to affect the energy metabolism in cancer cells. Mitochondria controls the majority of the chemical reactions needed to generate most of the energy demands of the cells. Accordingly, any variation in the mitochondrial enzymes will strongly affect the energy metabolism of the cancer cell. Studies have shown that several cancers display inherent reduced mitochondrial functions caused by mutations in the mitochondrial genome. This latter encloses around one to two thousand nuclear DNA (nDNA) and thousands of copies of mitochondrial DNA (mtDNA) that dwell inside the mitochondrion (Vyas, Zaganjor, & Haigis, 2016). Some of the enzymes that are encoded by the nDNA are the succinate dehydrogenase (SDH) and the fumarate hydratase (FH), which are enzymes of the tricarboxylic acid (TCA) cycle and moreover been demonstrated as tumor suppressors (Gottlieb & Tomlinson, 2005). On the other hand, mtDNA have a high mutation rate that can be due to the accumulation of damage during replication, oxidative stress and many other factors. In consequences, mtDNA mutations, either oncogenic germline mutations or tumor-specific somatic mutations, contribute to cancer etiology (Brandon, Baldi, & Wallace, 2006).

Oxidative stress, apart from being mutagenic, is also directly involved in altering cellular energy metabolism by either activating or inactivating certain metabolic enzymes. High levels of reactive oxygen species (ROS) cause activation of proteins involved in glycolysis such as HIF-1α, AKT and the oncogenes RAS, SRC and MYC, and also the oxidation and inactivation of protein tyrosine phosphatases such as phosphate and tensin homolog "PTEN" (Panieri & Santoro, 2016). Furthermore, a number of signaling pathways are activated in response to oxidative stress to neutralize the impact of elevated ROS. It has been demonstrated that ROS are actively suppressed by K-Ras, B-Raf and Myc oncogenes that increases the transcription of Nrf2 (Nuclear factor erythroid 2-related factor 2) to promote the basal Nrf2 antioxidant program (Denicola et al., 2011).

Another metabolic alteration in cancer is induced by hypoxia. Hyperplastic growth in tumors causes substantial hypoxia, which in its turn increases glycolysis through stabilization of hypoxia-inducible transcription factor HIF-1α (Peppicelli, Bianchini, & Calorini, 2014). In fact, this mechanism is beneficial for cancer cells as it enhances the activity of pHi-regulating systems to promote cell survival and invasion (Chiche, Brahimi-Horn, & Pouysségur, 2010). Hypoxia causes acidosis of the tumor environment, low extracellular pH, and a neutral/alkaline intracellular pH (pHi) (Alfarouk et al., 2014).

Gene expression have a huge impact on the cellular energy metabolism. Its alteration in cancer is presented by an activation of oncogenes and/or inactivation of tumor suppressor genes. A large number of studies showed that a coordination between c-MYC, HIF-1α and TP53 take place and influence the energy metabolism and cell cycle progression in cancer cells (Yeung, Pan, & Lee, 2008). C-MYC is a proto-oncogene that stimulate the transcription of PDK1 and LDH, consequently it positively modulates the glycolysis pathway. HIF-1α is responsible for the transcription of GLUT-1, HK-2, LDH and PDK-1. The expression of PDK1 leads to the inactivation of PDH, therefore to a decreased conversion of pyruvate to acetyl-coA and eventually the reduction of the OXPHOS pathway (Yeung et al., 2008). However, TP53 is a tumor suppressor gene, it is shown to be mutated in the majority of human cancers. TP53 mutation influences energy metabolism at multiple levels. For instance, TIGAR (TP53-induced glycolysis and apoptosis regulator) is an enzyme induce by p53 that decreases the activity of PFK-1 and thereby inhibits glycolysis, the opposite take place when there is loss of TP53 (Bensaad & Vousden, 2007). Another tumor suppressor gene is PTEN, similarly, its loss causes alteration in metabolic pathways. PTEN controls the dephosphorylation of PIP3 and therefor the activation of PI3K, which in turn stimulate the activity of AKT and mTOR (Jia et al., 2008).

II.2.d Metabolic Switch during Skin Carcinogenesis

UV exposure affect mtDNA integrity. This latter is shown to affect cell invasion and tumor progression (Amuthan et al., 2002; Petros et al., 2005). UV-radiation was proved to affect D-loop mtDNA in a 260 bp mtDNA tandem duplication and mtDNA deletions in a study performed on sun-exposed skin and NMSCs (Harbottle & Birch-Machin, 2006; Krishnan & Birch-Machin, 2006; Krishnan, Harbottle, & Birch-Machin, 2004; Powers, Murphy, Ralph, O'Gorman, & Murphy, 2016). Being useful biomarkers for photoaging and skin cancers, mtDNA mutations are able to affect energy metabolism as its common deletions affect regions encoding for ATPase8, ATPase6, COXIII, ND3, ND4, ND4L and ND5 (Russell & Turnbull, 2014).

DNA damage response (DDR) pathway promotes altered energy metabolism. DDR network is induced by DNA damage, like that resulting from UV radiations, and refers to the process by which the cell maintains the integrity of the genome after a damage. This pathway comprises DNA repair and cell-cycle checkpoint pathways to finally define cell fate (Branzei & Foiani, 2008). A failure in this response is associated with cancer development. Recently, a link

between genomic mutations and metabolic alterations in keratinocyte cells was explored. From the variety of proteins belonging to the DDR network, we studied the role of XPC protein on metabolic reprogramming in human keratinocytes. XPC plays an important role in recognition of DNA damage in nucleotide excision repair, and patients with XPC deficiencies have higher incidence of skin cancer and other malignancies. In this study, XPC knockdown induced the activation of AKT1 and NADPH oxidase-1 (NOX1), resulting in the accumulation of ROS and specific deletions in mtDNA (Rezvani et al., 2011). Nonetheless, XPC knockdown in human keratinocytes escalated glycolysis with a reduction in OXPHOS. Implanted into immunodeficient mice, XPC-deficient cells with mtDNA deletions were capable of forming SCC. However, inactivation of AKT or NOX in these cells blocked neoplastic transformation (Rezvani et al., 2011). This highlights an important link between metabolic reprogramming and neoplastic transformation. In another study, using a multistage model of UVB-induced skin cancer, we discovered that cSCC formation is conditional to a certain cellular energy metabolism, that once rewired cancer formation will be inhibited. It was demonstrated that at a very early stage of photo-carcinogenesis glycolysis, TCA cycle and fatty acid ß-oxidation were decreased, while the distal part of the electron transport chain (ETC) were upregulated. These specific metabolic modifications that precede primary skin tumor formation, were accompanied with activated DHODH and glutamine metabolism. DHODH activity is essential for maintaining an increased ETC activity. Mice with decreased DHODH activity or impaired ETC failed to develop pre-malignant or malignant lesions, concluding that DHODH create a major link between DNA repair efficiency and bioenergetic pattering during skin carcinogenesis (Hosseini et al., 2018).

II.2.e Metabolic Heterogeneity in Skin Cancer

Metabolic heterogeneity is responsible for differences in treatment response among patients (Grande et al., 2018).

This **inter-patient heterogeneity** is characterized by different metabolic reprogramming, observed in many cancers including small cell lung cancer (NSCLC) and high grade ovarian cancer (Amoedo et al., 2021; Gentric et al., 2019).

Amoedo et al. identified two metabolic subgroups in lung cancer, an OXPHOS+ group with a strong capacity to use oxidative phosphorylation and an OXPHOS- group not dependent on this energy pathway. The recognition of the two subgroups allowed them to identify a metabolic

modulator allowing to inhibit the tumor growth of OXPHOS+ cells in xenografted mice and thus to highlight its therapeutic potential (Amoedo et al., 2021).
The same approach was used in high-grade serous ovarian cancer where the OXPHOS+ and OXPHOS- groups were identified; the team was able to demonstrate that the OXPHOS+ subgroup showed sensitivity to chemotherapy induced by activation of the PML-PGC-1α axis, involved in the regulation of metabolic pathways (Gentric et al., 2019).

Heterogeneity can also be **intra-tumoral**, as shown by Xiao Z et al., with co-existing of different types of reprogramming within the same tumor (Z. Xiao, Dai, & Locasale, 2019).
Indeed, tumor cells induce a metabolic reprogramming of the cells of the microenvironment leading to an intra-tumor heterogeneity of these cells. For example, fibroblasts present in oral squamous cell carcinomas can be metabolically modified by the increased glycolytic metabolism of cancer cells. This change in phenotype provides a favorable environment for tumor progression (Hensley et al., 2016; Zhang et al., 2020).

Conclusion

To conclude, metabolic heterogeneity has never been studied in cSCC. One of the objectives of my thesis was to characterize the metabolic heterogeneity of cSCC at different stages of carcinogenesis. Another objective was to determine if the effect of DHODH inhibition that we identified in mice was dependent on heterogeneity in cSCC.

References

Ahmady, S., Jansen, M. H. E., Nelemans, P. J., Kessels, J. P. H. M., Arits, A. H. M. M., De Rooij, M. J. M., … Mosterd, K. (2022). Risk of Invasive Cutaneous Squamous Cell Carcinoma After Different Treatments for Actinic Keratosis: A Secondary Analysis of a Randomized Clinical Trial. *JAMA Dermatology*, *158*(6), 634–640. https://doi.org/10.1001/JAMADERMATOL.2022.1034

Alam, M., & Ratner, D. (2001). Cutaneous squamous-cell carcinoma. *The New England Journal of Medicine*, *344*(13), 975–983. https://doi.org/10.1056/NEJM200103293441306

Alfarouk, K. O., Verduzco, D., Rauch, C., Muddathir, A. K., Bashir, A. H. H., Elhassan, G. O., … Harguindey, S. (2014). Erratum: Glycolysis, tumor metabolism, cancer growth

and dissemination. A new pH-based etiopathogenic perspective and therapeutic approach to an old cancer question. *Oncoscience*, *2*(4), 317. https://doi.org/10.18632/ONCOSCIENCE.158

Amin, M. B., Greene, F. L., Edge, S. B., Compton, C. C., Gershenwald, J. E., Brookland, R. K., … Winchester, D. P. (2017). The Eighth Edition AJCC Cancer Staging Manual: Continuing to build a bridge from a population-based to a more "personalized" approach to cancer staging. *CA: A Cancer Journal for Clinicians*, *67*(2), 93–99. https://doi.org/10.3322/CAAC.21388

Amoedo, N. D., Sarlak, S., Obre, E., Esteves, P., Bégueret, H., Kieffer, Y., … Rossignol, R. (2021). Targeting the mitochondrial trifunctional protein restrains tumor growth in oxidative lung carcinomas. *Journal of Clinical Investigation*. https://doi.org/10.1172/JCI133081

Amuthan, G., Biswas, G., Ananadatheerthavarada, H. K., Vijayasarathy, C., Shephard, H. M., & Avadhani, N. G. (2002). Mitochondrial stress-induced calcium signaling, phenotypic changes and invasive behavior in human lung carcinoma A549 cells. *Oncogene*, *21*(51), 7839–7849. https://doi.org/10.1038/SJ.ONC.1205983

Andrejeva, G., & Rathmell, J. C. (2017). Similarities and Distinctions of Cancer and Immune Metabolism in Inflammation and Tumors. *Cell Metabolism*, *26*(1), 49–70. https://doi.org/10.1016/J.CMET.2017.06.004

Asgari, M. M., Ray, G. T., Quesenberry, C. P., Katz, K. A., & Silverberg, M. J. (2017). Association of Multiple Primary Skin Cancers With Human Immunodeficiency Virus Infection, CD4 Count, and Viral Load. *JAMA Dermatology*, *153*(9), 892–896. https://doi.org/10.1001/JAMADERMATOL.2017.1716

Basset Seguin, N., Malvehy, J., Nadal, F., Creancier, L., Rauly-Lestienne, I., Beauchamp, R., … Ulianov, L. (2019). Risk behaviour and patient preferences for an improved non-melanoma skin cancer prevention modality for organ-transplanted patients; a European, multi-country, online patient community study. *European Journal of Dermatology : EJD*. https://doi.org/10.1684/ejd.2019.3639

Baysal, B. E., Ferrell, R. E., Willett-Brozick, J. E., Lawrence, E. C., Myssiorek, D., Bosch, A., … Devlin, B. (2000). Mutations in SDHD, a mitochondrial complex II gene, in hereditary paraganglioma. *Science (New York, N.Y.)*, *287*(5454), 848–851. https://doi.org/10.1126/SCIENCE.287.5454.848

Bensaad, K., & Vousden, K. H. (2007). p53: new roles in metabolism. *Trends in Cell Biology*, *17*(6), 286–291. https://doi.org/10.1016/J.TCB.2007.04.004

Berens, P. J. T., & Molinier, J. (2020). Formation and Recognition of UV-Induced DNA Damage within Genome Complexity. *International Journal of Molecular Sciences*, *21*(18), 1–23. https://doi.org/10.3390/IJMS21186689

Blechman, A. B., Carucci, J. A., & Stevenson, M. L. (2019). Stratification of Poor Outcomes for Cutaneous Squamous Cell Carcinoma in Immunosuppressed Patients Using the American Joint Committee on Cancer Eighth Edition and Brigham and Women's Hospital Staging Systems. *Dermatologic Surgery : Official Publication for American Society for Dermatologic Surgery [et Al.]*, *45*(9), 1117–1124. https://doi.org/10.1097/DSS.0000000000001774

Boulton, D. P., & Caino, M. C. (2022). Mitochondrial Fission and Fusion in Tumor Progression to Metastasis. *Frontiers in Cell and Developmental Biology*, *10*. https://doi.org/10.3389/FCELL.2022.849962

Brandon, M., Baldi, P., & Wallace, D. C. (2006). Mitochondrial mutations in cancer. *Oncogene*, *25*(34), 4647–4662. https://doi.org/10.1038/SJ.ONC.1209607

Brantsch, K. D., Meisner, C., Schönfisch, B., Trilling, B., Wehner-Caroli, J., Röcken, M., & Breuninger, H. (2008a). Analysis of risk factors determining prognosis of cutaneous squamous-cell carcinoma: a prospective study. *The Lancet. Oncology*, *9*(8), 713–720. https://doi.org/10.1016/S1470-2045(08)70178-5

Brantsch, K. D., Meisner, C., Schönfisch, B., Trilling, B., Wehner-Caroli, J., Röcken, M., & Breuninger, H. (2008b). Analysis of risk factors determining prognosis of cutaneous squamous-cell carcinoma: a prospective study. *The Lancet Oncology*, *9*(8), 713–720. https://doi.org/10.1016/S1470-2045(08)70178-5

Branzei, D., & Foiani, M. (2008). Regulation of DNA repair throughout the cell cycle. *Nature Reviews. Molecular Cell Biology*, *9*(4), 297–308. https://doi.org/10.1038/NRM2351

Bray, F., Ferlay, J., Soerjomataram, I., Siegel, R. L., Torre, L. A., & Jemal, A. (2018). Global cancer statistics 2018: GLOBOCAN estimates of incidence and mortality worldwide for 36 cancers in 185 countries. *CA: A Cancer Journal for Clinicians*, *68*(6), 394–424. https://doi.org/10.3322/CAAC.21492

Brewer, J. D., Shanafelt, T. D., Khezri, F., Sosa Seda, I. M., Zubair, A. S., Baum, C. L., … Otley, C. C. (2015). Increased incidence and recurrence rates of nonmelanoma skin cancer in patients with non-Hodgkin lymphoma: a Rochester Epidemiology Project population-based study in Minnesota. *Journal of the American Academy of Dermatology*, *72*(2), 302–309. https://doi.org/10.1016/J.JAAD.2014.10.028

Brougham, N. D. L. S., Dennett, E. R., Cameron, R., & Tan, S. T. (2012). The incidence of

metastasis from cutaneous squamous cell carcinoma and the impact of its risk factors. *Journal of Surgical Oncology*, *106*(7), 811–815. https://doi.org/10.1002/JSO.23155

Brown, K. K., Spinelli, J. B., Asara, J. M., & Toker, A. (2017). Adaptive reprogramming of De novo pyrimidine synthesis is a metabolic vulnerability in triple-negative breast cancer. *Cancer Discovery*. https://doi.org/10.1158/2159-8290.CD-16-0611

Cañueto, J., Cardeñoso, E., García, J. L., Santos-Briz, Castellanos-Martín, A., Fernández-López, E., … Román-Curto, C. (2017). Epidermal growth factor receptor expression is associated with poor outcome in cutaneous squamous cell carcinoma. *The British Journal of Dermatology*, *176*(5), 1279–1287. https://doi.org/10.1111/BJD.14936

Caro, P., Kishan, A. U., Norberg, E., Stanley, I. A., Chapuy, B., Ficarro, S. B., … Danial, N. N. (2012). Metabolic signatures uncover distinct targets in molecular subsets of diffuse large B cell lymphoma. *Cancer Cell*, *22*(4), 547–560. https://doi.org/10.1016/J.CCR.2012.08.014

Carter, J. B., Johnson, M. M., Chua, T. L., Karia, P. S., & Schmults, C. D. (2013). Outcomes of primary cutaneous squamous cell carcinoma with perineural invasion: an 11-year cohort study. *JAMA Dermatology*, *149*(1), 35–42. https://doi.org/10.1001/JAMADERMATOL.2013.746

Chahoud, J., Semaan, A., Chen, Y., Cao, M., Rieber, A. G., Rady, P., & Tyring, S. K. (2016). Association Between β-Genus Human Papillomavirus and Cutaneous Squamous Cell Carcinoma in Immunocompetent Individuals-A Meta-analysis. *JAMA Dermatology*, *152*(12), 1354–1364. https://doi.org/10.1001/JAMADERMATOL.2015.4530

Chapalain, M., Baroudjian, B., Dupont, A., Lhote, R., Lambert, J., Bagot, M., … Basset-Seguin, N. (2020). Stage IV cutaneous squamous cell carcinoma: treatment outcomes in a series of 42 patients. *Journal of the European Academy of Dermatology and Venereology : JEADV*, *34*(6), 1202–1209. https://doi.org/10.1111/JDV.16007

Chiche, J., Brahimi-Horn, M. C., & Pouysségur, J. (2010). Tumour hypoxia induces a metabolic shift causing acidosis: a common feature in cancer. *Journal of Cellular and Molecular Medicine*, *14*(4), 771–794. https://doi.org/10.1111/J.1582-4934.2009.00994.X

Christian, S., Merz, C., Evans, L., Gradl, S., Seidel, H., Friberg, A., … Janzer, A. (2019). The novel dihydroorotate dehydrogenase (DHODH) inhibitor BAY 2402234 triggers differentiation and is effective in the treatment of myeloid malignancies. *Leukemia*, *33*(10), 2403–2415. https://doi.org/10.1038/s41375-019-0461-5

Condeelis, J., & Pollard, J. W. (2006). Macrophages: obligate partners for tumor cell migration, invasion, and metastasis. *Cell*, *124*(2), 263–266.

https://doi.org/10.1016/J.CELL.2006.01.007

Conforti, C., Paolini, F., Venuti, A., Dianzani, C., & Zalaudek, I. (2019). The detection rate of human papillomavirus in well-differentiated squamous cell carcinoma and keratoacanthoma: is there new evidence for a viral pathogenesis of keratoacanthoma? *The British Journal of Dermatology*, *181*(6), 1309–1311. https://doi.org/10.1111/BJD.18212

D'orazio, J., Jarrett, S., Amaro-Ortiz, A., & Scott, T. (2013). UV Radiation and the Skin. *Int. J. Mol. Sci*, *14*, 12222–12248. https://doi.org/10.3390/ijms140612222

Dang, C. V., Lewis, B. C., Dolde, C., Dang, G., & Shim, H. (1997). Oncogenes in tumor metabolism, tumorigenesis, and apoptosis. *Journal of Bioenergetics and Biomembranes*, *29*(4), 345–354. https://doi.org/10.1023/A:1022446730452

de Martel, C., & Franceschi, S. (2009). Infections and cancer: established associations and new hypotheses. *Critical Reviews in Oncology/Hematology*, *70*(3), 183–194. https://doi.org/10.1016/J.CRITREVONC.2008.07.021

De Visser, K. E., Eichten, A., & Coussens, L. M. (2006). Paradoxical roles of the immune system during cancer development. *Nature Reviews. Cancer*, *6*(1), 24–37. https://doi.org/10.1038/NRC1782

Deady, S., Sharp, L., & Comber, H. (2014). Increasing skin cancer incidence in young, affluent, urban populations: a challenge for prevention. *The British Journal of Dermatology*, *171*(2), 324–331. https://doi.org/10.1111/BJD.12988

Denicola, G. M., Karreth, F. A., Humpton, T. J., Gopinathan, A., Wei, C., Frese, K., … Tuveson, D. A. (2011). Oncogene-induced Nrf2 transcription promotes ROS detoxification and tumorigenesis. *Nature*, *475*(7354), 106–110. https://doi.org/10.1038/NATURE10189

Dhup, S., Kumar Dadhich, R., Ettore Porporato, P., & Sonveaux, P. (2012). Multiple biological activities of lactic acid in cancer: influences on tumor growth, angiogenesis and metastasis. *Current Pharmaceutical Design*, *18*(10), 1319–1330. https://doi.org/10.2174/138161212799504902

Dotto, G. P., & Rustgi, A. K. (2016). Squamous Cell Cancers: A Unified Perspective on Biology and Genetics. *Cancer Cell*, *29*(5), 622–637. https://doi.org/10.1016/J.CCELL.2016.04.004

Durinck, S., Ho, C., Wang, N. J., Liao, W., Jakkula, L. R., Collisson, E. A., … Cho, R. J. (2011). Temporal dissection of tumorigenesis in primary cancers. *Cancer Discovery*, *1*(2), 137–143. https://doi.org/10.1158/2159-8290.CD-11-0028

Dusendang, J. R., Carlson, E., Lee, D. S., Marwaha, S., Madani, S., Alexeeff, S. E., … Herrinton, L. J. (2022). Cohort and nested case-control study of cutaneous squamous cell carcinoma in solid organ transplant recipients, by medication. *Journal of the American Academy of Dermatology*, *86*(3), 598–606. https://doi.org/10.1016/J.JAAD.2021.07.065

Dusingize, J. C., Olsen, C. M., Pandeya, N. P., Subramaniam, P., Thompson, B. S., Neale, R. E., … Whiteman, D. C. (2017). Cigarette Smoking and the Risks of Basal Cell Carcinoma and Squamous Cell Carcinoma. *The Journal of Investigative Dermatology*, *137*(8), 1700–1708. https://doi.org/10.1016/J.JID.2017.03.027

Ecker, J., & Liebisch, G. (2014). Application of stable isotopes to investigate the metabolism of fatty acids, glycerophospholipid and sphingolipid species. *Progress in Lipid Research*, *54*(1), 14–31. https://doi.org/10.1016/J.PLIPRES.2014.01.002

Essen, L. O., & Klar, T. (2006). Light-driven DNA repair by photolyases. *Cellular and Molecular Life Sciences : CMLS*, *63*(11), 1266–1277. https://doi.org/10.1007/S00018-005-5447-Y

Feng, Y., Ye, Z., Song, F., He, Y., & Liu, J. (2022). The Role of TAMs in Tumor Microenvironment and New Research Progress. *Stem Cells International*, *2022*, 1–11. https://doi.org/10.1155/2022/5775696

Fernandez Figueras, M. T. (2017). From actinic keratosis to squamous cell carcinoma: pathophysiology revisited. *Journal of the European Academy of Dermatology and Venereology : JEADV*, *31 Suppl 2*, 5–7. https://doi.org/10.1111/JDV.14151

Feuerhahn, S., & Egly, J. M. (2008). Tools to study DNA repair: what's in the box? *Trends in Genetics : TIG*, *24*(9), 467–474. https://doi.org/10.1016/J.TIG.2008.07.003

Frit, P., Kwon, K., Coin, F., Auriol, J. érôme, Dubaele, S., Salles, B., & Egly, J. M. (2002). Transcriptional Activators Stimulate DNA Repair. *Molecular Cell*, *10*(6), 1391–1401. https://doi.org/10.1016/S1097-2765(02)00732-3

Galluzzi, L., Kepp, O., Heiden, M. G. V., & Kroemer, G. (2013). Metabolic targets for cancer therapy. *Nature Reviews. Drug Discovery*, *12*(11), 829–846. https://doi.org/10.1038/NRD4145

Gandini, S., Palli, D., Spadola, G., Bendinelli, B., Cocorocchio, E., Stanganelli, I., … Caini, S. (2018). Anti-hypertensive drugs and skin cancer risk: a review of the literature and meta-analysis. *Critical Reviews in Oncology/Hematology*, *122*, 1–9. https://doi.org/10.1016/J.CRITREVONC.2017.12.003

García-Foncillas, J., Tejera-Vaquerizo, A., Sanmartín, O., Rojo, F., Mestre, J., Martín, S., … Mesía, R. (2022). Update on Management Recommendations for Advanced Cutaneous

Squamous Cell Carcinoma. *Cancers*, *14*(3). https://doi.org/10.3390/CANCERS14030629

Garrett, G. L., Blanc, P. D., Boscardin, J., Lloyd, A. A., Ahmed, R. L., Anthony, T., … Arron, S. T. (2017). Incidence of and Risk Factors for Skin Cancer in Organ Transplant Recipients in the United States. *JAMA Dermatology*, *153*(3), 296–303. https://doi.org/10.1001/JAMADERMATOL.2016.4920

Geltink, R. I. K., Kyle, R. L., & Pearce, E. L. (2018). Unraveling the Complex Interplay Between T Cell Metabolism and Function. *Annual Review of Immunology*, *36*, 461–488. https://doi.org/10.1146/ANNUREV-IMMUNOL-042617-053019

Gentric, G., Kieffer, Y., Mieulet, V., Goundiam, O., Bonneau, C., Nemati, F., … Mechta-Grigoriou, F. (2019). PML-Regulated Mitochondrial Metabolism Enhances Chemosensitivity in Human Ovarian Cancers. *Cell Metabolism*. https://doi.org/10.1016/j.cmet.2018.09.002

George, E. A., Baranwal, N., Kang, J. H., Qureshi, A. A., Drucker, A. M., & Cho, E. (2021). Photosensitizing Medications and Skin Cancer: A Comprehensive Review. *Cancers*, *13*(10). https://doi.org/10.3390/CANCERS13102344

Gordon, L. G., Leung, W., Johns, R., McNoe, B., Lindsay, D., Merollini, K. M. D., … Whiteman, D. C. (2022). Estimated Healthcare Costs of Melanoma and Keratinocyte Skin Cancers in Australia and Aotearoa New Zealand in 2021. *International Journal of Environmental Research and Public Health*, *19*(6). https://doi.org/10.3390/IJERPH19063178

Gottlieb, E., & Tomlinson, I. P. M. (2005). Mitochondrial tumour suppressors: a genetic and biochemical update. *Nature Reviews. Cancer*, *5*(11), 857–866. https://doi.org/10.1038/NRC1737

Grande, S., Palma, A., Ricci-Vitiani, L., Luciani, A. M., Buccarelli, M., Biffoni, M., … Rosi, A. (2018). Metabolic Heterogeneity Evidenced by MRS among Patient-Derived Glioblastoma Multiforme Stem-Like Cells Accounts for Cell Clustering and Different Responses to Drugs. *Stem Cells International*, *2018*. https://doi.org/10.1155/2018/3292704

Gross, N. D., Miller, D. M., Khushalani, N. I., Divi, V., Ruiz, E. S., Lipson, E. J., … Rischin, D. (2022). Neoadjuvant Cemiplimab for Stage II to IV Cutaneous Squamous-Cell Carcinoma. *The New England Journal of Medicine*. https://doi.org/10.1056/NEJMOA2209813

Guerra, C., Schuhmacher, A. J., Cañamero, M., Grippo, P. J., Verdaguer, L., Pérez-Gallego,

L., … Barbacid, M. (2007). Chronic pancreatitis is essential for induction of pancreatic ductal adenocarcinoma by K-Ras oncogenes in adult mice. *Cancer Cell*, *11*(3), 291–302. https://doi.org/10.1016/J.CCR.2007.01.012

Hanahan, D., & Weinberg, R. A. (2011). Hallmarks of cancer: the next generation. *Cell*, *144*(5), 646–674. https://doi.org/10.1016/J.CELL.2011.02.013

Harbottle, A., & Birch-Machin, M. A. (2006). Real-time PCR analysis of a 3895 bp mitochondrial DNA deletion in nonmelanoma skin cancer and its use as a quantitative marker for sunlight exposure in human skin. *British Journal of Cancer*, *94*(12), 1887–1893. https://doi.org/10.1038/SJ.BJC.6603178

Heiden, M. G. V., Cantley, L. C., & Thompson, C. B. (2009). Understanding the warburg effect: The metabolic requirements of cell proliferation. *Science*. https://doi.org/10.1126/science.1160809

Hensley, C. T., Faubert, B., Yuan, Q., Lev-Cohain, N., Jin, E., Kim, J., … DeBerardinis, R. J. (2016). Metabolic Heterogeneity in Human Lung Tumors. *Cell*. https://doi.org/10.1016/j.cell.2015.12.034

Hillen, U., Leiter, U., Haase, S., Kaufmann, R., Becker, J., Gutzmer, R., … Livingstone, E. (2018). Advanced cutaneous squamous cell carcinoma: A retrospective analysis of patient profiles and treatment patterns-Results of a non-interventional study of the DeCOG. *European Journal of Cancer (Oxford, England : 1990)*, *96*, 34–43. https://doi.org/10.1016/J.EJCA.2018.01.075

Hosseini, M., Dousset, L., Mahfouf, W., Serrano-Sanchez, M., Redonnet-Vernhet, I., Mesli, S., … Rezvani, H. R. (2018). Energy Metabolism Rewiring Precedes UVB-Induced Primary Skin Tumor Formation. *Cell Reports*, *23*(12), 3621–3634. https://doi.org/10.1016/j.celrep.2018.05.060

Hosseini, M., Ezzedine, K., Taieb, A., & Rezvani, H. R. (2015). Oxidative and energy metabolism as potential clues for clinical heterogeneity in nucleotide excision repair disorders. *The Journal of Investigative Dermatology*, *135*(2), 341–351. https://doi.org/10.1038/JID.2014.365

Hsu, P. P., & Sabatini, D. M. (2008). Cancer cell metabolism: Warburg and beyond. *Cell*, *134*(5), 703–707. https://doi.org/10.1016/J.CELL.2008.08.021

Hu, S., Balakrishnan, A., Bok, R. A., Anderton, B., Larson, P. E. Z., Nelson, S. J., … Goga, A. (2011). 13C-pyruvate imaging reveals alterations in glycolysis that precede c-Myc-induced tumor formation and regression. *Cell Metabolism*, *14*(1), 131–142. https://doi.org/10.1016/J.CMET.2011.04.012

Hussein, M. R. (2005). Ultraviolet radiation and skin cancer: molecular mechanisms. *Journal of Cutaneous Pathology*, *32*(3), 191–205. https://doi.org/10.1111/J.0303-6987.2005.00281.X

Jansen, M. H. E., Kessels, J. P. H. M., Nelemans, P. J., Kouloubis, N., Arits, A. H. M. M., van Pelt, H. P. A., … Mosterd, K. (2019). Randomized Trial of Four Treatment Approaches for Actinic Keratosis. *The New England Journal of Medicine*, *380*(10), 935–946. https://doi.org/10.1056/NEJMOA1811850

Jia, S., Liu, Z., Zhang, S., Liu, P., Zhang, L., Lee, S. H., … Zhao, J. J. (2008). Essential roles of PI(3)K-p110beta in cell growth, metabolism and tumorigenesis. *Nature*, *454*(7205), 776–779. https://doi.org/10.1038/NATURE07091

Jin, H., Wang, S., Zaal, E. A., Wang, C., Wu, H., Bosma, A., … Bernards, R. (2020). A powerful drug combination strategy targeting glutamine addiction for the treatment of human liver cancer. *ELife*, *9*, 1–20. https://doi.org/10.7554/ELIFE.56749

Jose, C., Bellance, N., & Rossignol, R. (2011). Choosing between glycolysis and oxidative phosphorylation: a tumor's dilemma? *Biochimica et Biophysica Acta*, *1807*(6), 552–561. https://doi.org/10.1016/J.BBABIO.2010.10.012

Karia, P. S., Han, J., & Schmults, C. D. (2013a). Cutaneous squamous cell carcinoma: estimated incidence of disease, nodal metastasis, and deaths from disease in the United States, 2012. *Journal of the American Academy of Dermatology*, *68*(6), 957–966. https://doi.org/10.1016/J.JAAD.2012.11.037

Karia, P. S., Han, J., & Schmults, C. D. (2013b). Cutaneous squamous cell carcinoma: Estimated incidence of disease, nodal metastasis, and deaths from disease in the United States, 2012. *Journal of the American Academy of Dermatology*, *68*(6), 957–966. https://doi.org/10.1016/j.jaad.2012.11.037

Karia, P. S., Han, J., & Schmults, C. D. (2013c). Cutaneous squamous cell carcinoma: Estimated incidence of disease, nodal metastasis, and deaths from disease in the United States, 2012. *Journal of the American Academy of Dermatology*, *68*(6), 957–966. https://doi.org/10.1016/j.jaad.2012.11.037

Karia, P. S., Morgan, F. C., Ruiz, E. S., & Schmults, C. D. (2017). Clinical and Incidental Perineural Invasion of Cutaneous Squamous Cell Carcinoma: A Systematic Review and Pooled Analysis of Outcomes Data. *JAMA Dermatology*, *153*(8), 781–788. https://doi.org/10.1001/JAMADERMATOL.2017.1680

Kim, S. T., Sancar, A., & Heelis, P. F. (1992). Energy transfer (deazaflavin-->FADH2) and electron transfer (FADH2-->T T) kinetics in Anacystis nidulans photolyase.

Biochemistry, *31*(45), 11244–11248. https://doi.org/10.1021/BI00160A040

Kitamura, S., Yanagi, T., Imafuku, K., Hata, H., Abe, R., & Shimizu, H. (2017). Drp1 regulates mitochondrial morphology and cell proliferation in cutaneous squamous cell carcinoma. *Journal of Dermatological Science*, *88*(3), 298–307. https://doi.org/10.1016/J.JDERMSCI.2017.08.004

Knuutila, J. S., Riihilä, P., Kurki, S., Nissinen, L., & Kähäri, V. M. (2020). Risk Factors and Prognosis for Metastatic Cutaneous Squamous Cell Carcinoma: A Cohort Study. *Acta Dermato-Venereologica*, *100*(16), 1–9. https://doi.org/10.2340/00015555-3628

Koundinya, M., Sudhalter, J., Courjaud, A., Lionne, B., Touyer, G., Bonnet, L., … Morris, A. (2018). Dependence on the Pyrimidine Biosynthetic Enzyme DHODH Is a Synthetic Lethal Vulnerability in Mutant KRAS-Driven Cancers. *Cell Chemical Biology*, *25*(6), 705-717.e11. https://doi.org/10.1016/J.CHEMBIOL.2018.03.005

Krawczyk, C. M., Holowka, T., Sun, J., Blagih, J., Amiel, E., DeBerardinis, R. J., … Pearce, E. J. (2010). Toll-like receptor-induced changes in glycolytic metabolism regulate dendritic cell activation. *Blood*, *115*(23), 4742–4749. https://doi.org/10.1182/BLOOD-2009-10-249540

Krishnan, K. J., & Birch-Machin, M. A. (2006). The incidence of both tandem duplications and the common deletion in mtDNA from three distinct categories of sun-exposed human skin and in prolonged culture of fibroblasts. *The Journal of Investigative Dermatology*, *126*(2), 408–415. https://doi.org/10.1038/SJ.JID.5700099

Krishnan, K. J., Harbottle, A., & Birch-Machin, M. A. (2004). The use of a 3895 bp mitochondrial DNA deletion as a marker for sunlight exposure in human skin. *The Journal of Investigative Dermatology*, *123*(6), 1020–1024. https://doi.org/10.1111/J.0022-202X.2004.23457.X

Küsters-Vandevelde, H. V. N., Leeuwen, A. Van, Verdijk, M. A. J., De Koning, M. N. C., Quint, W. G. V., Melchers, W. J. G., … Blokx, W. A. M. (2010). CDKN2A but not TP53 mutations nor HPV presence predict poor outcome in metastatic squamous cell carcinoma of the skin. *International Journal of Cancer*, *126*(9), 2123–2132. https://doi.org/10.1002/IJC.24871

Lanz, J., Bouwes Bavinck, J. N., Westhuis, M., Quint, K. D., Harwood, C. A., Nasir, S., … Hofbauer, G. F. L. (2019). Aggressive Squamous Cell Carcinoma in Organ Transplant Recipients. *JAMA Dermatology*, *155*(1), 66–71. https://doi.org/10.1001/JAMADERMATOL.2018.4406

Li, L., Ng, S. R., Colón, C. I., Drapkin, B. J., Hsu, P. P., Li, Z., … Jacks, T. (2019).

Identification of DHODH as a therapeutic target in small cell lung cancer. *Science Translational Medicine*, *11*(517). https://doi.org/10.1126/scitranslmed.aaw7852

Li, Y. Y., Hanna, G. J., Laga, A. C., Haddad, R. I., Lorch, J. H., & Hammerman, P. S. (2015). Genomic analysis of metastatic cutaneous squamous cell carcinoma. *Clinical Cancer Research*. https://doi.org/10.1158/1078-0432.CCR-14-1773

Likhacheva, A., Awan, M., Barker, C. A., Bhatnagar, A., Bradfield, L., Brady, M. S., … Devlin, P. M. (2020). Definitive and Postoperative Radiation Therapy for Basal and Squamous Cell Cancers of the Skin: Executive Summary of an American Society for Radiation Oncology Clinical Practice Guideline. *Practical Radiation Oncology*, *10*(1), 8–20. https://doi.org/10.1016/J.PRRO.2019.10.014

Lindelöf, B., Sigurgeirsson, B., Gäbel, H., & Stern, R. S. (2000). Incidence of skin cancer in 5356 patients following organ transplantation. *British Journal of Dermatology*, *143*(3), 513–519. https://doi.org/10.1111/J.1365-2133.2000.03703.X

Lobl, M. B., Clarey, D. D., Higgins, S., Sutton, A., & Wysong, A. (2022). Sequencing of Cutaneous Squamous Cell Carcinoma Primary Tumors and Patient-Matched Metastases Reveals ALK as a Potential Driver in Metastases and Low Mutational Concordance in Immunocompromised Patients. *JID Innovations : Skin Science from Molecules to Population Health*, *2*(4), 100122. https://doi.org/10.1016/J.XJIDI.2022.100122

Lomas, A., Leonardi-Bee, J., & Bath-Hextall, F. (2012). A systematic review of worldwide incidence of nonmelanoma skin cancer. *The British Journal of Dermatology*, *166*(5), 1069–1080. https://doi.org/10.1111/J.1365-2133.2012.10830.X

Lui, V. W. Y., Peyser, N. D., Ng, P. K. S., Hritz, J., Zeng, Y., Lu, Y., … Grandis, J. R. (2014). Frequent mutation of receptor protein tyrosine phosphatases provides a mechanism for STAT3 hyperactivation in head and neck cancer. *Proceedings of the National Academy of Sciences of the United States of America*, *111*(3), 1114–1119. https://doi.org/10.1073/PNAS.1319551111

Mantovani, A., Allavena, P., Sica, A., & Balkwill, F. (2008). Cancer-related inflammation. *Nature*, *454*(7203), 436–444. https://doi.org/10.1038/NATURE07205

Mantovani, A., Marchesi, F., Malesci, A., Laghi, L., & Allavena, P. (2017). Tumour-associated macrophages as treatment targets in oncology. *Nature Reviews. Clinical Oncology*, *14*(7), 399–416. https://doi.org/10.1038/NRCLINONC.2016.217

Marks, R., Rennie, G., & Selwood, T. S. (1988). MALIGNANT TRANSFORMATION OF SOLAR KERATOSES TO SQUAMOUS CELL CARCINOMA. *The Lancet*, *331*(8589), 795–797. https://doi.org/10.1016/S0140-6736(88)91658-3

Martincorena, I., & Campbell, P. J. (2015, September 25). Somatic mutation in cancer and normal cells. *Science*. American Association for the Advancement of Science. https://doi.org/10.1126/science.aab4082

Martínez-Reyes, I., Cardona, L. R., Kong, H., Vasan, K., McElroy, G. S., Werner, M., … Chandel, N. S. (2020). Mitochondrial ubiquinol oxidation is necessary for tumour growth. *Nature*, *585*(7824), 288–292. https://doi.org/10.1038/S41586-020-2475-6

Maubec, E., Petrow, P., Scheer-Senyarich, I., Duvillard, P., Lacroix, L., Gelly, J., … Avril, M. F. (2011). Phase II study of cetuximab as first-line single-drug therapy in patients with unresectable squamous cell carcinoma of the skin. *Journal of Clinical Oncology : Official Journal of the American Society of Clinical Oncology*, *29*(25), 3419–3426. https://doi.org/10.1200/JCO.2010.34.1735

Michalek, R. D., Gerriets, V. A., Jacobs, S. R., Macintyre, A. N., MacIver, N. J., Mason, E. F., … Rathmell, J. C. (2011). Cutting edge: distinct glycolytic and lipid oxidative metabolic programs are essential for effector and regulatory CD4+ T cell subsets. *Journal of Immunology (Baltimore, Md. : 1950)*, *186*(6), 3299–3303. https://doi.org/10.4049/JIMMUNOL.1003613

Migden, M. R., Rischin, D., Schmults, C. D., Guminski, A., Hauschild, A., Lewis, K. D., … Fury, M. G. (2018). PD-1 blockade with cemiplimab in advanced cutaneous squamous-cell carcinoma. *New England Journal of Medicine*, *379*(4), 341–351. https://doi.org/10.1056/NEJMoa1805131

Moreno-Sánchez, R., Rodríguez-Enríquez, S., Marín-Hernández, A., & Saavedra, E. (2007). Energy metabolism in tumor cells. *The FEBS Journal*, *274*(6), 1393–1418. https://doi.org/10.1111/J.1742-4658.2007.05686.X

Morris, K. L., Luke, M. C., & Perna, F. M. (2018). Prevalence of Skin Cancer Examination Among Users of Indoor Tanning Beds. *JAMA Dermatology*, *154*(7), 840–842. https://doi.org/10.1001/JAMADERMATOL.2018.1118

Mota, J. M., Leite, C. A., Souza, L. E., Melo, P. H., Nascimento, D. C., De-Deus-Wagatsuma, V. M., … Rego, E. M. (2016). Post-Sepsis State Induces Tumor-Associated Macrophage Accumulation through CXCR4/CXCL12 and Favors Tumor Progression in Mice. *Cancer Immunology Research*, *4*(4), 312–322. https://doi.org/10.1158/2326-6066.CIR-15-0170

Mourouzis, C., Boynton, A., Grant, J., Umar, T., Wilson, A., Macpheson, D., & Pratt, C. (2009). Cutaneous head and neck SCCs and risk of nodal metastasis - UK experience. *Journal of Cranio-Maxillo-Facial Surgery : Official Publication of the European*

Association for Cranio-Maxillo-Facial Surgery, *37*(8), 443–447. https://doi.org/10.1016/J.JCMS.2009.07.007

Muzic, J. G., Schmitt, A. R., Wright, A. C., Alniemi, D. T., Zubair, A. S., Olazagasti Lourido, J. M., … Baum, C. L. (2017). Incidence and Trends of Basal Cell Carcinoma and Cutaneous Squamous Cell Carcinoma: A Population-Based Study in Olmsted County, Minnesota, 2000 to 2010. *Mayo Clinic Proceedings*, *92*(6), 890–898. https://doi.org/10.1016/j.mayocp.2017.02.015

Nakamura, K., Okuyama, R., Saida, T., & Uhara, H. (2013). Platinum and anthracycline therapy for advanced cutaneous squamous cell carcinoma. *International Journal of Clinical Oncology*, *18*(3), 506–509. https://doi.org/10.1007/S10147-012-0411-Y

Nelson, T. G., & Ashton, R. E. (2017). Low incidence of metastasis and recurrence from cutaneous squamous cell carcinoma found in a UK population: Do we need to adjust our thinking on this rare but potentially fatal event? *Journal of Surgical Oncology*, *116*(6), 783–788. https://doi.org/10.1002/JSO.24707

O'Neill, L. A. J., Kishton, R. J., & Rathmell, J. (2016). A guide to immunometabolism for immunologists. *Nature Reviews Immunology 2016 16:9*, *16*(9), 553–565. https://doi.org/10.1038/nri.2016.70

O'Sullivan, D. (2019). The metabolic spectrum of memory T cells. *Immunology and Cell Biology*, *97*(7), 636–646. https://doi.org/10.1111/IMCB.12274

Olsen, E. A., Lisa Abernethy, M., Kulp-Shorten, C., Callen, J. P., Glazer, S. D., Huntley, A., … Wolf, J. E. (1991). A double-blind, vehicle-controlled study evaluating masoprocol cream in the treatment of actinic keratoses on the head and neck. *Journal of the American Academy of Dermatology*, *24*(5 Pt 1), 738–743. https://doi.org/10.1016/0190-9622(91)70113-G

Omland, S. H., Ahlström, M. G., Gerstoft, J., Pedersen, G., Mohey, R., Pedersen, C., … Omland, L. H. (2018). Risk of skin cancer in patients with HIV: A Danish nationwide cohort study. *Journal of the American Academy of Dermatology*, *79*(4), 689–695. https://doi.org/10.1016/J.JAAD.2018.03.024

Omland, S. H., Gniadecki, R., Hædersdal, M., Helweg-Larsen, J., & Omland, L. H. (2016). Skin Cancer Risk in Hematopoietic Stem-Cell Transplant Recipients Compared With Background Population and Renal Transplant Recipients: A Population-Based Cohort Study. *JAMA Dermatology*, *152*(2), 177–183. https://doi.org/10.1001/jamadermatol.2015.3902

Orth, M., & Schapira, A. H. V. (2001). Mitochondria and degenerative disorders. *American*

Journal of Medical Genetics, *106*(1), 27–36. https://doi.org/10.1002/AJMG.1425

Pandeya, N., Olsen, C. M., & Whiteman, D. C. (2017). The incidence and multiplicity rates of keratinocyte cancers in Australia. *Medical Journal of Australia*, *207*(8), 339–343. https://doi.org/10.5694/mja17.00284

Panieri, E., & Santoro, M. M. (2016). ROS homeostasis and metabolism: a dangerous liason in cancer cells. *Cell Death & Disease*, *7*(6). https://doi.org/10.1038/CDDIS.2016.105

Pavlova, N. N., & Thompson, C. B. (2016). The Emerging Hallmarks of Cancer Metabolism. *Cell Metabolism*, *23*(1), 27–47. https://doi.org/10.1016/J.CMET.2015.12.006

Pe, K. C. S., Saetung, R., Yodsurang, V., Chaotham, C., Suppipat, K., Chanvorachote, P., & Tawinwung, S. (2022). Triple-negative breast cancer influences a mixed M1/M2 macrophage phenotype associated with tumor aggressiveness. *PloS One*, *17*(8), e0273044. https://doi.org/10.1371/JOURNAL.PONE.0273044

Pedersen, S. A., Gaist, D., Schmidt, S. A. J., Hölmich, L. R., Friis, S., & Pottegård, A. (2018). Hydrochlorothiazide use and risk of nonmelanoma skin cancer: A nationwide case-control study from Denmark. *Journal of the American Academy of Dermatology*, *78*(4), 673-681.e9. https://doi.org/10.1016/J.JAAD.2017.11.042

Peppicelli, S., Bianchini, F., & Calorini, L. (2014). Extracellular acidity, a "reappreciated" trait of tumor environment driving malignancy: perspectives in diagnosis and therapy. *Cancer Metastasis Reviews*, *33*(2–3), 823–832. https://doi.org/10.1007/S10555-014-9506-4

Petros, J. A., Baumann, A. K., Ruiz-Pesini, E., Amin, M. B., Sun, C. Q., Hall, J., … Wallace, D. C. (2005). mtDNA mutations increase tumorigenicity in prostate cancer. *Proceedings of the National Academy of Sciences of the United States of America*, *102*(3), 719–724. https://doi.org/10.1073/PNAS.0408894102

Pickering, C. R., Zhou, J. H., Lee, J. J., Drummond, J. A., Peng, S. A., Saade, R. E., … Frederick, M. J. (2014). Mutational landscape of aggressive cutaneous squamous cell carcinoma. *Clinical Cancer Research*. https://doi.org/10.1158/1078-0432.CCR-14-1768

Pirie, K., Beral, V., Heath, A. K., Green, J., Reeves, G. K., Peto, R., … Green, A. C. (2018). Heterogeneous relationships of squamous and basal cell carcinomas of the skin with smoking: the UK Million Women Study and meta-analysis of prospective studies. *British Journal of Cancer*, *119*(1), 114–120. https://doi.org/10.1038/S41416-018-0105-Y

Porceddu, S. V., Bressel, M., Poulsen, M. G., Stoneley, A., Veness, M. J., Kenny, L. M., … Rischin, D. (2018). Postoperative Concurrent Chemoradiotherapy Versus Postoperative Radiotherapy in High-Risk Cutaneous Squamous Cell Carcinoma of the Head and Neck:

The Randomized Phase III TROG 05.01 Trial. *Journal of Clinical Oncology : Official Journal of the American Society of Clinical Oncology*, *36*(13), 1275–1283. https://doi.org/10.1200/JCO.2017.77.0941

Porporato, P. E., Payen, V. L., Pérez-Escuredo, J., De Saedeleer, C. J., Danhier, P., Copetti, T., … Sonveaux, P. (2014). A mitochondrial switch promotes tumor metastasis. *Cell Reports*, *8*(3), 754–766. https://doi.org/10.1016/J.CELREP.2014.06.043

Pospisilova, J., Vit, O., Lorkova, L., Klanova, M., Zivny, J., Klener, P., & Petrak, J. (2013). Resistance to TRAIL in mantle cell lymphoma cells is associated with the decreased expression of purine metabolism enzymes. *International Journal of Molecular Medicine*, *31*(5), 1273–1279. https://doi.org/10.3892/IJMM.2013.1302

Powers, J. M., Murphy, G., Ralph, N., O'Gorman, S. M., & Murphy, J. E. J. (2016). Mitochondrial DNA deletion percentage in sun exposed and non sun exposed skin. *Journal of Photochemistry and Photobiology. B, Biology*, *165*, 277–282. https://doi.org/10.1016/J.JPHOTOBIOL.2016.10.030

Rastogi, R. P., Richa, Kumar, A., Tyagi, M. B., & Sinha, R. P. (2010). Molecular mechanisms of ultraviolet radiation-induced DNA damage and repair. *Journal of Nucleic Acids*, *2010*. https://doi.org/10.4061/2010/592980

Rawls, J., Knecht, W., Diekert, K., Lill, R., & Löffler, M. (2000). Requirements for the mitochondrial import and localization of dihydroorotate dehydrogenase. *European Journal of Biochemistry*, *267*(7), 2079–2087. https://doi.org/10.1046/J.1432-1327.2000.01213.X

Rezvani, H. R., Kim, A. L., Rossignol, R., Ali, N., Daly, M., Mahfouf, W., … Bickers, D. R. (2011). XPC silencing in normal human keratinocytes triggers metabolic alterations that drive the formation of squamous cell carcinomas. *Journal of Clinical Investigation*. https://doi.org/10.1172/JCI40087

Rich, P. R. (2003). The molecular machinery of Keilin's respiratory chain. *Biochemical Society Transactions*, *31*(Pt 6), 1095–1105. https://doi.org/10.1042/BST0311095

Rischin, D., Khushalani, N. I., Schmults, C. D., Guminski, A., Chang, A. L. S., Lewis, K. D., … Migden, M. R. (2021). Integrated analysis of a phase 2 study of cemiplimab in advanced cutaneous squamous cell carcinoma: extended follow-up of outcomes and quality of life analysis. *Journal for Immunotherapy of Cancer*, *9*(8). https://doi.org/10.1136/JITC-2021-002757

Robsahm, T. E., Helsing, P., & Veierød, M. B. (2015). Cutaneous squamous cell carcinoma in Norway 1963-2011: increasing incidence and stable mortality. *Cancer Medicine*, *4*(3),

472–480. https://doi.org/10.1002/CAM4.404

Rodier, F., Coppé, J. P., Patil, C. K., Hoeijmakers, W. A. M., Muñoz, D. P., Raza, S. R., … Campisi, J. (2009). Persistent DNA damage signalling triggers senescence-associated inflammatory cytokine secretion. *Nature Cell Biology*, *11*(8), 973–979. https://doi.org/10.1038/NCB1909

Röwert-Huber, J., Patel, M. J., Forschner, T., Ulrich, C., Eberle, J., Kerl, H., … Stockfleth, E. (2007). Actinic keratosis is an early in situ squamous cell carcinoma: a proposal for reclassification. *The British Journal of Dermatology*, *156 Suppl 3*(SUPPL. 3), 8–12. https://doi.org/10.1111/J.1365-2133.2007.07860.X

Ruiz, E. S., Karia, P. S., Besaw, R., & Schmults, C. D. (2019). Performance of the American Joint Committee on Cancer Staging Manual, 8th Edition vs the Brigham and Women's Hospital Tumor Classification System for Cutaneous Squamous Cell Carcinoma. *JAMA Dermatology*, *155*(7), 819–825. https://doi.org/10.1001/JAMADERMATOL.2019.0032

Russell, O., & Turnbull, D. (2014). Mitochondrial DNA disease-molecular insights and potential routes to a cure. *Experimental Cell Research*, *325*(1), 38–43. https://doi.org/10.1016/J.YEXCR.2014.03.012

Schmults, C. D., Blitzblau, R., Aasi, S. Z., Alam, M., Andersen, J. S., Baumann, B. C., … Nguyen, M. Q. (2021). NCCN Guidelines® Insights: Squamous Cell Skin Cancer, Version 1.2022. *Journal of the National Comprehensive Cancer Network : JNCCN*, *19*(12), 1382–1394. https://doi.org/10.6004/JNCCN.2021.0059

Schmults, C. D., Karia, P. S., Carter, J. B., Han, J., & Qureshi, A. A. (2013a). Factors predictive of recurrence and death from cutaneous squamous cell carcinoma: a 10-year, single-institution cohort study. *JAMA Dermatology*, *149*(5), 541–547. https://doi.org/10.1001/JAMADERMATOL.2013.2139

Schmults, C. D., Karia, P. S., Carter, J. B., Han, J., & Qureshi, A. A. (2013b). Factors predictive of recurrence and death from cutaneous squamous cell carcinoma: A 10-year, single-institution cohort study. *JAMA Dermatology*, *149*(5), 541–547. https://doi.org/10.1001/jamadermatol.2013.2139

Shao, E. X., Khosrotehrani, K., Campbell, S., Isbel, N., & Green, A. (2022). Pathways from Diagnosis to Death from Keratinocyte Cancer in Kidney Transplant Recipients. *Dermatology (Basel, Switzerland)*. https://doi.org/10.1159/000524120

Singh, A., Compe, E., Le May, N., & Egly, J. M. (2015). TFIIH subunit alterations causing xeroderma pigmentosum and trichothiodystrophy specifically disturb several steps during transcription. *American Journal of Human Genetics*, *96*(2), 194–207.

https://doi.org/10.1016/J.AJHG.2014.12.012

Smolková, K., Plecitá-Hlavatá, L., Bellance, N., Benard, G., Rossignol, R., & Ježek, P. (2011). Waves of gene regulation suppress and then restore oxidative phosphorylation in cancer cells. *International Journal of Biochemistry and Cell Biology*. https://doi.org/10.1016/j.biocel.2010.05.003

Sparmann, A., & Bar-Sagi, D. (2004). Ras-induced interleukin-8 expression plays a critical role in tumor growth and angiogenesis. *Cancer Cell*, *6*(5), 447–458. https://doi.org/10.1016/j.ccr.2004.09.028

Speiser, D. E., Ho, P. C., & Verdeil, G. (2016). Regulatory circuits of T cell function in cancer. *Nature Reviews. Immunology*, *16*(10), 599–611. https://doi.org/10.1038/NRI.2016.80

Stratigos, A. J., Garbe, C., Dessinioti, C., Lebbe, C., Bataille, V., Bastholt, L., … Grob, J. J. (2020). European interdisciplinary guideline on invasive squamous cell carcinoma of the skin: Part 2. Treatment. *European Journal of Cancer*, *128*, 83–102. https://doi.org/10.1016/j.ejca.2020.01.008

Su, K. A., Habel, L. A., Achacoso, N. S., Friedman, G. D., & Asgari, M. M. (2018). Photosensitizing antihypertensive drug use and risk of cutaneous squamous cell carcinoma. *The British Journal of Dermatology*, *179*(5), 1088–1094. https://doi.org/10.1111/BJD.16713

Sykes, D. B., Kfoury, Y. S., Mercier, F. E., Wawer, M. J., Law, J. M., Haynes, M. K., … Scadden, D. T. (2016). Inhibition of Dihydroorotate Dehydrogenase Overcomes Differentiation Blockade in Acute Myeloid Leukemia. *Cell*. https://doi.org/10.1016/j.cell.2016.08.057

Tang, H., Fu, S., Zhai, S., Song, Y., Asgari, M. M., & Han, J. (2018). Use of antihypertensive drugs and risk of keratinocyte carcinoma: A meta-analysis of observational studies. *Pharmacoepidemiology and Drug Safety*, *27*(3), 279–288. https://doi.org/10.1002/PDS.4384

Tannahill, G. M., Curtis, A. M., Adamik, J., Palsson-Mcdermott, E. M., McGettrick, A. F., Goel, G., … O'Neill, L. A. J. (2013). Succinate is an inflammatory signal that induces IL-1β through HIF-1α. *Nature*, *496*(7444), 238–242. https://doi.org/10.1038/NATURE11986

Tokez, S., Wakkee, M., Kan, W., Venables, Z. C., Mooyaart, A. L., Louwman, M., … Hollestein, L. M. (2022). Cumulative incidence and disease-specific survival of metastatic cutaneous squamous cell carcinoma: A nationwide cancer registry study.

Journal of the American Academy of Dermatology, *86*(2), 331–338. https://doi.org/10.1016/J.JAAD.2021.09.067

Tomlinson, I. P. M., Alam, N. A., Rowan, A. J., Barclay, E., Jaeger, E. E. M., Kelsell, D., … Aaltonen, L. A. (2002). Germline mutations in FH predispose to dominantly inherited uterine fibroids, skin leiomyomata and papillary renal cell cancer. *Nature Genetics*, *30*(4), 406–410. https://doi.org/10.1038/NG849

Tornaletti, S., & Pfeifer, G. P. (1996). UV damage and repair mechanisms in mammalian cells. *BioEssays : News and Reviews in Molecular, Cellular and Developmental Biology*, *18*(3), 221–228. https://doi.org/10.1002/BIES.950180309

Van Kuilenburg, A. B. P., Van Lenthe, H., Löffler, M., & Van Gennip, A. H. (2004). Analysis of pyrimidine synthesis "de novo" intermediates in urine and dried urine filter-paper strips with HPLC-electrospray tandem mass spectrometry. *Clinical Chemistry*, *50*(11), 2117–2124. https://doi.org/10.1373/CLINCHEM.2004.038869

Vasan, K., Werner, M., & Chandel, N. S. (2020). Mitochondrial Metabolism as a Target for Cancer Therapy. *Cell Metabolism*, *32*(3), 341–352. https://doi.org/10.1016/J.CMET.2020.06.019

Venables, Z. C., Autier, P., Nijsten, T., Wong, K. F., Langan, S. M., Rous, B., … Leigh, I. M. (2019). Nationwide Incidence of Metastatic Cutaneous Squamous Cell Carcinoma in England. *JAMA Dermatology*, *155*(3), 298–306. https://doi.org/10.1001/jamadermatol.2018.4219

Vercellino, I., & Sazanov, L. A. (2022). The assembly, regulation and function of the mitochondrial respiratory chain. *Nature Reviews. Molecular Cell Biology*, *23*(2), 141–161. https://doi.org/10.1038/S41580-021-00415-0

Vyas, S., Zaganjor, E., & Haigis, M. C. (2016). Mitochondria and Cancer. *Cell*, *166*(3), 555–566. https://doi.org/10.1016/J.CELL.2016.07.002

Wang, C., Lin, Y., Zhu, H., Zhou, Y., Mao, F., Huang, X., … Li, C. (2022). The Prognostic and Clinical Value of Tumor-Associated Macrophages in Patients With Breast Cancer: A Systematic Review and Meta-Analysis. *Frontiers in Oncology*, *12*. https://doi.org/10.3389/FONC.2022.905846

Wang, W., Cui, J., Ma, H., Lu, W., & Huang, J. (2021). Targeting Pyrimidine Metabolism in the Era of Precision Cancer Medicine. *Frontiers in Oncology*, *11*. https://doi.org/10.3389/FONC.2021.684961

Wang, X., Yang, K., Wu, Q., Kim, L. J. Y., Morton, A. R., Gimple, R. C., … Rich, J. N. (2019). Targeting pyrimidine synthesis accentuates molecular therapy response in

glioblastoma stem cells. *Science Translational Medicine*, *11*(504). https://doi.org/10.1126/scitranslmed.aau4972

Wang, Z. C., Wang, X. M., Jiao, B. H., Jin, Y. X., Miao, M. Y., Zhu, K. J., & Ni, Q. G. (2003). Detection of mitochondrial DNA deletion by a modified PCR method in a 60Co radiation-exposed patient. *IUBMB Life*, *55*(3), 133–137. https://doi.org/10.1080/1521654031000110181

Warburg, O. (1956). On the origin of cancer cells. *Science (New York, N.Y.)*, *123*(3191), 309–314. https://doi.org/10.1126/SCIENCE.123.3191.309

Ward, P. S., & Thompson, C. B. (2012a). Metabolic reprogramming: a cancer hallmark even warburg did not anticipate. *Cancer Cell*, *21*(3), 297–308. https://doi.org/10.1016/J.CCR.2012.02.014

Ward, P. S., & Thompson, C. B. (2012b). Metabolic Reprogramming: A Cancer Hallmark Even Warburg Did Not Anticipate. *Cancer Cell*. https://doi.org/10.1016/j.ccr.2012.02.014

Watmough, N. J., & Frerman, F. E. (2010). The electron transfer flavoprotein: ubiquinone oxidoreductases. *Biochimica et Biophysica Acta*, *1797*(12), 1910–1916. https://doi.org/10.1016/J.BBABIO.2010.10.007

Weinberg, S. E., & Chandel, N. S. (2015). Targeting mitochondria metabolism for cancer therapy. *Nature Chemical Biology*, *11*(1), 9–15. https://doi.org/10.1038/NCHEMBIO.1712

Werner, R. N., Sammain, A., Erdmann, R., Hartmann, V., Stockfleth, E., & Nast, A. (2013). The natural history of actinic keratosis: a systematic review. *The British Journal of Dermatology*, *169*(3), 502–518. https://doi.org/10.1111/BJD.12420

Whitaker-Menezes, D., Martinez-Outschoorn, U. E., Flomenberg, N., Birbe, R. C., Witkiewicz, A. K., Howell, A., … Sotgia, F. (2011). Hyperactivation of oxidative mitochondrial metabolism in epithelial cancer cells in situ: visualizing the therapeutic effects of metformin in tumor tissue. *Cell Cycle (Georgetown, Tex.)*, *10*(23), 4047–4064. https://doi.org/10.4161/CC.10.23.18151

White, R. M., Cech, J., Ratanasirintrawoot, S., Lin, C. Y., Rahl, P. B., Burke, C. J., … Zon, L. I. (2011). DHODH modulates transcriptional elongation in the neural crest and melanoma. *Nature*, *471*(7339), 518–522. https://doi.org/10.1038/nature09882

Wise, D. R., Deberardinis, R. J., Mancuso, A., Sayed, N., Zhang, X. Y., Pfeiffer, H. K., … Thompson, C. B. (2008). Myc regulates a transcriptional program that stimulates mitochondrial glutaminolysis and leads to glutamine addiction. *Proceedings of the*

National Academy of Sciences of the United States of America, *105*(48), 18782–18787. https://doi.org/10.1073/PNAS.0810199105

Wu, P. A., Stern, R. S., Huang, V., Liu, K. X., Chen, C. (Amy), Tzachanis, D., … Ho, V. T. (2019). Reduced-Intensity Conditioning Regimens, Prior Chronic Lymphocytic Leukemia, and Graft-Versus-Host Disease Are Associated with Higher Rates of Skin Cancer after Allogeneic Hematopoietic Stem Cell Transplantation. *The Journal of Investigative Dermatology*, *139*(3), 591–599. https://doi.org/10.1016/J.JID.2018.08.025

Xiao, Y., Wang, Z., Zhao, M., Deng, Y., Yang, M., Su, G., … Fan, R. (2022). Single-Cell Transcriptomics Revealed Subtype-Specific Tumor Immune Microenvironments in Human Glioblastomas. *Frontiers in Immunology*, *13*. https://doi.org/10.3389/FIMMU.2022.914236

Xiao, Z., Dai, Z., & Locasale, J. W. (2019). Metabolic landscape of the tumor microenvironment at single cell resolution. *Nature Communications*, *10*(1). https://doi.org/10.1038/S41467-019-11738-0

Xu, M. J., Lazar, A. A., Garsa, A. A., Arron, S. T., Ryan, W. R., El-Sayed, I. H., … Yom, S. S. (2018). Major prognostic factors for recurrence and survival independent of the American Joint Committee on Cancer eighth edition staging system in patients with cutaneous squamous cell carcinoma treated with multimodality therapy. *Head & Neck*, *40*(7), 1406–1414. https://doi.org/10.1002/HED.25114

Yeung, S. J., Pan, J., & Lee, M. H. (2008). Roles of p53, MYC and HIF-1 in regulating glycolysis - the seventh hallmark of cancer. *Cellular and Molecular Life Sciences : CMLS*, *65*(24), 3981–3999. https://doi.org/10.1007/S00018-008-8224-X

Zhang, Z., Gao, Z., Rajthala, S., Sapkota, D., Dongre, H., Parajuli, H., … Liang, X. (2020). Metabolic reprogramming of normal oral fibroblasts correlated with increased glycolytic metabolism of oral squamous cell carcinoma and precedes their activation into carcinoma associated fibroblasts. *Cellular and Molecular Life Sciences : CMLS*, *77*(6), 1115–1133. https://doi.org/10.1007/S00018-019-03209-Y

Chapter III

Immune System and Cancer

The impact of the immune system on the development of SCC is illustrated by their high incidence in immunocompromised patients. Immunosuppressed solid organ transplant recipients (SOTRs) have a 65- to 250-fold greater incidence of cSCC than the general population, a more aggressive progression and a higher risk of metastasis and death (Lanz *et al.*, 2019). In a recent Australian study, the median time from the diagnosis of primary cSCC to metastasis in kidney transplant recipients was 5 months (0, 29), indicating the aggressive nature of cSCC in this subpopulation of patients (Shao *et al.*, 2022).

III.1. Immunity, Inflammation and Cancer

Inflammatory responses play decisive roles at different stages of tumor development, including initiation, promotion, malignant transformation, invasion, and metastasis. Inflammation also affects immune surveillance and responses to therapy. Immune cells that infiltrate tumors engage in an extensive and dynamic crosstalk with cancer cells, and some of the molecular events that mediate this dialog have recently been revealed.

Only a minority of all cancers are caused by germline mutations, whereas the vast majority (90%) are linked to somatic mutations and environmental factors and they are associated with some form of chronic inflammation. In cSCC, the induction of inflammation by bacterial or viral infections (human Papillomavirus, HPV) increases cancer risk because of its ability to trigger chronic inflammation (de Martel and Franceschi, 2009). We also know that cSCC appears in older individuals, and old age and cell senescence are postulated to be tumor promoters that act through inflammatory mechanisms (Rodier *et al.*, 2009).

III.1.a The Protumorigenic Effects of Inflammation

The inflammatory response triggered by infection precedes tumor development and is a part of normal host defense, whose goal is pathogen elimination. So how this normal reaction may promote cancer development and progression?

Solid malignancies trigger an intrinsic inflammatory response that builds up a protumorigenic microenvironment (Figure 21) (Mantovani *et al.*, 2008). Tumors can affect their microenvironment by releasing cell signaling molecules, promoting angiogenesis, and by inducing immune tolerance, while immune cells in the microenvironment can affect the growth and development of cancer cells (Mantovani *et al.*, 2008). Some immune and inflammatory

components may be dispensable during one stage of tumorigenesis but absolutely critical in another stage.

For example, the oncogene RAS induce a transcriptional program that leads to remodeling of the tumor microenvironment (TME) through recruitment of leukocytes, expression of tumor-promoting chemokines and cytokines, and induction of an angiogenic switch (Sparmann and Bar-Sagi, 2004). But in adult animals, K-Ras is unable to induce cancer unless accompanied by injury and subsequent tissue regeneration (Guerra *et al.*, 2007). So, inflammation is an important trigger for tumor formation.

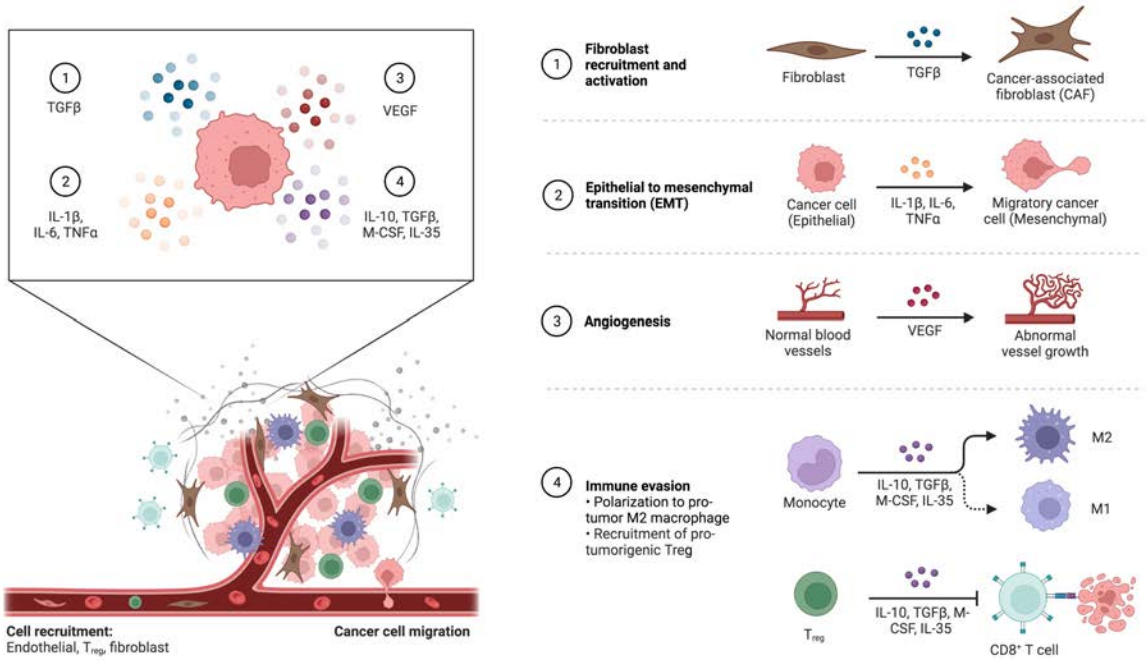

Figure 21. The Tumor Microenvironment: Overview of Cancer-associated Changes. A snapshot of the tumor microenvironment changes: induction of normal fibroblasts in cancer-associated fibroblasts; cancer cells that undergone an epithelial to mesenchymal transition; neoangiongenesis; and immune evasion phenomenon. Adapted from Mantovanni et al, 2008. IFN-γ, interferon-γ; TNF-α, tumor necrosis factor-α; LPS, lipopolysaccharide; TGF, transforming growth factor-β; VEGF, vascular endothelial growth factor.

III.1.b Immune cells in Tumorigenesis

As a result of inflammation, the TME contains innate immune cells (including macrophages, neutrophils, mast cells, myeloid-derived suppressor cells, dendritic cells, and natural killer cells) and adaptive immune cells (T and B lymphocytes) in addition to the cancer cells and their surrounding stroma (which consists of fibroblasts, endothelial cells, pericytes,

and mesenchymal cells) (Table 6). It has been suggested that an inflammatory microenvironment can increase mutation rates, in addition to enhancing the proliferation of mutated cells (De Visser, Eichten and Coussens, 2006). Activated inflammatory cells serve as sources of reactive oxygen species (ROS) and reactive nitrogen intermediates (RNI) that are capable of inducing DNA damage, damage to other macromolecules (lipid peroxidation, protein carbonylation and oxidation of the thio groups in methionine and cysteine) and genomic instability. Alternatively, inflammatory cells may use cytokines such as tumor necrosis factor-α (TNF-α) to stimulate ROS accumulation in neighboring epithelial cells or premalignant cells. In addition, inflammation can result in epigenetic changes that favor tumor initiation.

Table 6. Roles of Different Subtypes of Immune and Inflammatory Cells in Antitumor Immunity and Tumor-Promoting Inflammation

Cell Types	Antitumor	Tumor-Promoting
Macrophages, dendritic cells, myeloid-derived suppressor cells	Antigen presentation; production of cytokines (IL-12 and type I IFN)	Immunosuppression; production of cytokines, chemokines, proteases, growth factors, and angiogenic factors
Mast cells		Production of cytokines
B cells	Production of tumor-specific antibodies?	Production of cytokines and antibodies; activation of mast cells; immunosuppression
CD8+ T cells	Direct lysis of cancer cells; production of cytotoxic cytokines	Production of cytokines?
CD4+ Th2 cells		Education of macrophages; production of cytokines; B cell activation
CD4+ Th1 cells	Help to cytotoxic T lymphocytes (CTLs) in tumor rejection; production of cytokines (IFNg)	Production of cytokines
CD4+ Th17 cells	Activation of CTLs	Production of cytokines
CD4+ Treg cells	Suppression of inflammation (cytokines and other suppressive mechanisms)	Immunosuppression; production of cytokines
Natural killer cells	Direct cytotoxicity toward cancer cells; production of cytotoxic cytokines	
Natural killer T cells	Direct cytotoxicity toward cancer cells; production of cytotoxic cytokines	
Neutrophils	Direct cytotoxicity; regulation of CTL responses	Production of cytokines, proteases, and ROS

The host's defense mechanisms consist of innate immunity and adaptive immunity. The former is responsible for the initial protection against infections and pathogens. The second develops

more slowly and implements a late and more effective defense against infections thanks to the phenomenon of immunological memory (Figure 22).

However, the adaptive immune system often uses the mechanisms of innate immunity to eradicate infections. There is thus a constant bidirectional exchange between these 2 immune mechanisms.

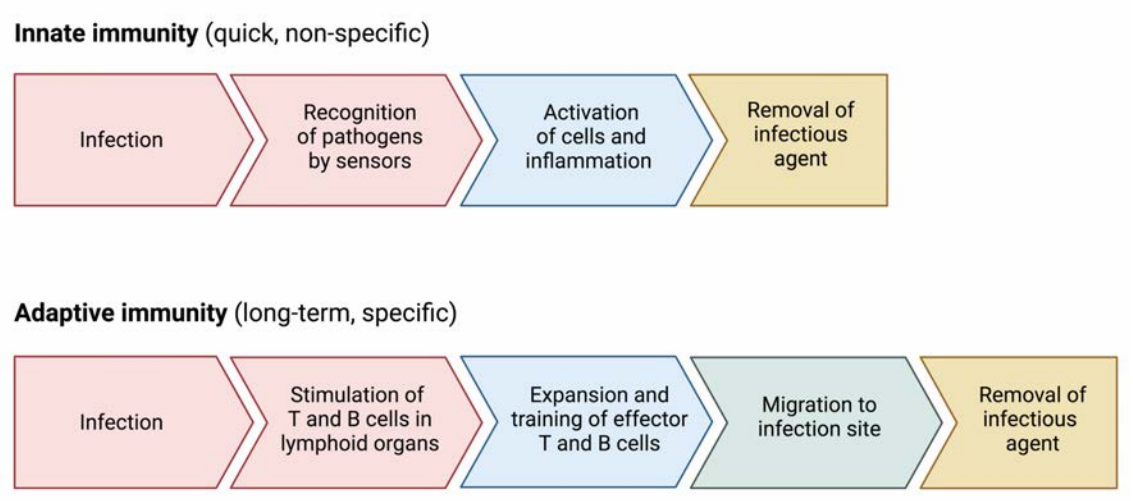

Figure 22. Innate and Adaptative Immunity. Adapted from Geltink et al, 2018.

Like the innate system, the adaptive immune system includes both humoral immunity components and cell-mediated immunity components and destroys invading pathogens. Unlike the innate immune system, which is pre-programmed to react to common broad categories of pathogen, the adaptive immune system is highly specific to each particular pathogen the body has encountered.

i. Innate Immunity

This system is composed of epithelia, dendritic cells, Natural Killer Lymphocytes, granulocytes, and monocytes. The latter two are derived from the myeloid lineage (Figure 23). This immune process is represented by phagocytosis, the non-specific inflammatory reaction (i.e., vasodilatation and local edema) and diapedesis, defined by all the mechanisms allowing immunocompetent cells to penetrate the tissues by crossing the endothelial barrier. Innate immunity is the first line of defense against physical, chemical and infectious aggression. The response to these aggressions is non-specific (independent of the nature of the antigen).

Macrophages are myeloid cells of the innate immune system, present in almost all tissues. Resident Tissue Macrophages (RTM) exhibit highly specialized functions (eg, Kupffer cells in the liver or microglia in the central nervous system). Monocytes can also be recruited to inflamed or injured tissues, where they undergo local differentiation into macrophages.

macrophages are plastic, meaning that they continuously adapt their phenotype to the demands of the tissue, as they permanently screen their environment (Monnier *et al.*, 2022).

Recent years have brought paradigm shift on macrophages functions in tissues, especially regarding the RTM, generating more complexity. Although it was assumed for decades that RTMs arose from short-lived circulating monocytes, it is now clear that most RTMs have an embryonic origin and have therefore established a long and deep relationship with the tissue of residence-the niche (Ginhoux *et al.*, 2016) (Figure 24).

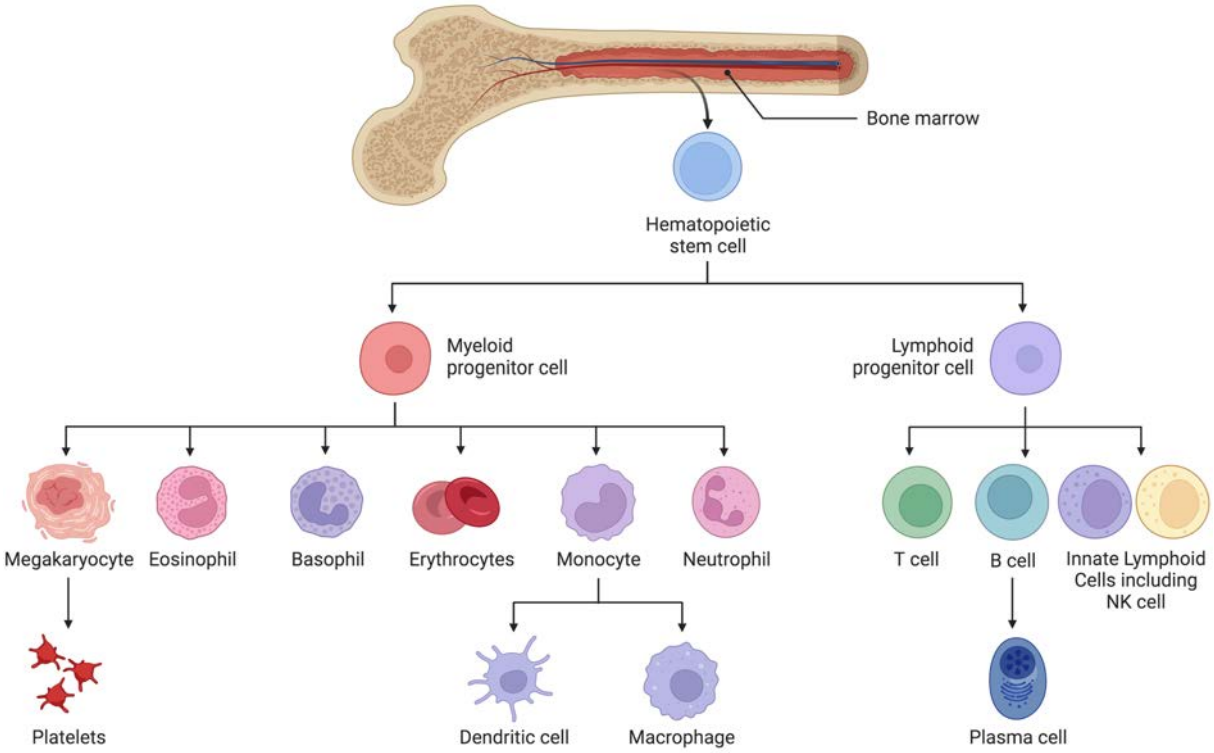

Figure 23. Stem Cells Differentiation from Bone Marrow. Adapted from Geltink et al, 2018. Hematopoietic stem cells give rise to different types of blood cells: myeloid and lymphoid progenitor cells. Myeloid cells include monocytes, macrophages, neutrophils, basophils, eosinophils, erythrocytes, and megakaryocytes to platelets. Lymphoid cells include T cells, B cells, natural killer cells, and innate lymphoid cells.

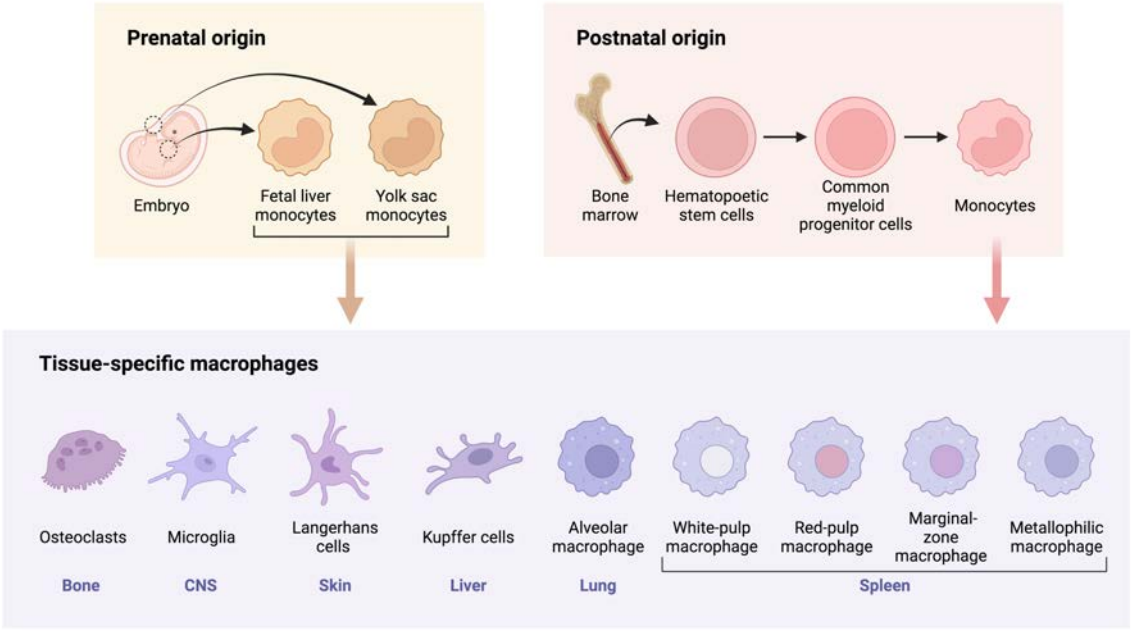

Figure 24. Origin and development of macrophages.
The resident macrophages (RTM) have an embryonic origin and a deep and long relationship with the tissue of residence, and not from short-lived circulating macrophages

ii. Adaptive Immunity

Adaptive lymphocytes

This system is derived from the lymphoid lineage and consists of T and B lymphocytes including their products, notably antibodies (Figure 23). These cells specifically recognize antigens through receptors on their cell surface that are specialized in the recognition of antigens that are specific to them (B cell receptor, BCR, and T cell receptor, TCR). Adaptive immune responses are triggered when lymphocyte antigen receptors, BCR and TCR, recognize antigens. B and T cells differ in the types of antigens they are able to recognize and the means by which they recognize the antigen to activate the immune response (Figure 25). In the subset of T cells, memory T cells play a central role in the adaptive immune response, switching from a resting phase to a highly active stage, transferring an experience gained before from a past situation to a future event. Memory T cell populations are antigen-specific T cells that remain long-term after elimination of an infection. They include central memory T cell (TCM), effector memory (TEM), and tissue resident memory (TRM). The memory T cells are quickly converted into large numbers of effector T cells upon reexposure to the specific invading antigen, thus providing a rapid response to past infection.

Innate lymphocytes

Innate lymphoid cells (ILCs) are newly identified members of the lymphoid lineage that have emerging roles in mediating immune responses and in regulating tissue homeostasis and inflammation. The ILCs produce many T Helper (TH) cell-associated cytokines, but they do not express cell-surface markers that are associated with other immune cell lineages (Walker, Barlow and McKenzie, 2013) (Figure 25). The group 1 ILC lineage comprises ILCs such as natural killer (NK) cells that produce type 1 cytokines, notably interferon-γ and tumour necrosis factor (Eberl *et al.*, 2015). ILCs activate tissue resident DCs to migrate to lymph nodes, where they elicit specific T cell responses, which in turn regulate ILCs. ILCs also directly regulate T cells through the presentation of peptide antigens on major histocompatibility complex II. However, ILCs are also involved in immunopathology, during which their production of cytokines exacerbates the inflammatory process.

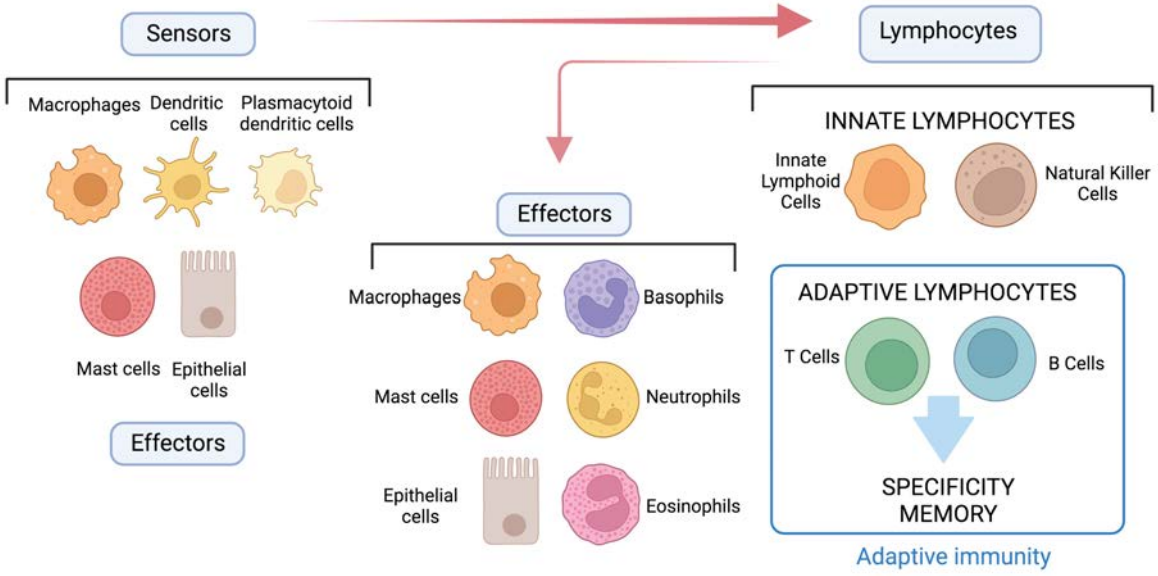

Figure 25. Immune Response. The immune Players. Adapted from Geltink et al, 2018. As with B cells and T cells, ILCs develop from the common lymphoid progenitor. ILC precursors may migrate from their primary site of production into infected and injured tissues, where they complete their maturation, similar to the differentiation of naïve T cells into T Helper effectors.

Yet it is difficult to assess the overall impact of immunity and inflammation on early tumorigenic events, because direct *in vivo* models are missing. In skin carcinogenesis, cSCC

mostly rise on a cancerization field or surrounded by precancerous lesion (Figure 26). So, studying the spatial modification rising in tumor formation is possible.

Figure 26. Cancerization field with multiples lesions at different stages of carcinogenesis (*actinic keratosis, **in situ cSCC, arrow: invasive cSCC) triggered by a chronic inflammation caused by erosive pustular dermatosis of the scalp. (Dermatology department, Pr Beylot-Barry, Bordeaux University Hospital)

iii. Tumor-associated Macrophages (TAMs)

Macrophages existing in the TME are called tumor-associated macrophages (TAMs). TAMs mostly promote tumor growth by producing inflammatory cytokines and growth factors, and may be required for angiogenesis, invasion, and metastasis (Condeelis and Pollard, 2006; Feng *et al.*, 2022); they also decrease effector $CD8^+$T cell recruitment and function (Mantovani *et al.*, 2017). High TAM content generally correlates with poor prognosis in several malignancies (glioblastoma, breast cancer, hepatocarcinoma, melanoma) (Mota *et al.*, 2016; Pe *et al.*, 2022; Wang *et al.*, 2022; Xiao *et al.*, 2022). They are one of the most important players in the inflammation in the cancer area and an important source of cytokines. TAMs participate in tumor progression by regulating the expression of chemokines, growth factors and scavenger receptors, and tumor cells regulate TAMs polarization, by releasing various cytokines (Mantovani *et al.*, 2017).

For a long time, macrophages have been classified into M1 and M2 types (Figure 27) (Feng *et al.*, 2022). Traditionally, M1 macrophages, activated by interferon-γ (IFN- γ) and microbial products, express high levels of proinflammatory cytokines (TNF-α, IL-1, IL-6, IL-12 or IL-23), major histocompatibility complex (MHC) molecules, and inducible nitric oxide

synthase, and are capable of killing pathogens and priming antitumor immune responses. By contrast, M2 or ‘‘alternatively’’ activated macrophages, which are induced *in vitro* by IL-4, IL-10, and IL-13, downregulate MHC class II and IL-12 expression and show increased expression of the anti-inflammatory cytokine IL-10. But this classification is now obsolete because originally defined by in vitro generated murine macrophage subsets (Monnier *et al.*, 2022). Cancer development is associated with a sustained inflammation and profound immune suppression involving Th1, Th17 and Treg cells, rather than Th2 accumulation (Murray *et al.*, 2014). Moreover, although the expression of IL-4 and IL-13 has been detected in some cancers, M2 cells generated in the presence of IL-4 are considered as tissue repair macrophages rather than protumor macrophages. Altogether, recent single-cell analysis studies in different tumors confirmed that human TAM exhibit mixed M1-like and M2-like signatures, showing the importance that the definition of TAMs cannot be reduced to macrophage polarization alone (Müller *et al.*, 2017; Azizi *et al.*, 2018).

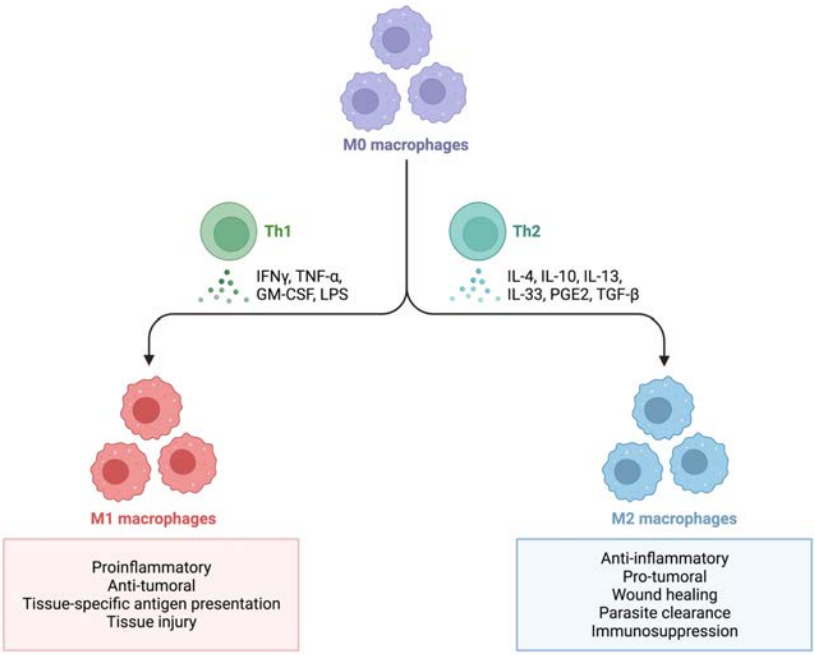

Figure 27. Macrophages Polarization by T-helper Cells. Created with Biorender. The M1/M2 classification was originally defined by in vitro generated murine macrophage subsets and is based on well characterized phenotypic signatures. However, such signatures are rarely, if ever, observed in human macrophages. Abbreviations: IFN-γ, interferon-γ; TNF-α, tumor necrosis factor-α; LPS, lipopolysaccharide; TGF, transforming growth factor-β.

Taken together, tumor-associated inflammation drives tumor growth and angiogenesis and can perpetuate itself through an extensive network of cytokines and chemokines, which are produced by immune, stromal, and malignant cells in response to several and different signals.

III.2. Energy Metabolism in Immune Cells

Metabolic reprogramming occurs in the immune system as cells transition from resting state to stimulated effectors (Andrejeva and Rathmell, 2017). Immunometabolism describes the changes that occur in intracellular metabolic pathways in immune cells during activation.

2.a An Overview of Metabolism of Immune Cell Subtypes

Six major pathways have been studied in immune cells in detail: glycolysis, the tricarboxylic acid (TCA) cycle, the pentose phosphate pathway, fatty acid oxidation, fatty acid synthesis and amino acid metabolism (O'Neill, Kishton and Rathmell, 2016). Historically, oxygen levels and nutrient supply were seen as the key drivers of metabolic pathways. Normoxia supports the tricarboxylic acid (TCA) cycle and oxidative phosphorylation, whereas hypoxia leads to the activation of hypoxia-inducible factor 1α (HIF1α) and the expression of glycolytic enzymes. More recently, it has become apparent that immune stimuli can also cause metabolic reprogramming in cells (Figure 28) (Krawczyk *et al.*, 2010). For example, stimulation of cells with interleukin-4 (IL-4) can induce oxidative phosphorylation, whereas the activation of cells through pattern recognition receptors (PRRs), such as Toll-like receptor 4 (TLR4), induces HIF-1α expression to promote glycolysis (Tannahill *et al.*, 2013).

Glycolysis and fatty acid synthesis seem to be key features of lipopolysaccharide (LPS)-activated macrophages; by contrast, interleukin-4 (IL-4)-activated macrophages mainly use oxidative phosphorylation and fatty acid oxidation to generate energy (Figure 28). Effector T cells are highly glycolytic whereas memory T cells have an oxidative metabolism (Michalek *et al.*, 2011).

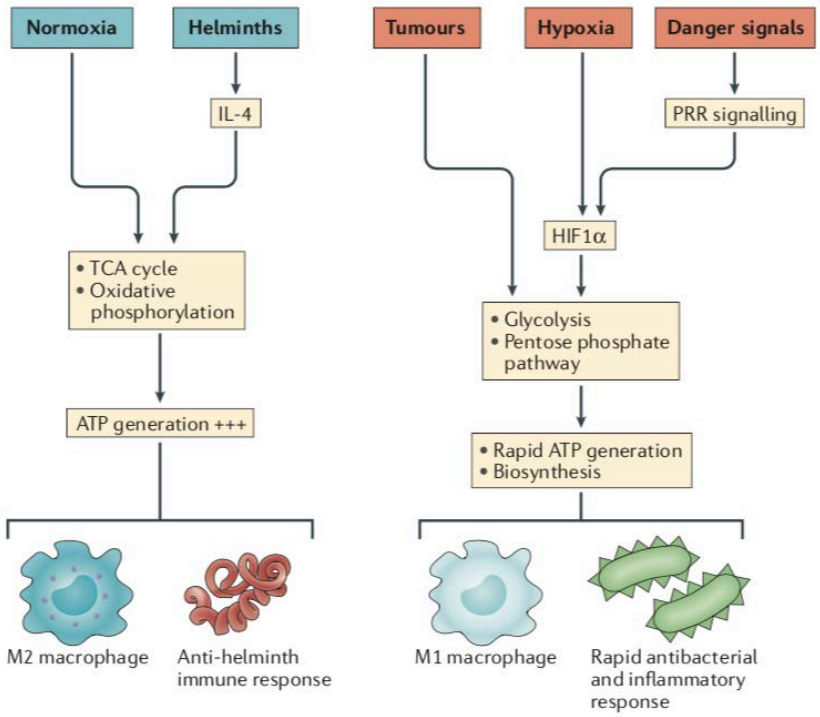

Figure 28. Metabolic Reprogramming by the Immune System. Adapted from O'Neill et al, 2016. Glycolysis also predominates in tumors under normoxia in the form of aerobic glycolysis, presumably giving tumors a growth advantage in oxygen-replete tissues. Abbreviations: PPRs, pattern recognition receptors; IL-4, interleukine-4.

Inflammatory macrophages use glycolysis, the TCA cycle, the pentose phosphate pathway, fatty acid synthesis and amino acid metabolism to proliferate and to support the production of inflammatory cytokines.

M2 macrophages, which exhibit a more tolerant phenotype, use the TCA cycle, fatty acid oxidation and arginine flux into the arginase pathway.

Rapidly proliferating effector T cells, including T helper 1 (TH1), TH17 and cytotoxic $CD8^+$ T cells, use glycolysis, fatty acid synthesis and amino acid metabolism to promote proliferation and cytokine production.

Immunosuppressive regulatory T (Treg) cells use the TCA cycle and fatty acid oxidation. Similarly, **memory CD8+ T cells** also require the use of the TCA cycle and fatty acid oxidation to promote increased cell lifespan.

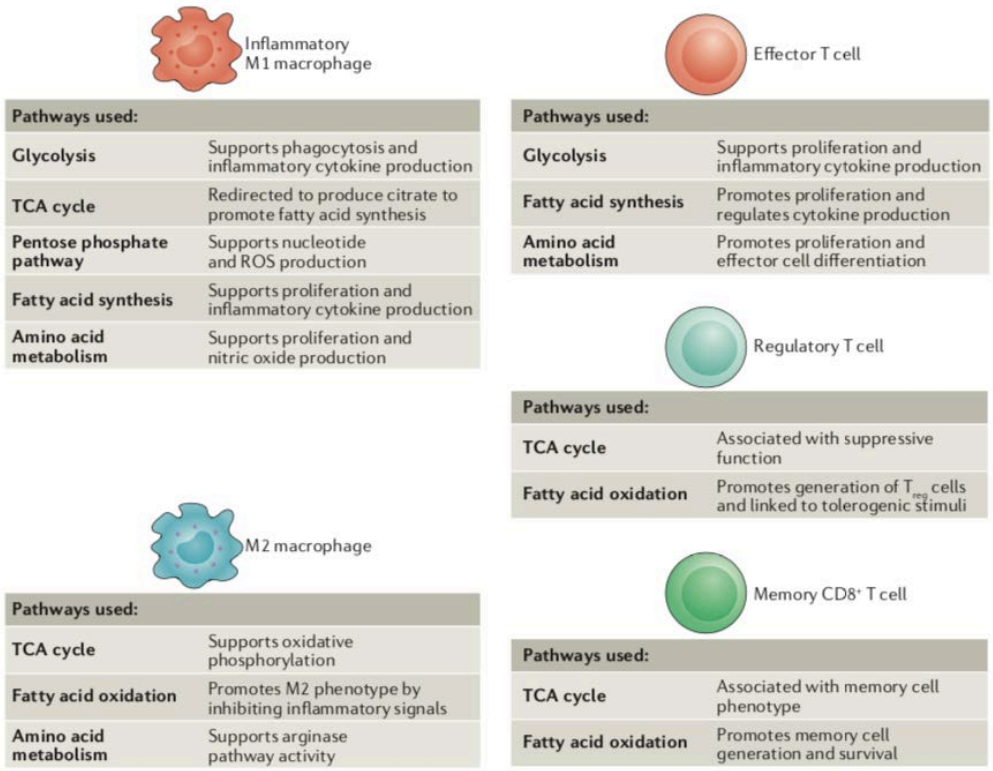

Figure 29. An overview of Metabolism of Immune Cell Subtypes.
Adapted from O'Neill et al, 2016. The various immune cell subsets exhibit a reliance on distinct metabolic pathways to promote cell survival, lineage generation and function. Abbreviations: ROS, reactive oxygen species.

2.b Metabolism in T cells

Because of their different functions, memory T-cell subsets have distinct metabolic propensities, influenced by their environmental conditions and transcriptional regulation. The most predominant form of metabolism in memory T cells is mitochondrial oxidative phosphorylation (OXPHOS), fueled by a number of substrates derived from carbon sources including amino acids, fatty acids and glucose (Figure 30) (O'Sullivan, 2019). Memory T cells are composed by: TRM, resident memory T cells; TCM, central memory T cells; TEM, effector memory T cells. TCM, which are typically long-lived and exhibit robust proliferative response and cytokine production, rely on OXPHOS. On the contrary, TRM and TCM have a preference for fatty acid oxidation and so utilization of exogenous fatty acids is required for TRM survival. Finally, the development of TEM required an upregulation of aerobic glycolysis as they have to exhibit rapid expression of effector function.

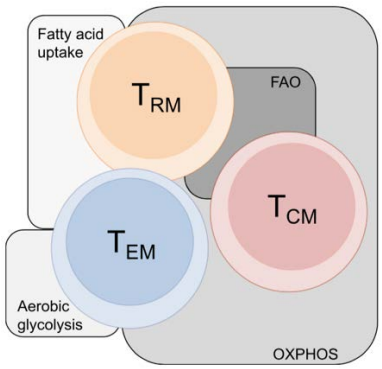

Figure 30. Major Metabolic Pathways used for Memory T Cells.
Distinct metabolic propensities depending on memory T cells function. Abbreviations: TRM, resident memory T cells; TCM, central memory T cells; TEM, effector memory T cells, FAO, fatty acid oxidation; OXPHOS, oxidative phosphorylation. Adapted from O'Sullivan et al, 2019.

Activation of T Cell Subtypes

$CD8^+$ T cells

Naïve $CD8^+$ T cells rely on OXPHOS and use glucose to generate energy to maintain homeostatic proliferation and survival. Upon activation, $CD8^+$ T cells increase OXPHOS and progressively increase their glycolytic rate. Fully differentiated $CD8^+$ T effector cells utilize glycolysis and OXPHOS. When CD8+ T cells switch on a "T memory state", they decrease their glycolytic rate, coinciding with the engagement with FAO to fuel OXPHOS. At this time they are endowed with more spare respiratory capacity in order to have the capacity to rapidly change their state when been called (Figure 31a) (Geltink, Kyle and Pearce, 2018).

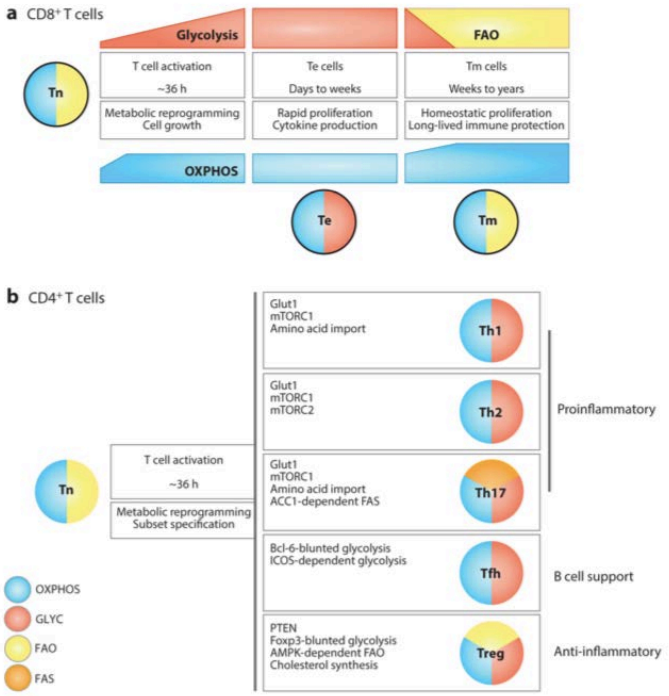

Figure 31. Metabolic phenotypes of CD8+ and CD4+ subtypes. Adapted from Geltink RI et al, 2018. Naïve $CD8^+$T cells and naïve $CD4^+$ T cells rely on OXPHOS. Metabolic reprogramming occurs upon activation: $CD8^+$T cells increase OXPHOS and steadily increase their glycolytic rate and $CD4^+$T cells differentiate into diverse subsets with distinct metabolic requirements.
Abbreviations: ACC1, acetyl-CoA carboxylase 1; AMPK, adenosine monophosphate–activated protein kinase; Bcl-6, B-cell CLL/lymphoma 6; FAO, fatty acid oxidation; FAS, fatty acid synthesis; Foxp3, forkhead box P3; ICOS, inducible T cell costimulator; OXPHOS, oxidative phosphorylation; SRC, spare respiratory capacity; Te, effector T cell; Tfh, T follicular helper cell; Th, T helper cell; Tm, memory T cell; Tn, naive T cell; Treg, regulatory T cell.

$CD4^+$ T Cells

Like CD8+ naïve T cells, CD4+ naïve T cells rely on OXPHOS and use glucose to generate energy to maintain homeostatic proliferation and survival. Upon activation, CD4+ T cells differentiate into diverse subsets with distinct roles and metabolic requirements (Figure 31b) (Geltink, Kyle and Pearce, 2018). While all subsets engage glycolysis, Th2 and Th17 cells display high levels of glucose uptake. The master transcription factors of the Treg (Foxp3) and Tfh (Bcl-6) cell lineages repress glycolytic gene transcription, although depending on context Tregs also engage glycolysis. All subsets sustain OXPHOS at varying levels. Tregs engage FAO for suppressive function, whereas Th17 cells rely on de novo fatty acid synthesis (FAS). The balance of FAO and FAS contributes to the divergence between Th17 and Tregs.

III.2.c T Cell Metabolism during an Immune Response

When naïve T cells are activated (thanks to antigen-presenting cells) in secondary lymphoid organs such as lymph nodes or spleen, they proliferate and differentiate into T effector cells and travel to peripheral tissues to mediate immune response (Figure 32) (Geltink, Kyle and Pearce, 2018). During this immune response, Tregs regulate inflammation to limit tissue damage. After the resolution of the infection, long-lived $CD8^+$ T memory cells form and remain metabolically quiescent until they reencounter antigen and become reactivated, at which time they rapidly reengage glycolysis and promote OXPHOS. In TME, limited reliance on glycolysis allows Tregs to persist in the glucose-depleted environment, whereby they inhibit antitumor T effector cell function.

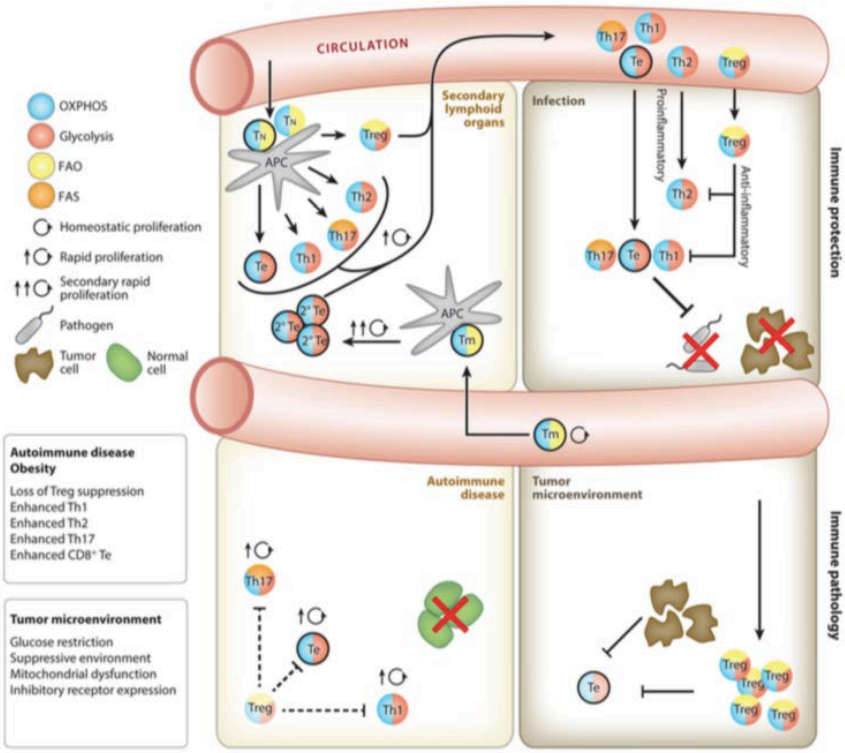

Figure 32. T cell metabolism during an immune response. Adapted from Geltink et al, 2018. Tregs inhabit tumors, and the accumulation of suppressive Tregs in the TME is associated with poor prognosis, as Tregs blunt effector T cell (Te) responses. Abbreviations: APC, antigen-presenting cell; FAO, fatty acid oxidation; FAS, fatty acid synthesis; OXPHOS, oxidative phosphorylation; Te, effector T cell; Th, T helper cell; Tm, memory T cell; Tn, naive T cell; Treg, regulatory T cell.

III.2.d Microenvironmental Factors instructing T Cell Dysfunction.

In the TME, T cell functions are regulated by nutrient availability, immune-modulatory cells and cytokines. These factors interact with each other to deactivate antitumour T cell responses. Immunostimulatory nutrients that support T cell expansion and activation are depleted by high consumption rates of tumour cells and immunosuppressive cells. In addition, tumour and immunosuppressive cells produce multiple immunosuppressive metabolites and cytokines, altering the transcriptional landscape of the T cells and promoting their dysfunction (Figure 33) (Speiser, Ho and Verdeil, 2016).

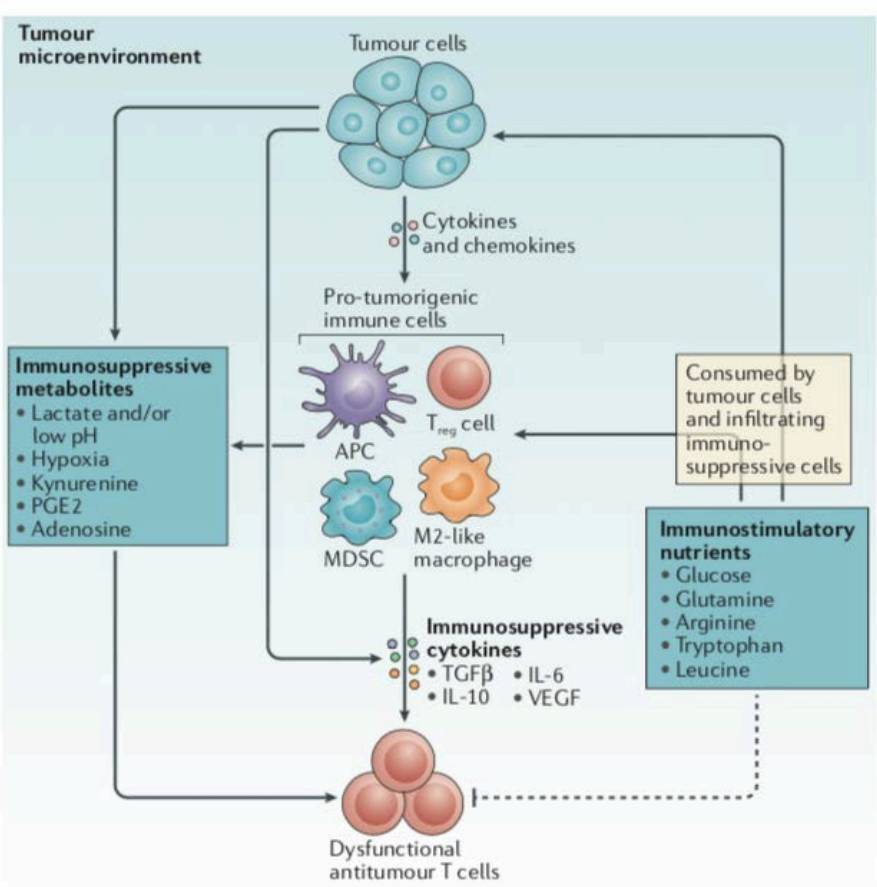

Figure 33. High concentrations of immunosuppressive metabolites accumulate in the tumor microenvironment and nutrient deprivation promote T cell dysfunction and facilitate cancer growth. Adapted from Speiser et al, 2016.
Abbreviations: APC, antigen-presenting cell; IL, interleukin; MDSC, myeloid-derived suppressor cell; PGE2, prostaglandin E2; TGFβ, transforming growth factor-β; Treg cell, regulatory T cell; VEGF, vascular endothelial growth factor.

Conclusion

All immune cells and metabolic reprogramming can be considered separately, but we know that they are interlinked and co-regulated adding to the complexity. Immune cells also communicate with their environment, especially with epithelial cells.

References

Andrejeva, G. and Rathmell, J. C. (2017) 'Similarities and Distinctions of Cancer and Immune Metabolism in Inflammation and Tumors', *Cell metabolism*. Cell Metab, 26(1), pp. 49–70. doi: 10.1016/J.CMET.2017.06.004.

Azizi, E. *et al.* (2018) 'Single-Cell Map of Diverse Immune Phenotypes in the Breast Tumor Microenvironment', *Cell*. Cell, 174(5), pp. 1293-1308.e36. doi: 10.1016/J.CELL.2018.05.060.

Condeelis, J. and Pollard, J. W. (2006) 'Macrophages: obligate partners for tumor cell migration, invasion, and metastasis', *Cell*. Cell, 124(2), pp. 263–266. doi: 10.1016/J.CELL.2006.01.007.

Eberl, G. *et al.* (2015) 'Innate lymphoid cells. Innate lymphoid cells: a new paradigm in immunology', *Science (New York, N.Y.)*. Science, 348(6237). doi: 10.1126/SCIENCE.AAA6566.

Feng, Y. *et al.* (2022) 'The Role of TAMs in Tumor Microenvironment and New Research Progress', *Stem cells international*. Edited by M. Muddassir Ali. Stem Cells Int, 2022, pp. 1–11. doi: 10.1155/2022/5775696.

Geltink, R. I. K., Kyle, R. L. and Pearce, E. L. (2018) 'Unraveling the Complex Interplay Between T Cell Metabolism and Function', *Annual review of immunology*. Annu Rev Immunol, 36, pp. 461–488. doi: 10.1146/ANNUREV-IMMUNOL-042617-053019.

Ginhoux, F. *et al.* (2016) 'New insights into the multidimensional concept of macrophage ontogeny, activation and function', *Nature immunology*. Nat Immunol, 17(1), pp. 34–40. doi: 10.1038/NI.3324.

Guerra, C. *et al.* (2007) 'Chronic pancreatitis is essential for induction of pancreatic ductal adenocarcinoma by K-Ras oncogenes in adult mice', *Cancer cell*. Cancer Cell, 11(3), pp. 291–302. doi: 10.1016/J.CCR.2007.01.012.

Krawczyk, C. M. *et al.* (2010) 'Toll-like receptor-induced changes in glycolytic metabolism regulate dendritic cell activation', *Blood*. Blood, 115(23), pp. 4742–4749. doi: 10.1182/BLOOD-2009-10-249540.

Lanz, J. *et al.* (2019) 'Aggressive Squamous Cell Carcinoma in Organ Transplant Recipients', *JAMA dermatology*. JAMA Dermatol, 155(1), pp. 66–71. doi: 10.1001/JAMADERMATOL.2018.4406.

Mantovani, A. *et al.* (2008) 'Cancer-related inflammation', *Nature*. Nature, 454(7203), pp.

436–444. doi: 10.1038/NATURE07205.
Mantovani, A. *et al.* (2017) 'Tumour-associated macrophages as treatment targets in oncology', *Nature reviews. Clinical oncology*. Nat Rev Clin Oncol, 14(7), pp. 399–416. doi: 10.1038/NRCLINONC.2016.217.
de Martel, C. and Franceschi, S. (2009) 'Infections and cancer: established associations and new hypotheses', *Critical reviews in oncology/hematology*. Crit Rev Oncol Hematol, 70(3), pp. 183–194. doi: 10.1016/J.CRITREVONC.2008.07.021.
Michalek, R. D. *et al.* (2011) 'Cutting edge: distinct glycolytic and lipid oxidative metabolic programs are essential for effector and regulatory CD4+ T cell subsets', *Journal of immunology (Baltimore, Md. : 1950)*. J Immunol, 186(6), pp. 3299–3303. doi: 10.4049/JIMMUNOL.1003613.
Monnier, M. *et al.* (2022) 'Antitumor strategies targeting macrophages: the importance of considering the differences in differentiation/polarization processes between human and mouse macrophages', *Journal for immunotherapy of cancer*. J Immunother Cancer, 10(10). doi: 10.1136/JITC-2022-005560.
Mota, J. M. *et al.* (2016) 'Post-Sepsis State Induces Tumor-Associated Macrophage Accumulation through CXCR4/CXCL12 and Favors Tumor Progression in Mice', *Cancer immunology research*. Cancer Immunol Res, 4(4), pp. 312–322. doi: 10.1158/2326-6066.CIR-15-0170.
Müller, S. *et al.* (2017) 'Single-cell profiling of human gliomas reveals macrophage ontogeny as a basis for regional differences in macrophage activation in the tumor microenvironment', *Genome biology*. Genome Biol, 18(1). doi: 10.1186/S13059-017-1362-4.
Murray, P. J. *et al.* (2014) 'Macrophage activation and polarization: nomenclature and experimental guidelines', *Immunity*. Immunity, 41(1), pp. 14–20. doi: 10.1016/J.IMMUNI.2014.06.008.
O'Neill, L. A. J., Kishton, R. J. and Rathmell, J. (2016) 'A guide to immunometabolism for immunologists', *Nature Reviews Immunology 2016 16:9*. Nature Publishing Group, 16(9), pp. 553–565. doi: 10.1038/nri.2016.70.
O'Sullivan, D. (2019) 'The metabolic spectrum of memory T cells', *Immunology and cell biology*. Immunol Cell Biol, 97(7), pp. 636–646. doi: 10.1111/IMCB.12274.
Pe, K. C. S. *et al.* (2022) 'Triple-negative breast cancer influences a mixed M1/M2 macrophage phenotype associated with tumor aggressiveness', *PloS one*. Edited by D. Heymann. PLoS One, 17(8), p. e0273044. doi: 10.1371/JOURNAL.PONE.0273044.
Rodier, F. *et al.* (2009) 'Persistent DNA damage signalling triggers senescence-associated

inflammatory cytokine secretion', *Nature cell biology*. Nat Cell Biol, 11(8), pp. 973–979. doi: 10.1038/NCB1909.

Shao, E. X. *et al.* (2022) 'Pathways from Diagnosis to Death from Keratinocyte Cancer in Kidney Transplant Recipients', *Dermatology (Basel, Switzerland)*. Dermatology. doi: 10.1159/000524120.

Sparmann, A. and Bar-Sagi, D. (2004) 'Ras-induced interleukin-8 expression plays a critical role in tumor growth and angiogenesis', *Cancer Cell*. Cell Press, 6(5), pp. 447–458. doi: 10.1016/j.ccr.2004.09.028.

Speiser, D. E., Ho, P. C. and Verdeil, G. (2016) 'Regulatory circuits of T cell function in cancer', *Nature reviews. Immunology*. Nat Rev Immunol, 16(10), pp. 599–611. doi: 10.1038/NRI.2016.80.

Tannahill, G. M. *et al.* (2013) 'Succinate is an inflammatory signal that induces IL-1β through HIF-1α', *Nature*. Nature, 496(7444), pp. 238–242. doi: 10.1038/NATURE11986.

De Visser, K. E., Eichten, A. and Coussens, L. M. (2006) 'Paradoxical roles of the immune system during cancer development', *Nature reviews. Cancer*. Nat Rev Cancer, 6(1), pp. 24–37. doi: 10.1038/NRC1782.

Walker, J. A., Barlow, J. L. and McKenzie, A. N. J. (2013) 'Innate lymphoid cells--how did we miss them?', *Nature reviews. Immunology*. Nat Rev Immunol, 13(2), pp. 75–87. doi: 10.1038/NRI3349.

Wang, C. *et al.* (2022) 'The Prognostic and Clinical Value of Tumor-Associated Macrophages in Patients With Breast Cancer: A Systematic Review and Meta-Analysis', *Frontiers in oncology*. Front Oncol, 12. doi: 10.3389/FONC.2022.905846.

Xiao, Yong *et al.* (2022) 'Single-Cell Transcriptomics Revealed Subtype-Specific Tumor Immune Microenvironments in Human Glioblastomas', *Frontiers in immunology*. Front Immunol, 13. doi: 10.3389/FIMMU.2022.914236.

GENERAL DESCRIPTION OF THESIS PROJECT, RESEARCH HYPOTHESIS, APPLIED METHODOLOGIES, AND ACHIEVEMENTS

Historical context

In a recent project, on which I worked during my master 2, we found, using a multistage model of UVB radiation-induced skin cancer, that specific metabolic modifications (upregulation of the distal part of the electron transport chain in the mitochondria) was preceding primary skin tumor formation, and that DHODH plays a critical role in this UVB-induced energy metabolism reprogramming (Hosseini *et al.*, 2018). The importance of DHODH for nucleotide biosynthesis suggests that its inhibition could be a promising target for cancer therapy. To test this hypothesis, at the beginning of my thesis, I continued working on that project aiming at testing the effect of leflunomide (LFN), an inhibitor of the enzyme DHODH and a FDA-approved drug for the treatment of rheumatoid arthritis, on the growth of cSCC cell lines transplanted into immunodeficient mice (please see first article presented in the result section). Altogether, our results in these two papers suggested that DHODH can be targeted for both skin tumor prevention and curative combination therapy to develop metabolic targeted therapies for cSCC.

As a logical follow-up of these results, I then decided to focus on two following objectives:
-To characterize the molecular and metabolic features of human cSCCs at different stages of carcinogenesis (Second article in results section)
-To identify at a single-cell resolution the early metabolic changes of cancer progression and immunoediting (third article in results section)

Biological resources and the major used techniques for my thesis projects:

To achieve my objectives, following models and approaches were used:
In vitro: We used several human cSCC cell lines (such as A431, SCC15, PM1, MET1, MET2, MET4, IC1, IC1Met, IC12, IC18).
In vivo: Well-defined SKH-1 mouse multistep photocarcinogenesis model, transplantation of patient-derived tumor cell (PDC) and in-house patient-derived xenograft (PDX) into immuno-deficient mice were used.

Down- and up-regulation of proteins: Specific lentiviral vectors were delivered to cSCC cell lines.

Metabolic characterization: Metabolism reprogramming were assessed by multiplex techniques of mRNA and protein expressions, enzymatic activities of key proteins involved in OXPHOS, extracellular flux analyzer Seahorse and measurement of ATP concentration. Proteomic and metabolomics approaches such as LC-MS/MS mass spectrometry were also used.

Analysis at single-cell resolution: Digital spatial profiling (DSP) on paraffin-embedded samples and single-cell RNA sequencing (scRNA-seq) from fresh dissociated cells from locally advanced tumor-precancerous skin-paired lesions were used.

Summary of achievements:

My works will be presented in the result section within three articles:

1- **UVB-induced DHODH upregulation, which is driven by STAT3, is a promising target for chemoprevention and combination therapy of photocarcinogenesis**

This first article, which is published in Oncogenesis in 2019, presents the results obtained during my master 2 and the onset of my thesis. In this article, we sought to identify if metabolic vulnerabilities of cSCC could be targeted as a therapeutic strategy. Precisely, we asked whether inhibiting DHODH prevent the tumor formation and whether the observed phenotype in leflunomide-treated mice was due to decreased pyrimidine biosynthesis.

2- **Metabolism-based scoring of cutaneous squamous cell carcinoma to predict tumor features and responses to treatment by DHODH inhibitor**.

In the second article (*in preparation*), we wondered whether cSCCs at different stages of carcinogenesis exhibit heterogeneous metabolic features? And if so, what is the functional impact of metabolic profiles on tumor features? Our last objective in this work was to identify whether sensitivity of a tumor to a particular treatment (here DHODH inhibition) is dependent on its metabolic profile?

3- **The early metabolic changes of progression and immunoediting in advanced cutaneous squamous cell carcinoma at single-cell resolution**

Single-cell transcriptomics has been recently used to identify intra-tumoral heterogeneity (ITH) within many cancer types, to characterize cell populations that drive drug resistance, and cancer metastasis. However, little is known about the difference between precancerous

lesion AKs and cSCC at single cell resolution. Therefore, in the third article (*in preparation*), we sought to identify the difference between composition and spatial architecture of precancerous lesion AKs and cSCC as well as the metabolic changes in the era of cSCC. To this end, we performed single-cell and spatial transcriptomics (ST) on a series of primary human cSCCs, along with matched precancerous or in situ surrounded lesion. We used digital spatial profiling (DSP) and single-cell RNA sequencing (scRNA-seq) to maximize the resolution and depth of data.

ARTICLE 1

UVB-induced DHODH upregulation, which is driven by STAT3, is a promising target for chemoprevention and combination therapy of photocarcinogenesis

Published in Oncogenesis

Hosseini et al. *Oncogenesis* (2019)8:52
https://doi.org/10.1038/s41389-019-0161-z

ARTICLE Open Access

UVB-induced DHODH upregulation, which is driven by STAT3, is a promising target for chemoprevention and combination therapy of photocarcinogenesis

Mohsen Hosseini[1], Léa Dousset[1], Pauline Michon[1], Walid Mahfouf[1], Elodie Muzotte[1], Vanessa Bergeron[1], Doriane Bortolotto[1], Rodrigue Rossignol[2], François Moisan[1], Alain Taieb[1,3,4], Anne-Karine Bouzier-Sore[5] and Hamid R. Rezvani[1,3]

Abstract

The leading cause of cutaneous squamous cell carcinomas (cSCCs) is exposure to ultraviolet radiation (UV). Unlike most other cancers, the incidence rates of cSCCs are still on the rise and the treatment options currently available are limited. We have recently found that dihydroorotate dehydrogenase (DHODH), which is the rate-limiting enzyme in the de novo pyrimidine synthesis pathway, plays a critical role in UVB-induced energy metabolism reprogramming. Using a multistage model of UVB radiation-induced skin cancer, we show that UVB-induced DHODH upregulation is mainly regulated transcriptionally by STAT3. Our results indicate that chronic inhibition of DHODH by leflunomide (LFN) blocks UVB-induced tumor initiation. Human tumor xenograft studies showed that LFN treatment reduces growth of established tumors when used in combination with a genotoxic agent, 5-fluorouracil (5-FU). Our data suggest that DHODH is a promising target for chemoprevention and combination therapy of UVB-induced cSCCs.

Introduction

Exposure to ultraviolet (UV) radiation from the sun is the most significant risk factor resulting in non-melanoma skin cancers (NMSCs), including basal cell carcinomas and cutaneous squamous cell carcinomas (cSCCs), the most common types of human malignancies worldwide. An estimated 5.4 million cases of NMSCs were affecting 3.3 million patients among the US population in 2012[1]. The rate of NMSCs is increasing by 5–7% per year, mainly due to UV exposure and population ageing[2]. cSCCs typically manifest as a spectrum of progressively advanced malignancies, ranging from precursor actinic keratosis (AK) to in situ, invasive, and finally metastatic cSCCs[3]. A recent US study estimated that 3900–9000 patients died from cSCCs in 2012[4]. Thus, it is crucial to preserve the general high chances of cure of cSCCs by a careful evaluation and proper early management of all cases, and not underestimate the potential aggressiveness of this tumor[5,6].

The most commonly used therapies to treat AKs, such as cryotherapy, laser or FDA-approved topical 5-fluorouracil (5-FU) or imiquimod[7], have significant painful side-effects and a high level of post-treatment recurrence. For cSCCs, surgery is the curative treatment, followed by radiotherapy and chemotherapy, which are mainly used as adjuvant or palliative treatment in advanced cSCCs[7]. The most commonly used chemotherapy agents for cSCCs in stage III and IV with nodal or distant metastasis are 5-FU/cisplatin, 5-FU/carboplatin, and paclitaxel/carboplatin combinations[8]. Targeted therapies such as epidermal growth factor receptor (EGFR) inhibitors have shown efficacy but no sustained

Correspondence: Hamid R. Rezvani (hamid-reza.rezvani@u-bordeaux.fr)
[1]Univ. Bordeaux, INSERM, BMGIC, UMR 1035, F-33076 Bordeaux, France
[2]Univ. Bordeaux, INSERM, MRGM, U1211, F-33076 Bordeaux, France
Full list of author information is available at the end of the article.

remission. More recently, immunotherapy and checkpoint inhibitors showed promising results[9]. Overall, these data suggests the urgent necessity to improve the level of prevention and protection for skin cancer and the evaluation of new therapeutic strategies.

Leflunomide (LFN), an FDA-approved drug for the treatment of rheumatoid arthritis, is an inhibitor of the enzyme dihydroorotate dehydrogenase (DHODH)[10–12]. As the rate-limiting enzyme in the de novo pyrimidine synthesis pathway, DHODH catalyzes the conversion of dihydroorotate to orotate in the fourth step of the six enzymatic reactions of this pathway. Inhibition of DHODH prevents the synthesis of pyrimidines and consequently impairs the synthesis of pyrimidine derivatives, such as the nucleotide bases cytosine and thymine. We have recently shown that this enzyme, which is located in the inner mitochondrial membrane, plays a critical role in UVB-induced energy metabolism reprogramming[13]. Indeed, upregulation of DHODH was shown to be important in maintaining higher electron transport chain (ETC) activity in irradiated skin and in ensuring the coordination of ATP generation and persistent nucleotide biosynthesis. The latter is indeed necessary for the repair of damaged DNA, which is one of the major deleterious effects of exposure to UVB[13]. The most frequent lesions arising from UVB exposure are cyclobutane pyrimidine dimers (CPDs) and pyrimidine (6–4) pyrimidone photoproducts (6-4PPs). They are mainly repaired by the nucleotide excision DNA repair (NER) pathway whose action results in the release of a 24-mer to 32-mer oligonucleotide comprising the damaged base(s) and its replacement by a newly synthesized DNA[14].

In this study, we show that UVB-induced DHODH upregulation is mainly regulated transcriptionally by STAT3. Furthermore, we show that inhibition of DHODH by LFN blocks UVB-induced tumorigenic transformation of keratinocytes. Given the importance of DHODH for nucleotide biosynthesis, we finally tested the efficiency of LFN for the therapy of cSCC. Results indicate that the growth of established A431 and SCC-15 cell xenografts is significantly reduced when LFN is used in combination with a genotoxic agent. Our data demonstrate the potential of DHODH as a novel target for the prevention and combination therapy of UVB-induced cSCCs.

Results

UVB irradiation results in DHODH upregulation

We have recently shown that UVB-induced skin tumorigenesis is associated with altered metabolism[13] and that DHODH fuels mitochondrial respiration to coordinate DNA repair and ATP synthesis. To investigate the effects of chronic UVB irradiation on DHODH expression, SKH-1 hairless mice which closely mimic photocarcinogenesis in humans[13] were irradiated three times a week with 150 mJ/cm^2 UVB. We measured the expression and the activity of DHODH in mouse skin at different stages of UVB-induced carcinogenesis (Fig. 1a–c). DHODH mRNA (Fig. 1a) and protein expression (Fig. 1b) levels as well as its enzyme activity (Fig. 1c) were markedly upregulated at a very early phase of UVB-induced tumorigenesis and this up-regulation persisted during the subsequent steps of carcinogenesis. As already mentioned, DHODH catalyzes the conversion of dihydroorotate to orotate in the fourth step of pyrimidine synthesis, in which glutamine and aspartate are used as precursors (Fig. 1d). Functional activation of this pathway was then verified by tracing analysis. To this end, epidermal cells isolated from non-irradiated and irradiated mice were incubated for 5 h in the medium supplemented with labeled [1,4-^{13}C] aspartate. Results indicated that orotate, a central intermediate of pyrimidine synthesis, became labeled on carbons 2 and 5 only in irradiated cells (Fig. 1e). Given that specific DHODH activity was only about 1.5-fold higher in irradiated skin than in non-irradiated skin (Fig. 1f), we concluded that DHODH was mainly regulated transcriptionally in irradiated skin.

UVB-induced transcriptional upregulation of DHODH is driven by STAT3

To establish what accounts for *DHODH* gene overexpression following irradiation, software analysis of the promoter region of *DHODH* gene was performed. Results revealed that eight putative interferon-gamma-activated sequences (GAS), with the general consensus sequence of TTNNNNNAA[15], are located in the 1.4 kb region upstream from the ATG translation initiation codon (Fig. 2a, b). Of note, the protein family that can bind to GAS sequences is the signal transducer and activator of transcription (STAT). Among the members of this family, STAT3 has been shown to play a critical role during UVB-induced carcinogenesis. Indeed, *Stat3*-deficient mice were resistant to UVB-induced skin carcinogenesis and, inversely, the formation of skin tumors was accelerated in mice overexpressing *STAT3*[16]. These data prompted us to examine whether STAT3 may account for *DHODH* overexpression in irradiated skin by direct binding to the promoter region of *DHODH*. To examine this hypothesis, we first verified the expression of STAT3 and its phosphorylated form at tyrosine-705 (pY-STAT3) at different stages of carcinogenesis. STAT3 and pY-STAT3 were upregulated at a very early phase of UVB-induced tumorigenesis and this up-regulation persisted at different stages of carcinogenesis (Fig. 2c). We then performed ChIP experiments with the primers spanning eight putative GAS (Fig. 2a, d). While the region containing GAS-6 and 7 immunoprecipitated in both non-irradiated and irradiated skin, immunoprecipitation of GAS-2 to GAS-5

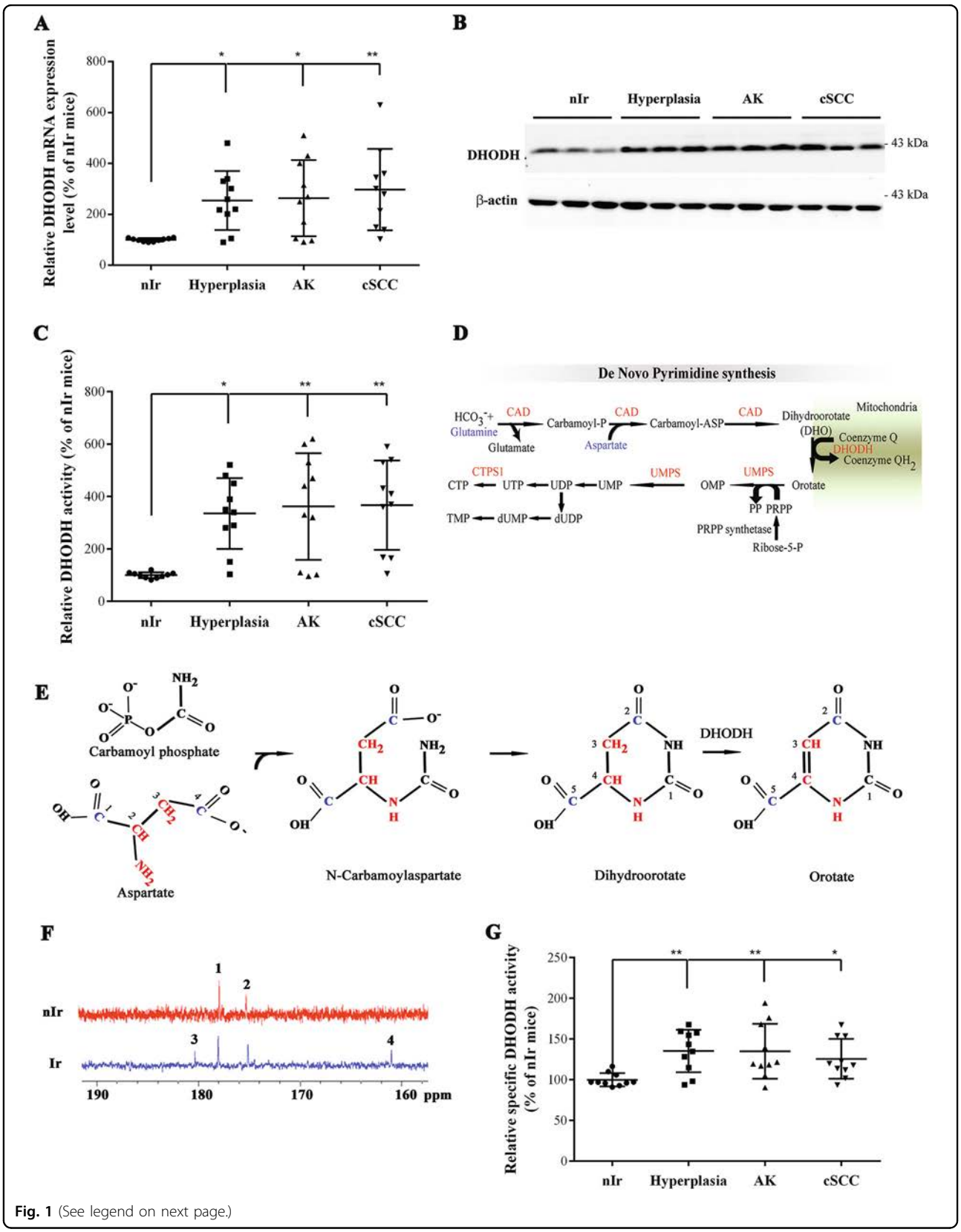

Fig. 1 (See legend on next page.)

(see figure on previous page)

Fig. 1 Chronic UVB exposure results in DHODH overactivation SKH-1 mice exposed to chronic UVB irradiation. a The relative levels of DHODH mRNA were quantified by quantitative reverse transcription PCR. **b** Total protein extracts of skin biopsies at different stages of tumorigenesis were assessed for expression of DHODH by western blot. β-actin was used as a loading control. Full-length blots are presented in Fig. S1. **c** DHODH activity was measured in skin biopsies at different stages of UVB-induced carcinogenesis. **d** DHODH is the only mitochondrial enzyme of the de novo pyrimidine synthesis pathway that converts dihydroorotate to orotate. **e**, **f** Cells were incubated for 4 h with [1,4-^{13}C] aspartate. **e** Schematic depicting atoms of orotate that are derived from aspartate and carbamoyl phosphate. Blue color represents labeled carbons from aspartate, red color represents non-labeled carbons and nitrogen from aspartate, and black color represents carbon and nitrogen derived from carbamoyl phosphate. **f** ^{13}C-NMR spectra of perchloric acid cell extract after 4 h of incubation with [1,4-^{13}C] aspartate. nIr non-irradiated cell, Ir irradiated cell. 1: Aspartate C4, 2: Aspartate C1, 3: orotate C2, and 4: orotate C5. **g** Specific DHODH activity was measured by normalization of DHODH activity to its expression level in each sample. $N = 10$ [(A–C, G)] and 6 [(F)] mice per group $^{*}P < 0.05$ and $^{**}P < 0.01$ for irradiated versus non-irradiated mice. PRPP phophoribosylpyrophosphate, CAD carbamoyl-phosphate synthetase 2, aspartate transcarbamylase, and dihydroorotase, CTPS1 CTP synthase, DHODH DHO dehydrogenase, OMP orotidine 5′-monophosphate, UMPS uridine 5′-monophosphate synthase

was substantially increased in UVB-irradiated skin. Luciferase reporter plasmid, in which the 1.4 kb region upstream from the ATG translation initiation codon of *DHODH* had been cloned upstream of luciferase, was then used to further characterize the role of GASs in the regulation of *DHODH* expression following UVB-irradiation. This construct was transiently transfected into epidermal cells isolated from non-irradiated and irradiated mice. Results revealed that the basal activity of this promoter in irradiated cells was higher than that of non-irradiated cells (Fig. 2e). STAT3 downregulation or truncating the promoter to −450 bp led to a significant decrease in basal activity of this promoter and totally abrogated the chronic UVB irradiation-induced upregulation of the luciferase activity (Fig. 2e). Of note, to rule out "off target" effects of siSTAT3, these experiments were performed with two distinct siRNAs against STAT3. Since both siRNAs had similar effects, only the results of one of them have been shown in this figure. Moreover, substituting two T nucleotides in the GAS-2, 3, 4, and 5 of the luciferase reporter plasmid for two G nucleotides totally abrogated the chronic UVB irradiation-induced upregulation of the luciferase activity (Fig. 2e). Overall, our results show that STAT3 plays a positive role both in basal and chronic UVB-induced DHODH expression.

Inhibition of DHODH activity blocks UVB-induced tumor formation

To investigate the impact of DHODH upregulation on the susceptibility to UVB-induced skin cancer, DHODH activity was inhibited using LFN, a non-specific inhibitor of DHODH and an FDA-approved drug for the treatment of rheumatoid arthritis. LFN (20 mg/kg/day) was administered intraperitoneally each day and 1 h before each UVB exposure. In the absence of UVB exposure, neither placebo nor the LFN treatment showed any adverse effect on skin (data not shown). Assessment of DHODH activity at 8 weeks after irradiation indicated its efficient inhibition in LFN-treated mice (Fig. 3a). Monitoring placebo-treated and LFN-treated mice during chronic UVB irradiation indicated that the latter failed to develop malignant lesions (Fig. 3b–d). Indeed, while none of the placebo-treated mice had any obvious abnormalities up to week 12 of irradiation, 7 out of the 12 mice exhibited at least one AK lesion at 18 weeks (Fig. 3c–e). More than 90% of these mice had an average of 14 tumors of variable size, exhibiting an exponential increase in size at 28 weeks of irradiation (Fig. 3e–h). In contrast, 8 out of the 12 LFN-treated mice developed moderate squamous hyperkeratotic plaques 12 weeks after UVB irradiation (Fig. 3b–d). Eighteen weeks after chronic UVB irradiation, all these mice presented desquamative features with a hyperkeratotic epidermis (Fig. 3b–d). However, only 1 of these 12 mice displayed three keratotic tumors up to 28 weeks after irradiation (Fig. 3c, g).

Pyrimidine supplementation restores UVB-induced tumorigenic transformation of keratinocytes in LFN-treated mice

Since DHODH is a critical enzyme in the pyrimidine de novo biosynthesis pathway, we next sought to investigate whether the DHODH inhibition-mediated reduction in pyrimidine synthesis and subsequent decreased DNA repair efficiency could explain the absence of tumor formation in LFN-treated mice despite their UVB-hypersensitive phenotype. To test this hypothesis, we first assessed the repair capacity of placebo-treated and LFN-treated mice irradiated for 12 weeks by quantifying the levels of CPDs in the whole skin (Fig. 3i). Results obtained by immuno-dot blot indicated a substantial increase in the CPD level in epidermal DNA of LFN-treated mice compared to control counterparts.

To test functionally whether the observed phenotype in LFN-treated mice was due to the decreased pyrimidine biosynthesis, supplementation with uridine (i.p. injection of 100 mg/kg/day uridine) was tested. Of note, uridine levels in the plasma peaked rapidly after each injection and returned to pretreatment levels within 8 h (Fig. 4a). Monitoring the mice during chronic UVB irradiation indicated that supplementation with uridine blocked the

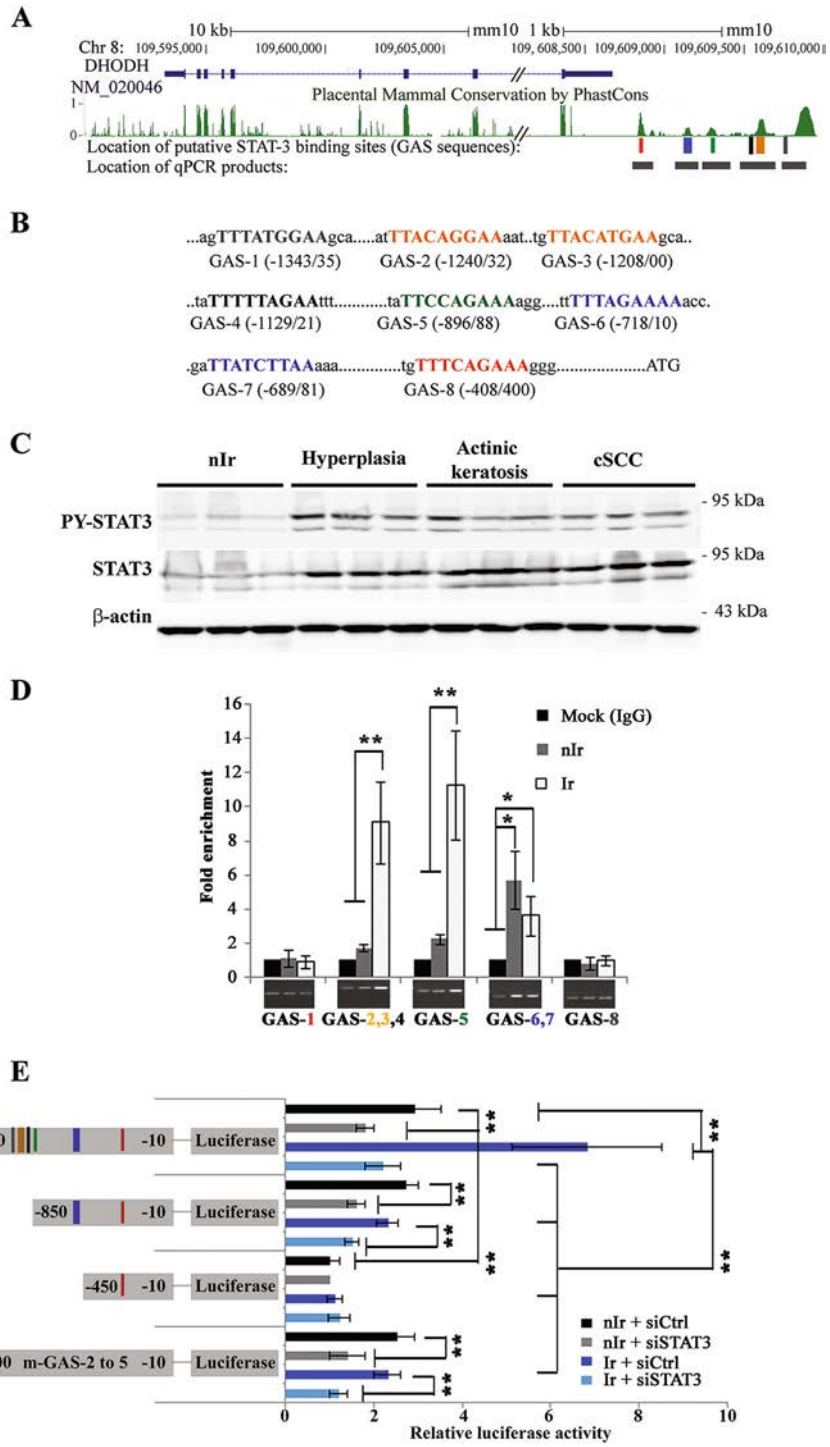

Fig. 2 UVB-induced DHODH overexpression is regulated via a STAT3-dependent mechanism. a Representation of the DHODH gene and its promoter in the UCSC genome browser, including location of the eight motifs matching the consensus STAT3-binding site [TTNNNNNAA)] and the location of PCR products for ChIP-qPCR. **b** Eight nucleotide-sequences matching the consensus STAT3-binding site (GAS-1–GAS-8) in the upstream region of mouse DHODH gene are numbered in relation to the translational start codon, ATG. **c** The expression of STAT3 was assessed in mouse skin specimens at different stages of tumorigenesis. Upregulation of STAT3 expression persisted at different stages of UVB-induced carcinogenesis. Full-length blots are presented in Fig. S2. **d** Irradiated and non-irradiated skin were subjected to ChIP assay using an anti-STAT3 antibody. Bands indicate PCR products using primers that span the indicated GASs. The relative levels of corresponding precipitated GAS fragments following ChIP were quantified by qRT-PCR. **e** Luciferase reporter plasmids containing indicated fragments were transfected into siCtrl-transfected or siSTAT3-transfected keratinocytes isolated from irradiated or non-irradiated skin. $N = 6$ mice per group. $^{*}P < 0.05$ and $^{**}P < 0.01$

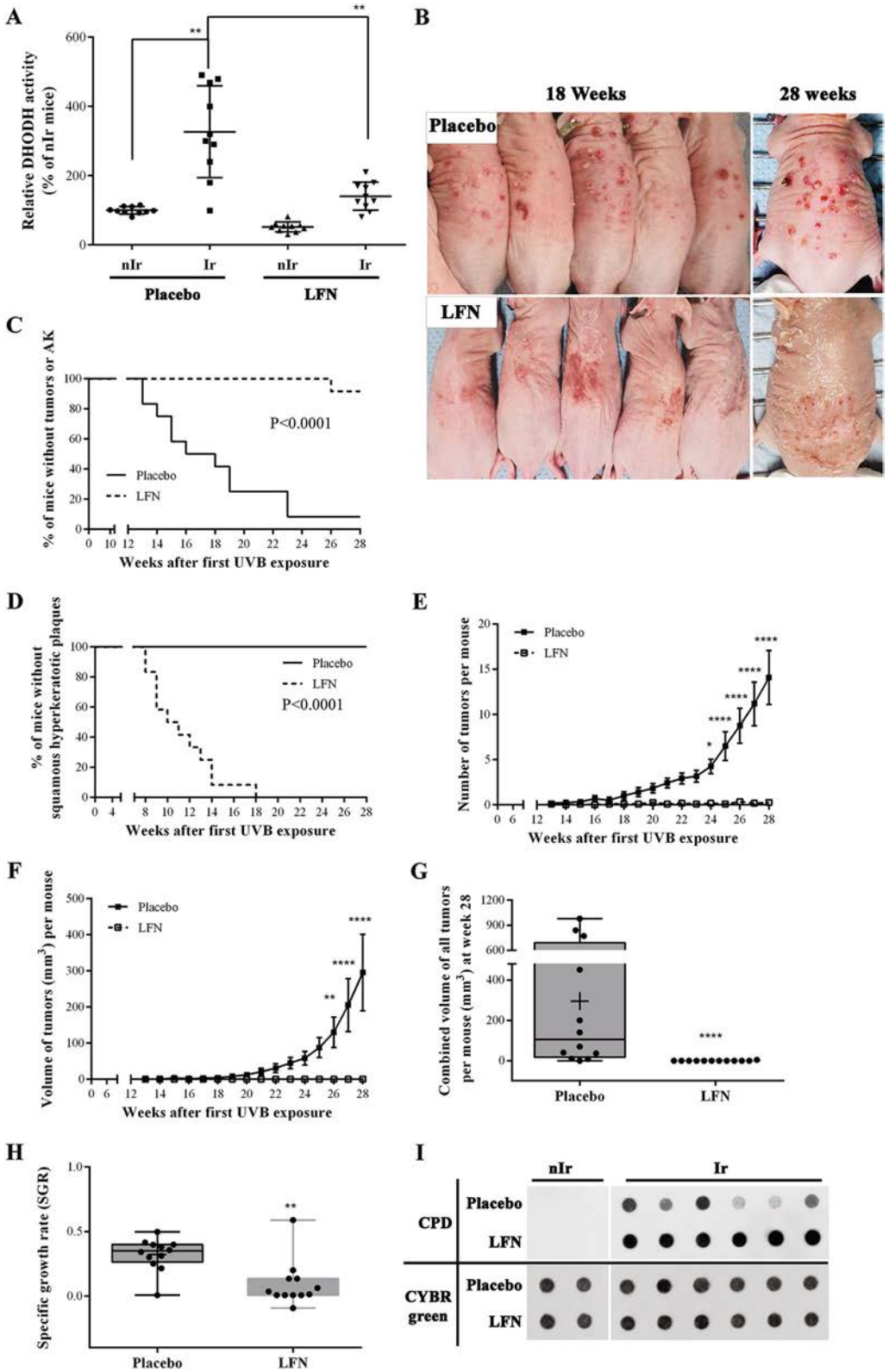

Fig. 3 (See legend on next page.)

(see figure on previous page)
Fig. 3 Inhibition of DHODH using LFN treatment results in hypersensitivity to UVB exposure. One-month-old SKH-1 mice were subjected to chronic UVB irradiation ± intraperitoneal injection of either LFN (20 mg/kg/day) or placebo. **a** The relative DHODH activity in irradiated and non-irradiated skin was measured at 8 weeks after irradiation. Increased DHODH activity in UVB-irradiated skin samples was blocked following treatment of mice with LFN. **b** Photographs are representative examples of placebo-treated and LFN-treated mice after 18 and 28 weeks of chronic UVB irradiation. **c**, **d** The percentage of tumor-free mice **c** and desquamative feature-free mice **d** were assessed at indicated times. **e**, **f** the numbers **e**, and the combined volumes **f** of tumors per mouse were recorded at different intervals. **g** The distribution of the mean volume of all single tumors/mouse is presented at week 28 of chronic UVB irradiation. **h** The specific tumor growth rate SGR was estimated for each mouse according to the following equation: SGR = Ln2/DT, in which DT = doubling time. **i** Cyclopyrimidine dimer (CPD) levels were quantified in mouse skin at 8 weeks of chronic UVB irradiation by immuno-dot blot analysis. Full-length blots are presented in Fig. S3. $N = 12$ [(A–I)] mice per group $^{*}P < 0.05$, $^{**}P < 0.01$, and $^{****}P < 0.0001$

formation of hyperkeratotic plaques (Fig. 4b). Indeed, assessment of the incidence, number, volume, and growth rate of tumors revealed no significant difference between the group receiving LFN and uridine and mice treated with uridine alone (Fig. 4c–g). Furthermore, there was no significant difference between the two groups concerning the efficiency to remove the UV photoproduct (Fig. 4h).

Altogether, these results showed that uridine supplementation restored UVB-induced tumor formation in LFN-treated mice and blocked formation of hyperkeratotic plaques in them.

Synergistic anti-tumoral effect of LFN and 5-FU on established human tumors

We then sought whether LFN could slow the progression of human SCC. To this end, we first characterized the effect of LFN on the viability of A431 and SCC-15 cell lines. As a control, we used the genotoxic anti-cancer drug 5-flurouracil (5-FU). Neither A431 nor SCC-15 were sensitive to LFN (Fig. 5a, b). However, when LFN was used in combination with 5-FU, a remarkable synergistic effect was detected (Fig. 5a, b). The most statistically significant combination of LFN and 5-FU was 50 µM LFN and 1 µM 5-FU, i.e. a ratio of 50:1.

To test the effect of LFN on SCC growth in vivo, we transplanted both cell lines into immunocompromised mice. After 4 weeks of tumor growth, mice were divided into four groups receiving either placebo alone, LFN alone, 5-FU alone, or combined LFN and 5-FU (10 animals/group) (Fig. 6a). As shown in Fig. 6b, c, body weight loss was not observed in any treatment group. Moreover, any difference in mouse behavior among the different groups was noted, suggesting that all treatments were well-tolerated. In the placebo group, the average A431 tumor volume increased from 239 mm^3 on day 0–760 mm^3 on day 18, indicating a steady increase in tumor growth over the course of the experiment (Fig. 6d). LFN treatment alone did not reduce tumor volume when compared to placebo-treated tumors. In contrast, 5-FU treatment significantly reduced the average tumor volume, even though the tumors continued to grow during the course of the experiment. However, when combined LFN and 5-FU was administered, tumor growth was suppressed, with tumor volumes remaining steady at the same size over the 18-day treatment period (Fig. 6d, e). When weighed at the end of experiment, tumors weighed significantly less in mice treated with combined LFN and 5-FU than in the other groups (Fig. 6f). Similar results were obtained when SCC-15 were transplanted into NSG mice and treated with placebo, LFN, 5-FU, and 5-FU plus LFN (Fig. 6g–i), even though these tumors were more sensitive to 5-FU than the A431 tumors.

Taken together, our data show that the combination of LFN and 5-FU prevents tumor growth in vivo.

Discussion

We found that DHODH was upregulated at a very early phase of UVB-induced carcinogenesis and its inhibition blocked the tumorigenic transformation of damaged keratinocytes. Indeed, despite manifesting hyperkeratosis, mice treated with an inhibitor of DHODH developed neither actinic keratosis nor skin tumors following exposure to chronic UVB irradiation.

There is now growing evidence showing that several branches of metabolism are affected during malignant transformation to support both the energy demands of cancer cells and their anaplerotic fluxes, which that are necessary for providing cellular building blocks, such as nucleic acids, proteins, and membranes[17–19]. We have already shown that reprogramming of the energy metabolism occurs at a very early phase of UVB-induced carcinogenesis and that mice harboring an impaired ETC fail to develop premalignant and malignant lesions owing to their decreased DNA repair capacity and increased apoptotic cell death[13]. We now show that inhibition of the mitochondrial DHODH enzyme, which couples the de novo pyrimidine biosynthesis pathway to ETC fluxes, results in decreased DNA repair capacity and prevents tumor formation in mice chronically exposed to UVB. The appearance of tumors and the blocking of hyperkeratotic plaque development in LFN-treated mice upon uridine supplementation confirms the importance of nucleotide biosynthesis in determining the fate of cells upon exposure to genotoxic stressors such as UV

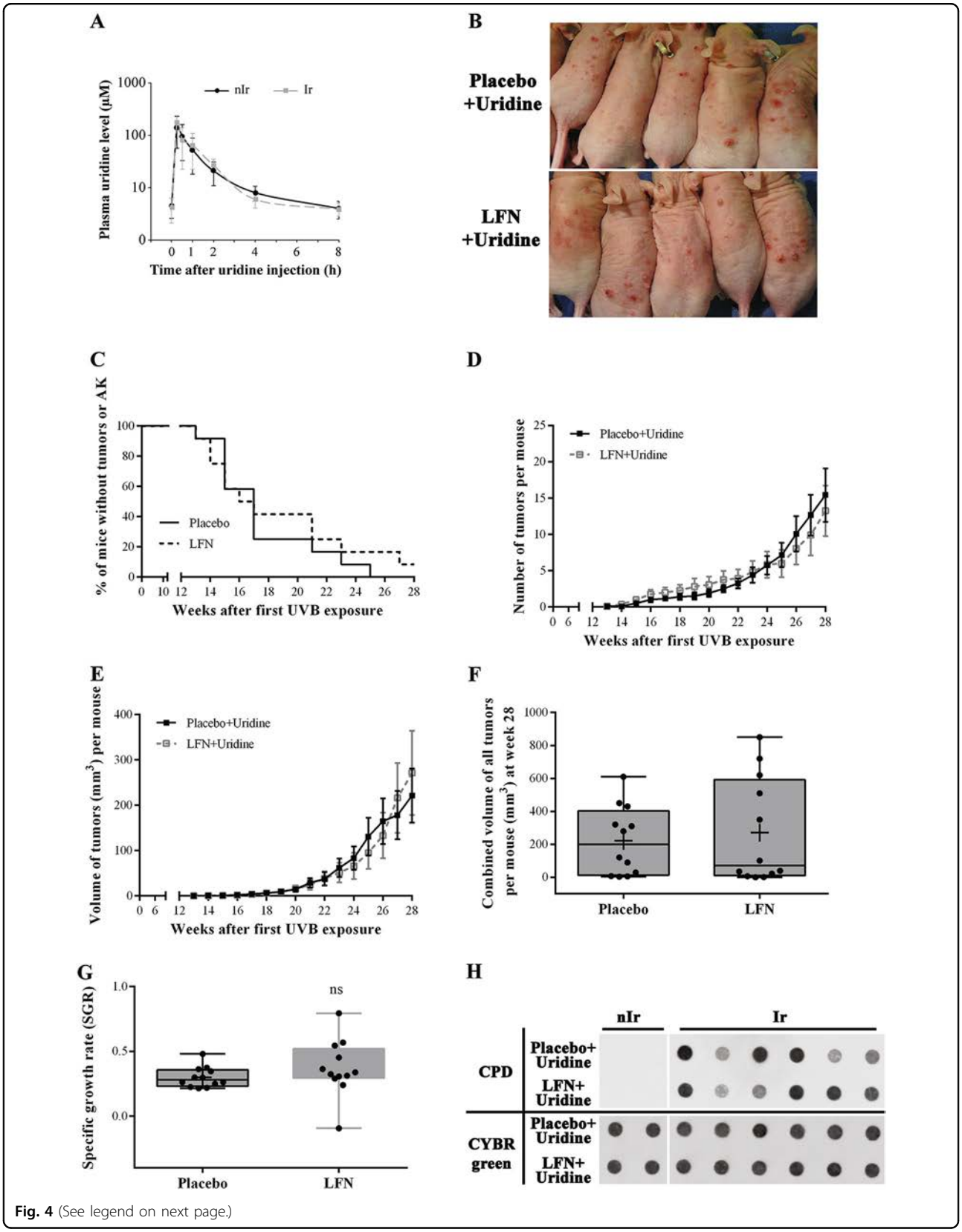

Fig. 4 (See legend on next page.)

(see figure on previous page)

Fig. 4 Uridine supplementation largely restored DHODH inhibition-mediated decreased DNA repair capacity and hypersensitivity to UVB. One-month-old SKH-1 mice were subjected to chronic UVB irradiation + intraperitoneal injection of either LFN (20 mg/kg/day) or placebo + intraperitoneal uridine. **a** Time courses of plasma uridine concentrations after an i.p. injection of exogenous uridine at week 8 of chronic UVB exposure. **b** Photographs are representative examples of mice treated with either placebo + uridine or LFN + uridine after 18 weeks of chronic UVB irradiation. **c–e** The percentage of tumor-free mice **c**, the tumor numbers **d**, and the volume **e** of tumors per mouse were assessed at indicated times. **f** The distribution of the mean volume of all single tumors/mouse is presented at week 28 of chronic UVB irradiation. **g** The specific tumor growth rate SRG was estimated for each mouse. **h** Immuno-dot blot analysis reveals the same quantity of cyclopyrimidine dimer (CPD) in both LFN-treated and placebo-treated mice supplemented with uridine upon chronic UVB irradiation. Full-length blots are presented in Fig. S3. $N = 12$[(A–H)] mice per group

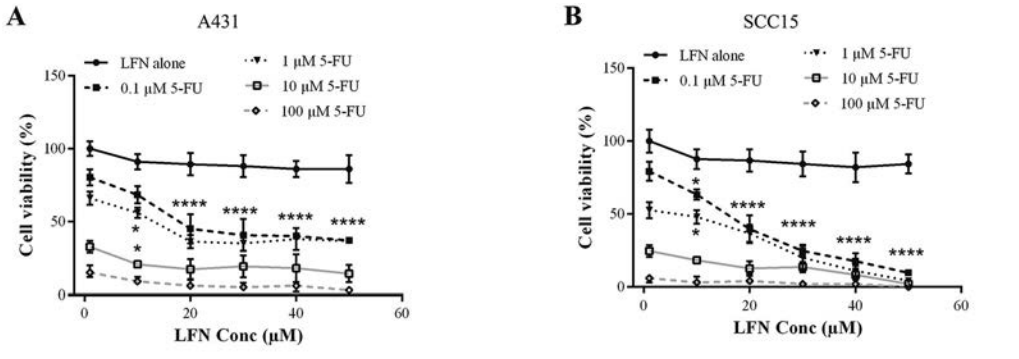

Treatment condition	IC50 (μM)	Treatment condition	IC50 (μM)
LFN alone	n/a	5-FU alone	4.46
LFN+0.1μM 5-FU	13.26	5-FU+10μM LFN	1.05
LFN+1μM 5-FU	11.47	5-FU+20μM LFN	0.19
LFN+10μM 5-FU	n/a	5-FU+30μM LFN	0.11
LFN+100μM 5-FU	n/a	5-FU+40μM LFN	0.09
		5-FU+50μM LFN	0.08

Treatment condition	IC50 (μM)	Treatment condition	IC50 (μM)
LFN alone	n/a	5-FU alone	1.01
LFN+0.1μM 5-FU	17.22	5-FU+10μM LFN	0.86
LFN+1μM 5-FU	24.02	5-FU+20μM LFN	0.16
LFN+10μM 5-FU	n/a	5-FU+30μM LFN	0.04
LFN+100μM 5-FU	n/a	5-FU+40μM LFN	0.03
		5-FU+50μM LFN	0.02

Fig. 5 The combination of LFN and 5-FU reduces tumor growth in vivo. a, **b** The effect of different concentrations of LFN and 5-FU on the viabilities of A431 **a** and SCC-15 **b** was measured at 24 h after treatment. The statistical analysis on the graphs compares the drug combinations to each respective treatment alone. All values are represented as a percentage (%) relative to the placebo. Data is presented as the mean ± SEM of three independent experiments each performed in triplicate

irradiation. These results suggest that the importance of DHODH in malignant transformation of a cell is dependent on cellular demands for nucleotide biosynthesis and that DHODH plays a key role in malignant transformation of a cell under chronic genotoxic stress.

Increased intracellular pyrimidine nucleotide levels have also been reported when cells are exposed to other genotoxic stressors such as chemotherapy agents[20]. Therefore, the pyrimidine biosynthesis pathway is a promising metabolic target for enhancing the efficacy of chemotherapy and limiting the emergence of resistance. In support of this notion, the combination of doxorubicin and LFN, as well as the combination of MEK inhibitor and LFN have recently been proposed as a promising combination therapy for breast cancer[20] and melanoma[21], respectively. In line with these data, our results show that if A431 xenografted tumors are subjected to LFN in combination with a genotoxic agent such as 5-FU, a significant synergistic anti-tumor effect occurs (Fig. 6). Considering the high cytotoxicity of chemotherapy agents especially in elderly patients, this combination therapy could reasonably be expected to be efficient.

Although several drugs target DHODH[22–25], it has received little attention as a therapeutic target for cancer. As the rate-limiting enzyme in pyrimidine biosynthesis, DHODH is now becoming an attractive target for anticancer therapy. DHODH inhibitors have been shown to inhibit the growth of a wide variety of human solid tumors both in vitro and in vivo[21,26–29]. Moreover, it has been recently shown that cancer cells without mitochondrial DNA (mtDNA) do not form tumors unless they import functional mtDNA from host stroma cells. The key step in this event is reconstitution of DHODH-driven pyrimidine biosynthesis[30]. Several studies have also highlighted the significant anti-tumoral effect of DHODH inhibitors on patient-derived tumors[31–34]. The effects of LFN and other DHODH inhibitors on tumor growth, such as brequinar sodium and 4SC-101 have been ascribed to their ability to affect the expression of cell cycle regulators, such as cyclin D2 and pRb expression, the phosphorylation of some

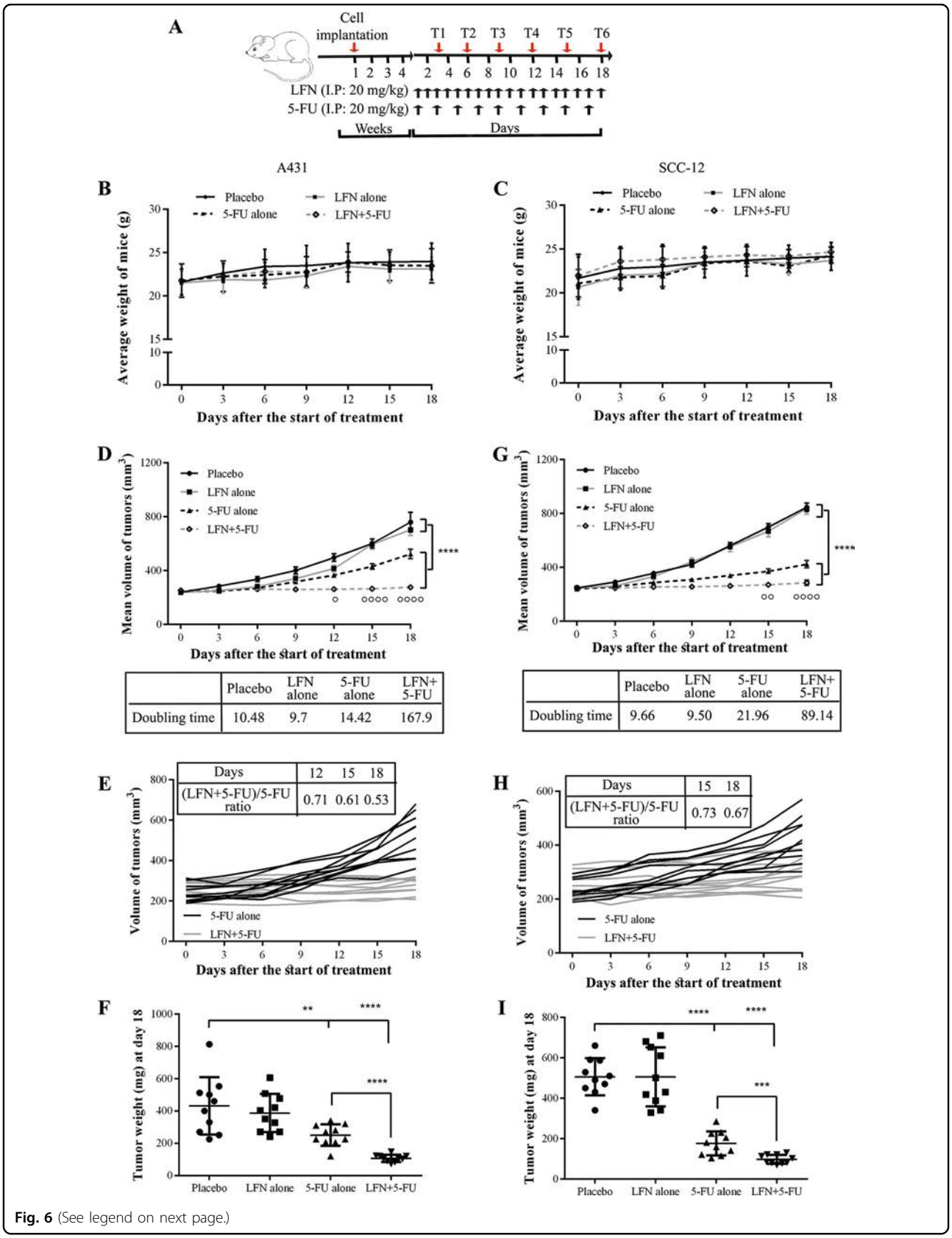

Fig. 6 (See legend on next page.)

(see figure on previous page)
Fig. 6 The combination of LFN and 5-FU reduces tumor growth in vivo. a A431 and SCC-15 cell (5×10^5) were injected subcutaneously into NSG mice. When tumors were palpable (4-weeks post-xenografting), mice were treated daily with placebo, LFN, 5-FU, or combined 5-FU and LFN for 18 days. Tumor volumes were measured at six time points (T1–T6). **b**, **c** The body weight of mice after treatment was measured at the indicated time points. Results represent the mean ± SD. **d** The combination of LFN and 5-FU reduced the average A431 tumor volume greater than either drug alone. Data is presented as the mean ± SEM of one independent experiment. Statistical analysis (two-way ANOVA with Bonferroni's post-hoc test) compares the combination therapy versus each drug alone. ****$P \leq 0.0001$. °$P \leq 0.05$, °°°°$P \leq 0.0001$ for combined 5-FU and LFN vs. 5-FU. **e** Tumor growth curves of individual A431 tumors in mice treated with 5-FU (black lines) and 5-FU plus LFN (gray lines). The effect of each treatment on mean volume of tumors at indicated day are shown at the top of the panel. **f** The combination of leflunomide and 5-FU reduced tumor weight greater than either drug alone. **g–i** The mean volume of tumors at indicated time points **g**, individual tumor growth curves **h**, and the weight of tumors at day 18 **i** are shown for transplanted SCC-15 cells. $N = 10$ mice per group, one injection per mice. *$P < 0.05$, **$P \leq 0.01$, ***$P \leq 0.001$, ****$P \leq 0.0001$

proteins, such as protein kinase B, p70S6K, and eukaryotic translation initiation factor 4E-binding protein-1, and/or cellular energy metabolism[13,25,27,35]. Moreover, activation of p53 and p53-dependent apoptosis as a downstream effect of DHODH inhibition-mediated depletion of pyrimidines has been proposed as the fourth mechanism[36]. A recent study showed that there is a strong link between expression of DHODH, tumor growth rate and sensitivity to DHODH inhibitors[35]. Along this line, it has been shown that relatively slow-growing A431 tumors have either no or very moderate sensitivity to DHODH inhibitors[37,38]. In accordance with these data, our results show that LFN treatment has a very limited effect on A431 and SCC-15 growth rate when used as a monotherapy.

Numerous cytokines, growth factors, and oncogenes activate STAT3 by affecting its post-translational modifications. Not surprisingly, therefore, over-activation of STAT3 and its pro-tumoral activity has been reported in a wide variety of tumors[39,40]. However, an increasing body of evidence supports the idea that STAT3 could have pro-tumorigenic or anti-tumorigenic activities depending on the specific tumor type, mutational landscape, stage of carcinogenesis, and metabolic conditions[41]. Therefore, targeting the downstream effectors of STAT3 with more narrow activities might increase the likelihood of developing an efficient anti-cancer drug. As a downstream effector, DHODH would be a promising target whose inhibition could be an effective anti-cancer strategy.

Altogether, our results suggest that DHODH can be targeted for both skin tumor prevention and curative combination therapy.

Materials and methods

Cell lines and culture

The origin and characteristics of the human cancer cell lines A431 and SCC-15 used in the present study are as follows. The A431 and SCC-15 lines, which were derived respectively, from the malignant epidermal carcinoma of an old female and old man, was obtained from the American Type Culture Collection (ATCC). Cells were grown in DMEM medium supplemented with 10% fetal calf serum (Gibco BRL Invitrogen, USA) and cultured in a humidified atmosphere of 5% CO_2 at 37 °C. Both cell strains were cryopreserved within three passages and no cell aliquot was cultured continuously for more than 6 months. A431 and SCC-15 cell cultures were tested every 2 weeks for mycoplasma contamination by PCR and always came back negative. A431 and SCC-15 cell cultures were tested every 2 weeks for mycoplasma contamination by PCR and always came back negative. The cell lines were authenticated by short tandem repeat (STR) genotyping. The last authentication were performed just before transplantation of cells into mice. Cell lines used were 100% matched with those of ATCC and no cross-contamination of other human cells was observed.

Animals and experimental protocol

SKH-1 hairless mice were purchased at 4–6 weeks of age from Charles River (L'arbresle, France). Mice were bred and maintained in a pathogen-free mouse facility. Female mice were used in these experiments. Mice were randomly assigned to each group before the start and experiments were performed blinded with respect to genotype and/or treatment. Experimental subgroups consisted of at least 10 mice per group. A UV Irradiation Unit (Daavlin, Bryan, OH) equipped with an electronic controller to regulate the dosage was used[42,43]. The UV dose was quantified with an X-96 dosimeter obtained from Daavlin. SKH-1 mice were exposed to UVB for 28 weeks (150 mJ/cm^2, three times a week). Tumor numbers and volume were recorded every week. Tumor volume was estimated by measuring the shortest (width, '*W*') and longest (length, '*L*') axes, based on the volume of a cylinder with hemispherical ends, according to the following equation: calculated volume (mm^3) $= [\pi(W/2)^2 (L-W)] + [4/3\pi\ (W/2)^3]$.

For xenograft studies, NOD/Shi-SCID IL2Rγnull mice (NSG) were bred in standard conditions compliant with regulations and housed in a pathogen-free animal facility. Experimental subgroups consisted of 10 mice per group, with each subgroup caged separately. 5×10^5 of A431 or

SCC-15 cells combined with Matrigel® Matrix High Concentration (Corning, USA) were subcutaneously (s.c.) injected in the right flank of mice. When the tumors reached 200–300 mm^3 in volume, mice were randomly assigned to four groups. Treatments consisted of LFN alone (intraperitoneal injections of 20 mg/kg/day), 5-FU alone (intraperitoneal injections 20 mg/kg *t* times a week/day), or the combination of both drugs. Counterpart control groups received intraperitoneal injection of phosphate buffered saline (PBS). To assess the tumor volumes and growth rate of tumors, caliper measurements of the tumors were obtained every 3 days. Tumor volumes were calculated by the following formula: volume = $(\text{width})^2 \times \text{length}/2$. After 18 days of treatment, mice were euthanized, and tumors were extracted and weighed.

All mouse experiments were carried out with the approval of Bordeaux University Animal Care and Use Committee and in accordance with relevant guidelines and regulations.

Measurement of DHODH activity

The skin samples were put in a hypotonic buffer (2.5 mM Tris/HCl, pH 7.5 and 2.5 mM $MgCl_2$) on ice for 15 min, homogenized and then sonicated for 15 s. The protein concentration for each sample was measured by BCA protein assay. DHO-ubiquinone oxidoreductase activity was measured spectrophotometrically (U-3210; Hitachi) at 37 °C by monitoring the decrease in absorbance at 600 nm of reduced DCPIP (2,6-dichlorophenol–indophenol; used as an artificial electron acceptor). Briefly, the reaction was initiated with 20 mM DHO in 1 ml of standard reaction buffer (containing 50 mM potassium phosphate, 5 mg/ml BSA and 2.5 mM $MgCl_2$) supplemented with 50 µM DCPIP, 2 µg of rotenone (a complex I inhibitor), 2 µg of antimycin A (a complex III inhibitor), 5 mM NaN_3 (a complex IV inhibitor) and 25 µg of skin lysate. The data were expressed as nmol min^{-1} μg^{-1} of protein. The reaction was stopped by the addition of 50 µM terileflunomide.

RNA extraction and quantitative real-time RT-PCR (qRT-PCR)

Total epidermal RNA was extracted using TRIzol (Invitrogen) according to the manufacturer's instructions. Total cellular RNA (2 µg) was reverse-transcribed at 42 °C for 60 min using the First Strand cDNA synthesis kit (Roche Applied Science). Quantitative real-time PCR was carried out for DHODH and tubulin using the SYBR Green method with a Bio-Rad instrument. Primer sequences used for PCR were as follows: *Dhodh*, forward primer (AGAGAGCTGGGCATCGAC) and reverse primer (AACCCCGATGATGGGAAT); *Tubulin* forward primer (CAAGGAGGATGCTGCCAATAA) and reverse primer (GCTGTGGAAAACCAAGAAGC). The reactions were cycled 40 times after initial polymerase activation (50 °C, 2 min) and initial denaturation (95 °C, 15 min) using the following parameters: denaturation at 95 °C for 15 s; and annealing and extension at 60 °C for 1 min. A final fusion cycle (95 °C, 30 s; 60 °C, 30 s; 95 °C, 30 s) terminated these reactions. The standard curve demonstrated a linear relationship between the Ct values and the cDNA concentration. The relative expression of each gene was assessed by considering the Ct and efficiency values and normalized according to the tubulin expression level.

Determination of uridine concentration in plasma by HPLC

Blood samples from mice were collected in heparinized capillaries. The plasma was prepared by centrifugation. Perchloric acid (final concentration of 0.5 M) was added to the plasma followed by incubation on ice for 5 min prior to centrifugation (12,000 × *g*, 2 min at 4 °C). Supernatants were kept at −20 °C and directly used for HPLC analysis. The uridine was resolved on a Phenomenex Kinetex C_{18} (100 × 4.6 mm, 2.6 µm) column eluted with 100 mM ammonium acetate, pH 5.16 (solvent A) and acetonitrile (solvent B) with a linear gradient from 35% A (65%B) to 50% A (50%B) in 0.8 min with a flow rate of 0.35 ml/min. Uridine elutes at 0.51 min. Twenty microliters of standard and samples were injected. All standards were freshly prepared and dissolved in 35% 100 mM ammonium acetate/65% acetonitrile and frozen at −20 °C. The following standard calibration curve was used: 20, 50, 100, 200, 500, 1500, 2000, 5000, 10,000, 15,000 ng/mL.

Quantification of CPDs by immunodot blot analysis

Mouse skin biopsies were incubated overnight at 65 °C in DirectPCR Lysis Reagent (Euromedex) and 2% proteinase K (Sigma). DNA was extracted by using sodium acetate/ethanol precipitation and quantified on a Nanodrop spectrophotometer. 500 ng of genomic DNA were mixed with 1% SYBR Green (*Brilliant III Ultra-Fast* SYBR®), dot-blotted onto a Hybond N+ nitrocellulose membrane (Amersham) and dried at 80 °C for 30 min. Membranes were blocked for 20 min (20 mM TBS, 5% non-fat dry milk, 0.5% Tween 20, pH 7.6) and incubated with anti-CPD monoclonal antibody (1:1000, Kamiya Biomedical) overnight at 4 °C. Membranes were washed in TBS and incubated for 1 h with an HRP-conjugated secondary antibody (1:2000, Vector Laboratories). Blots were developed using an ECL reagent (Biorad). Chemiluminescence signals were quantified and normalized against SYBR green fluorescence.

Western blotting procedure

Western blotting was performed as previously described[44,45]. Briefly, equal amounts of total protein were resolved by SDS–polyacrylamide gel electrophoresis (SDS–PAGE) and electrophoretically transferred to PVDF

membranes. The membranes were then incubated overnight at 4 °C with a 1:1000 dilution of the anti-DHODH (ab174288), anti-STAT3 (ab119352), anti-phosphorylated STAT3 (Abcam, Paris, France), and anti-β-actin (A2228, Sigma-Aldrich, Saint Quentin Fallavier, France) antibodies. After additional incubation with a 1:10,000 dilution of an anti-immunoglobulin horseradish peroxidase-linked antibody (Vector Laboratories, Biovalley S.A., Marne la Vallée, France) for 1 h, blots were developed using the chemiluminescence ECL reagent (Perkin Elmer, Courtaboeuf, France).

Chromatin immunoprecipitation assay

The assay was performed using the EpiQuik^{TM} tissue Chromatin Immunoprecipitation Kit (Euromedex, Mundolsheim, France) in accordance with the manufacturer's instructions. Briefly, to cross-link the proteins to DNA, skin specimens were incubated in medium containing 1% formaldehyde for 15 min at 37 °C. After adding glycine and lysis buffer, obtained chromatin lysate was sonicated to produce DNA of ~500 bp. Protein–DNA complexes were immunoprecipitated with anti-STAT3 antibody (ab119352, Abcam) or normal mouse IgG (negative control). The immunoprecipitated DNA was then purified and eluted with 50 µl of elution buffer. PCR amplification was done using 2 µl of DNA sample with different sets of primers (Supplementary Table S1). Amplification of soluble chromatin prior to immunoprecipitation was used as an input positive control. qRT-PCR was carried out on eluted DNA with the same primer sets, using the SYBR Green method with a Bio-Rad instrument. The reactions were cycled 40 times after initial polymerase activation (50 °C, 2 min) and initial denaturation (95 °C, 15 min) using the following parameters: denaturation at 95 °C for 15 s; and annealing and extension at 60 °C for 1 min. A final fusion cycle (95 °C, 30 s; 60 °C, 30 s; 95 °C, 30 s) terminated these reactions. The fold enrichment was calculated for each primer/antibody/treatment. The normalized ChIP Ct values were calculated: $\Delta C_{t(\text{normalized ChIP})} = \{C_t(\text{ChIP}) - [C_t(\text{Input}) - \text{Log}_2 \text{ (input dilution factor)}]\}$. The % Input was then calculated: % Input $= 100 \times 2^{(-\Delta C_t(\text{normalized ChIP}))}$. Finaly, fold enrichment was calculated using the following formula: fold enrichment = (% Input of antibody/%Input of IgG).

Plasmid constructs and luciferase assays

A DHODH promoter reporter plasmid, in which 1.4 kb promoter region upstream from the ATG translation initiation codon of DHODH was cloned into pEZX-PG04 plasmid, was purchased from Tebu-bio (Le Perray-en-Yvelines, France). The mutations in GAS-2 to 5 were generated using a site-directed mutagenesis kit (Promega, Madison, WI, USA) according to the manufacturer's instructions. The primers used to mutate the GAS-2 to 5 sites were as follows: GAS-2, 3: 5′-atgaggtaa t***ttacaggGG***Gatgtatgggactggagatcatg***ttacatgGG***gcaagccaat-3′, GAS-4: 5′-aaaggactta***tttttagGG***ttatgtgta-3′, GAS-5: 5′-ggaagtatta***ttccagaGG***aggaaggga-3′, in which the GAS sequences are marked in bold italics and the mutated bases are marked in bold uppercase italics. The promoter regions containing 450 and 850 bp upstream from the ATG translation initiation codon of DHODH were amplified from this plasmid by PCR and cloned into pEZX-PG04 plasmid, which codes for a secreted Gaussia Luciferase (Gluc) as the promoter reporter and secreted alkaline phosphatase (SEAP) as the internal control for signal normalization. Keratinocytes isolated from non-irradiated and irradiated skin were co-transfected with siRNA-STAT3 (Santa Cruz technology) and 32 ng of promoter reporter plasmid. Medium were then collected 24 h after transfection, kept at −80 °C and then subjected to luciferase assays using the Secrete-Pair Dual Luminescence Assay Kit (Gluc, SEAP) (Tebu-Bio) in accordance with the manufacturer's instructions. The Gluc activity expressed in each well was normalized by SEAP. For all transfection assays, at least three independent experiments were performed in triplicate.

Statistics

For all groups that were statistically compared, the variance between the groups was very similar. Comparisons between two groups were calculated using Student's *t*-test (two tailed) and a *P*-value < 0.05 (*) was considered significant. Results are presented as means ± SD. Comparisons between more than two groups were calculated with one-way analysis of variance (ANOVA) followed by Bonferroni's multiple comparison tests. To assess the number and the volume of tumors, a two-way ANOVA analysis of variance test followed by a post hoc Bonferroni's test was used. A *P*-value < 0.05 (*) was considered significant. Results are presented as means ± SEM.

Acknowledgements

The authors wish to thank P. Costet (University of Bordeaux) and Véronique Guyonnet-Duperat (FR TransBioMed, Plateforme de Vectorologie, University of Bordeaux). H.R.R. gratefully acknowledges support from the Institut National du Cancer "INCA_6654", INCa-Canceropôle GSO, and "Société Française de Dermatologie (SFD). A.-K.B.-S. is supported by the Labex TRAIL (ANR-10-LABX-57). L.D. was supported by grant from "Société Française de Dermatologie (SFD)".

Author details

[1]Univ. Bordeaux, INSERM, BMGIC, UMR 1035, F-33076 Bordeaux, France. [2]Univ. Bordeaux, INSERM, MRGM, U1211, F-33076 Bordeaux, France. [3]Centre de Référence pour les Maladies Rares de la Peau, CHU de Bordeaux, Bordeaux, France. [4]Service de Dermatologie Adulte et Pédiatrique, CHU de Bordeaux, Bordeaux, France. [5]Centre de Résonance Magnétique des Systèmes Biologiques, CNRS-Université Bordeaux UMR, 5536 Bordeaux, France

Author contributions

M.H., L.D., W.M., and E.M. performed investigation, formal analysis and contributed in methodology, validation, visualization, and writing original draft; P.M., V.B., D.B., F.M., R.R., and A.-K.B.-S. performed some investigation; A.T. contributed in conceptualization, supervision, writing—original draft and

writing—review and editing, H.R.R. contributed in supervision, conceptualization, formal analysis, visualization funding acquisition, writing—original draft and writing—review and editing.

Data availability

The authors declare that the data supporting the findings of this study are available within the paper and its Supplementary Information files. Additional data are available from the corresponding author upon reasonable request.

Conflict of interest

The authors declare that they have no conflict of interest.

Publisher's note

Springer Nature remains neutral with regard to jurisdictional claims in published maps and institutional affiliations.

Supplementary Information accompanies this paper at (https://doi.org/10.1038/s41389-019-0161-z).

Received: 23 May 2019 Revised: 8 July 2019 Accepted: 21 August 2019
Published online: 24 September 2019

References

1. Rogers, H. W., Weinstock, M. A., Feldman, S. R. & Coldiron, B. M. Incidence estimate of nonmelanoma skin cancer (keratinocyte carcinomas) in the US population, 2012. *JAMA Dermatology*. **151**, 1081–1086, https://doi.org/10.1001/jamadermatol.2015.1187 (2015).
2. Donaldson, M. R. & Coldiron, B. M. No end in sight: the skin cancer epidemic continues. *Semin. Cutan. Med. Surg.* **30**, 3–5 (2011).
3. Ratushny, V., Gober, M. D., Hick, R., Ridky, T. W. & Seykora, J. T. From keratinocyte to cancer: the pathogenesis and modeling of cutaneous squamous cell carcinoma. *J. Clin. Invest.* **122**, 464–472 (2012).
4. Karia, P. S., Han, J. & Schmults, C. D. Cutaneous squamous cell carcinoma: estimated incidence of disease, nodal metastasis, and deaths from disease in the United States, 2012. *J. Am. Acad. Dermatol.* **68**, 957–966 (2013).
5. Cranmer, L. D., Engelhardt, C. & Morgan, S. S. Treatment of unresectable and metastatic cutaneous squamous cell carcinoma. *Oncologist* **15**, 1320–1328 (2010).
6. Stratigos, A. et al. Diagnosis and treatment of invasive squamous cell carcinoma of the skin: European consensus-based interdisciplinary guideline. *Eur. J. Cancer* **51**, 1989–2007 (2015).
7. Que, S. K. T., Zwald, F. O. & Schmults, C. D. Cutaneous squamous cell carcinoma: management of advanced and high-stage tumors. *J. Am. Acad. Dermatol.* **78**, 249–261 (2018).
8. Martinez, J. C., Otley, C. C., Okuno, S. H., Foote, R. L. & Kasperbauer, J. L. Chemotherapy in the management of advanced cutaneous squamous cell carcinoma in organ transplant recipients: theoretical and practical considerations. *Dermatol. Surg.* **30**, 679–686 (2004).
9. Migden, M. R. et al. PD-1 blockade with cemiplimab in advanced cutaneous squamous-cell carcinoma. *N. Engl. J. Med.* **379**, 341–351 (2018).
10. Kaplan, M. J. Leflunomide Aventis Pharma. *Curr. Opin. Investig. Drugs* **2**, 222–230 (2001).
11. McLean, J. E., Neidhardt, E. A., Grossman, T. H. & Hedstrom, L. Multiple inhibitor analysis of the brequinar and leflunomide binding sites on human dihydroorotate dehydrogenase. *Biochemistry* **40**, 2194–2200 (2001).
12. Schiff, M. H., Strand, V., Oed, C. & Loew-Friedrich, I. Leflunomide: efficacy and safety in clinical trials for the treatment of rheumatoid arthritis. *Drugs Today* **36**, 383–394 (2000).
13. Hosseini, M. et al. Energy metabolism rewiring precedes UVB-induced primary skin tumor formation. *Cell Rep.* **23**, 3621–3634 (2018).
14. Hosseini, M., Ezzedine, K., Taieb, A. & Rezvani, H. R. Oxidative and energy metabolism as potential clues for clinical heterogeneity in nucleotide excision repair disorders. *J. Invest. Dermatol.* **135**, 341–351 (2015).
15. Vallania, F. et al. Genome-wide discovery of functional transcription factor binding sites by comparative genomics: the case of Stat3. *Proc. Natl Acad. Sci. USA* **106**, 5117–5122 (2009).
16. Kim, D. J., Angel, J. M., Sano, S. & DiGiovanni, J. Constitutive activation and targeted disruption of signal transducer and activator of transcription 3 (Stat3) in mouse epidermis reveal its critical role in UVB-induced skin carcinogenesis. *Oncogene* **28**, 950–960 (2009).
17. Galluzzi, L., Kepp, O., Vander Heiden, M. G. & Kroemer, G. Metabolic targets for cancer therapy. *Nat. Rev. Drug Discov.* **12**, 829–846 (2013).
18. Smolkova, K. et al. Waves of gene regulation suppress and then restore oxidative phosphorylation in cancer cells. *Int. J. Biochem. Cell Biol.* **43**, 950–968 (2011).
19. Ward, P. S. & Thompson, C. B. Metabolic reprogramming: a cancer hallmark even warburg did not anticipate. *Cancer Cell* **21**, 297–308 (2012).
20. Brown, K. K., Spinelli, J. B., Asara, J. M. & Toker, A. Adaptive reprogramming of de novo pyrimidine synthesis is a metabolic vulnerability in triple-negative breast cancer. *Cancer Discov.* **7**, 391–399 (2017).
21. Hanson, K. et al. The anti-rheumatic drug, leflunomide, synergizes with MEK inhibition to suppress melanoma growth. *Oncotarget* **9**, 3815–3829 (2018).
22. Fitzpatrick, L. R. et al. 4SC-101, a novel immunosuppressive drug, inhibits IL-17 and attenuates colitis in two murine models of inflammatory bowel disease. *Inflamm. Bowel Dis.* **16**, 1763–1777 (2010).
23. Fox, R. I. Mechanism of action of leflunomide in rheumatoid arthritis. *J. Rheumatol. Suppl.* **53**, 20–26 (1998).
24. He, D. et al. Teriflunomide for multiple sclerosis. *Cochrane Database Syst. Rev.* **12**, CD009882 (2012).
25. Leban, J., Saeb, W., Garcia, G., Baumgartner, R. & Kramer, B. Discovery of a novel series of DHODH inhibitors by a docking procedure and QSAR refinement. *Bioorg. Med. Chem. Lett.* **14**, 55–58 (2004).
26. Braakhuis, B. J., van Dongen, G. A., Peters, G. J., van Walsum, M. & Snow, G. B. Antitumor activity of brequinar sodium (Dup-785) against human head and neck squamous cell carcinoma xenografts. *Cancer Lett.* **49**, 133–137 (1990).
27. Chen, S. F., Perrella, F. W., Behrens, D. L. & Papp, L. M. Inhibition of dihydroorotate dehydrogenase activity by brequinar sodium. *Cancer Res.* **52**, 3521–3527 (1992).
28. Dexter, D. L. et al. Activity of a novel 4-quinolinecarboxylic acid, NSC 368390 [6-fluoro-2-(2′-fluoro-1,1′-biphenyl-4-yl)-3-methyl-4-quinolinecarb oxylic acid sodium salt], against experimental tumors. *Cancer Res.* **45**, 5563–5568 (1985).
29. Strawn, L. M. et al. Effects of SU101 in combination with cytotoxic agents on the growth of subcutaneous tumor xenografts. *Clin. Cancer Res.* **6**, 2931–2940 (2000).
30. Bajzikova, M. et al. Reactivation of dihydroorotate dehydrogenase-driven pyrimidine biosynthesis restores tumor growth of respiration-deficient cancer cells. *Cell Metab.* **29**, 399–416 (2019). e310.
31. Arteaga, C. L. et al. Phase I clinical and pharmacokinetic trial of Brequinar sodium (DuP 785; NSC 368390). *Cancer Res.* **49**, 4648–4653 (1989).
32. Peters, G. J. et al. In vivo inhibition of the pyrimidine de novo enzyme dihydroorotic acid dehydrogenase by brequinar sodium (DUP-785; NSC 368390) in mice and patients. *Cancer Res.* **50**, 4644–4649 (1990).
33. Schwartsmann, G. et al. Pharmacokinetics of Brequinar sodium (NSC 368390) in patients with solid tumors during a phase I study. *Eur. J. Cancer Clin. Oncol.* **25**, 1675–1681 (1989).
34. Sykes, D. B. et al. Inhibition of dihydroorotate dehydrogenase overcomes differentiation blockade in acute myeloid leukemia. *Cell* **167**, 171–186 (2016). e115.
35. Mohamad Fairus, A. K., Choudhary, B., Hosahalli, S., Kavitha, N. & Shatrah, O. Dihydroorotate dehydrogenase (DHODH) inhibitors affect ATP depletion, endogenous ROS and mediate S-phase arrest in breast cancer cells. *Biochimie* **135**, 154–163 (2017).
36. Khutornenko, A. A. et al. Pyrimidine biosynthesis links mitochondrial respiration to the p53 pathway. *Proc. Natl Acad. Sci. USA* **107**, 12828–12833 (2010).
37. Shawver, L. K. et al. Inhibition of platelet-derived growth factor-mediated signal transduction and tumor growth by N-[4-(trifluoromethyl)-phenyl]5-methylisoxazole-4-carboxamide. *Clin. Cancer Res.* **3**, 1167–1177 (1997).
38. Xu, X. et al. In vitro and in vivo antitumor activity of a novel immunomodulatory drug, leflunomide: mechanisms of action. *Biochem. Pharmacol.* **58**, 1405–1413 (1999).
39. Yu, H., Lee, H., Herrmann, A., Buettner, R. & Jove, R. Revisiting STAT3 signalling in cancer: new and unexpected biological functions. *Nat. Rev. Cancer* **14**, 736–746 (2014).
40. Yuan, J., Zhang, F. & Niu, R. Multiple regulation pathways and pivotal biological functions of STAT3 in cancer. *Sci. Rep.* **5**, 17663 (2015).
41. Avalle, L., Camporeale, A., Camperi, A. & Poli, V. STAT3 in cancer: a double edged sword. *Cytokine* **98**, 42–50 (2017).

42. Mahfouf, W. et al. Loss of epidermal HIF-1alpha blocks UVB-induced tumorigenesis by affecting DNA repair capacity and oxidative stress. *J. Invest. Dermatol.* **139**, 2016–2028.e7, https://doi.org/10.1016/j.jid.2019.01.035 (2019).
43. Raad, H. et al. NADPH oxidase-1 plays a key role in keratinocyte responses to UV radiation and UVB-induced skin carcinogenesis. *J. Invest. Dermatol.* **137**, 1311–1321 (2017).
44. Rezvani, H. R. et al. XPC silencing in normal human keratinocytes triggers metabolic alterations that drive the formation of squamous cell carcinomas. *J. Clin. Invest.* **121**, 195–211 (2011).
45. Rezvani, H. R. et al. XPC silencing in normal human keratinocytes triggers metabolic alterations through NOX-1 activation-mediated reactive oxygen species. *Biochim. Biophys. Acta* **1807**, 609–619 (2011).

ARTICLE 2

Metabolism-based scoring of cutaneous squamous cell carcinoma to predict tumor features and responses to treatment by DHODH inhibitor

Article submitted

Metabolism-based scoring of cutaneous squamous cell carcinoma to predict tumor features and responses to treatment by DHODH inhibitor

Léa Dousset[1,2]*, Pauline Michon[1]*, Walid Mahfouf[1], Elodie Muzotte[1], Giulia Guzzo[1], Corinne Faucheux[1], Benoît Rousseau[3], Nivea Amoedo[4,5], Stéphane Claverol[6], Alain Taieb[1], Laure Favot-Laforge[7], François Moisan[1], Rodrigue Rossignol[3], Marie Beylot-Barry[1,5], Hamid-Reza Revani[1,8§]

[1] Univ. Bordeaux, Inserm, BRIC, UMR 1312, F-33076 Bordeaux, France.

[2] Dermatology Department, Hôpital Saint-André, Bordeaux, France.

[3] Animalerie A2, University of Bordeaux, F-33000 Bordeaux, France.

[4] Inserm U1211 Maladies Rares: Génétique et Métabolisme (MRGM), Université de Bordeaux, Bordeaux, France;

[5] CELLOMET, Centre de Génomique Fonctionnelle de Bordeaux, Université de Bordeaux, Bordeaux, France.

[6] Plateforme de protéomique, Centre de Génomique Fonctionnelle de Bordeaux, Université de Bordeaux, Bordeaux, France.

[7] LITEC EA 4331, Poitier, France

[8] Aquiderm, Univ. Bordeaux, Bordeaux, France

***** These authors contributed equally

§ **Corresponding Author**

Postal address: INSERM U1312, Bordeaux, F-33000 France

Email address: hamid-reza.rezvani@u-bordeaux.fr

Phone: +33-557-575-683 Fax: +33-557-571-374

Summary

Alteration in metabolic activities is a critical point in cancer progression and myriad of metabolic-based therapy approaches are now proposed for human cancers. However, emerging evidence highlight interpatient metabolic heterogeneity and the importance of metabolic phenotyping in cancer therapy. To investigate metabolic heterogeneity in cutaneous squamous cell carcinoma (cSCC), combined proteomic and bioenergetic analyses were applied on patient samples with various stages of cSCC ranging from precancerous actinic keratosis (AK) to metastatic cSCC. Three subgroups with low-, medium- and high-metabolic scores were detected in all stages of carcinogenesis. To examine the functional impact of the detected metabolic heterogeneities on tumor features and their responses to treatment, we used patient-derived tumor cell (PDC) and patient-derived xenograft (PDX) models by transplantation of tumor cells and freshly resected patient tumors into immunocompromised mice. Results showed that, in both models (PDC and PDX), the sensitivities of tumors to leflunomide, an inhibitor of dihydroorotate dehydrogenase (DHODH), were inversely correlated with their metabolic scores and directly correlated with the protein expression level of DHODH. Moreover, DHODH overexpression in nonresponding groups render them sensitive to leflunomide. These findings demonstrate the pragmatism of metabolic profiling/scoring in designing of therapeutic approaches targeting bioenergetic vulnerabilities of tumors and propose DHODH as a promising therapeutic target in low-metabolic score subgroup of cSCC.

Introduction

Cutaneous squamous cell carcinomas (cSCC) are the second most frequent non-melanoma skin cancer (NMSCs) which incidence continues to rise because of population ageing and UV exposure (Donaldson and Coldiron, 2011; Rogers *et al.*, 2015). It can manifest as a spectrum of progressively advanced malignancies, ranging from precursor actinic keratosis (AK) to *in situ*, invasive, and finally metastatic cSCC (Ratushny *et al.*, 2012). While most patients have a good prognosis, if left untreated, cSCC can lead to death (Brantsch *et al.*, 2008; García-Foncillas *et al.*, 2022). Although European guidelines recently worked to create a definition of high risk factors of recurrence and progression for cSCC (Stratigos *et al.*, 2020; Basset-Seguin and Maubec, 2022), a recent study pointed out that among 190 advanced cSCC patients, 58% started with a primary low stage tumor (Tis, T1 and T2) (Hillen *et al.*, 2018), emphasizing the need of new profiling methods and precision medicine.

Given the key contribution of metabolic reprogramming in carcinogenesis (Gentric, Mieulet and Mechta-Grigoriou, 2017), targeting tumor bioenergetics vulnerabilities may be promising targets as an innovative therapeutic strategy (Obre and Rossignol, 2015; Hosseini, Kasraian and Rezvani, 2017). Of note, a large number of profiles has been discovered in diverse tumor types, some of them with a preference for aerobic glycolysis (Warburg effect) (Heiden, Cantley and Thompson, 2009; Ward and Thompson, 2012) and others with a higher dependency on oxidative phosphorylation (OXPHOS) (Smolková *et al.*, 2011). Our previous work showed that metabolic reprogramming occurs at an early stage of carcinogenesis during cSCC tumor formation through the activation of dihydroorotate dehydrogenase (DHODH)(Hosseini *et al.*, 2018). DHODH participates in the fourth step of de novo pyrimidine synthesis, as a rate-limiting enzyme, by converting dihydroorotate to orotate. This enzyme, by its localization in the inner membrane of mitochondria, also takes part in the electron transport chain (ETC) through reduction of ubiquinone to ubiquinol, generating electrons that are transferred via redox cycling of ubiquinone to complex III. DHODH was found upregulated in UVB-induced tumors and its inhibition by leflunomide (LFN), a FDA-approved drug for treatment of rheumatoid arthritis (Schiff *et al.*, 2000; Kaplan, 2001), blocked UVB-induced tumorigenic transformation of keratinocytes in chronic irradiated SKH-1 mice (Hosseini *et al.*, 2019). Those results strongly suggested a potential of DHODH as a novel target for prevention and therapy of cSCC.

Bioenergetic vulnerabilities-based therapies of human cancers have been recently received great attention (Kim and DeBerardinis, 2019). However, several studies highlighted interpatient metabolic heterogeneities and thus the importance of metabolic phenotyping in cancer therapy. For instance, it has been shown that a subgroup of lung cancers characterized by high mitochondrial respiration capacity (Hensley *et al.*, 2016), was sensitive to the inhibition of fatty acid α-oxidation pathway (Amoedo *et al.*, 2021). In the same line, Gentric *et al*, have identified low- and high-OXPHOS subgroups in high-grade serous ovarian and found that the second group was more sensitive to conventional chemotherapies (Gentric *et al.*, 2019). These data indicate that metabolic profiling of tumors should be considered for a better designing of bioenergetic-based therapy approaches.

Here, we investigated metabolic heterogeneity among cSCC samples at different stages of carcinogenesis and uncovered that metabolic heterogeneity can be detected even at a precancerous stage. Indeed, three subgroups with low-, medium- and high-metabolic scores were detected at all stages of carcinogenesis. By transplanting of patient-derived tumor cells and fresh tumor samples belongs to low-, medium- and high-metabolic score subgroups into mice, we found that low-metabolic score tumors grew faster than medium- and high-metabolic score tumors. The treatment efficacy of DHODH inhibition on tumor growth depends on their metabolic score and DHODH expression level. Finally, we found that lentiviral-mediated DHODH overexpression in nonresponding groups rendered them sensitive to LFN. Our data emphasize the usefulness of metabolism scoring to predict drug efficiency and the potential of leflunomide for the low-metabolic score subgroup of cSCC.

Results

Proteomic-based metabolic profiling defines 3 bioenergetic cSCC subgroups.

To assess interpatient metabolic heterogeneity, surgical pieces obtained from 60 patients with actinic keratosis (16), *in situ* cSCC (15), invasive cSCC (14) and recurrent or metastatic cSCC (15) (**supplemental Table S1, Figure 1A**) were subjected to a label-free proteomic analysis. Of note, for each patient, a paired healthy tissue far from the tumor lesion (≥5 cm) was taken and was also subjected to proteomic analysis. We first characterized the large-scale changes in the expression levels of proteins involved in OXPHOS, glycolysis, TCA cycle and fatty-acid β-oxidation among patients at different stages of carcinogenesis using Ingenuity Computational Pathway Analysis (IPA®) software (www.ingenuity.com) (**Figure 1B**). It should be noted that the relative expression levels of proteins, which were obtained by comparing the protein expression levels in tumor lesions versus their respective healthy tissue, were compared among patients. Hierarchical clustering highlighted three metabolic subgroups (low-, medium-, and high-metabolic score) within each clinicopathologic stage based on the expression levels of the majority of enzymes involved in mentioned pathways **(Figure 1B-C)**. We then analyzed the metabolic canonical pathways that were differentially regulated among patients using IPA. Canonical pathway analysis revealed the same trend **(Figure 2A-D)**. The high metabolic score subgroup was associated with an upregulation of metabolic pathways and the low metabolic score subgroup with a downregulation of those pathways **(Figure 2E-H)**.

Overall, our results show a large metabolic heterogeneity among cSCC patients and further heterogeneity at different stages of carcinogenesis.

ECAR- and OCR-based profiling classify cSCC cell lines into three bioenergetic subsets

To examine the functional impact of the metabolic heterogeneities on tumor features and their responses to treatment, we then used 8 cSCC cell lines isolated from different stages of carcinogenesis (**Figure 3A, Table S2**). PM1, MET1, MET2 and MET4 were isolated from the same patient (patient 1) and correspond to different stages of carcinogenesis. IC1 and IC1 MET were isolated from the same patient and IC12 and IC18 were two primary tumors from unrelated patients **(Figure 3A and Table S2)**.

We first characterized the metabolic features of these cell lines. Extracellular acidification rate (ECAR) levels were different among the cell lines. PM1 and IC1 exhibited lower ECAR level than the other cells lines **(Figure 3B-E).** Moreover, the levels of glycolytic capacity, which is defined as the maximum capacity to convert glucose to lactate following inhibition of ATP synthase by oligomycin (as shown in **Figure 3D**), were lower in PM1 and IC1 cells than other cells, indicating their low metabolic flexibilities to switch to glycolysis even when mitochondrial respiration is inhibited (**Figure 3A-C**). High-resolution respirometry investigation revealed that oxygen consumption rate (OCR) levels were lower in PM1 and IC1 than other cells (**Figure 3F-G**). We then classified these cells via their OCR/ECAR ratios in an energy map (**Figure 3H**). As obtained by proteomic analysis of human tumors, we could classify these cells on low-, medium- and high-metabolic score cell lines. Of note, IC1 cells, in which ECAR level was lowest among all tested cell lines, exhibited also the lowest OCR rate, indicating that this cell line could be mapped as low metabolic score cell line (**Figure 3F**). On the contrary, MET4 and IC18 cells were classed as high metabolic score cell lines (**Figure 3H**).

Focusing on intra-patient metabolic phenotyping of tumors, metastatic MET4 cell line displayed 3.90 and 1.95- fold higher ECAR and OCR levels than PM1 respectively, the precancerous cell line of the same patient (**Figure 3E-F, H**). Likewise, ECAR and OCR levels in metastatic IC1 MET were higher than IC1 (6.82 and 19-fold, respectively) (**Figure 3E, G, H**). Therefore, regardless of their initial bioenergetic state, the metabolic score of tumors will be increased during their tumor progression toward metastatic disease.

We finally measured complex I-, III- and IV-linked mitochondrial respirations and compared them among cell lines. A topography 3D map showing the activities of mitochondrial complexes revealed a distribution of cells similar to the energy map with IC1 and MET4 as cells with lowest and highest activities **(Figure 3I)**. Protein expression levels of mitochondrial complexes' subunits were also lower in IC1 cells (**Figure 3J**).

Human cSCC cell lines with distinct metabolic profiles exhibit different growth features *in vitro and in vivo*

To determine the impact of the different metabolic scores on tumor growth, we selected two cell lines from the high-metabolic scored subgroup (MET4 and IC18), two from the medium-metabolic scored subgroup (IC1 MET and IC12) and one from the low-metabolic scored subgroup (IC1) **(Figure 4A)** for *in vitro* and *in vivo* experiments. Measuring *in vitro* cell proliferation rate using SRB assay showed that low-metabolic IC1 cell line exhibited the highest proliferation rate among tested cells **(Figure 4B),** followed by the two high-metabolic scored MET4 and IC18 cells line **(Figure 4B).** The same trend was also found *in vivo,* following their subcutaneous transplantation into immunocompromised NOD-SCID gamma (NSG) mice (**Figure 4C**). Indeed low-metabolic score IC1 cells were grown significantly faster than other metabolic score subgroups, and high-metabolic score cell lines tend to grow faster than medium-metabolic score tumors (p value in between 0,05-0,054) (**Figure 4C, D).**

Overall, our data suggests that metabolic score, reflecting metabolic capacity, impacts cSCC tumor growth *in vitro* and *in vivo*.

Metabolic profiles of cells determine the inhibitory efficiency of leflunomide on tumor growth and their metastatic potency

We have previously shown that DHODH, through coordinating energy production and nucleotide biosynthesis (**Figure 5A**), intervenes in photocarcinogenesis (Hosseini *et al.*, 2018) and its inhibition by leflunomide reduces tumor growth (Hosseini *et al.*, 2019). In order to investigate the response sensitivity of the cell lines with different metabolic status to DHODH inhibition, low-metabolic score IC1, medium-metabolic IC1 MET and IC12, and high-metabolic score MET4 and IC18 cell lines were subcutaneously transplanted into NSG mice. Of note, to be able to evaluate the metastatic potency of cells by bioluminescence imaging, cells were transduced with a lentiviral vector expressing luciferase before xenografting. After transplantation and when the tumors reached an average volume of 200 mm^3, mice were divided in two groups receiving oral administration of either vehicle alone or LFN (35mg/kg/d, 7day/7). After monitoring tumor growth for one month, tumors were resected, and mice were undergoing imaging one week later to detect metastasis **(Figure 5B)**. Treatment with LFN was well-

tolerated in mice as neither body weight loss was observed (**Figure S1A**) nor any difference in mouse behavior among the different groups.

The average IC1 tumor volume increased from 179.34 mm^3 at treatment starting point to 1412 cm^3 on day 35 post-treatment (**Figure 5C**), indicating a steady increase in tumor growth overtime (**Figure 5C**). LFN treatment reduced remarkably the growth of IC1 tumors (**Figure 5C, S1B**). Examining the outcome of LFN treatment on the growth of IC1 MET tumors showed a modest but significant reducing effect (**Figure 5D, S1C**). MET4 tumors in vehicle- and LFN-treated mice continued to grow during the course of the experiment with no difference in tumor growth rates between the two groups (**Figure 5E, S1D**). Weighting the tumors at the end of experiment confirmed that LFN treatment significantly reduced the growth of IC1 tumors, whereas the weight of LFN-treated MET4 tumors was significantly higher in LFN-treated MET4 tumors than vehicle-treated tumors **(Figure S1E-G)**, suggesting that the efficiency of LFN treatment was dependent on the metabolic score of cell lines. Of note, while transplanted into mice with the same procedure, IC12 and IC18 failed to form tumors.

The histological examining of resected tumors at the end of the experiments with H&E staining, revealed that vehicle-treated IC1 and IC1 MET tumors were less differentiated than LFN-treated tumors **(Figure 5F)**. Such a difference was not detected between vehicle- and LFN-treated MET4 tumors. Of interest, LFN-treated IC1 tumors were less angiogenic than vehicle-treated tumors as evidenced macroscopically (**Figure 5F**) and following CD31 staining (**Figure 5G**). The GLUT1 staining in LFN-treated tumors were also dramatically increased in IC1 and IC1 MET compared to vehicle-treated tumors, as shown in figure 5G, showing the upregulation of GLUT1 transporter to promote glucose uptake under DHODH inhibition.

Finally, the effect of LFN treatment on the metastatic behavior of cells transplanted into NSG mice was analyzed using bioluminescence imaging. Results indicated that while 30% of mice in vehicle-treated IC1 group (3 out of 10 mice) developed metastasis, no metastasis was detected in LFN-treated IC1 mice (**Figure 5H, 5I and table 2**). LFN treatment reduced the frequency of metastasis in IC1 MET, too. Indeed, while all mice in vehicle-treated IC1 MET group displayed at least one metastasis, only 60% of mice in LFN-treated IC1 MET group developed metastasis (**Figure 5H, 5I and table 2**). In mice with MET4 tumors, the percentage of mice bearing metastasis was not different between vehicle- and LFN-treated mice (**Figure 5H, 5I and table 2**). Of note, the

metastasis were mostly found in inguinal and axillary lymph nodes, lungs and liver. A small number of mice bore metastasis in ovary, uterus and pancreas **(Figure 5I, Table 2).**

Altogether, our data show that LFN limits tumor growth and metastasis formation in the low- and medium-metabolic score groups.

Energy metabolism score and DHODH expression level could be used to predict sensitivity to LFN treatment.

To evaluate whether sensitivity of tumors to leflunomide could be related to the expression level of DHODH, western blotting was conducted on IC1, IC1 MET and MET4 cell lines **(Figure 6A)**. Results revealed that DHODH protein expression levels in low- and medium-metabolic score cells (i.e., IC1 and IC1 MET) were close to each other and were much higher than the level found in MET4, suggesting that the absence of response of MET4 cells to LFN could be ascribed to the low level of DHODH expression **(Figure 6A)**. However, this result cannot explain the difference in sensitivity to LFN between IC1 and IC1 MET. To verify whether the respective sensitivity of IC1 and IC1 MET to LFN was related to its action on of DHODH, the expression of DHODH was downregulated in IC1 and IC1 MET cells using lentiviral vector expressing shRNA against DHODH. Of note, 5 different shDHODH were tested *in vitro* for their efficacy in reduction of DHODH expression (**Figure S2 A and B**). Six days after transduction, cells were engrafted subcutaneously into NSG mice. Tumor growths were followed until reaching the maximum volume limit. Results showed significant reduction in kinetics of tumor growth rate and specific growth rate (SGR) in shDHODH-transduced IC1 and IC1 MET group compared to shControl-transduced cells (**Figure 6B-E**).

To examine whether upregulation of DHODH in MET4 cells could render them sensitive to LFN, MET4 cells were transduced by a lentiviral vector expressing human DHODH (**Figure S2 A and B**). Following transplantation of MET4 cells into NSG mice, vehicle and LFN were administrated orally (35mg/kg/d, 7/7). Monitoring the kinetics of tumor growth rates and specific growth rate (SGR) indicated that DHODH upregulation in MET4 render them sensitive to LFN (**Figure 6F-G**). Indeed, the average tumor volume in DHODH-overexpressed MET4 treated with LFN was significantly lower than the one found in vehicle-treated MET4 overexpressing DHODH (**Figure 6E**).

Altogether, our results show that sensitivity of cSCC cells to LFN treatment is dependent on their metabolic score and on the level of DHODH expression.

Sensitivities of human cSCC PDXs to LFN were dependent on energy metabolism score of primary human tumors

Fresh tumor samples at different stages of carcinogenesis were collected by physicians from consenting patients who underwent at the University Hospital in Bordeaux. Tissue samples were carried out within the 1-3 hours following biopsy and implanted subcutaneously in NSG mice to stablish a PDX biobank of human cSCC. Of note, a part of those samples was subjected to proteomic analysis. Among 30 tumor cases (2 normal-looking skin in UV exposed areas, 5 AK, 8 *in situ* cSCC, 12 invasive cSCC and 3 locally advanced (acSCC) or metastatic cSCC) engrafted into mice, 7 tumors grew up in immunocompromised mice (F1) within two to eight months post implantation. 14 out of 30 F1 tumors continued growth after implantation into NSG mice (F2) and were passageable for more than three passages (≥F3), giving a final success rate of 23% (7/30).

To investigate whether the effect of LFN in PDX model is dependent on their energy metabolism score, 3 invasive cSCC with low-, medium-, and high-metabolism score were then selected and transplanted into 8 NSG mice per group for the F3 generation. When tumors reached 200mm^3, vehicle and LFN were administrated orally (35mg/kg/d, 7/7). Interestingly low metabolic-scored tumors were highly sensitive to LFN (**Figure 7B**). Medium-metabolism scored tumors were less sensitive whereas high-metabolism scored tumors did not showed any sensitivity to LFN (**Figure 7C-D**). Clinical and histological data of patients are shown in (**figure 7E**).

Discussion

Here, we present one of the largest proteomic analysis on human cSCC and highlight an unexpected metabolic heterogeneity among samples at the same cSCC progression stage as well as between samples at different stages of carcinogenesis. Cells isolated from the tumors with low-, medium- and high-metabolism scores exhibit distinct growth profiles and sensitivities to metabolic vulnerability-targeted treatment (i.e., LFN). In our study, we deciphered the functional status of energy metabolism pathways on freshly excised surgical pieces or biopsy punch using proteomic and biochemical functional analysis. These approaches may eventually be considered for

metabolic profiling of cSCC in the clinical setting. Indeed, we provide functional and molecular evidence of metabolic heterogeneity in cSCC and the vital importance of metabolic profiling for efficient response of cSCC to new anti-cancer agents.

Accumulating evidence indicates that metabolic rewiring has a vital importance in cancer progression and that targeting metabolic vulnerabilities of tumors can be considered as a promising therapeutic approach in the treatment of cancer (Luengo, Gui and Vander Heiden, 2017; Kim and DeBerardinis, 2019). However, the response to bioenergetic vulnerabilities-based therapies varies between patients (Kim and DeBerardinis, 2019). That is why interpatient metabolic heterogeneity of tumors must be considered in the designing of such therapies, as recently proposed for lung and ovarian cancers (Gentric *et al.*, 2019; Amoedo *et al.*, 2021). We previously reported that metabolic reprogramming precedes UVB-induced primary tumor formation and evolves during the following stages (Hosseini *et al.*, 2018). In current study, we show that human cSCCs at different stages of carcinogenesis could be stratified based on their metabolic profiles which play a key role in their responses to metabolic-based treatment.

Genomic analyses have previously identified several mutational signatures and heterogeneity in significantly mutated genes in cSCC (Pickering *et al.*, 2014; Li *et al.*, 2015; Inman *et al.*, 2018). Interestingly, mutation signature patterns were very similar in PM1, MET1, MET2 and MET4 cells, which were isolated from the same patient, except that MET4 harbored one more signature that was absent in others (Shimizu *et al.*, 2001; Inman *et al.*, 2018). However, our results showed that these cells have distinct metabolic features, in that PM1 was characterized as low-metabolic score subgroup, MET1 and MET 2 as medium-metabolic score group, and MET4 as high-metabolic score cells (**Figure 3**). Likewise, IC1 and IC1 MET, which are the cells from the same patients with similar mutational signature patterns, present different metabolic features (**Figure 3**). These data indicate that mutational analysis needs to be completed by metabolic profiling to optimize the therapeutic strategy.

DHODH, which couples the *de novo* pyrimidine biosynthesis pathway to OXPHOS, is now becoming an attractive target for treatment of cancer. Indeed, DHODH inhibition has been shown to reduce the growth of various human solid tumors both *in vitro* and *in vivo* (Dexter *et al.*, 1985; Schwartsmann *et al.*, 1989; Shen *et al.*, 1989; Braakhuis *et al.*, 1990; Peters *et al.*, 1990; Chen *et al.*, 1992; Strawn *et al.*, 2000;

Sykes *et al.*, 2016; Hanson *et al.*, 2018). We have already shown that inhibition of the DHODH blocks tumor formation in mice chronically exposed to UVB irradiation through diminishing DNA repair capacity (Hosseini *et al.*, 2018) . Here, we showed that some cSCC cells are sensitive to DHODH inhibition in a metabolic score-dependent manner. Enhanced expression of DHODH was correlated with a shortened overall patient survival in oral squamous cell carcinoma (OSCC) and DHODH inhibition resulted in impaired tumor growth in a xenograft model (Qiu *et al.*, 2021). Mohamad-Fairus *et al*. have shown that DHODH expression level play a critical role in the sensitivity of tumors to DHODH inhibitors (Mohamad Fairus *et al.*, 2017).

Along this line, we showed that MET4 cells, in which the expression level of DHODH was very low, did not respond to LFN treatment. However, overexpression of DHODH in these cells render them sensitive to LFN (**Figure 6D**). An upregulation of pyrimidine nucleotides has been noticed when cells are treated with genotoxic agents, such as chemotherapy components (Brown *et al.*, 2017). Given that the upregulation of pyrimidine biosynthesis pathway needs as its prerequisite an increase in the rate-limiting enzyme of this pathway (i.e., DHODH), targeting DHODH could thus enhance the efficacy of other treatment such as PD-1 inhibitors or chemotherapy. In accordance with this hypothesis, we have already proposed the combination of 5-FU (5-flurouracil) and LFN for cSCC (Hosseini *et al.*, 2019). The combination of LFN with other drugs (such as, MEK inhibitor for melanoma treatment (Hanson *et al.*, 2018) and doxorubicin for breast cancer (Brown *et al.*, 2017) has also been proposed. Along the same direction, the *in vivo* selection of patient-derived primary and metastatic tumor xenografts (PDX) based on their enhanced metastatic capacity resulted in the enrichment of tumor cells engineered with an upregulation in the pyrimidine biosynthesis pathway, which render them very sensitive to LFN (Yamaguchi *et al.*, 2019). Our results also indicate that the metastatic potency of cells with low- and medium-metabolic features was reduced with LFN, whereas no difference was observed in high-metabolic MET4 cells between vehicle- and LFN-treated groups (**Figure 5G, H, table 1**).

The anti-tumor effect of LFN and other DHODH inhibitors has been attributed to their effect on cell cycle progression, apoptosis and/or cellular metabolism (Chen *et al.*, 1992; Leban *et al.*, 2004; Mohamad Fairus *et al.*, 2017; Hosseini *et al.*, 2018). From a histological standpoint, tumors formed by low-metabolic IC1 cells were composed of

poorly differentiated cells, which is usually associated with bad prognosis (Stratigos *et al.*, 2015). Treatment of tumors with LFN led to formation of tumors with more differentiated cells. On the contrary, the tumors formed by MET4 cells were composed of more differentiated cells, which are associated with a better prognosis. In this case, there was not obvious histological difference between vehicle- and LFN-treated tumors.

Overall, our data indicate that metabolic profiles of cSCCs have pivotal effects on tumor growth, metastatic potency and, response to treatment. Therefore, we propose metabolism scoring of cSCC, especially in the case of clinically/histologically aggressive (invasive/metastatic) behavior, as a key step in a precision medicine approach.

CONTACT FOR REAGENT AND RESOURCE SHARING

Further information and requests for resources should be directed to and will be fulfilled by the lead contact, Hamid Rezvani (hamid.reza-rezvani@u-bordeaux.fr).

EXPERIMENTAL MODEL AND SUBJECT DETAILS

Cohort of Patients

The MITOSKIN project is a translational prospective study conducted in the dermatology department of Bordeaux University Hospital. Every patient presented with a suspected lesion at different stages of carcinogenesis (actinic keratosis, in situ cSCC, invasive cSCC, locally advanced cSCC, recurrent cSCC and cutaneous metastasis of cSCC), were subjected after consent to two biopsies in the tumor (one in formol for histopathological analyze; the other frozen in liquid nitrogen), and one in the normal tissue also frozen in liquid nitrogen. Main clinical features of these cohorts are summarized in Table 1. Analysis of tumor samples were performed according to the relevant national law providing protection to people taking part in the biomedical research. The patients/participants provided their written informed consent to participate in the study. In case of patient refusal, expressed either orally or written, residual tumor samples were excluded. The National Commission for Data Processing and Liberties approved all analyses realized in this study (n° approval: ID-RCB 2018-A03096 delivered on January 04, 2019). NCT04389112

Xenograft Models

NOD/Shi-SCID IL2Rγnull mice (NSG) were bred in standard conditions compliant with regulations and housed in pathogens-free animal facility. Female mice were used in all experiments. Experimental subgroups consisted of 10 mice per groups with each group caged separately. 1×10^6 of each cell lines combined with Matrigel® Matrix High Concentration (Corning, USA) were subcutaneously injected in the right flank of mice. When the tumors reached 200mm3 in volume, mice were randomly assigned to four groups. Treatments consisted of LFN (oral gavage of 35 mg/kg/day) or Carboxymethyl cellulose (CMC, oral gavage as vehicle). To assess the tumor volumes and growth rate of tumors, caliper measurements of the tumors were performed twice a week. Tumor volumes were calculated by the following formula: volume = (width)2 × length/2. After 30-45 days of treatment, mice received an intraperitoneal injection of 300 µg/kg

buprenorphine (Vetergesic, Centavet, Dinan, France) and were then anesthetized with isoflurane while tumors were resected. The wound was disinfected with a spray of chlortetracycline (Cyclo spray, Centavet, Dinan, France). One week after resection, mice were monitored by an *in vivo* bioluminescence imaging (Biospace Lab, Nesles-la-Vallée, France) upon intraperitoneal injection of 3.3 mg of D-Luciferin (Promega, Charbonnières-les-Bains, France). At the end point, mice were sacrificed, and organs were analyzed macroscopically, photographed by *in vivo* bioluminescence imaging and embedded in paraffin for histological analyses. In the luciferase-expressing models, photon emission on recovered organs was measured after their incubation for 5 min in a solution of 3.3 mg/mL D-luciferin. All mouse experiments were in accordance with the approval of Bordeaux University Animal Care and Use Committee and in accordance with relevant.

Human cutaneous Squamous Cell Carcinoma cell lines

We used human cutaneous squamous cell carcinoma cell lines at different stages of carcinogenesis (**Table 2**) including PM1, MET1, IC1, IC12, IC18, IC1 MET and MET4 from Ximbio (Ximbio, https://ximbio.com/). Of note, their isolation from the patients at different stages of carcinogenesis were previously explained (Inman *et al.*, 2018). All cell lines, except PM1 and IC1, were grown in Keratinocyte Serum Free Media (KSFM) supplemented with 50 µg/mL of bovine pituitary extract and 10 ng/mL of epidermal growth factor (Gibco; Thermo Fisher Scientific), penicillin (100U/mL) and streptomycin (100µg/mL; Thermo Fisher Scientific). PM1 and IC1 cell lines were grown in Dulbecco′s Modified Eagle′s Medium (DMEM) with glucose (4,5g/L) supplemented with 10% fetal calf serum (Gibco; Thermo Fisher Scientific), penicillin (100U/mL) and streptomycin (100µg/mL; Thermo Fisher Scientific). Cell were cultured in a humidified atmosphere of 5%(v/v) CO_2 in air at 37°C, maintained for a maximum of 20 passages and testing confirmed the absence of mycoplasma contamination.

METHOD DETAILS

Measurement of cell growth

A sulforhodamine B (SRB) assay (Vichai and Kirtikara, 2006) was performed to examine cell viability. Cells were seeded in 96-well plates at a density of 5000 and 7500 cells/well, and settled overnight. After 1, 3, 5 and 7 days, cells were fixed in situ

with cold 10% (w/v) trichloroacetic acid (TCA). The plates were washed with water, stained with 0.4% SRB (w/v, dissolved in 1% acetic acid), and washed with 1% acetic acid. The protein-bound dye was subsequently dissolved in 10 mmol/L Tris. Absorbance values at 540 nm were recorded using a colorimetric plate reader (ClarioStar). The percent cell survival was calculated as follows: Percent cell survival=Mean OD day n/ Mean OD day 1×100%.

Lentiviral vectors and cell transduction

Cells were transduced with lentiviral vectors (pSin-EF1aL-MCS-IRES-puro for IC1 and MET4; and pRRLsin-MND-Luc-IRES2-ZsGreen-WPRE for IC1 MET). Briefly, 100 000 cells were seeded in a 6-well plate. The next day, cell were incubated with the lentivirus particles for 24h and cultured in fresh media for 1 week. Luciferase expression in transduced cells was verified by incubation in a 150mg/mL solution of luciferine D-luciferin (Interchim), followed by bioluminescence imaging using in vivo bioluminescence imaging (Biospace Lab, Nesles-la-Vallée, France).

Lentiviral vectors expressing shRNA against DHODH were purchased from Sigma-Aldrich (TRCN0000025839). Transduction of cells were done as for luciferase vectors. Specific inhibition of mRNA and protein expression of human DHODH were verified by quantitative PCR and western blotting, respectively, at one week before their transplantation into mice.

Lentiviral vectors expressing DHODH was purchased from Origene (RC209034L4). Transduction of cells were done as for luciferase and shDHODH vectors.

Oxygen consumption and glycolytic capacity

A Seahorse XF24 Extracellular Flux Analyzer (Seahorse Bioscience) was used to analyze the metabolic profile of cSCC cell lines. Results were normalized with total protein level. The assay medium for measurement of glycolytic capacity was XF Base medium (Sigma) supplemented with penicillin (100 IU/mL) and streptomycin (100 mg/mL) adjusted to pH 7.4. The assay medium for measurement of OXPHOS capacity consisted in XF Base medium supplemented with D-glucose (10 mM), sodium pyruvate (1 mM), penicillin (100 IU/mL), and streptomycin (100 mg/mL) adjusted to pH 7.4. The assay medium for measurement of complexes activities consisted in XF Base medium supplemented with D-glucose (10 mM), sodium pyruvate (1 mM), digitonin (10µM),

penicillin (100 IU/mL), and streptomycin (100 mg/mL) adjusted to pH 7.4. Four wells contained no cells to control for temperature-sensitive fluctuations in O2 fluorophore emission. One hour before monitoring, plates were incubated in a CO2-free incubator at 37°C for 1 hour to allow temperature and pH equilibration. Microplates were then put into XF96 and allowed to equilibrate for 15 min prior to first measurement. XF assays consisted of 3 min mix, 3 min wait, and 2 min measurement cycles and were performed at 37°C as described elsewhere (Wu et al., 2007)(Wu *et al.*, 2007). Using this protocol, it was possible to calculate an O2 consumption rate every 8 min. Drugs of interest prepared in the requisite assay medium were preloaded into reagent delivery chambers A, B, C, and D at 10X,11X,12X, and 13X the final working concentration, respectively, and injected sequentially at intervals of 24 min as indicated. The substrates were added as indicated in the figures at the following final working concentrations for glycolytic capacity and OXPHOS capacity: oligomycin (10µM), glucose (20g/L), 2-DG (50mM), rotenone (10µM), antimycin A (10µM), digitonin (4 mM), succinate (25 mM), DNP (50µM). The substrates concentration to measure the different complexes activities were: rotenone (1µM), succinate (100mM), antimycin A (10 µM), ascorbate (10mM) and TMPD (100 µM). In each 96-well plate, each cell lines were put in 4 or 6 wells.

Proteomic analysis

Dry pellet of cSCC cell lines were subjected to proteomic analysis. Of note, each sample was taken from a distinct T75 flask. Samples were lysed in RIPA buffer containing a protease inhibitor cocktail (Sigma). 10 µg of protein was used for the proteomic analysis at the proteomic facility of the University of Bordeaux, as recently described (Hosseini *et al.*, 2018).

Western Blot procedure

Western blotting was performed as previously described(Rezvani *et al.*, 2011; Mahfouf *et al.*, 2019). Briefly, equal amounts of total protein were resolved by SDS–polyacrylamide gel electrophoresis (SDS–PAGE) and electrophoretically transferred to Nitocellulose membrane for DHODH and PDVF membrane for OXPHOS tot. The membranes were then incubated overnight at 4 °C with a 1:300 dilution of the anti-DHODH (ab 174288) and OXPHOStot (ab110411) antibodies. After additional

incubation with a 1:1000 dilution of an anti-immunoglobulin horseradish peroxidase-linked antibody (Vector Laboratories, Biovalley S.A., Marne la Vallée, France) for 1 h, blots were developed using the chemiluminescence ECL reagent (Biorad).

Measurement of DHODH activity

DHODH activity was measured as already explained(Hosseini *et al.*, 2018). Briefly, the skin samples were put in a hypotonic buffer (2.5 mM Tris/HCl, pH 7.5 and 2.5mM MgCl2) and grinded with Precellys® Evolution. The protein concentration for each sample was measured by BCA protein assay. DHO-ubiquinone oxidoreductase activity was measured spectrophotometrically (ClarioStar) at 37 °C by monitoring the decrease in absorbance at 600 nm of reduced DCPIP (2,6-dichlorophenol–indophenol; used as an artificial electron acceptor). Briefly, the reaction was initiated with 20mM DHO in 1ml of standard reaction buffer (containing 50mM potassium phosphate, 5mg/ml BSA and 2.5mM MgCl2) supplemented with 50 µM DCPIP, 2 µg of rotenone (a complex I inhibitor), 2 µg of antimycin A (a complex III inhibitor), 5mM NaN3 (a complex IV inhibitor) and 25 µg of skin lysate. The data were expressed as $nmol.min^{-1}.\mu g^{-1}$ of protein.

Immunohistochemical and immunofluorescence staining

For both immunohistochemistry and immunofluorescence, formalin-fixed, paraffin-embedded skin sections were deparaffinized and rehydrated by following standard protocols. For immunofluorescence, after deparaffinization, antigen retrieval was performed using microwave oven treatment in a citric acid solution (Vector Laboratories). The sections were then incubated overnight at 4°C with anti-DHODH (ab54621, Abcam) and anti-CD31 (ab2836, Abcam) antibodies. After washing the slides, the section was incubated with Alexa Fluor 488-conjugated secondary antibody for 60 min. The nuclei were counterstained with DAPI.

Statistics

Comparisons between two groups were calculated using Student's t-test (two tailed) when the values followed normality. If not a Mann-Whitney test was realized. A p-value < 0.05 (*) was considered significant. Results are presented as means +/- SEM.

Comparisons between more than two groups were calculated with a one-way analysis of variance (ANOVA), and if two independent variables were needed to be tested, a two-way ANOVA analysis of variance. Both test were followed by Bonferroni's multiple comparison tests (Shapiro and Wilk test). If the normality wasn't followed, a non-parametric Krustal-Wallis test associated with a Dunn's multiple comparison tests was realized or a Mixed-effect model followed by Bonferroni's test for multiple comparison were calculated. p-value < 0.05 was considered significant. Results are presented as means +/- SEM. PCA analyses were done using the GraphPad Prism software

Data availability

The authors declare that the data supporting the findings of this study are available within the paper and its Supplementary Information files. Additional data are available from the corresponding author upon reasonable request.

Acknowledgments

The authors wish to thank Dr. Véronique Guyonnet-Duperat (TBMCore, Plateforme de Vectorologie, University of Bordeaux), Christine Alfaro (CHU Bordeaux, human sample collection), Pr. Beatrice Vergier and Dr. Marie-Laure Julié (Dermatopathology, CHU Bordeaux), Pr Pierre Dubus and Pr Jean-Philippe Merlio (CRB Cancer). **Funding:** H.R.R. gratefully acknowledges supports from the Institut National du Cancer "INCa_2021-105", the « Société Française de Dermatologie (SFD) », the « Fondation SILAB-Jean Peaufique » and the « groupe de Cancérologie cutané (GCC) ». LD was supported by institutional grants from INSERM and University Hospital of Bordeaux. PM was supported by grant from "Aquitaine region" and "La Ligue contre le cancer". **Competing interests:** The authors declare that they have no financial or non-financial conflict of interest.

Bibliography

Amoedo, N. D. *et al.* (2021) 'Targeting the mitochondrial trifunctional protein restrains tumor growth in oxidative lung carcinomas', *Journal of Clinical Investigation*. doi: 10.1172/JCI133081.

Basset-Seguin, N. and Maubec, E. (2022) 'Recent Advanced in the Treatment of Advanced SCC Tumors', *Cancers*. Cancers (Basel), 14(3). doi: 10.3390/CANCERS14030550.

Braakhuis, B. J. M. *et al.* (1990) 'Antitumor activity of brequinar sodium (Dup-785) against human head and neck squanmous cell carcinoma xenografts', *Cancer Letters*. doi: 10.1016/0304-3835(90)90149-R.
Brantsch, K. D. *et al.* (2008) 'Analysis of risk factors determining prognosis of cutaneous squamous-cell carcinoma: a prospective study', *The Lancet Oncology*. Elsevier, 9(8), pp. 713–720. doi: 10.1016/S1470-2045(08)70178-5.
Brown, K. K. *et al.* (2017) 'Adaptive reprogramming of De novo pyrimidine synthesis is a metabolic vulnerability in triple-negative breast cancer', *Cancer Discovery*. doi: 10.1158/2159-8290.CD-16-0611.
Chen, S. F. *et al.* (1992) 'Inhibition of Dihydroorotate Dehydrogenase Activity by Brequinar Sodium', *Cancer Research*.
Dexter, D. L. *et al.* (1985) 'Activity of a novel 4-quinolinecarboxylic acid, NSC 368390 [6-fluoro-2-(2'-fluoro-1,1'-biphenyl-4-yl)-3-methyl-4-quinolinecarboxylic acid sodium salt], against experimental tumors', *Cancer Research*.
Donaldson, M. R. and Coldiron, B. M. (2011) 'No End in Sight: The Skin Cancer Epidemic Continues', *Seminars in Cutaneous Medicine and Surgery*. doi: 10.1016/j.sder.2011.01.002.
García-Foncillas, J. *et al.* (2022) 'Update on Management Recommendations for Advanced Cutaneous Squamous Cell Carcinoma', *Cancers*, 14(3), pp. 1–19. doi: 10.3390/cancers14030629.
Gentric, G. *et al.* (2019) 'PML-Regulated Mitochondrial Metabolism Enhances Chemosensitivity in Human Ovarian Cancers', *Cell Metabolism*. doi: 10.1016/j.cmet.2018.09.002.
Gentric, G., Mieulet, V. and Mechta-Grigoriou, F. (2017) 'Heterogeneity in Cancer Metabolism: New Concepts in an Old Field', *Antioxidants and Redox Signaling*. doi: 10.1089/ars.2016.6750.
Hanson, K. *et al.* (2018) 'The anti-rheumatic drug, leflunomide, synergizes with MEK inhibition to suppress melanoma growth', *Oncotarget*. doi: 10.18632/oncotarget.23378.
Heiden, M. G. V., Cantley, L. C. and Thompson, C. B. (2009) 'Understanding the warburg effect: The metabolic requirements of cell proliferation', *Science*. doi: 10.1126/science.1160809.
Hensley, C. T. *et al.* (2016) 'Metabolic Heterogeneity in Human Lung Tumors', *Cell*. doi: 10.1016/j.cell.2015.12.034.
Hillen, U. *et al.* (2018) 'Advanced cutaneous squamous cell carcinoma: A retrospective analysis of patient profiles and treatment patterns-Results of a non-interventional study of the DeCOG', *European journal of cancer (Oxford, England : 1990)*. Eur J Cancer, 96, pp. 34–43. doi: 10.1016/J.EJCA.2018.01.075.
Hosseini, M. *et al.* (2018) 'Energy Metabolism Rewiring Precedes UVB-Induced Primary Skin Tumor Formation', *Cell Reports*, 23(12), pp. 3621–3634. doi: 10.1016/j.celrep.2018.05.060.
Hosseini, M. *et al.* (2019) 'UVB-induced DHODH upregulation, which is driven by STAT3, is a promising target for chemoprevention and combination therapy of photocarcinogenesis', *Oncogenesis*. Nature Publishing Group, 8(10). doi: 10.1038/s41389-019-0161-z.
Hosseini, M., Kasraian, Z. and Rezvani, H. R. (2017) 'Energy metabolism in skin cancers: A therapeutic perspective', *Biochimica et Biophysica Acta (BBA) - Bioenergetics*, 1858(8), pp. 712–722. doi: 10.1016/j.bbabio.2017.01.013.
Inman, G. J. *et al.* (2018) 'The genomic landscape of cutaneous SCC reveals drivers and a novel

azathioprine associated mutational signature', *Nature Communications*. Nature Publishing Group, 9(1). doi: 10.1038/s41467-018-06027-1.
Kaplan, M. J. (2001) 'Leflunomide Aventis Pharma', *Current Opinion in Investigational Drugs*.
Kim, J. and DeBerardinis, R. J. (2019) 'Mechanisms and Implications of Metabolic Heterogeneity in Cancer', *Cell Metabolism*. doi: 10.1016/j.cmet.2019.08.013.
Leban, J. *et al.* (2004) 'Discovery of a novel series of DHODH inhibitors by a docking procedure and QSAR refinement', *Bioorganic and Medicinal Chemistry Letters*. doi: 10.1016/j.bmcl.2003.10.021.
Li, Y. Y. *et al.* (2015) 'Genomic analysis of metastatic cutaneous squamous cell carcinoma', *Clinical Cancer Research*. doi: 10.1158/1078-0432.CCR-14-1773.
Luengo, A., Gui, D. Y. and Vander Heiden, M. G. (2017) 'Targeting Metabolism for Cancer Therapy', *Cell Chemical Biology*. doi: 10.1016/j.chembiol.2017.08.028.
Mahfouf, W. *et al.* (2019) 'Loss of Epidermal HIF-1α Blocks UVB-Induced Tumorigenesis by Affecting DNA Repair Capacity and Oxidative Stress', *Journal of Investigative Dermatology*. Elsevier B.V., 139(9), pp. 2016-2028.e7. doi: 10.1016/j.jid.2019.01.035.
Mohamad Fairus, A. K. *et al.* (2017) 'Dihydroorotate dehydrogenase (DHODH) inhibitors affect ATP depletion, endogenous ROS and mediate S-phase arrest in breast cancer cells', *Biochimie*. doi: 10.1016/j.biochi.2017.02.003.
Obre, E. and Rossignol, R. (2015) 'Emerging concepts in bioenergetics and cancer research: Metabolic flexibility, coupling, symbiosis, switch, oxidative tumors, metabolic remodeling, signaling and bioenergetic therapy', *International Journal of Biochemistry and Cell Biology*. doi: 10.1016/j.biocel.2014.12.008.
Peters, G. J. *et al.* (1990) 'In Vivo Inhibition of the Pyrimidine de Novo Enzyme Dihydroorotic Acid Dehydrogenase by Brequinar Sodium (DUP-785; NSC 368390) in Mice and Patients', *Cancer Research*.
Pickering, C. R. *et al.* (2014) 'Mutational landscape of aggressive cutaneous squamous cell carcinoma', *Clinical Cancer Research*. doi: 10.1158/1078-0432.CCR-14-1768.
Qiu, X. *et al.* (2021) 'SOX2-dependent expression of dihydroorotate dehydrogenase regulates oral squamous cell carcinoma cell proliferation', *International Journal of Oral Science*. doi: 10.1038/s41368-020-00109-x.
Ratushny, V. *et al.* (2012) 'From keratinocyte to cancer: The pathogenesis and modeling of cutaneous squamous cell carcinoma', *Journal of Clinical Investigation*. doi: 10.1172/JCI57415.
Rezvani, H. R. *et al.* (2011) 'XPC silencing in normal human keratinocytes triggers metabolic alterations that drive the formation of squamous cell carcinomas', *Journal of Clinical Investigation*. doi: 10.1172/JCI40087.
Rogers, H. W. *et al.* (2015) 'Incidence estimate of nonmelanoma skin cancer (keratinocyte carcinomas) in the us population, 2012', *JAMA Dermatology*. American Medical Association, 151(10), pp. 1081–1086. doi: 10.1001/jamadermatol.2015.1187.
Schiff, M. H. *et al.* (2000) 'Leflunomide: Efficacy and safety in clinical trials for the treatment of rheumatoid arthritis', *Drugs of Today*. doi: 10.1358/dot.2000.36.6.584259.
Schwartsmann, G. *et al.* (1989) 'Pharmacokinetics of Brequinar sodium (NSC 368390) in patients with

solid tumors during a phase I study', *European Journal of Cancer and Clinical Oncology*. doi: 10.1016/0277-5379(89)90334-9.
Shen, H. S. L. *et al.* (1989) 'Phase I Clinical and Pharmacokinetic Trial of Brequinar Sodium (DUP 785; NSC 368390)', *Cancer Research*.
Shimizu, T. *et al.* (2001) 'Epidermal growth factor receptor overexpression and genetic aberrations in metastatic squamous-cell carcinoma of the skin', *Dermatology*. doi: 10.1159/000051637.
Smolková, K. *et al.* (2011) 'Waves of gene regulation suppress and then restore oxidative phosphorylation in cancer cells', *International Journal of Biochemistry and Cell Biology*. doi: 10.1016/j.biocel.2010.05.003.
Stratigos, A. *et al.* (2015) 'Diagnosis and treatment of invasive squamous cell carcinoma of the skin: European consensus-based interdisciplinary guideline', *European Journal of Cancer*. Elsevier Ltd, 51(14), pp. 1989–2007. doi: 10.1016/j.ejca.2015.06.110.
Stratigos, A. J. *et al.* (2020) 'European interdisciplinary guideline on invasive squamous cell carcinoma of the skin: Part 1. epidemiology, diagnostics and prevention', *European journal of cancer (Oxford, England : 1990)*. Eur J Cancer, 128, pp. 60–82. doi: 10.1016/J.EJCA.2020.01.007.
Strawn, L. M. *et al.* (2000) 'Effects of SU101 in combination with cytotoxic agents on the growth of subcutaneous tumor xenografts', *Clinical Cancer Research*.
Sykes, D. B. *et al.* (2016) 'Inhibition of Dihydroorotate Dehydrogenase Overcomes Differentiation Blockade in Acute Myeloid Leukemia', *Cell*. doi: 10.1016/j.cell.2016.08.057.
Vichai, V. and Kirtikara, K. (2006) 'Sulforhodamine B colorimetric assay for cytotoxicity screening', *Nature Protocols*. doi: 10.1038/nprot.2006.179.
Ward, P. S. and Thompson, C. B. (2012) 'Metabolic Reprogramming: A Cancer Hallmark Even Warburg Did Not Anticipate', *Cancer Cell*. doi: 10.1016/j.ccr.2012.02.014.
Wu, M. *et al.* (2007) 'Multiparameter metabolic analysis reveals a close link between attenuated mitochondrial bioenergetic function and enhanced glycolysis dependency in human tumor cells', *American Journal of Physiology - Cell Physiology*. doi: 10.1152/ajpcell.00247.2006.
Yamaguchi, N. *et al.* (2019) 'PCK1 and DHODH drive colorectal cancer liver metastatic colonization and hypoxic growth by promoting nucleotide synthesis', *eLife*. doi: 10.7554/eLife.52135.

Table 1. Patients characteristics

Patient no.	gender	Age	Location	Histologic subtype	Immunocompromised Yes/No
1	M	87	Scalp	AK	Yes
2	M	93	Scalp	AK	Yes
3	M	81	Scalp	AK	No
4	M	77	Face	AK	No
5	M	90	Scalp	AK	No
6	M	68	Face	AK	Yes
7	F	84	Face	AK	No
8	M	82	Scalp	AK	Yes
9	M	68	Face	AK	Yes
10	M	87	Face	AK	No
11	M	67	Scalp	AK	Yes
12	M	61	scalp	AK	No
13	M	76	hand	AK	Yes
14	M	77	face	AK	Yes
15	M	89	face	AK	No
16	F	69	arm	AK	No
1	M	55	leg	in situ cSCC	Yes
2	M	85	face	in situ cSCC	Yes
3	F	80	leg	in situ cSCC	No
4	F	90	face	in situ cSCC	No
5	M	93	scalp	in situ cSCC	No
6	M	77	arm	in situ cSCC	No
7	F	85	ear	in situ cSCC	Yes
8	M	68	face	in situ cSCC	Yes
9	F	91	neck	in situ cSCC	No
10	M	81	neck	in situ cSCC	Yes
11	M	89	scalp	in situ cSCC	No
12	M	76	face	in situ cSCC	Yes
13	M	83	scalp	in situ cSCC	No
14	M	92	back	in situ cSCC	No
15	F	69	arm	in situ cSCC	Yes
1	M	85	face	invasive cSCC	Yes
2	M	81	face	invasive cSCC	Yes
3	M	87	scalp	invasive cSCC	Yes
4	M	84	face	invasive cSCC	Yes
5	F	83	neck	invasive cSCC	No
6	M	78	face	invasive cSCC	No
7	M	90	scalp	invasive cSCC	No
8	M	68	neck	invasive cSCC	Yes
9	F	84	face	invasive cSCC	No
10	M	82	leg	invasive cSCC	Yes
11	M	69	scalp	invasive cSCC	Yes
12	F	93	face	invasive cSCC	Yes
13	M	67	scalp	invasive cSCC	No
14	M	89	scalp	invasive cSCC	Yes
1	F	72	scalp	recurrent cSCC	Yes
2	M	81	ear	recurrent cSCC	Yes
3	M	81	scalp	locally advanced cSCC	Yes
4	M	77	neck	subcutaneous metastasis	No
5	F	84	face	locally advanced cSCC	No
6	M	79	scalp	locally advanced cSCC	No
7	F	87	face	locally advanced cSCC	No
8	M	82	scalp	recurrent cSCC	Yes
9	M	68	face	recurrent cSCC	Yes
10	M	87	face	recurrent cSCC	No
11	F	98	face	locally advanced cSCC	No
12	M	67	scalp	locally advanced cSCC	Yes
13	F	82	face	locally advanced cSCC	No
14	M	80	arm	subcutaneous metastasis	No
15	M	76	scalp	recurrent cSCC	Yes

Abbreviations: M, male; F, female.

Table 2. Number of mice bearing metastasis in indicated organs

Group	Low metabolic		Medium metabolic		High Metabolic	
	IC1		IC1 MET		MET4	
Treatment	**Veh**	**LFN**	**Veh**	**LFN**	**Veh**	**LFN**
Inguinal nodes	3/10	0/10	3/8	2/10	1/10	1/9
Axilary nodes	0/10	0/10	0/8	0/10	1/10	1/9
Lungs	0/10	0/10	8/8	6/10	6/10	7/9
Liver	1/10	0/10	3/8	1/10	1/10	0/9
Ovary	0/10	0/10	1/8	0/10	1/10	0/9
Uterus	0/10	0/10	2/8	0/10	0/10	0/9
Pancreas	0/10	0/10	1/8	0/10	0/10	0/9

Figure Legends

Figure 1. Metabolic heterogeneity among human cSCC at different stages of carcinogenesis

A) Schematic representation of cSCC progression ranging from actinic keratosis (AK, *) to in situ (black arrow), invasive (black arrow) and metastatic or recurrent cSCC.

B) 16 AKs, 15 in situ cSCCs, 14 infiltrative cSCCs, 15 recurrent or metastatic cSCC and, their respective healthy tissues were subjected to a comprehensive label-free proteomic study (N= 120). Heatmap showing the fold change in the expression levels of proteins involved in OXPHOS, glycolysis, TCA cycle, and fatty acid β-oxidation in human patient lesions compared to their respective healthy skin. Each column is a sample, and each row a protein. Downregulated proteins are colored green, upregulated proteins are red and non-modified proteins are white.

C) Median of expression fold changes of proteins involved in OXPHOS, glycolysis, TCA cycle and fatty-acid β-oxidation from proteomic data (N = 60). Classification in low-, medium- and high-metabolic is based on the consensus clustering in (**B**). Mean +/- SEM are shown. p values from one-way ANOVA test.

Figure 2. cSCCs at different stages of carcinogenesis could be stratified into low-, medium- and high-metabolic score subgroups based on their metabolic features

(**A-D**) Heatmap of z-score for activated metabolic canonical pathways in AK (**A**), in situ cSCC (**B**), infiltrative cSCC (**C**), and metastatic/recurrent cSCC (**D**) patients. Z-score was calculated by considering the number of proteins involved in a particular pathway that were modified in each patient's lesion compared to its respective healthy tissue. The color indicates canonical pathway activation z-score values; blue: downregulation and red: upregulation.

E-H) Average of activation z-scores of metabolic canonical pathways enriched in low-, medium-, and high-metabolic score subgroups in AK (**E**), *in situ* cSCC *(**F**)*, infiltrative cSCC (**G**) and metastatic cSCC (**H**) (N= 60). Classification in low-, medium- and high-

metabolic score is based on the consensus clustering in A to D. mean +/- SEM are shown. p values from one-way ANOVA test.

Figure 3. Low-metabolic score cSCC cell lines exhibit a lower metabolic flexibility than medium- and high-metabolic score subgroups.

A) Characteristics of cell lines isolated from human patients**.**

B-C) Extracellular acidification rate (ECAR) in response to different metabolic modulator was measured by Seahorse analyzer in mentioned cell lines. Data are mean +/- SEM. P value were calculated by a Mixed-model analysis followed by a Bonferonni's multiple comparison test for (**B**) and (**C**). $6 \leq n \leq 8$. Of note, cSCC cell lines coming from the same patient exhibited ECAR capacities. ECAR level in PM1 cells was lowest among other cells and did not respond to oligomycin compared to MET1, MET2 and MET4 cells **(B)**. IC1 did not respond to oligomycin compared to IC1 MET (**C**).

D) Schematic representation of ECAR kinetics in cell response to glucose, oligomycin and 2-DG.

E) ECAR levels after adding glucose were compared among different cell lines. PM1 and IC1 exhibited the lowest ECAR levels among the tested cell lines. P value were calculated by Krustal Wallis test followed by a Dunn's multiple comparison test. $5 \leq n \leq 8$.

F-G). Oxygen consumption rate (OCR) levels in response to the metabolic modulators was measured by seahorse analyzer for each cell lines and normalized to its corresponding total protein levels. Data are mean +/- SEM. P value are from Mixed effect model for (**F**) and one-way ANOVA test (**G**). $5 \leq n \leq 8$.

H) Energy map of cSCC cell lines. MET4 and IC18 cells appeared in the upper-right quadrant were classified as high metabolic cells, IC1 and PM1 cells appeared in lower-left quadrant were considered as low-metabolic cells and the others were grouped in medium-metabolic subgroup.

I) Three dimentional representation of the complex activities (x: Complex I; y: Complex III; z: Complexe IV). Data are mean of all experiments ($3 \leq n \leq 5$).

J) Representative western blot showing the five proteins involved in OXPHOS (ATP5A, ATP synthase alpha subunit; UQCR2, ubiquinol-cytochrome c reductase core protein II; SDHB, succinate dehydrogenase complex iron sulfur subunit B; COXII, cytochrome c oxidase II; NDUFB8, NADH: ubiquinone oxidoreductase subunit B8. β-Actin was used as a loading control.

Figure 4. Difference in metabolic features is associated with difference in proliferation rates *in vivo* and *in vitro*

A) Schematic showing topology of cSCC cell lines on an energy map. Mapping OCR and ECAR rates of the different cell lines led to their classification into three metabolic subgroups: low-(blue), medium- (green) and high-metabolic (brown) subgroups. The cells written in red were used for further functional analyses.

B) Growth rates of the different cell lines were evaluated *in vitro*. Low-metabolic group grows faster than the medium- and high-metabolic groups. Data are mean +/- SEM. n=3.

C) *In vivo* growth kinetics of cSCC cell lines were evaluated after their transplantation into NSG mice. Low-metabolic score IC1 grew faster than cells with high- and medium-metabolic scores. Data are mean +/- SEM. p value are from Mixed effect model. n=10 mice.

Figure 5. Low-metabolic score IC1 was very sensitive to DHODH inhibition

A) Schematic showing DHODH contribution in de *novo* pyrimidine synthesis and OXPHOS.

B) Schematic representation of the experimental procedure. After transplantation of cSCC IC1, IC1 MET and MET4 cell lines into NSG mice and when the tumor reached 200mm^3, mice were administrated orally with leflunomide (LFN) or carboxymethylcellulose (vehicle, veh). Metastasis were monitored by *in vivo* bioluminescence imaging one week after tumor resection.

C-E) Tumor growths in vehicle- and LFN-treated mice were surveyed and measured. While LFN treatment reduced significantly the growth of IC1 tumors, growth rate of high-metabolic MET4 tumors did not affected by LFN. N=10 mice (IC1-VEH, LFN-IC1,

LFN-IC1 MET, VEH-MET4), 9 mice (LFN-MET4) and 8 mice (VEH-IC1 MET). ∗p < 0.05, ∗∗ < 0.01, ∗∗∗ < 0.001 for VEH- versus LFN-treated mice.

F) A representative photo of a tumor per group at the time of resection and histopathological evaluation of tumors with H&E staining. Tumor cells were poorly differentiated in vehicle-treated IC1 cells and moderately differentiated in LFN-treated IC1 cells. On the contrary there were no differences in differentiation between LFN or vehicle treated IC1 MET and MET4 cells (moderately to well differentiated with focus of keratinization).

G) CD31-stained blood vessels were compared among different tumors. The nuclei were marked in blue with DAPI.

H-I) Luciferase-expressing IC1, IC1 MET, and MET4 cells were transplanted subcutaneously into NSG mice. Mice were treated with vehicle or LFN. % of mice bearing at least one metastasis in vehicle- and LFN-treated mice (**H**). A representative photo corresponding to bioluminescence signal of tumor metastasis in different organs taken from one mouse per group. *Ex vivo* bioluminescence imaging was conducted for (left) IC1, (middle) IC1 MET, and (right) MET4 cells (**I**).

Figure 6. Overexpression of DHODH in non-responder MET4 cells render them sensitive to LFN treatment

A) A representative western blot showing DHODH protein levels in IC1, IC1 MET and MET4 cells. β-actin used a loading control.

B) IC1 cell lines were transduced with lentiviral vectors expressing shcontrol or shDHODH. Cells were transplanted into NSG mice. Tumor growths of shcontrol- and shDHODH-transduced IC1 MET cells assessed. Data are mean +/- SEM. p value are from Mixed-effect analysis. n=10.

C) MET4 cell lines were transduced with lentiviral vectors expressing DHODH. Cells were transplanted into NSG mice and then treated with vehicle or LFN. Tumor growth rates of MET4 overexpressing DHODH ($DHODH^{+}$) treated with vehicle or LFN were assessed. DHODH overexpression make these cells sensitives to LFN. Data are mean +/- SEM. p value were calculated with Two-way ANOVA test. n=7.

Figure 7. Treatment of patient-derived xenografts revealed that low-metabolic scored tumors were sensitive to DHODH inhibition.

A) Patient-derived xenograft (PDX) models were established by transplantation of freshly resected patient tumors into NSG immunodeficient mice. Following primary tumors collected from patients at different stages of carcinogenesis were used: normal-looking UV-skin, n=2; actinic keratosis (AK), n=5; in situ cSCC, n=8; invasive cSCC, n=12; locally advanced cSCC n=3). Only 7 out of 30 PDX were passageable for more than three passages (>>F3).

B-D) Punch biopsies taken from the F3 generation of three PDX of invasive cSCC with low-, medium-, and high-metabolism scores were transplanted subcutaneously into 24 NSG mice (8 mice per group). When tumors reached 200mm3, mice were administered orally leflunomide (LFN) or vehicle (carboxymethylcellulose). Tumors growths in vehicle- and LFN-treated mice were surveyed and measured in low- (**B),** medium (**C**), and high-(**D**) metabolism scored tumors. n=8 mice in each group. $*p < 0.05$, $** < 0.01$, $*** < 0.001$.

E) Clinical and histopathological characteristics of patients which PDX underwent a treatment with leflunomide.

Supplementary Data

Supplemental Tables

Table S1. Clinical and histological characteristics of patients who provided the samples that created the patient-derived xenografts (PDX).

Table S2. Clinical and histological characteristics of patients who provided the samples that created the patient-derived tumor cells (PDCs).

Characteristic of human cSCC cell lines.

Cell line	Immune Status	Immune Therapy	Site	Histology	Age	Sex	Tumour
IC1	IC	N/A	right temple	MD	77	M	primary
IC1 MET	IC	N/A	right preauricular lymph node	metastasis	77	M	metastasis of IC1
PM1	RT	A,P	scalp	dysplastic	45	M	pre-malignant lesion from MET series patient
MET1	RT	A,P	dorsum left hand	MD	45	M	primary
MET2	RT	A,P	dorsum left hand	MD	45	M	recurrence of MET1
MET4	RT	A,P	left axillary lymph node	metastasis	46	M	metastasis of MET 1/2
SCC IC12	IC	N/A	left calf	MD-PD	87	F	primary
SCC IC18	IC	N/A	right ear	MD	81	M	primary

IC = Immuno-competent, RT = renal transplant, PUVA= psoralen + ultraviolet A, CT = cardiac transplant.

Patients received imunosuppressive therapy as follows: A, azathioprine; C, Cyclosporine A; M, mycophenolate mofetil (MMF); P, prednisolone; *, patient had stopped treatment at the time of lesional biopsy

Table S3. List of antibodies used in this study.

Protein	Reference	Dilution
B-Actine	**A2228 - Sigma**	**1/5000**
OXPHOS tot	**ab110411**	**1/500**
DHODH	**ab174288**	**1/300**
CD31	**ab28364**	**1/100**

Supplemental figures

Figure S1. LFN treatment, which was well-tolerated in mice without affecting their weights, reduces significantly the growth of IC1 cells

A) The body weight of mice after treatment was measured at the indicated time points. Results represent the mean ± SEM. LFN treatment was well-tolerated in mice without affecting their weights.

B-D) The specific tumor growth rate (SGR) was estimated for vehicle- and LFN-treated IC1 (**B**), IC1 MET (**C**), and MET4 (**D**) according to the following equation: SGR = Ln (v2-V1)/(T2-T1).

E-G) Weights of tumors at resection time are shown for transplanted IC1 (**E**), IC1 MET (**F**) and MET4 (**G**) cells treated with vehicle or LFN.

N = 10 mice (IC1-VEH, LFN-IC1, LFN-IC1 MET, VEH-MET4), 9 mice (LFN-MET4) and 7 mice (VEH-IC1 MET). ∗p < 0.05, ∗∗ < 0.01, ∗∗∗ < 0.001 for VEH- versus LFN-treated mice. *P < 0.05, ***P ≤ 0.001, ****P ≤ 0.0001

Figure S2. ShDHODH was reduced efficiently the mRNA expression of DHODH

The lentiviral vectors expressing 5 different shRNA against DHODH were purchase from Sigma. Their efficiency in reduction of mRNA expression DHODH was tested by quantitative RT-PCR (A) and Western Blot (B).

B) WB showed shDHODH and $DHODH^{+}$ overexpressed in HACAT cells.

Figure 1.

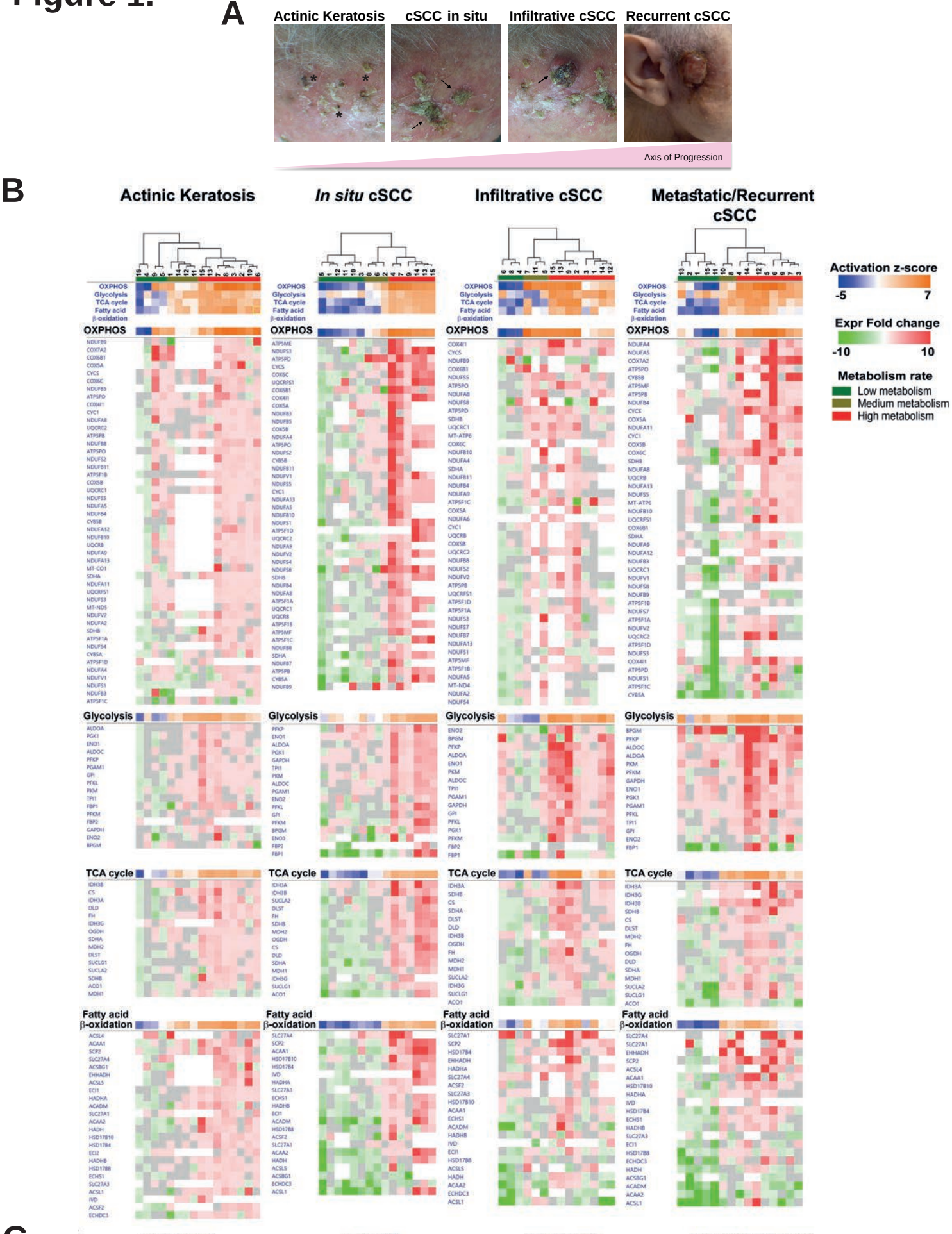
A
Actinic Keratosis
cSCC in situ
Infiltrative cSCC
Recurrent cSCC
Axis of Progression
B
Actinic Keratosis
In situ cSCC
Infiltrative cSCC
Metastatic/Recurrent cSCC
OXPHOS
Glycolysis
TCA cycle
Fatty acid β-oxidation
Activation z-score
-5
7
Expr Fold change
-10
10
Metabolism rate
Low metabolism
Medium metabolism
High metabolism
C
Actinic Keratosis
In situ cSCC
Infiltrative cSCC
Metastatic/Recurrent cSCC
Median fold change of proteins
Low Metabolism
Medium Metabolsim
High metabolism

Figure 2.

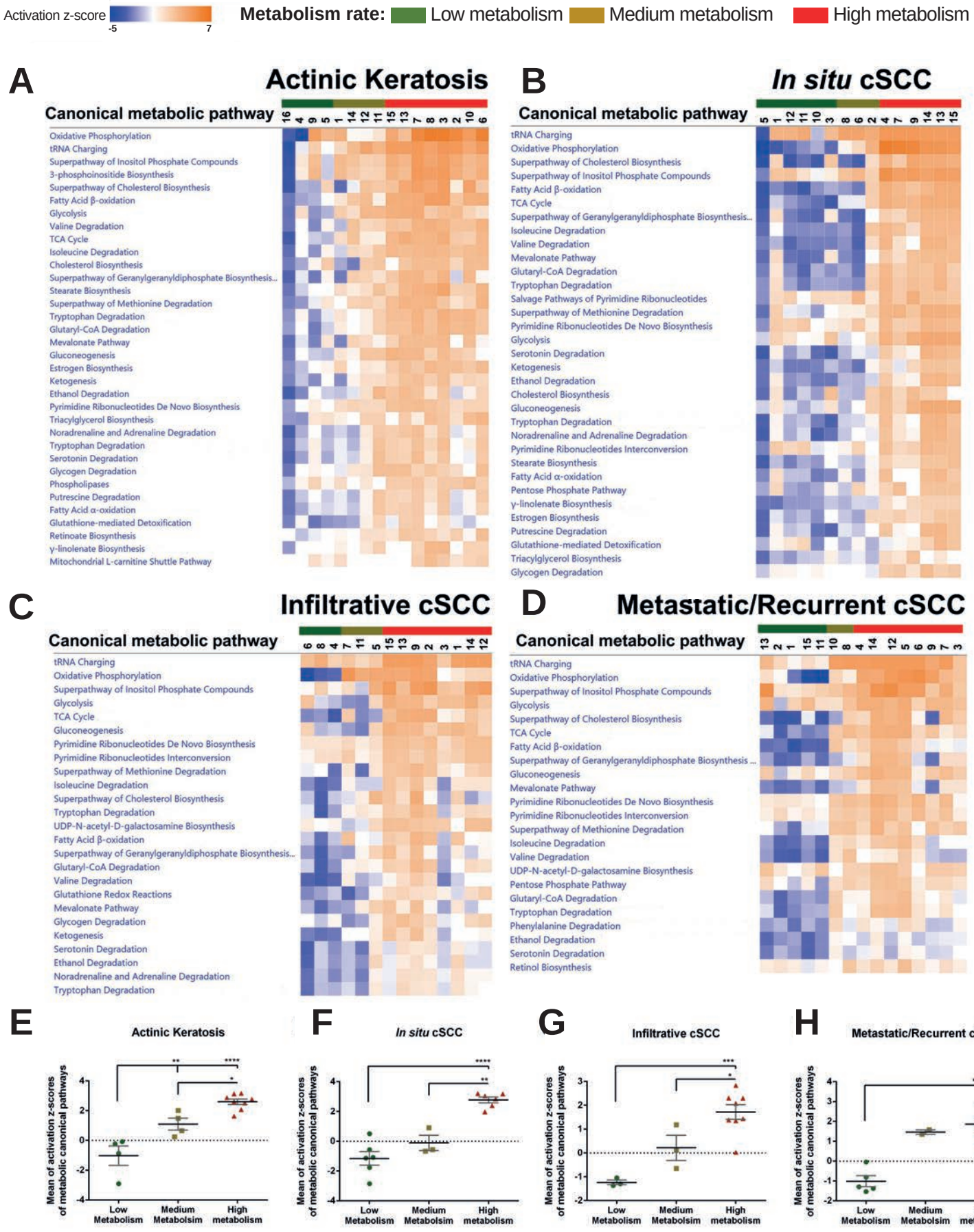
Activation z-score
-5
7
Metabolism rate: Low metabolism Medium metabolism High metabolism
A
Actinic Keratosis
Canonical metabolic pathway
16 4 9 5 1 14 12 11 15 13 7 8 3 2 10 6
Oxidative Phosphorylation
tRNA Charging
Superpathway of Inositol Phosphate Compounds
3-phosphoinositide Biosynthesis
Superpathway of Cholesterol Biosynthesis
Fatty Acid β-oxidation
Glycolysis
Valine Degradation
TCA Cycle
Isoleucine Degradation
Cholesterol Biosynthesis
Superpathway of Geranylgeranyldiphosphate Biosynthesis...
Stearate Biosynthesis
Superpathway of Methionine Degradation
Tryptophan Degradation
Glutaryl-CoA Degradation
Mevalonate Pathway
Gluconeogenesis
Estrogen Biosynthesis
Ketogenesis
Ethanol Degradation
Pyrimidine Ribonucleotides De Novo Biosynthesis
Triacylglycerol Biosynthesis
Noradrenaline and Adrenaline Degradation
Tryptophan Degradation
Serotonin Degradation
Glycogen Degradation
Phospholipases
Putrescine Degradation
Fatty Acid α-oxidation
Glutathione-mediated Detoxification
Retinoate Biosynthesis
γ-linolenate Biosynthesis
Mitochondrial L-carnitine Shuttle Pathway
B
In situ cSCC
Canonical metabolic pathway
5 1 12 11 10 3 8 6 2 4 7 9 14 13 15
tRNA Charging
Oxidative Phosphorylation
Superpathway of Cholesterol Biosynthesis
Superpathway of Inositol Phosphate Compounds
Fatty Acid β-oxidation
TCA Cycle
Superpathway of Geranylgeranyldiphosphate Biosynthesis...
Isoleucine Degradation
Valine Degradation
Mevalonate Pathway
Glutaryl-CoA Degradation
Tryptophan Degradation
Salvage Pathways of Pyrimidine Ribonucleotides
Superpathway of Methionine Degradation
Pyrimidine Ribonucleotides De Novo Biosynthesis
Glycolysis
Serotonin Degradation
Ketogenesis
Ethanol Degradation
Cholesterol Biosynthesis
Gluconeogenesis
Tryptophan Degradation
Noradrenaline and Adrenaline Degradation
Pyrimidine Ribonucleotides Interconversion
Stearate Biosynthesis
Fatty Acid α-oxidation
Pentose Phosphate Pathway
γ-linolenate Biosynthesis
Estrogen Biosynthesis
Putrescine Degradation
Glutathione-mediated Detoxification
Triacylglycerol Biosynthesis
Glycogen Degradation
C
Infiltrative cSCC
Canonical metabolic pathway
6 8 4 7 11 5 15 13 9 2 3 1 14 12
tRNA Charging
Oxidative Phosphorylation
Superpathway of Inositol Phosphate Compounds
Glycolysis
TCA Cycle
Gluconeogenesis
Pyrimidine Ribonucleotides De Novo Biosynthesis
Pyrimidine Ribonucleotides Interconversion
Superpathway of Methionine Degradation
Isoleucine Degradation
Superpathway of Cholesterol Biosynthesis
Tryptophan Degradation
UDP-N-acetyl-D-galactosamine Biosynthesis
Fatty Acid β-oxidation
Superpathway of Geranylgeranyldiphosphate Biosynthesis...
Glutaryl-CoA Degradation
Valine Degradation
Glutathione Redox Reactions
Mevalonate Pathway
Glycogen Degradation
Ketogenesis
Serotonin Degradation
Ethanol Degradation
Noradrenaline and Adrenaline Degradation
Tryptophan Degradation
D
Metastatic/Recurrent cSCC
Canonical metabolic pathway
13 2 1 15 11 10 8 4 14 12 5 6 9 7 3
tRNA Charging
Oxidative Phosphorylation
Superpathway of Inositol Phosphate Compounds
Glycolysis
Superpathway of Cholesterol Biosynthesis
TCA Cycle
Fatty Acid β-oxidation
Superpathway of Geranylgeranyldiphosphate Biosynthesis ...
Gluconeogenesis
Mevalonate Pathway
Pyrimidine Ribonucleotides De Novo Biosynthesis
Pyrimidine Ribonucleotides Interconversion
Superpathway of Methionine Degradation
Isoleucine Degradation
Valine Degradation
UDP-N-acetyl-D-galactosamine Biosynthesis
Pentose Phosphate Pathway
Glutaryl-CoA Degradation
Tryptophan Degradation
Phenylalanine Degradation
Ethanol Degradation
Serotonin Degradation
Retinol Biosynthesis
E
Actinic Keratosis
F
In situ cSCC
G
Infiltrative cSCC
H
Metastatic/Recurrent cSCC
Mean of activation z-scores of metabolic canonical pathways
Low Metabolism
Medium Metabolsim
High metabolism

Figure 3.

A

Patient no./gender	Age	Actinic keratosis	Invasive cSCC	Recurrent cSCC	Metastatic cSCC
1/M	45	PM1	MET1	MET2	MET4
2/M	77		IC1		IC1 MET
3/F	87		IC12		
4/M	81		IC18		

Abbreviations: M: male; F: female.

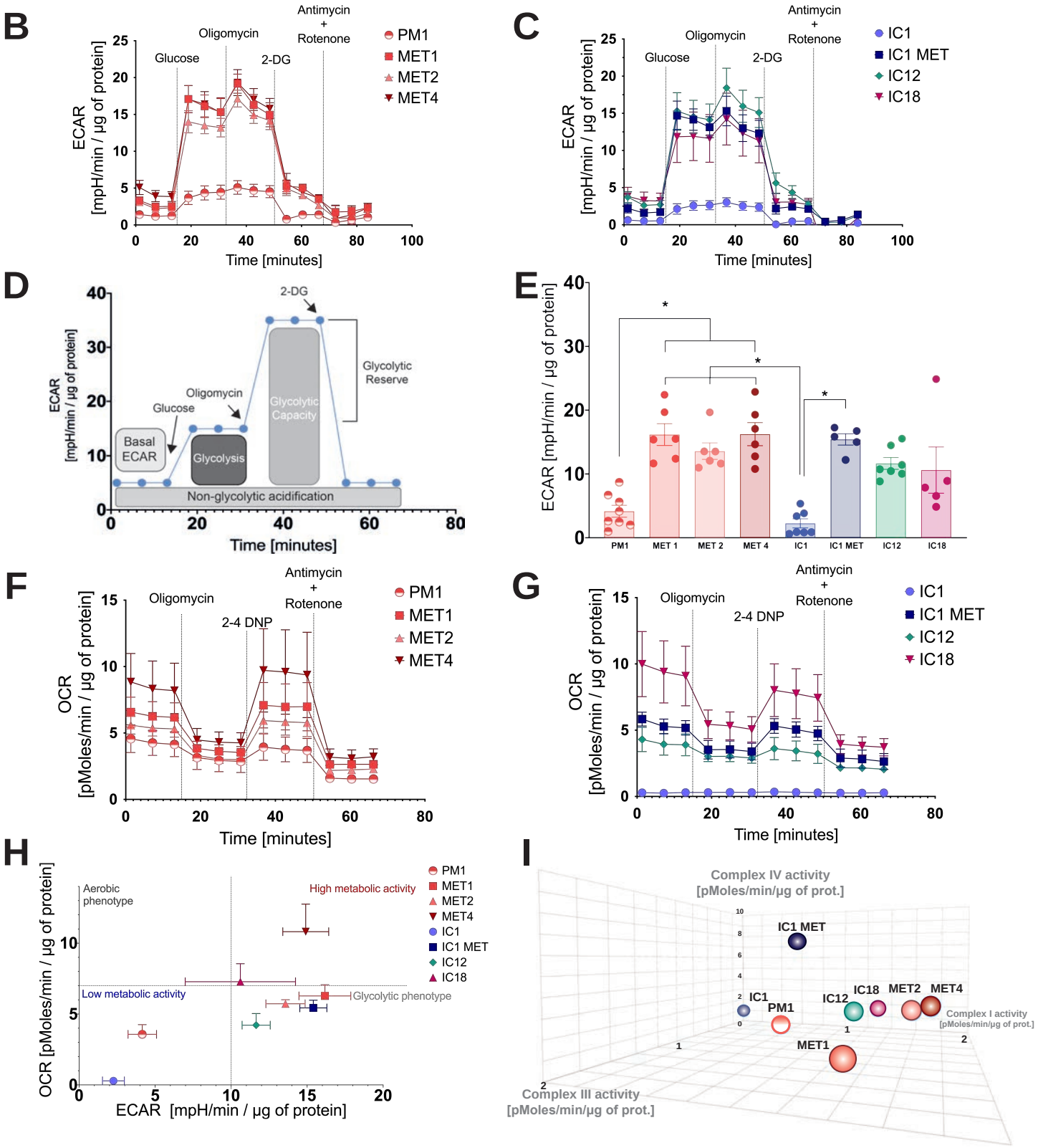

J

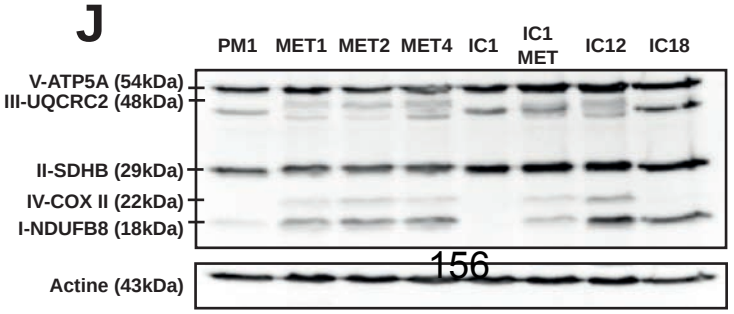

Figure 4.

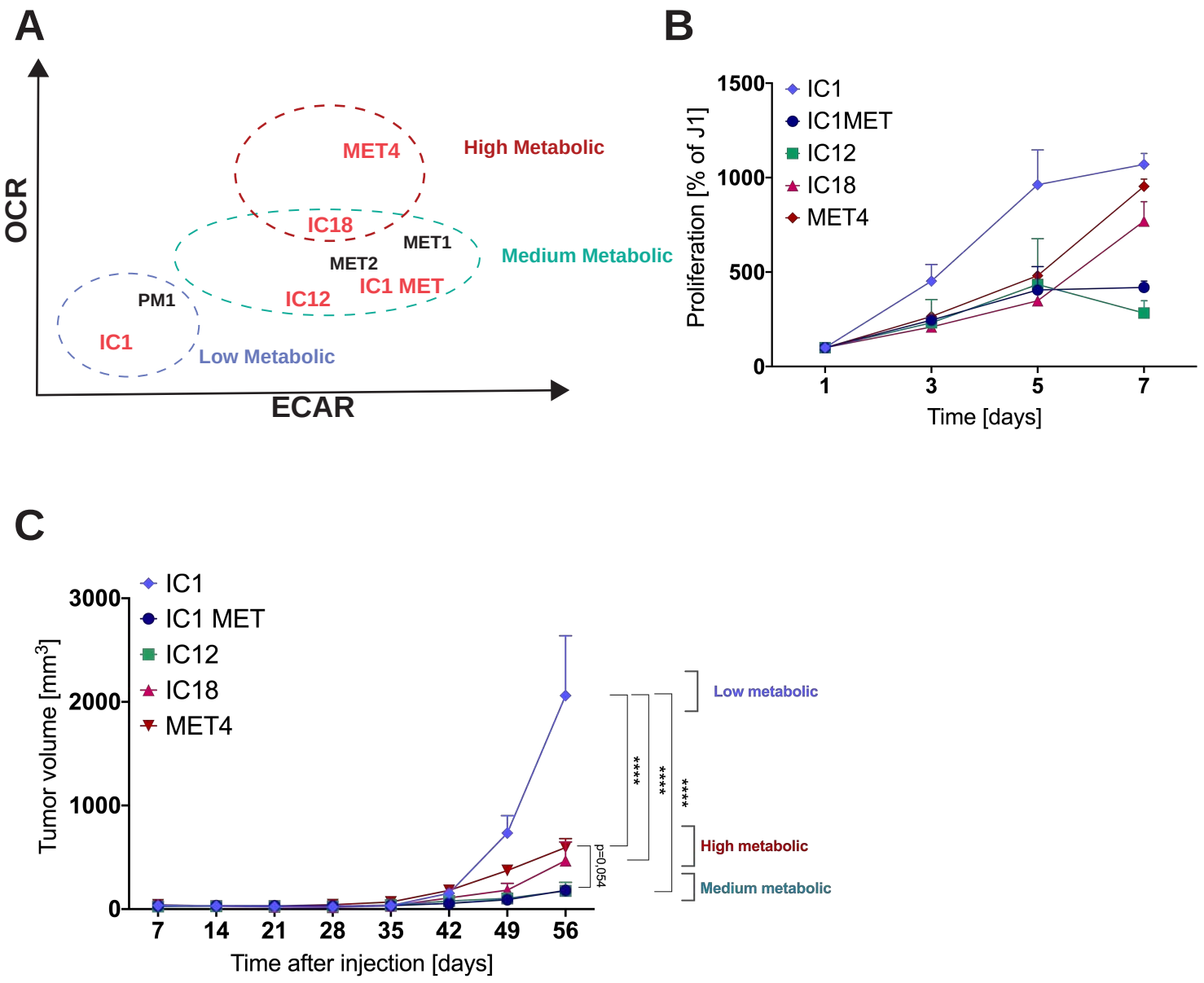
A
OCR
ECAR
MET4
High Metabolic
IC18
MET1
MET2
Medium Metabolic
IC1 MET
IC12
PM1
IC1
Low Metabolic
B
Proliferation [% of J1]
1500
1000
500
0
IC1
IC1MET
IC12
IC18
MET4
1
3
5
7
Time [days]
C
Tumor volume [mm3]
3000
2000
1000
0
IC1
IC1 MET
IC12
IC18
MET4
7
14
21
28
35
42
49
56
Time after injection [days]
****
****
****
p=0.054
Low metabolic
High metabolic
Medium metabolic

Figure 5.

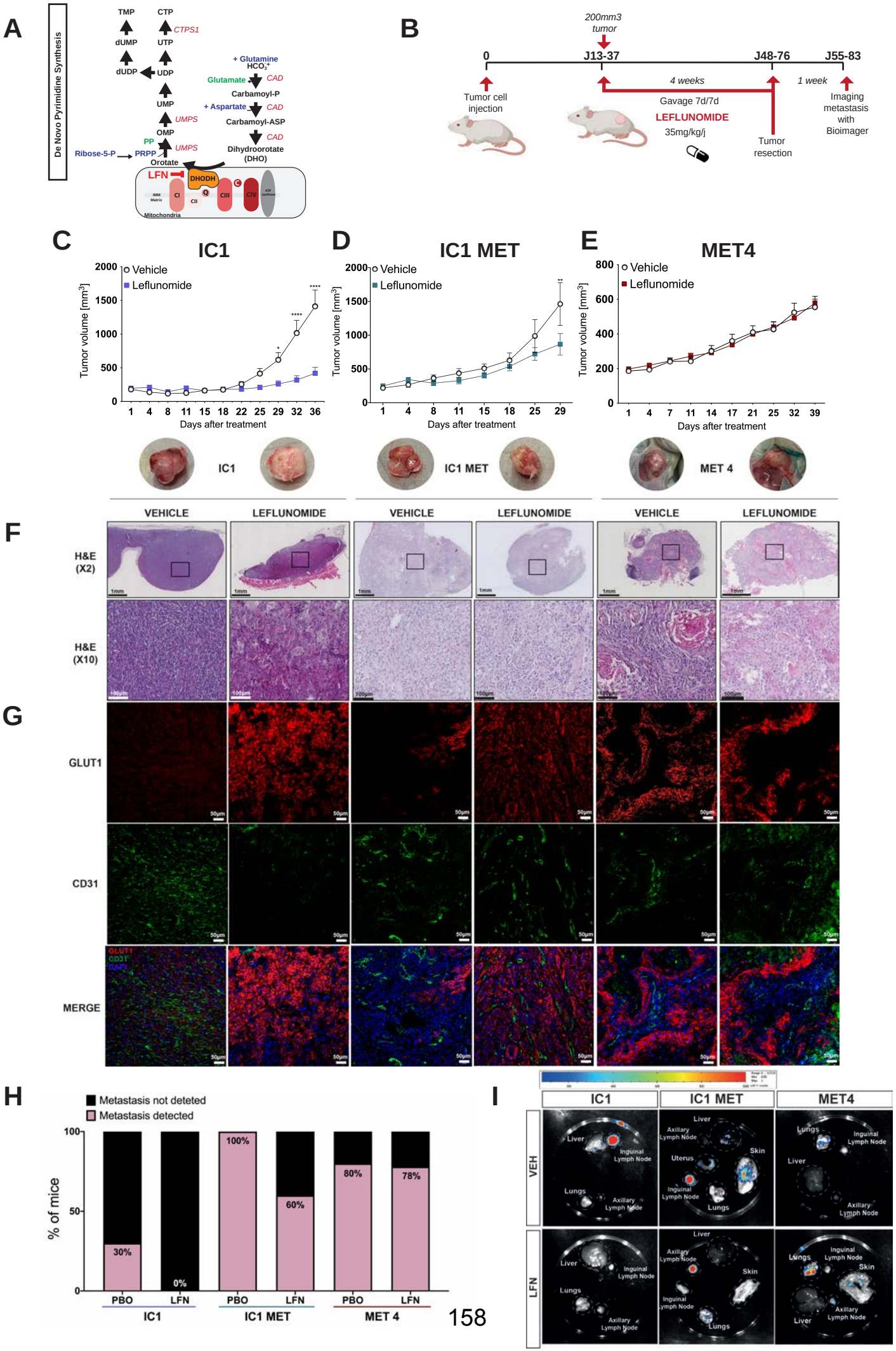
A
De Novo Pyrimidine Synthesis
TMP
CTP
CTPS1
dUMP
UTP
dUDP
UDP
UMP
UMPS
OMP
PP
UMPS
Ribose-5-P
PRPP
Orotate
+ Glutamine
HCO3+
Glutamate
CAD
Carbamoyl-P
+ Aspartate
CAD
Carbamoyl-ASP
CAD
Dihydroorotate
(DHO)
LFN
DHODH
Q
CI
CII
CIII
CIV
Mitochondria
B
200mm3
tumor
0
J13-37
J48-76
J55-83
4 weeks
1 week
Tumor cell
injection
Gavage 7d/7d
LEFLUNOMIDE
35mg/kg/j
Tumor
resection
Imaging
metastasis
with
Bioimager
C
IC1
Vehicle
Leflunomide
Tumor volume [mm3]
Days after treatment
D
IC1 MET
Vehicle
Leflunomide
Tumor volume [mm3]
Days after treatment
E
MET4
Vehicle
Leflunomide
Tumor volume [mm3]
Days after treatment
IC1
IC1 MET
MET 4
F
VEHICLE
LEFLUNOMIDE
VEHICLE
LEFLUNOMIDE
VEHICLE
LEFLUNOMIDE
H&E
(X2)
H&E
(X10)
G
GLUT1
CD31
MERGE
H
Metastasis not deteted
Metastasis detected
% of mice
30%
0%
100%
60%
80%
78%
PBO
LFN
PBO
LFN
PBO
LFN
IC1
IC1 MET
MET 4
I
IC1
IC1 MET
MET4
VEH
LFN
Liver
Lungs
Inguinal
Lymph Node
Axillary
Lymph Node
Uterus
Skin

Figure 6.

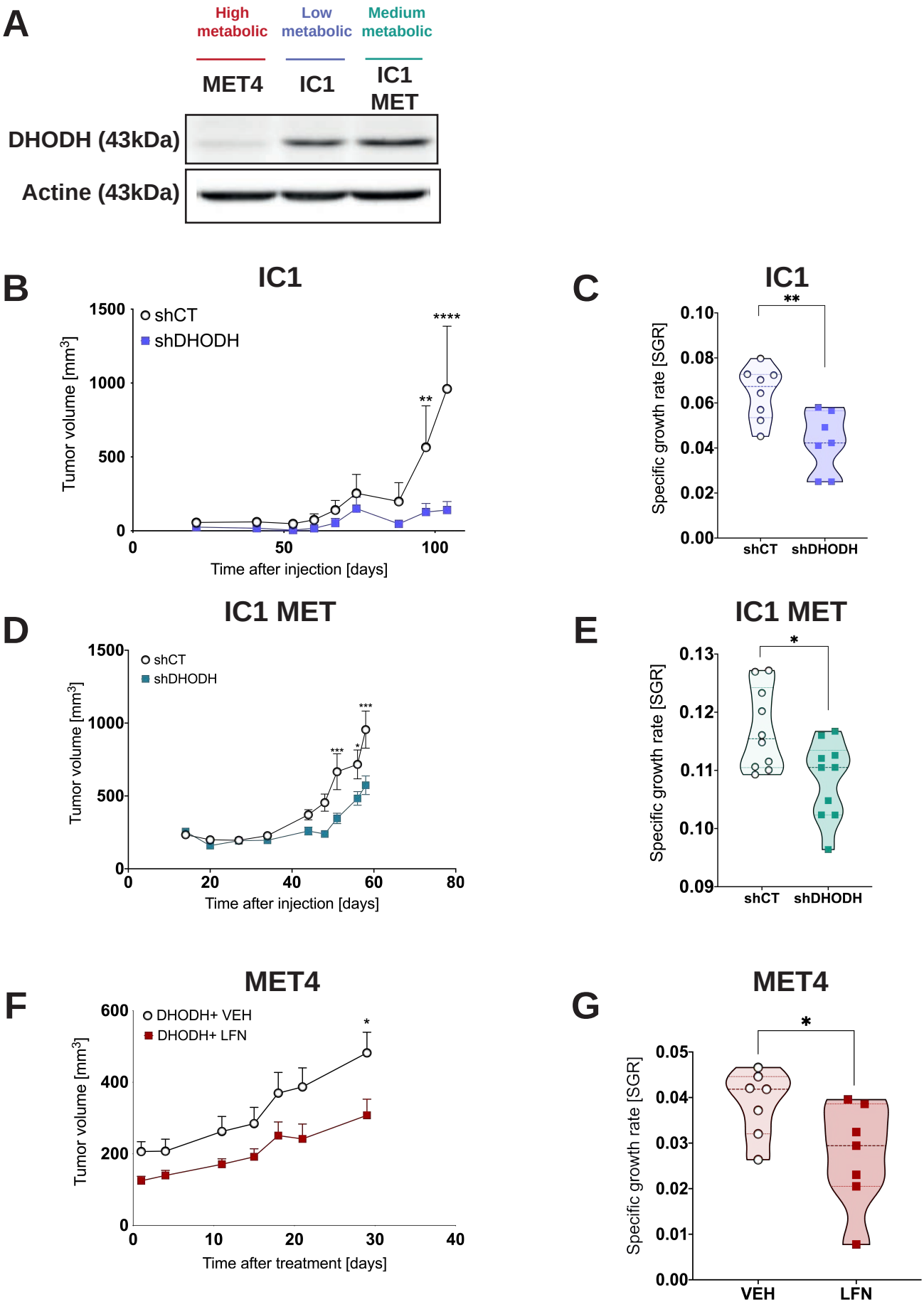
A
High metabolic
Low metabolic
Medium metabolic
MET4
IC1
IC1 MET
DHODH (43kDa)
Actine (43kDa)
B
IC1
shCT
shDHODH
Tumor volume [mm3]
Time after injection [days]
C
IC1
Specific growth rate [SGR]
shCT
shDHODH
D
IC1 MET
shCT
shDHODH
Tumor volume [mm3]
Time after injection [days]
E
IC1 MET
Specific growth rate [SGR]
shCT
shDHODH
F
MET4
DHODH+ VEH
DHODH+ LFN
Tumor volume [mm3]
Time after treatment [days]
G
MET4
Specific growth rate [SGR]
VEH
LFN

Figure 7.

A

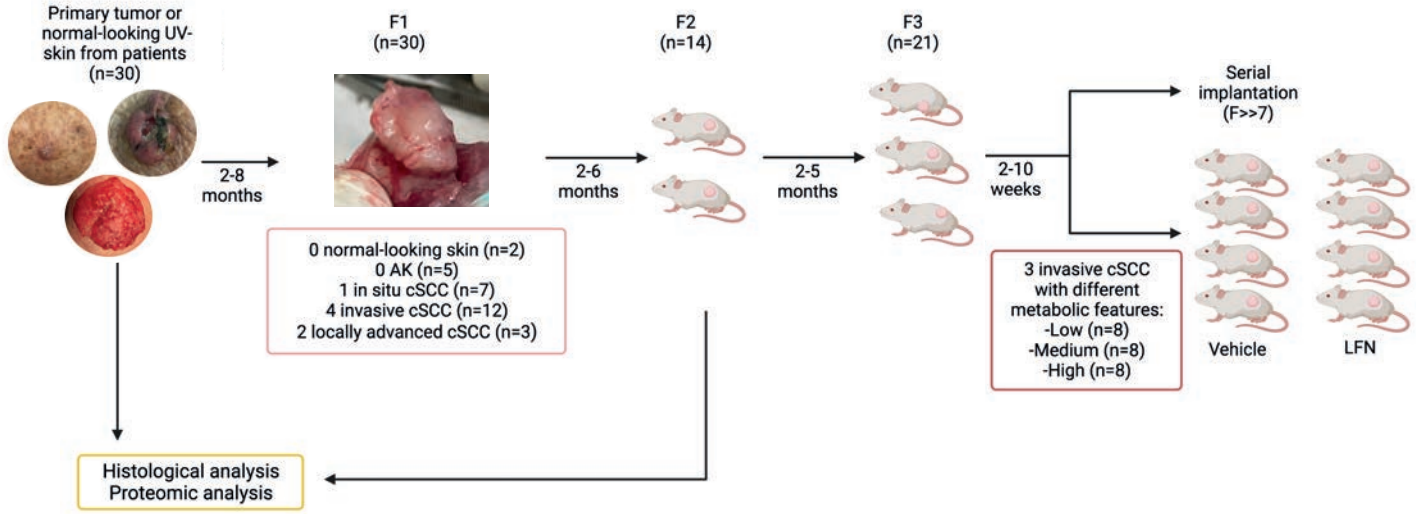

B

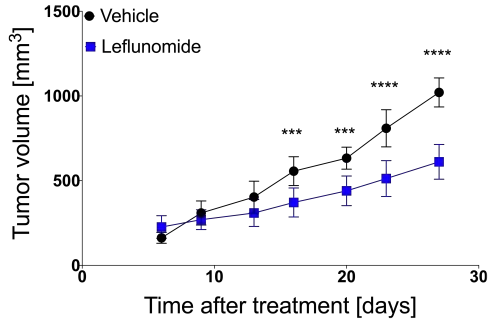

C

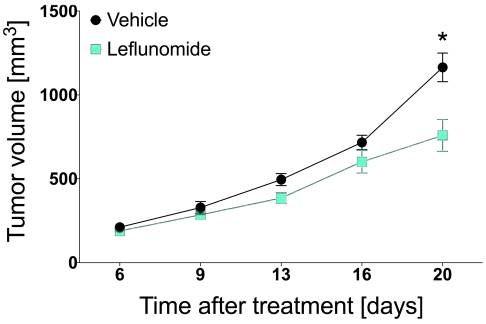

D

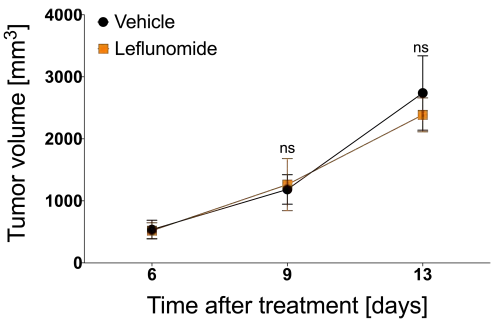

E

Patient gender	Age	Histology subtypes	Differentiation	Location	Organ transplant	Metabolic scoring
1/M	93	Invasive cSCC	Well	Scalp	No	Low
2/F	83	Invasive cSCC	Well	Neck	No	Medium
3/M	69	Invasive cSCC	Moderatly	Pre-tragus	Yes	High

Abbreviations: M, male; F, female; cSCC, cutaneous squamous cell carcinoma

Supplemental Data

Figure S1.

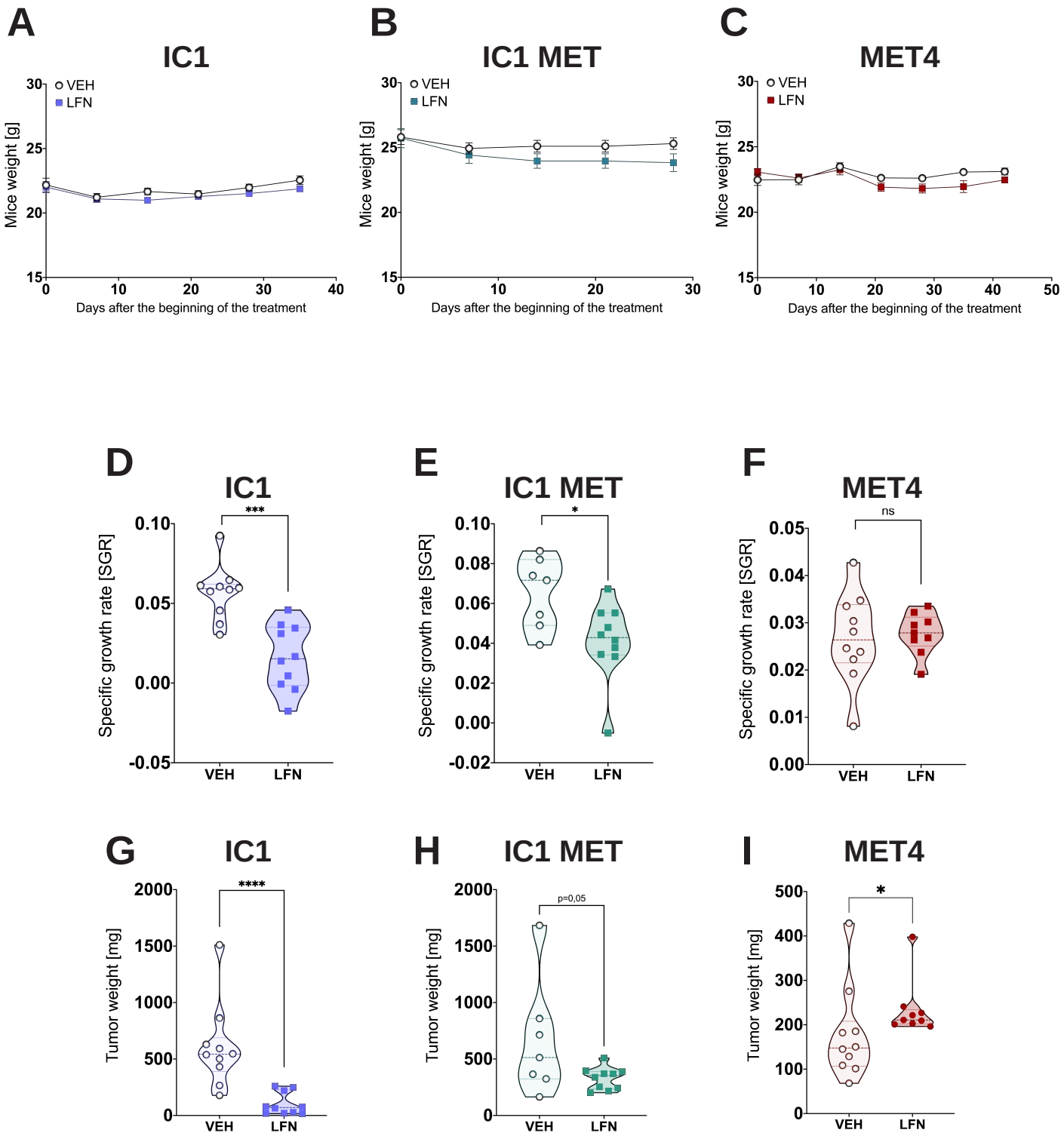

Figure S2.

A

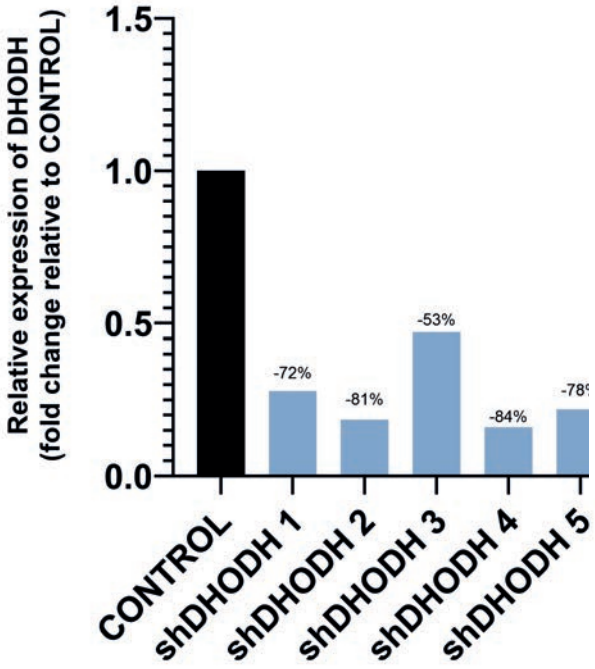
Relative expression of DHODH
(fold change relative to CONTROL)
1.5
1.0
0.5
0.0
-72%
-81%
-53%
-84%
CONTROL
shDHODH 1
shDHODH 2
shDHODH 3
shDHODH 4
shDHODH 5

B

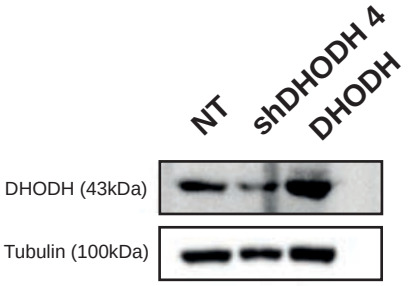
NT
shDHODH 4
DHODH
DHODH (43kDa)
Tubulin (100kDa)

ARTICLE 3

The Early Metabolic Changes of Progression and Immunoediting in Advanced Cutaneous Squamous Cell Carcinoma at Single-Cell Resolution

Article in preparation

The Early Metabolic Changes of Progression and Immunoediting in Advanced Cutaneous Squamous Cell Carcinoma at Single-Cell Resolution

Léa Dousset[1,2], Domitille Chalopin[3,4,5], Vitalina Bashynska[3,4], Jean-Philippe Guegan[6], Julie Giraud[3,4], Pauline Michon[1], Fanny Beltzung[1,7], Walid Mahfouf[1], Elodie Muzotte[1], Giulia Guzzo[1], Nivea Amoedo[8,9], Xavier Gauthereau[10], Alain Taieb[1], François Moisan[1], Rodrigue Rossignol[8,9], Maya Saleh[3], Marie Beylot-Barry[1,2], Macha Nikolski[3,4], Hamid-Reza Revani[1,11§]

[1]INSERM 1312, Bordeaux Institute of Oncology, Team 5 Translational Research on Oncodermatology and rare skin diseases, University of Bordeaux, F-33076 Bordeaux, France.
[2]Dermatology Department, CHU Bordeaux, France.
[3]University of Bordeaux, Bordeaux Bioinformatics Center, Bordeaux, France
[4]University of Bordeaux, CNRS, IBGC, UMR 5095, Bordeaux, France
[5]University of Bordeaux, CNRS, ImmunoConcEpt, UMR 5164, Bordeaux, France
[6]Explicyte Immuno-Oncology, Bordeaux, France
[7]Pathological Department, CHU Bordeaux, France.
[8]Inserm U1211 Maladies Rares: Génétique et Métabolisme (MRGM), Université de Bordeaux, Bordeaux, France;
[9]CELLOMET, Centre de Génomique Fonctionnelle de Bordeaux, Université de Bordeaux, Bordeaux, France.
[10]TransBioMed Core, PCRq'UB, University of Bordeaux, France
[11]Aquiderm, Univ. Bordeaux, Bordeaux, France

§ **Corresponding Author**
Email address: hamid-reza.rezvani@u-bordeaux.fr

Key words: advanced cutaneous squamous cell carcinoma, tumor microenvironment, single cell RNA seq, digital spatial profiling, tumor-associated macrophages, mesenchymal transition, metabolism, immunometabolism.

INTRODUCTION

Non-melanoma skin cancers (NMSC) are the most common cancer in white-skinned individuals (Rogers *et al.*, 2015; Venables *et al.*, 2019a). Among these cancers, cutaneous squamous cell carcinoma (cSCC) is a carcinogenesis process that develops in several stages. This carcinoma is most of the time surrounded by in situ or precancerous lesions (actinic keratosis, AK), allowing to have access at the same time to several lesions of different carcinogenic levels on the same patient (Fernandez Figueras, 2017). The majority of cSCC are curable when they are treated early, with 5-years survival rate of greater than 90% (Brougham *et al.*, 2012). However, despite its very good prognosis, around 1.5 to 5.2% of cSCC recurred in a very aggressive manner (called “advanced cSCC”, acSCC) with local and perineural invasion, metastatic spread and high mortality rate (Brantsch *et al.*, 2008; Schmults *et al.*, 2013; Venables *et al.*, 2019b; Knuutila *et al.*, 2020; Tokez *et al.*, 2022). Even if cemiplimab, an inhibitor of programmed death 1 (PD-1) has been recently approved for advanced cSCC, around 40% of patients will not respond to the therapy (Migden *et al.*, 2018; Gross *et al.*, 2022). Because of the risk of graft rejection, this PD-1 inhibitor is also contraindicated in organ transplant recipients (Fisher *et al.*, 2020), even if they have the most aggressive forms of cSCC (Basset-Seguin and Maubec, 2022; Menzies *et al.*, 2022). Thus, new therapeutic targets are needed in the era of acSCC.

Cancer cells upregulate both glycolysis and TCA cycle metabolism in order to provide the substrates required for the synthesis of macromolecules such as lipids and nucleotides that are required to sustain rapid cell proliferation (De Berardinis and Chandel, 2016). This metabolic reprogramming remains essential for cancer cells but also for the cells of the tumor microenvironment (TME) because of a continuous cell-to-cell communication (Mantovani *et al.*, 2008).

Single-cell transcriptomics has revealed intra-tumoral heterogeneity (ITH) within many cancer types, identifying cell populations that drive drug resistance, predict metastatic risk, and mediate plasticity (Tirosh *et al.*, 2016; Puram *et al.*, 2017; Neftel *et al.*, 2019). Ji et al recently characterize the composition and spatial architecture of cSCC in 10 tumor-normal skin pairs cSCC (Ji *et al.*, 2020), but little is known about the difference between composition and spatial architecture of

precancerous lesion AKs and cSCC as well as about the metabolic changes in the era of cSCC.

Here, we combine single-cell and spatial transcriptomics (ST) of a series of primary human cSCCs, along with matched precancerous or in situ surrounded lesion, using digital spatial profiling (DSP) and single-cell RNA sequencing (scRNA-seq) to maximize the resolution and depth of data. We used sequential fluorescence in situ hybridization, thanks to Nanostring technologies to directly visualize RNA molecules in their native environment. A total of 32526 single-cell transcriptomes of $CD45^+$immune cells were characterized from 2 tumor-precancerous skin-paired lesions (*a total of 4 patients is expected)* using scRNA-seq and integrated with DSP of cancer cells at different stages and tumor-associated macrophages to characterize the metabolic landscape of the TME.

RESULTS

Multimodal Profiling of Spatially Distinct Regions within Advanced Cutaneous Squamous Cell Carcinoma

A total of 44 areas of illumination (AOIs) with healthy, precancerous AK or in situ cSCC, or tumor were identified in FFPE specimens of two cSCC patients subjected to any treatment. The main clinical and pathological characteristics of the patients are presented in Table 1. To decipher the tissue segmentation, we performed immunostaining using pancytokeratin (PanCK) for epithelial cells, vimentin for cell in epithelial-mesenchymal transition on the invasion front of the tumor, and CD68 staining for macrophages localized in healthy, pretumoral, in situ or tumoral areas (Figure 1A and B). The four colour tumor tissue profiling that was used to demarcate tumor (center and invasion front), healthy tissue and macrophages is shown in Figure 1B. For each slide, Region Of Interests (ROIs) were drawn in order to analyze the expression of the WTA gene panel in the tumor (central or invasion front), peritumoral or healthy regions. Each ROI was further segmented in 2 or 3 AOIs based on the PanCK, Vimentin and CD68 staining. The number of AOI is summarized in figure 1C.

To examine whether it is possible to discriminate the lesions at different stages of carcinogenesis from its healthy tissue counterpart based on the gene expression profiles in $CD68^+$, $PanCK^+$ or $PanCK^+Vimentine^+$ cells, principal component analysis (PCA) was performed (Figure 1D). Results indicated that tumors and advanced tumors

could be discriminated from its healthy tissue counterpart based on the gene expression patterns in both PanCK$^+$ cells and CD68$^+$ cells. However, the gene expression features of PanCK$^+$ cells and CD68$^+$ cells in peritumoral tissue and precancerous lesions were very similar to the healthy tissues (Figure 1D). Interestingly, the gene expression profile of PanCK+ cells found in tumors could be distinguished from the profile of Panck+ cells found in invasion front. Furthermore, PanCK+ cells and PanCK+/vimentin+ cells in invasion front could be discriminated based on their gene expression profiles. Differentially expressed genes (DEG) were then screened for gene ontology (GO) analysis. Detailed comparison among the different clusters of cells showed that DEG were significantly enriched in following GO terms: cell junction organization, extracellular matrix organization, human immune response, keratinization and regulation of leukocyte activation (Figure 1E).

Intratumoral metabolic heterogeneity of malignant cells.

Thus, we aimed to characterize the intratumoral metabolic heterogeneity between cancer cells located in the center of the tumor and cancer cells in mesenchymal transition localized in the invasion front (Figure 2A-D). When epithelial cells started their tumor transformation, they stopped their keratinocyte and epidermal cell differentiation (Figure 2C). At the same time, the glycolysis was upregulated, and lipid biosynthesis was dowregulated (Figure 2D, E). Comparing metabolic features of PanCK+ cells between tumor and invasion front indicated that cells at mesenchymal transition state (PanCK$^+$, vimentin$^+$ cells) rewired their metabolic pathways favoring the oxidative phosphorylation pathway (OXPHOS) (Figure 2F-H).

Altogether, these results indicate that metabolism plays a key role in cancer progression. Indeed, both tumoral transformation of precancerous lesions and epithelial-mesenchymal transition process require specific metabolic demands, which will be achieved through metabolic rewiring mechanisms.

Metabolic heterogeneity in non-malignant cells

We next explored the metabolic heterogeneity of non-malignant cells. We first characterized the metabolic features of macrophages in healthy tissue compared to those located in the invasion front of the tumor (Figure 3A-B). As shown in the differential expression volcano plot, several genes were down and upregulated (Figure 3C). Both glycolysis and OXPHOS were upregulated in macrophages located in the

invasion front compared to macrophages in healthy tissue (Figure 3D), pointing out that both energetic pathways are activated in TAMs. Thus, similar to malignant cells, metabolic rewiring in macrophages seems to play a key role in cancer progression. *This DSP analysis has been done in one patient and we are now expecting the results for three other patients with same tumor sections to go deeper in the characterization of TAMs.*

To better characterize the metabolic landscape of immune cells in the TME, we conducted a scRNA-seq analysis on two cSCC paired with their matched precancerous surrounded lesion (Figure 4A). For patient 1, prior to dissociation, portions of tumors were formalin-fixed for DSP analysis (picture of the tumor and HE staining shown in Figure 1A). 45678 cells were sequenced at a median depth of 115 reads/cell, with 32526 cells passing filtering utilizing Seurat (Table 2).
Immune cell-type proportion analysis reflected sample processing, with 21 subsets of cells (Figure 4B-C). Comparing clusters between AK and cSCC, we found that some clusters of macrophages and T lymphocytes with gammadelta and cytotoxic properties were enriched in the tumor, while, at the other hand, B cells and plasmablasts were depleted (Figure 4D). Tumor and precancerous lesion exhibited differences in subset of immune cells in G2M phase (Figure 4E), pointing out a rapidly growing behavior for some subsets of cells or a senescent state for others. Focusing on metabolism, we found that glycolysis (Figure 5A) or OXPHOS (Figure 5C) were activated in different subsets of monocytes/macrophages in invasive cSCC. On the other hand, circulating T cells and Treg seemed to upregulate both glycolysis and OXPHOS pathways in order to go to a highly proliferative state (Figure 5A-C). We have now collected the data for two more patients to perform a deeper analysis on this different subset of cells.

Discussion

The impact of the immune system on the development of cSCC is illustrated by their high incidence in immunocompromised patient. Immunosuppressed solid organ transplant recipients (SOTRs) have a 65- to 250-fold greater incidence of cSCC than the general population, more aggressive progression and a higher risk of metastasis and death (Lanz *et al.*, 2019). In a recent Australian study, the median time from the

diagnosis of primary cSCC to metastasis was 5 months (0, 29), indicating the aggressive nature of cSCC in this subpopulation of patient (Shao *et al.*, 2022). *Discussion in preparation.*

EXPERIMENTAL MODEL AND SUBJECT DETAILS

Human Patient Samples

Cutaneous SCCs and patient-matched normal adjacent skin samples were collected under the MITOSKIN study, conducted in the dermatology department of Bordeaux University Hospital. Every patient presented with a suspected lesion at different stages of carcinogenesis (actinic keratosis, in situ cSCC, invasive cSCC, locally advanced cSCC, recurrent cSCC and cutaneous metastasis of cSCC), were subjected after informed consent to two biopsies in the tumor (one in formol for histopathological analyze; the other frozen in liquid nitrogen), and one in the normal tissue also frozen in liquid nitrogen. Analysis of tumor samples were performed according to the relevant national law providing protection to people taking part in the biomedical research. The patients/participants provided their written informed consent to participate in the study. In case of patient refusal, expressed either orally or written, residual tumor samples were excluded. The National Commission for Data Processing and Liberties approved all analyses realized in this study (n° approval: ID-RCB 2018-A03096 delivered on January 04, 2019). NCT04389112

METHOD DETAILS

Tissue Dissociation

Fresh tumor specimens and normal skin were minced with a scalpel in serum-free DMEM (GIBCO) with the tumor dissociation kit (Miltenyi). For normal skin, subcutaneous fat was removed with surgical scissors prior to mincing and trypsin-EDTA incubation.

Cell Sorting.

After dissociation, single cell suspensions were purified with a sequential cell sorting with magnetic bead coupled antibodies directed to CD45 using a column-based magnetic cell separation technology (Miltenyi).

Single-cell RNA-sequencing

scRNA-seq was performed immediately after FACS sorting by the Stanford Functional Genomics Facility (SFGF) with the 10X Chromium 30 v2 kit (10X Genomics, Pleasanton, CA) following the manufacturer's protocol. Target number of captured cells ranged from 5,000 to 10,000 cells. Sequencing libraries were prepared per manufacturer's protocol. Sequencing was performed on a HiSeq 4000 (Illumina, Inc., San Diego, CA) at a median depth of 115,216 reads/cell (Table S1). Raw sequencing data was processed with the cell- ranger pipeline (version 2.1.0, 10X Genomics) and mapped to the hg19 reference genome to generate matrices of gene counts by cell barcodes.

Tissue Preparation FFPE tissue

Tissue Preparation FFPE tissue (8 unstained x 5 µm) were prepared onto charged slides by Queensland pathology and one slide was H&E stained. The H&E slide was scanned at 20x and 40x magnification on the 3D Histech slide scanner and sent for demarcation of tumor and normal regions by a qualified pathologist. Four unstained slides were used for the Opal Multiplex IF staining (PerkinElmer) and two unstained slides were transported to Nanostring Technologies (Seattle) for DSP profiling. Multispectral Immunofluorescence Multispectral immunofluorescence staining was performed using the Opal four-color IHC Kit (NEL794001KT; Perkin Elmer, Waltham, MA) as per manufacturer's instructions. The Opal kit uses tyramide signal amplification (TSA) conjugated fluorophores to detect targets within an immunofluorescence assay. Briefly, the slides were deparaffinised with Xylene, rehydrated with a series of graded ethanol (100%, 95%, 70% for 2 min) and washed in Tris buffered saline with 0.1% Tween 20 (Merck). Slides were then heated using microwave treatment (MWT) for 45 seconds at 100% power followed by 15 min at 20% power in AR Buffer. Slides were blocked using the blocking diluent (Perkin Elmer) for 10 min at room temperature (RT). The primary antibody was incubated for 37°C for 32 min in the Dako Slide Hybridiser (Agilent, Ca, USA). Slides were washed in TBST and underwent MWT in AR buffer prior to probing with the next antibody. Slides were then counterstained with DAPI for 5 min and mounted with Prolong Gold (Invitrogen) and coverslipped prior to imaging. Slides were imaged using the Vectra 3.0 spectral imaging system (PerkinElmer) and image analysis performed using the InForm image analysis software (PerkinElmer). Low magnification scanning at 10x

was initially performed to get an overview of the slide and to compare to pathologist-demarcated H&E sections, next 10 regions of interest across the fields were chosen across tumor, immune, infiltrating edges, and the stroma to get representative images of the tissue section

Protein Digital Spatial Profiling

Protein Digital Spatial Profiling was carried out by Nanostring Technologies BioRxiv 2019. In brief, the protocol has five steps: standard FFPE tissue preparation; tissue incubation with a mixture of visualization markers (VMs) and DSP probes; imaging and region of interest (ROI) selection; ultraviolet (UV) exposure; and oligo collection step. This is then quantified using the Nanostring nCounter® system. Once the VM step have been completed to visualize the tissue morphology based on four-color fluorescence imaging of epithelial cells (PanCK), epithelial cells in EMT (PanCK_vimentin), macrophages (CD68), and nuclear stain (DAPI), 44 regions of interest (ROI) at 200µm circular diameter were selected in consultation with a pathologist. After UV illumination of the ROIs, the eluent was collected via microcapillary aspiration and transferred into individual wells of a microtiter plate. Once the 44 ROIs were processed, indexing oligos were hybridized to NanoString optical barcodes for digital counting on the nCouter®. Digital counts from barcodes corresponding to protein probes were then normalized to ERCC and housekeeping counts.

References

Basset-Seguin, N. and Maubec, E. (2022) ‘Recent Advanced in the Treatment of Advanced SCC Tumors’, *Cancers*. Cancers (Basel), 14(3). doi: 10.3390/CANCERS14030550.

De Berardinis, R. J. and Chandel, N. S. (2016) ‘Fundamentals of cancer metabolism’, *Science advances*. Sci Adv, 2(5). doi: 10.1126/SCIADV.1600200.

Brantsch, K. D. *et al.* (2008) ‘Analysis of risk factors determining prognosis of cutaneous squamous-cell carcinoma: a prospective study’, *The Lancet Oncology*. Lancet Oncol, 9(8), pp. 713–720. doi: 10.1016/S1470-2045(08)70178-5.

Brougham, N. D. L. S. *et al.* (2012) ‘The incidence of metastasis from cutaneous squamous cell carcinoma and the impact of its risk factors’, *Journal of surgical*

oncology. J Surg Oncol, 106(7), pp. 811–815. doi: 10.1002/JSO.23155.
Fernandez Figueras, M. T. (2017) 'From actinic keratosis to squamous cell carcinoma: pathophysiology revisited', *Journal of the European Academy of Dermatology and Venereology : JEADV*. J Eur Acad Dermatol Venereol, 31 Suppl 2, pp. 5–7. doi: 10.1111/JDV.14151.
Fisher, J. *et al.* (2020) 'Immune checkpoint inhibitor therapy in solid organ transplant recipients: A patient-centered systematic review', *Journal of the American Academy of Dermatology*. J Am Acad Dermatol, 82(6), pp. 1490–1500. doi: 10.1016/J.JAAD.2019.07.005.
Gross, N. D. *et al.* (2022) 'Neoadjuvant Cemiplimab for Stage II to IV Cutaneous Squamous-Cell Carcinoma', *The New England journal of medicine*. N Engl J Med. doi: 10.1056/NEJMOA2209813.
Ji, A. L. *et al.* (2020) 'Multimodal Analysis of Composition and Spatial Architecture in Human Squamous Cell Carcinoma.', *Cell*. Cell. doi: 10.1016/j.cell.2020.05.039.
Knuutila, J. S. *et al.* (2020) 'Risk Factors and Prognosis for Metastatic Cutaneous Squamous Cell Carcinoma: A Cohort Study', *Acta dermato-venereologica*. Acta Derm Venereol, 100(16), pp. 1–9. doi: 10.2340/00015555-3628.
Lanz, J. *et al.* (2019) 'Aggressive Squamous Cell Carcinoma in Organ Transplant Recipients', *JAMA dermatology*. JAMA Dermatol, 155(1), pp. 66–71. doi: 10.1001/JAMADERMATOL.2018.4406.
Mantovani, A. *et al.* (2008) 'Cancer-related inflammation', *Nature*. Nature, 454(7203), pp. 436–444. doi: 10.1038/NATURE07205.
Menzies, S. *et al.* (2022) 'A population-based comparison of organ transplant recipients in whom cutaneous squamous cell develops versus those in whom basal cell carcinoma develops', *Journal of the American Academy of Dermatology*. J Am Acad Dermatol, 86(6), pp. 1377–1379. doi: 10.1016/J.JAAD.2021.05.032.
Migden, M. R. *et al.* (2018) 'PD-1 blockade with cemiplimab in advanced cutaneous squamous-cell carcinoma', *New England Journal of Medicine*. Massachussetts Medical Society, 379(4), pp. 341–351. doi: 10.1056/NEJMoa1805131.
Neftel, C. *et al.* (2019) 'An Integrative Model of Cellular States, Plasticity, and Genetics for Glioblastoma', *Cell*. Cell, 178(4), pp. 835-849.e21. doi: 10.1016/J.CELL.2019.06.024.
Puram, S. V. *et al.* (2017) 'Single-Cell Transcriptomic Analysis of Primary and Metastatic Tumor Ecosystems in Head and Neck Cancer', *Cell*. Cell, 171(7), pp.

1611-1624.e24. doi: 10.1016/J.CELL.2017.10.044.
Rogers, H. W. *et al.* (2015) 'Incidence estimate of nonmelanoma skin cancer (keratinocyte carcinomas) in the us population, 2012', *JAMA Dermatology*. American Medical Association, 151(10), pp. 1081–1086. doi: 10.1001/jamadermatol.2015.1187.
Schmults, C. D. *et al.* (2013) 'Factors predictive of recurrence and death from cutaneous squamous cell carcinoma: a 10-year, single-institution cohort study', *JAMA dermatology*. JAMA Dermatol, 149(5), pp. 541–547. doi: 10.1001/JAMADERMATOL.2013.2139.
Shao, E. X. *et al.* (2022) 'Pathways from Diagnosis to Death from Keratinocyte Cancer in Kidney Transplant Recipients', *Dermatology (Basel, Switzerland)*. Dermatology. doi: 10.1159/000524120.
Tirosh, I. *et al.* (2016) 'Single-cell RNA-seq supports a developmental hierarchy in human oligodendroglioma', *Nature*. Nature, 539(7628), pp. 309–313. doi: 10.1038/NATURE20123.
Tokez, S. *et al.* (2022) 'Cumulative incidence and disease-specific survival of metastatic cutaneous squamous cell carcinoma: A nationwide cancer registry study', *Journal of the American Academy of Dermatology*. J Am Acad Dermatol, 86(2), pp. 331–338. doi: 10.1016/J.JAAD.2021.09.067.
Venables, Z. C. *et al.* (2019a) 'Nationwide Incidence of Metastatic Cutaneous Squamous Cell Carcinoma in England', *JAMA dermatology*. JAMA Dermatol, 155(3), pp. 298–306. doi: 10.1001/JAMADERMATOL.2018.4219.
Venables, Z. C. *et al.* (2019b) 'Nationwide Incidence of Metastatic Cutaneous Squamous Cell Carcinoma in England', *JAMA Dermatology*. American Medical Association, 155(3), pp. 298–306. doi: 10.1001/jamadermatol.2018.4219.

Table 1. Patients Clinicopathological Features

Patient	Gender	Age (years)	Location	Immunosupression	Type of tumor	AJCC Classification	Differentiation	Maximum tumor thickness	Perineural Invasion	Complete excision	Recurrence	Patient alive
1	female	82	Pretragian	No	Actinic keratosis aSCC	T3N0M0	Well differentiated	17mm	No	No	Yes	Yes
2	female	87	Pretragian	No	Actinic keratosis aSCC	T3N0M0	Moderatly differentiated	15mm	No	Yes	Yes	Yes

Abbreviations: asCC, advanced cutaneous squamous cell carcinoma; AJCC, American Joint Committee on Cancer

Table 2. Evaluation of Single Cell RNA Sequence Quality

Patient number	Lesion	Cell number	% of recovery	Fraction reads in cells	Mean reads/cell	Median UMIs	Total genes	Median genes
1	AK	10458	45.3%	91.2%	35907	4659	26602	1556
	Tumor	8209	34.6%	88.7%	40282	4457	26639	1697
2	AK	5769	25.8%	93.8%	49621	6404	25058	1990
	Tumor	8090	39.5%%	91.4%	37648	5808	24649	1963

Abbreviations: AK, actinic keratosis, UMI, unique molecular index.

Figure Legends

Figure 1. Multimodal profiling of advanced cutaneous squamous cell carcinoma using comparative staining across two multiplex technologies.

(A) Picture and corresponding H&E stain of advanced cutaneous squamous cell carcinoma (cSCC) of the pre-tragus, surrounded by an in situ cSCC (*) and normal-looking skin (**).

(**B-C**) ROI selection. (**B**) Opal four-color IHC staining of the tissue section for cytokeratin (red), vimentin (yellow), CD68 (green), DAPI (blue). (**C**) For each slide, Region Of Interests (ROIs) were drawn in order to analyze the expression of the WTA gene panel in the tumor (central or invasion front), peritumoral or healthy regions. Each ROI was further segmented in 2 or 3 AOIs (area of illumination) based on the PanCK, Vimentin and CD68 staining. The number of AOI is summarized in this table.

(**D-E**) Principal component analysis (PCA) (**D**) and hierarchical clustering (heatmap) of cells (**E**).

Figure 2. Characterization of metabolic features of PanCK$^+$ cells at invasion front, cSCC and peritumoral lesions.

(A) Opal four-color IHC staining of the tissue section for cytokeratin (red), vimentin (yellow), CD68 (green), DAPI (blue).

(B) Cell population estimates, using the SpatialDecon algorithm (Danaher, Nat Comm 2022) to estimate the cell populations within each AOIs. Difference between Peritumoral_PancK, Tumor_PancK and Mixed_Panck Vimentin areas are shown.

(C) Signaling pathways enriched in Peritumoral_PanCK and Tumor_PanCK cells were tested using fgsea R package and some dataset collection of MSigDB (GO, KEGG, REACTOME and Hallmarks).

(D) Genes differentially expressed between Peritumoral_PanCK and Tumor_PanCK cells were tested using the limma R pack

(E) Signaling pathways enriched in Peritumoral_PanCK and Tumor_PanCK cells were tested using our own metabolic pathway gene enrichment.
(F) Signaling pathways enriched in Tumor_PanCK and Mixed_PanCK.Vimentin cells were tested using fgsea R package and some dataset collection of MSigDB (Hallmarks). Top 10 of upregulated and downregulated pathways are illustrated. Cancer cells in vimentin areas highly expressed epithelial mesenchymal transition genes.
(G) Genes differentially expressed between Tumor_PanCK and Mixed_PanCK.Vimentin cells were tested using the limma R package.
(H) Signaling pathways enriched in Tumor_PanCK and Mixed_PanCK.Vimentin cells were tested using our own metabolic pathway gene enrichment.

Figure 3. Characterization of metabolic features of CD68$^+$ cells at invasion front and healthy tissue.

(A) Opal three-color IHC staining of the tissue section for cytokeratin (red), CD68 (green) and DAPI (blue).
(B) Macrophages population estimates, using the SpatialDecon algorithm (Danaher, Nat Comm 2022) to estimate the cell populations within each AOIs. Difference between Healthy_Macrophages and Mixed_Macrophages areas are shown.
(C) Genes differentially expressed between Healthy_Macrophages and Mixed_Macrophages cells were tested using the limma R package.
(D) Signaling pathways enriched in Tumor_PanCK and Mixed_PanCK.Vimentin cells were tested using our own metabolic pathway gene enrichment.

Figure 4. A Single-Cell Transcriptomic Atlas of the immune compartment of AK and cSCC.
(A) Workflow of patient sample processing for scRNA-seq in our study.
(B) Uniform manifold approximation and projection (UMAP) of scRNA-seq CD45$^+$ immune cells recovered from actinic keratosis sample and advanced cutaneous squamous cell carcinoma (cSCC) by cell type. Clusters were found when index Resolution in Seurat FindClusters was set as 0.05. UMAP visualization showing cells of individuals.
(C) Bar plots of proportion of cell type by patient, tumor or AK, and total cell number.

(D) UMAP projection of single CD45+ cells immune cells, across AK and cSCC. Major immune cell populations are annotated. Green and red arrows point respectively to a down or up direction of change in number of cells in the indicated clusters.
(E) scRNA-seq showing cell cycle phase using UMAP projection of single CD45+ cells immune cells recovered from actinic keratosis sample and cSCC by cell type. Clusters were found when index Resolution in Seurat FindClusters was set as 0.05. UMAP visualization showing cells of individuals.

Figure 5. Metabolic heterogeneity of non-malignant cells in precancerous skin and invasive cSCC

(A-C) Metabolic pathway enrichment among different types of immune cells in Ak and invasive cSS. Expression levels of genes involved in glycolysis (A), TCA cycle (B) and OXPHOS (C) were compared among different immune cell types in cSCC tumor samples compare to their paired precancerous lesion (n=2)

Figure 1

A-

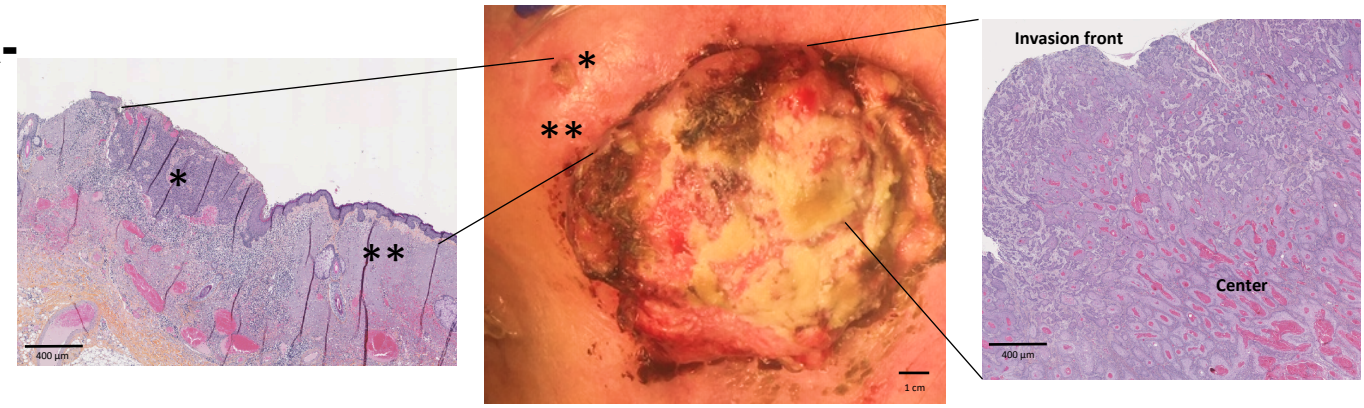

B-

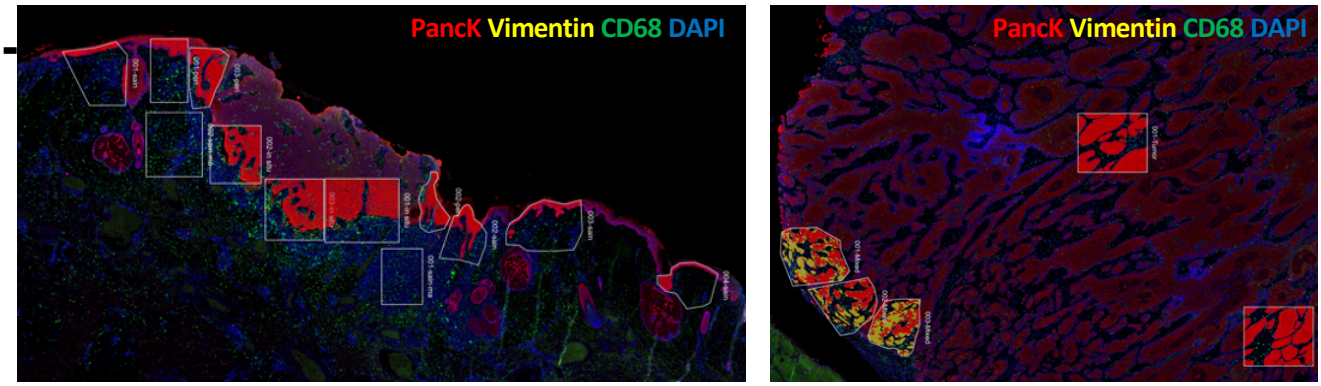

C-

tissue	segment	Number of AOIs
Healthy	Macrophages	5
	PanCK	4
in situ	Macrophages	3
	PanCK	3
Mixed	Macrophages	5
	PanCK	5
	PanCK.Vimentin	5
Peritumoral	Macrophages	3
	PanCK	3
Tumor	Macrophages	5
	PanCK	5

D-

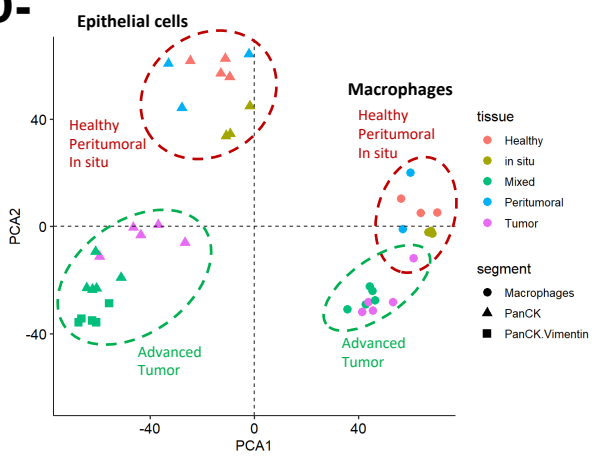

E-

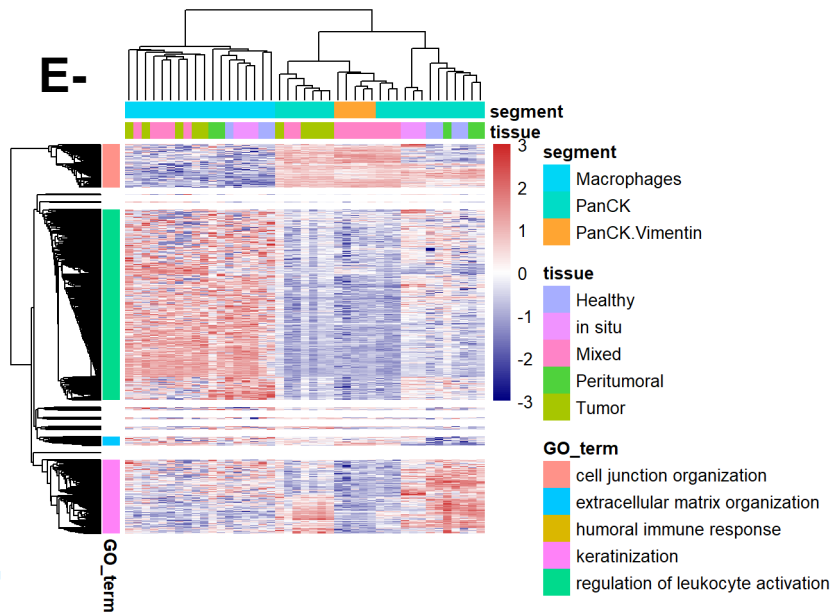

Figure 2

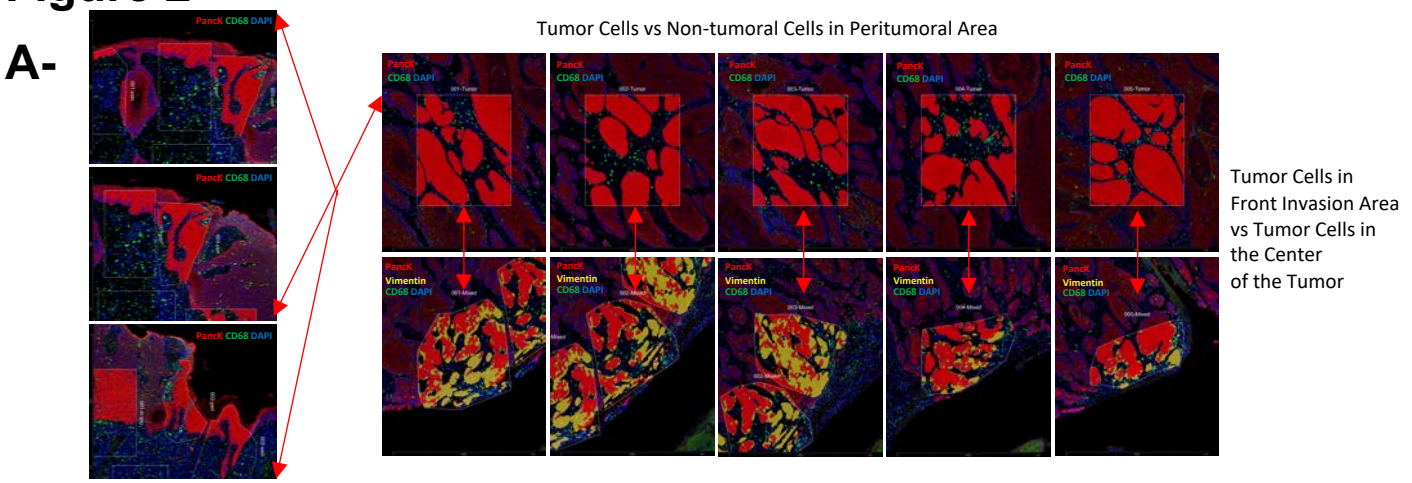
A-
Tumor Cells vs Non-tumoral Cells in Peritumoral Area
PancK CD68 DAPI
PancK Vimentin CD68 DAPI
Tumor Cells in Front Invasion Area vs Tumor Cells in the Center of the Tumor

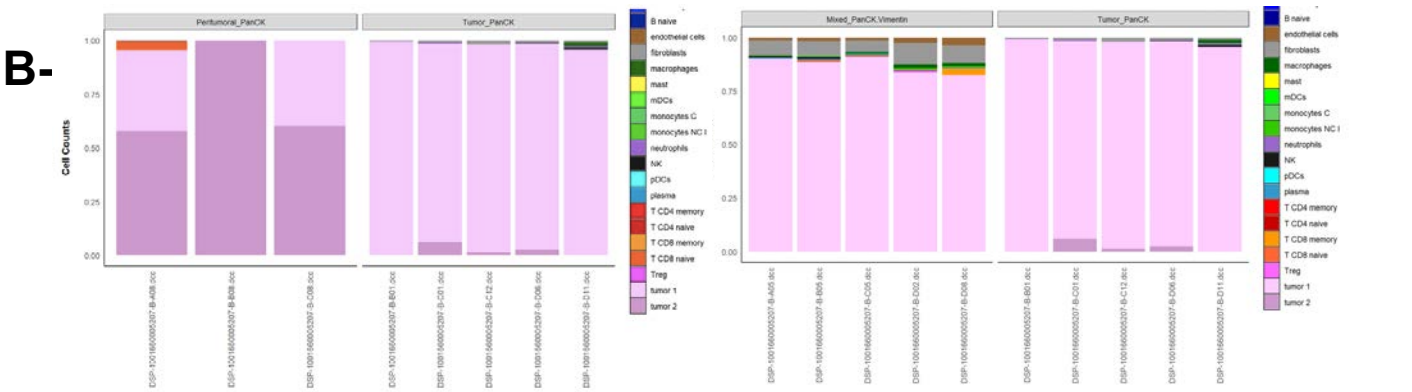
B-
Peritumoral_PancCK
Tumor_PancCK
Mixed_PancK.Vimentin
Cell Counts
B naive
endothelial cells
fibroblasts
macrophages
mast
mDCs
monocytes C
monocytes NC I
neutrophils
NK
pDCs
plasma
T CD4 memory
T CD4 naive
T CD8 memory
T CD8 naive
Treg
tumor 1
tumor 2


C-
GO pathway enrichment
Peritumoral_PancCK
Tumor_PancCK
ENDODERMAL CELL DIFFERENTIATION
EXTERNAL ENCAPSULATING STRUCTURE ORGANIZATION
COLLAGEN FIBRIL ORGANIZATION
ANAPHASE PROMOTING COMPLEX DEPENDENT CATABOLIC PR
CELL SUBSTRATE JUNCTION ORGANIZATION
REGULATION OF CELLULAR AMINO ACID METABOLIC PROCE
TRANSLATIONAL TERMINATION
MITOCHONDRIAL TRANSLATIONAL TERMINATION
NEGATIVE REGULATION OF CANONICAL WNT SIGNALING PA
CELLULAR COMPONENT DISASSEMBLY
INFLAMMATORY RESPONSE
RESPONSE TO BACTERIUM
ADAPTIVE IMMUNE RESPONSE
EPIDERMAL CELL DIFFERENTIATION
KERATINOCYTE DIFFERENTIATION
NUCLEAR TRANSCRIBED MRNA CATABOLIC PROCESS
ESTABLISHMENT OF PROTEIN LOCALIZATION TO ENDOPLAS
NUCLEAR TRANSCRIBED MRNA CATABOLIC PROCESS NONSEN
PHOSPHATIDYLCHOLINE ACYL CHAIN REMODELING
COTRANSLATIONAL PROTEIN TARGETING TO MEMBRANE
NES
padj
NES

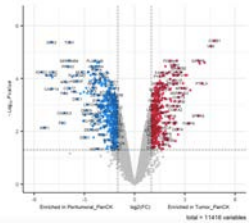
D-

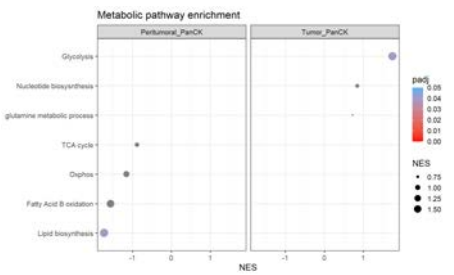
E-
Metabolic pathway enrichment
Peritumoral_PancCK
Tumor_PancCK
Glycolysis
Nucleotide biosynthesis
glutamine metabolic process
TCA cycle
Oxphos
Fatty Acid B oxidation
Lipid biosynthesis
NES
padj
NES

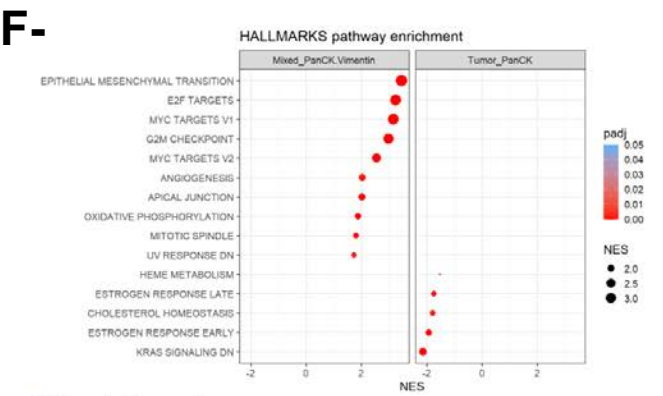
F-
HALLMARKS pathway enrichment
Mixed_PancK.Vimentin
Tumor_PancCK
EPITHELIAL MESENCHYMAL TRANSITION
E2F TARGETS
MYC TARGETS V1
G2M CHECKPOINT
MYC TARGETS V2
ANGIOGENESIS
APICAL JUNCTION
OXIDATIVE PHOSPHORYLATION
MITOTIC SPINDLE
UV RESPONSE DN
HEME METABOLISM
ESTROGEN RESPONSE LATE
CHOLESTEROL HOMEOSTASIS
ESTROGEN RESPONSE EARLY
KRAS SIGNALING DN
NES
padj
NES

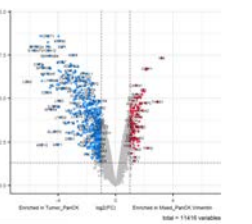
G-

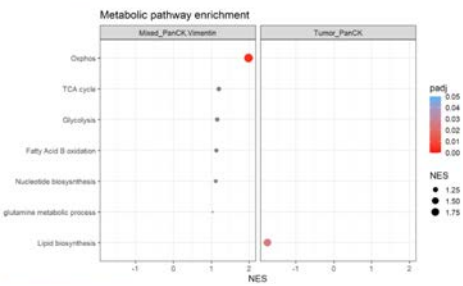
H-
Metabolic pathway enrichment
Mixed_PancK.Vimentin
Tumor_PancCK
Oxphos
TCA cycle
Glycolysis
Fatty Acid B oxidation
Nucleotide biosynthesis
glutamine metabolic process
Lipid biosynthesis
NES
padj
NES

Figure 3

A-

Healthy Macrophages
Vs
Macrophages in
Invasion front
Of Tumor Area

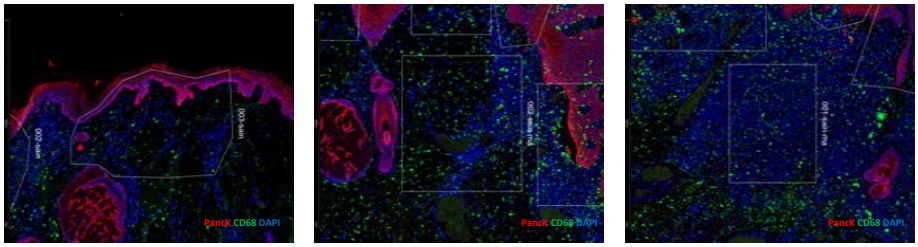

B-

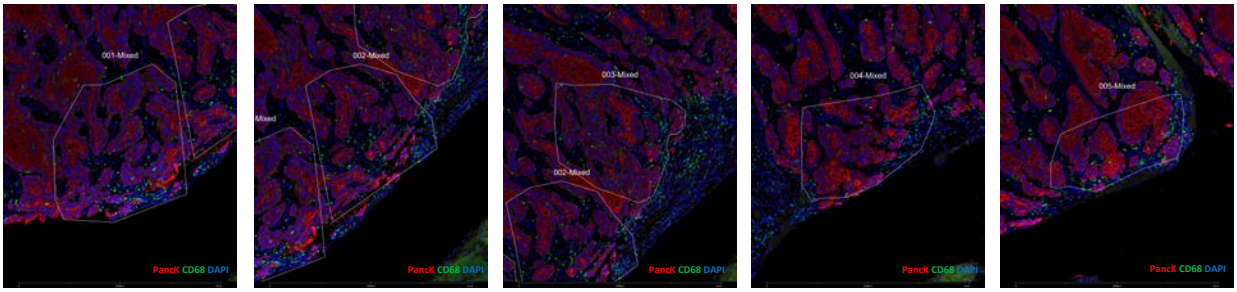

C-

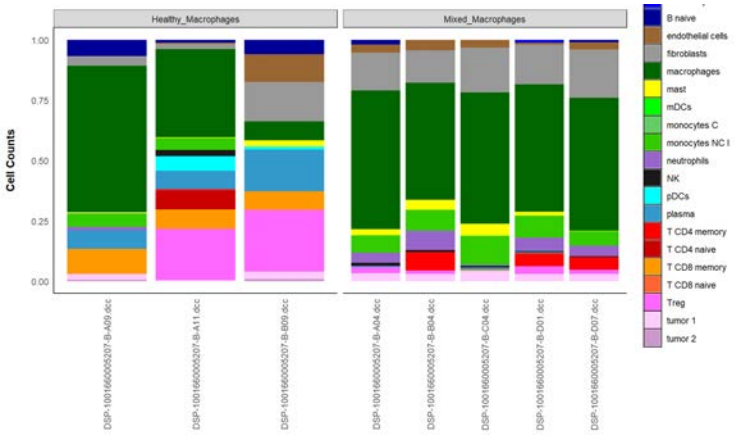

D-

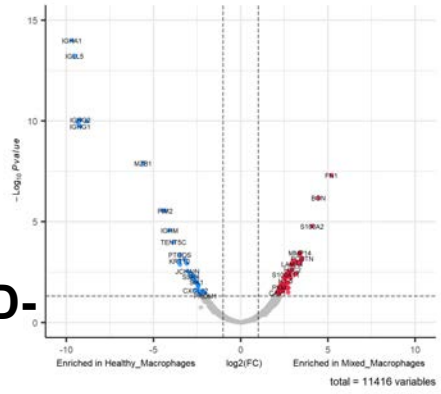

E-

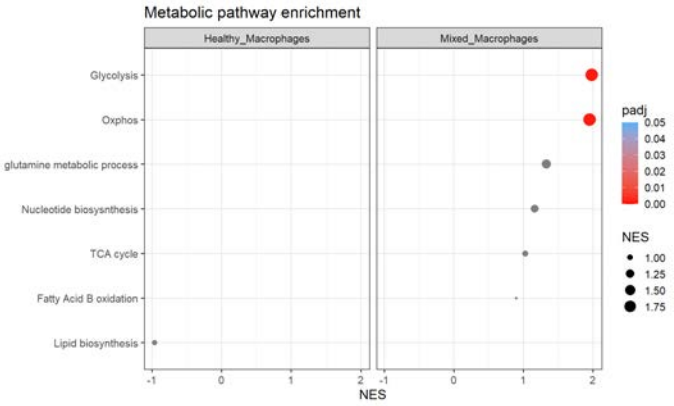

Figure 4

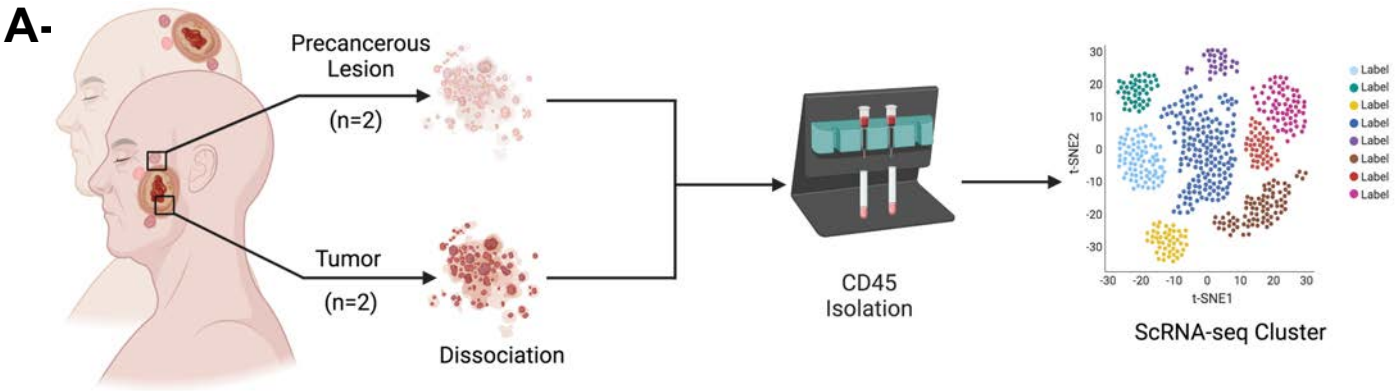
A-
Precancerous Lesion
(n=2)
Tumor
(n=2)
Dissociation
CD45 Isolation
t-SNE2
t-SNE1
ScRNA-seq Cluster

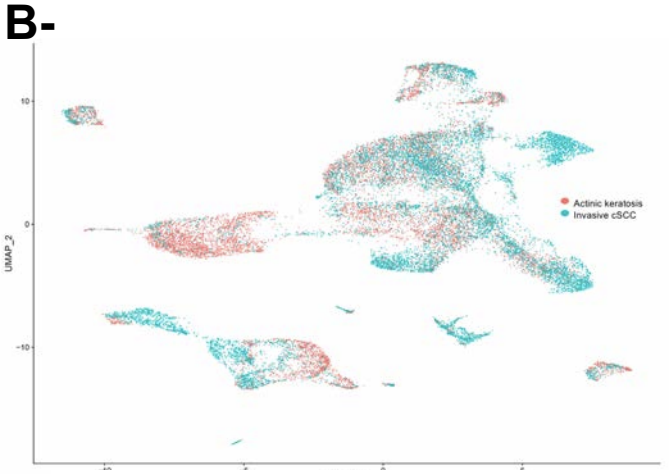
B-
Actinic keratosis
Invasive cSCC
UMAP_2

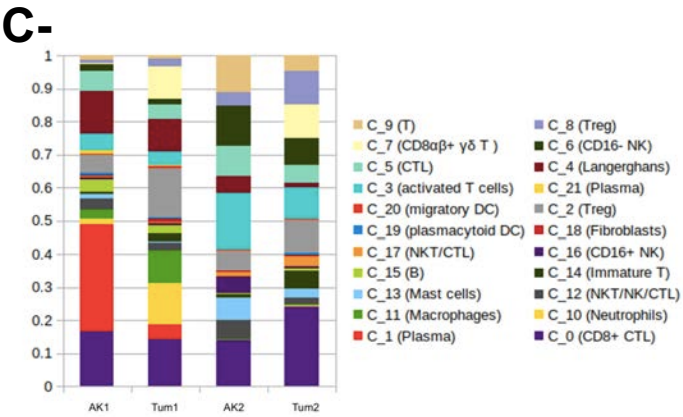
C-
AK1
Tum1
AK2
Tum2
C_9 (T)
C_7 (CD8αβ+ γδ T)
C_5 (CTL)
C_3 (activated T cells)
C_20 (migratory DC)
C_19 (plasmacytoid DC)
C_17 (NKT/CTL)
C_15 (B)
C_13 (Mast cells)
C_11 (Macrophages)
C_1 (Plasma)
C_8 (Treg)
C_6 (CD16- NK)
C_4 (Langerghans)
C_21 (Plasma)
C_2 (Treg)
C_18 (Fibroblasts)
C_16 (CD16+ NK)
C_14 (Immature T)
C_12 (NKT/NK/CTL)
C_10 (Neutrophils)
C_0 (CD8+ CTL)

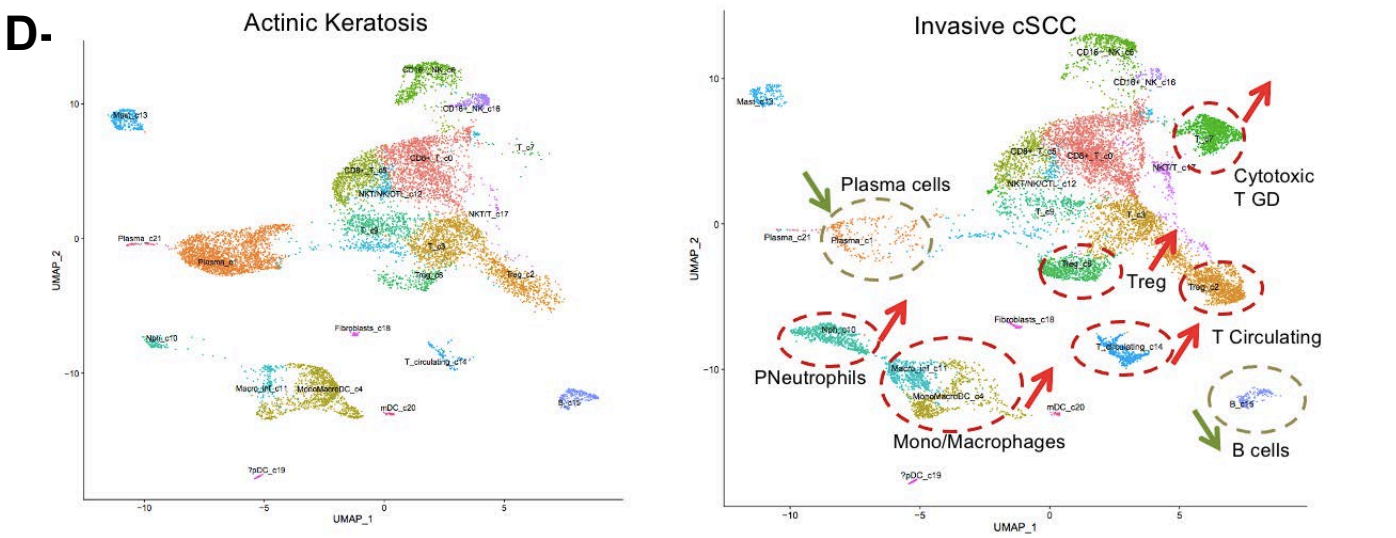
D-
Actinic Keratosis
Invasive cSCC
Plasma cells
Cytotoxic T GD
Treg
T Circulating
PNeutrophils
Mono/Macrophages
B cells
UMAP_1
UMAP_2

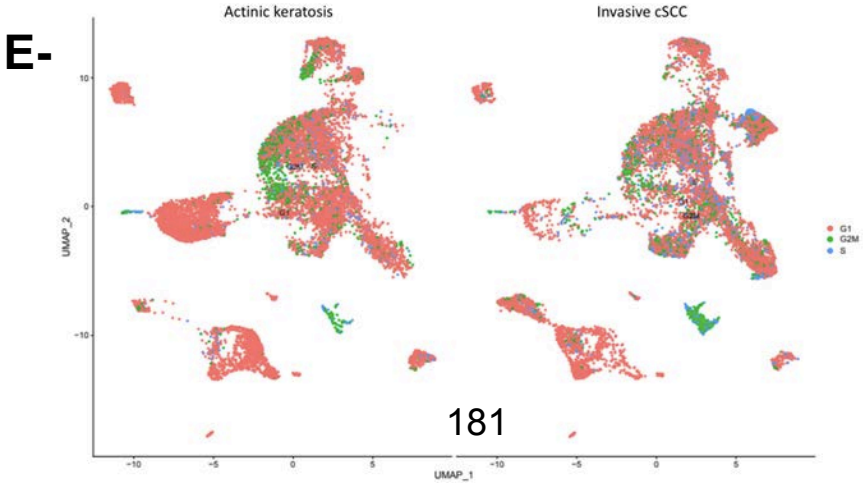
E-
Actinic keratosis
Invasive cSCC
G1
G2M
S
UMAP_1
UMAP_2

Figure 5

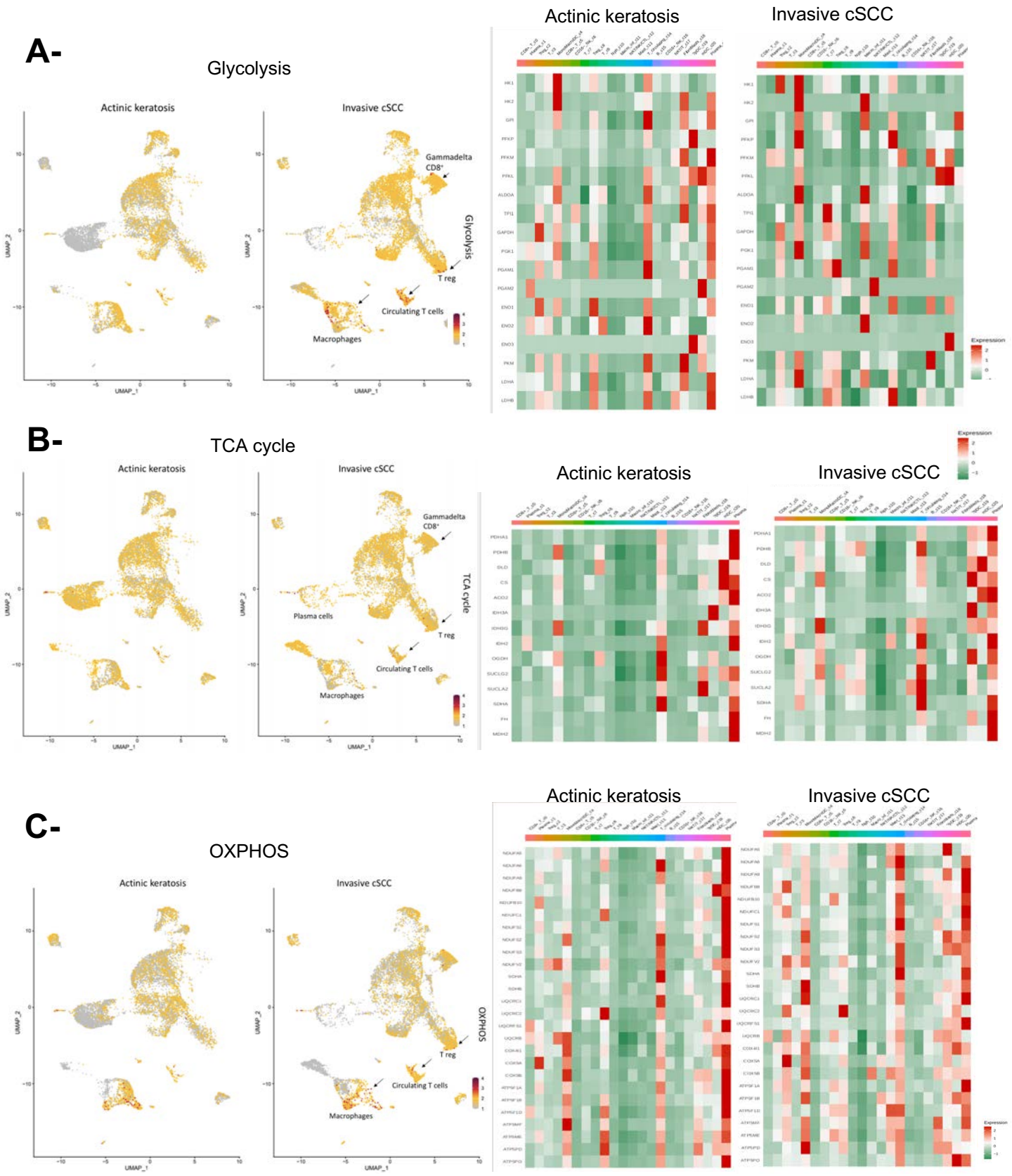
A-
Glycolysis
Actinic keratosis
Invasive cSCC
Actinic keratosis
Invasive cSCC
Gammadelta CD8+
Glycolysis
T reg
Circulating T cells
Macrophages
UMAP_1
UMAP_2
Expression
B-
TCA cycle
Actinic keratosis
Invasive cSCC
Actinic keratosis
Invasive cSCC
Gammadelta CD8+
TCA cycle
Plasma cells
T reg
Circulating T cells
Macrophages
Expression
C-
OXPHOS
Actinic keratosis
Invasive cSCC
Actinic keratosis
Invasive cSCC
OXPHOS
T reg
Circulating T cells
Macrophages
Expression

DISCUSSION

Recent evidence in humans and mice supports the notion that mitochondrial metabolism provides key metabolites for macromolecule synthesis and play a pivotal role in the tumor growth. Thus, inhibiting the altered pathways in mitochondrial metabolism might be/represent a new promising cancer therapeutic treatment, but in order for these treatments to be effective, patients need to be stratified/profiled, opening the way to personalized medicine.

1. Energy Metabolism in Skin Cancer Therapy

Our data showed that profiling cellular energy metabolism in cancer may be beneficial for prognosis and diagnosis. As it has been demonstrated, metabolic status is substantial in carcinogenesis, and every cancer cell has certainly altered metabolism. In fact, disorders related to cellular metabolism, such as obesity, hyperglycemia, hyperlipidemia and insulin resistance, are associated to an increased risk of developing several types of cancer, increased tumor progression and poor clinical outcome (Khandekar, Cohen, & Spiegelman, 2011; Pollak, 2012). Indeed, metformin (medication principally used for the treatment of type 2 diabetes) and statins (lipid-lowering medication) are associated with reduced incidence of cancer in patients receiving any of these drugs (Gronich & Rennert, 2013). Metformin has anti-neoplastic activity in *in vitro* models through inhibition of mitochondrial complex I, with an inhibitory effect on cell proliferation and by lowering glucose effects (Wu et al., 2013). In human melanoma cells, metformin has been shown to have an anti-melanoma cell growth via a cell death effect without affecting normal melanocytes (Checkley et al., 2014; Tomic et al., 2011).

In the same way, results on keratinocytes and mice indicated a protective role of metformin against UVB-induced skin carcinogenesis through an AMPK-independent pathway. Moreover, both topical and systemic administration of metformin on mice after 17 weeks of chronic UVB irradiation prevented the formation of new tumors (Wu *et al.*, 2013).

However, a recent meta-analysis also showed that metformin use was not significantly associated with decreased risk of SCC (OR 0.98, 95% CI 0.06-15.60) (Chang et al., 2021). Thus, targeting metabolism in order to have an anti-tumoral effect is not that simple and it requires precision and personalized medicine. Indeed, genomic alterations and cellular energy metabolism, affecting each other, communicate and influence carcinogenesis and tumor

progression. As noted, mutations in oncogenes and tumor suppressor genes influence metabolic reprogramming in cancer (Bensaad & Vousden, 2007; Ward & Thompson, 2012). As well, a continuous presence of an oncogene can stimulate a cancer cell to shift from highly glycolytic to highly oxidative metabolism during tumor development (Hu et al., 2011). Owing to the fact that UV-induced genomic alterations alone cannot account for the origin of cancer, as we recently demonstrated in the XPC knockout normal human keratinocytes and Tfam knockout keratinocytes, we can assure that the role of mitochondria and metabolic status is pivotal in skin carcinogenesis and that can be further used for preventative and curative objectives (Hosseini et al., 2018; Rezvani et al., 2011). However, since little attention has been given to the role of energy metabolism in the initiation and progression of skin carcinoma, we decided to focus our research on understanding the bioenergetic profiling in cancer and how it can be useful in treatment and prevention. Using a multi-stage model of UVB-induced skin cancer, we found that leflunomide completely inhibited the UVB-induced pre-malignant and malignant lesions, suggesting the importance of early modifications of energy metabolism in the initiation on cSCC (Hosseini et al., 2018). Accordingly, targeting energy metabolism could be reasonably anticipated as anti-cancer strategy.

In addition, there is growing evidence that cellular energy metabolism plays an important role in the emergence of resistant cells. Using drugs that target energy metabolism in combination with targeted therapies contribute to prominent results. For instance, vemurafenib-resistant BRAF-mutant melanoma cells, which rely on OXPHOS, have been shown to become sensitive to mitochondrial uncouplers or OXPHOS inhibitors (Haq et al., 2013). Besides relying on OXPHOS, other resistant BRAF-mutant cells have upregulated glutaminase (GLS) and increased glutamine uptake. The use of BPTES, which is a GLS inhibitor, re-sensitizes resistant cells to BRAF inhibition (Baenke et al., 2016). Furthermore, we already showed that DHODH could not only be targeted for the prevention from skin cancer, but also can be used in combination therapy for the treatment of cSCC. In this study, LFN was used in a combination therapy with 5-fluorouracil (5-FU), a genotoxic agent, on human tumor xenograft model. Results showed a reduction in tumor growth for both SCC-15 and A431 tumor transplants (Hosseini et al., 2019). Therefore, targeting energy metabolism could not only be studied for prevention or first-hand treatment, but it surely can be used in combination therapies. Cancer treatment faces various difficulties like drug resistance and drug toxicity, that's when combination therapies are adopted to overcome these obstacles.

Further research should be performed to investigate the precise role of energy metabolism in skin cancer, as targeting metabolism has been proposed as a promising mechanism to improve the efficacy of cancer therapy.

2. DHODH Inhibition in Cancer Therapy

Despite its role on cSCC formation and progression, several studies showed similar effects with DHODH inhibition, including highly aggressive small-cell lung cancer, acute myeloid leukemia (AML) and triple-negative breast cancers (Brown, Spinelli, Asara, & Toker, 2017; Koundinya et al., 2018; Sykes et al., 2016; Wang et al., 2019; White et al., 2011).

In the literature, 3 retrospective studies investigated if there was a protective effect of DHODH inhibitors on the development of cancers (Dolladille et al., 2021; Gil-Bernal, González-Caballero, Espinosa-Rosso, & Gómez-Gómez, 2021). Only one study investigated its effect on the development of non-melanoma skin cancers; leflunomide appeared to be insignificant (HR 0.89, 95%CI 0.68-1.18, p=0.424) based on 15789 American patients treated for rheumatoid arthritis (Chakravarty, Michaud, & Wolfe, 2005). The two other studies were conducted on multiple sclerosis patients and were looking at cancers in general, with no protective effect highlighted because of a lack of statistical design of studies (Dolladille et al., 2021; Gil-Bernal et al., 2021).

Because it is a matter of concern, our team is actually conducting a retrospective study on rheumatoid arthritis patient database to look at the protective role of Leflunomide for development of NMSC.

To assess alteration frequencies and mutation data for DHODH across different cancer types, we performed a query on the *cBioPortal* and COSMIC for Cancer Genomics. Results showed that genomic alterations of DHODH in various cancer types are not so frequent (Figure 33).

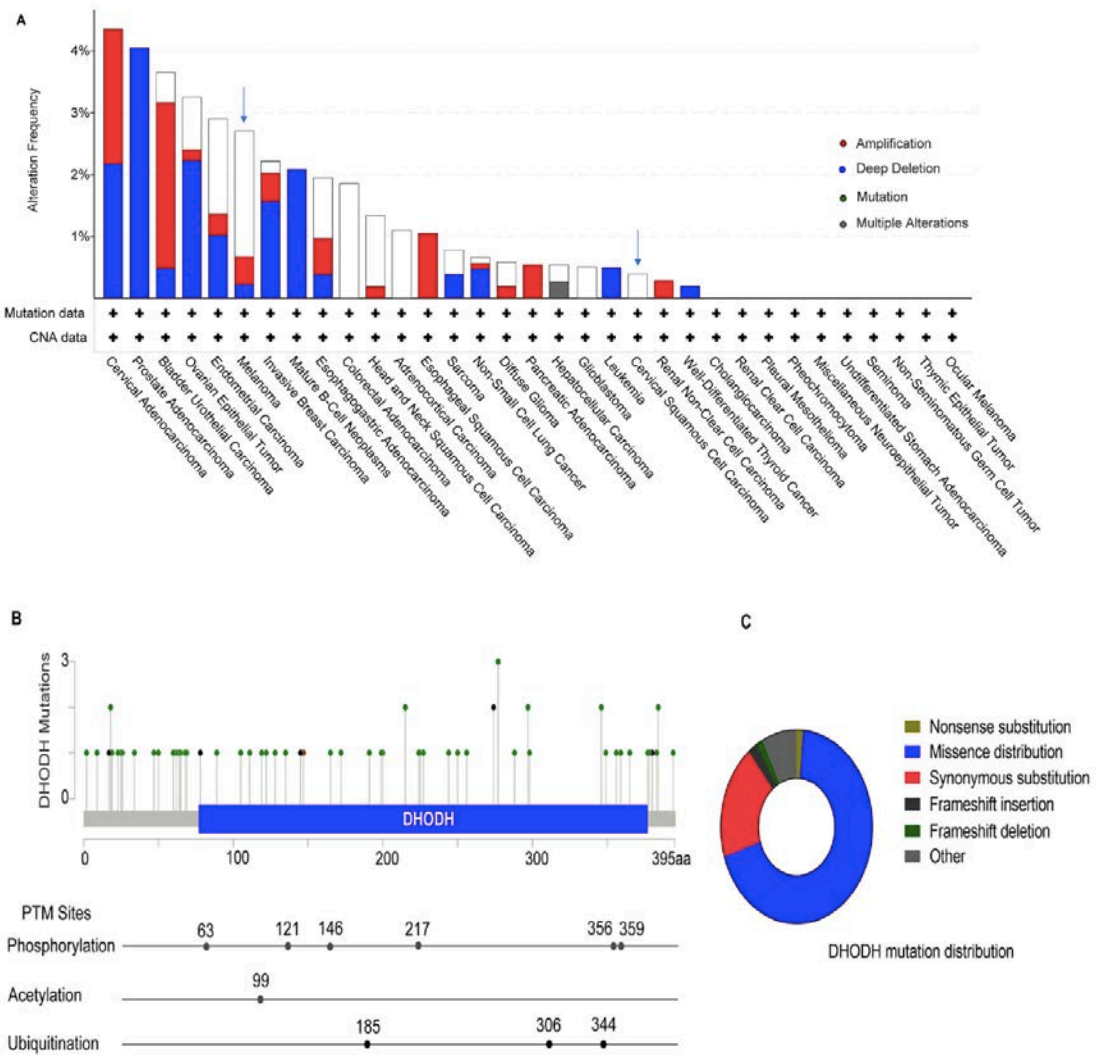

Figure 34. Cross-cancer queries of DHODH.

A. The alteration frequencies of DHODH across cancer studies. Data are from Cbioportal. **B.** DHODH post-translational modifications (PTMs) sites (available for the Ensembl transcript ENST00000219240). Mutation diagram circles are colored with respect to the corresponding mutation types. In case of different mutation types at a single position, color of the circle is determined with respect to the most frequent mutation type. Mutation types and corresponding color codes are as follow: green, missense mutations; black, truncating mutations (nonsense, nonstop, frameshift deletion, frameshift insertion, splice site); brown, inframe mutations (inframe deletion, inframe insertion). **C.** An overview of the types of DHODH mutation distribution from COSMIC.

i. New and Old Inhibitors of DHODH

The only clinically approved DHODH inhibitors are leflunomide and its metabolite teriflunomide, which are used for treating rheumatoid arthritis or multiple sclerosis (Table 7).

Table 7. DHODH inhibitors in the clinic, their dosing and adverse events.

Drug	Disease	Effective dose	Adverse events (one or more of the following)
Leflunomide	Rheumatoid and psoriatic arthritis (FDA approved)	20mg/day after a loading dose of 100mg/day for 3 days, oral administration (tablets)	Gastrointestinal complaints, skin rash, reversible alopecia, diarrhea, high blood pressure and asymptomatic transaminase elevation
Teriflunomide	Multiple Sclerosis (FDA approved)	14 mg/day, oral administration (tablets)	Diarrhea, nausea, hair thinning, elevated alanine aminotransferase levels

Leflunomide is currently evaluated in clinical trials for treatment of multiple myeloma (NCT02509052) and triple negative breast cancer (NCT03709446). Brequinar is also another "old DHODH inhibitors" which has shown efficiency in murine xenografts models of head and neck squamous cell carcinoma (Braakhuis, van Dongen, Peters, van Walsum, & Snow, 1990) but with also disappointed results on solid tumors (Maroun et al., 1993; Natale et al., 1992; Urba et al., 1992). But because its effects are directly linked to metabolism, which is constantly active, a right dosing schedule is necessary to reach a continuous inhibition. The necessity of sustained suppression of DHODH activity is supported by the observation that melanoma and breast cancer cells with deleted DHODH failed to form tumors when grafted into mice, while treatment with leflunomide twice a week showed only a partial anti-tumor effect in the same model (Bajzikova et al., 2019; Hubackova et al., 2020).

Despite leflunomide and its analogues, new classes of DHODH inhibitors are developed and studied in different clinical trials (Table 2). These new DHODH inhibitors have different specific hydrogen bonding and hydrophobic interactions, which make them more efficient (Zhang et al., 2022).

Table 8. DHODH inhibitors currently evaluated in clinical trials.
Adapted from clinicaltrials.gov.

Drug	Clinical trial	Disease	Clinicla trial identifier	Study start date	Status
RP7214	I/II	AML, MDS	NCT05246384	January 2023	Not yet recruiting
JNJ-7456665	I	AML, MDS	NCT04609826	February 2023	Not yet recruiting
AG-636	I	Advanced lymphoma	NCT03834584	May 2019	Terminated
PTC299	I	Refractory AML	NCT03761069	October 2018	Terminated
BREQUINAR	I/II	Refractory AML	NCT03760666	December 2018	Terminated
ASLAN003	II	AML	NCT03451084	January 2018	Completed
BAY2402234	I	Myeloid malignancies	NCT03404726	March 2018	Terminated
Leflunomide	I/II	Refractory MM	NCT02509052	December 2015	Active, not recruiting
Leflunomide	I/II	Triple negative breast cancers	NCT03709446	April 2019	Recruting

IMU-838	III	Relapsing MS	NCT05201638	January 2022	Recruting
IMU-838	II	Relapsing MS	NCT03846219	January 2019	Not Recruting
Vidoflumidus	II	Primary SC	NCT03722576	June 2019	Completed

Abbreviations: AML, Acute Myeloid Leukemia; MDS, myelodysplastic syndromes; MM, multiple myeloma; MS, multiple sclerosis; SC, Sclerosing Cholangitis

ii. How DHODH inhibition works on cancer cells?

Several studies investigated the antitumoral mechanisms elicited by DHODH inhibition (Boukalova et al., 2020). Its antitumoral effects rely on inhibition of pyrimidine synthesis, causing depletion on ribonucleotide pools, cell cycle arrest in S-phase, promotion of cell differentiation, causing preferential DNA damage and cell stress, and elevation of pro-apoptotic p53 protein level (Figure 34) (Baumgartner et al., 2006; Jiang, Zhang, Li, Ling, & Jiang, 2018; Ladds et al., 2018; Shi et al., 2022). In acute myeloid leukemia (AML), DHODH inhibition leads to differentiation of myeloid precursors due to a combining effect on nucleic acid synthesis, cell cycle arrest and post-translational glycosylation of important protein targets (Sykes et al., 2016). Interestingly, differentiation induced by DHODH inhibition in AML was suppressed in the presence of uridine (Sainas et al., 2022). We showed the same restored effect on skin tumor formation in leflunomide-treated mice supplemented with uridine (Hosseini et al., 2019). DHODH inhibition also promotes mitochondrial fusion expression and mitochondrial elongation and inhibits autophagy (Miret-Casals et al., 2018). Intriguingly, the authors also showed that there were no changes in mitochondrial respiration under LFN inhibition.

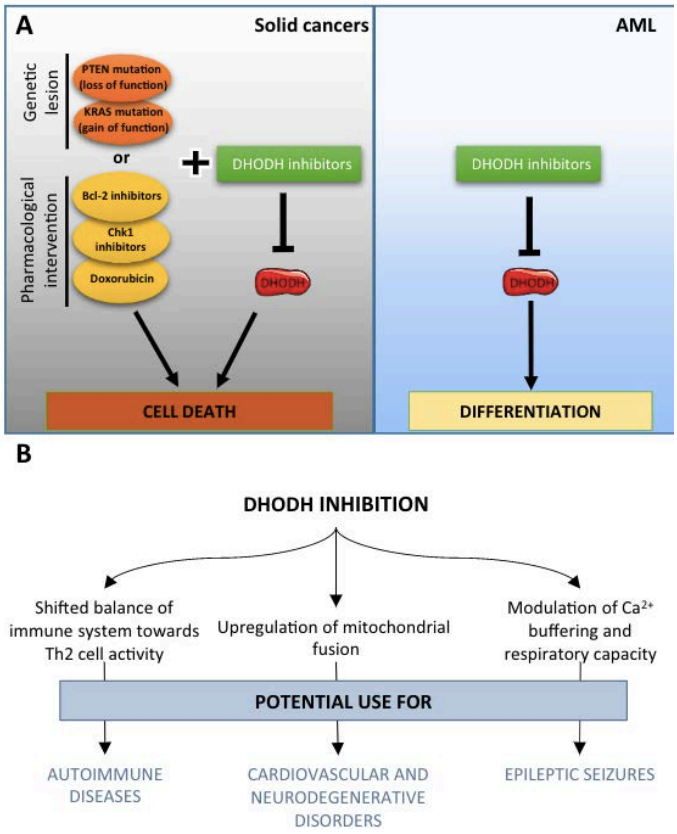

Figure 35. Consequences of DHODH inhibition in transformed and non-transformed cells. Adapted from Boukalova et al, 2020.
In non-transformed cells, DHODH inhibition can display immunosuppressive properties affecting Th1 and Th2 cells, shifting the balance in favor of Th2. By Modulating Ca2+ buffering system of mitochondrial fusion, DHODH inhibitors may be used in neurodegenerative disorders like multiple sclerosis.

3. DHODH Inhibition in Chemoprevention in Skin Carcinogenesis

Chemoprevention aims to prevent and reduce the risk of the development of new cSCC, especially for patients at risk of developing numerous and/or aggressive cSCC. Our work argues not only an antitumor role of DHODH inhibition but also a preventive role in tumor formation. Several molecules have already shown their preventive role in the appearance of cSCC.

i. Nicotinamide for Skin-Cancer Chemoprevention.

Chen et al. reported a protective effect of oral nicotinamide in people who are prone to skin cancer on the Oral Nicotinamide to Reduce Actinic Cancer (ONTRAC) trial (Chen et al., 2015). Nicotinamide is a water-soluble form of vitamin B3 (niacin). It may enhance repair of photodamaged DNA and prevent the immune-inhibitory effects of UV radiation.
Nicotinamide for 12 months reduced the rate of new cSCC by 30%, but only during active

treatment. This study was the only one phase III, double-blind, randomized and controlled, able to show prospectively a safe effectiveness in reducing the rates of new nonmelanoma skin cancers and actinic keratoses.

It must be payed attention that nicotinamide is also a precursor of NAD+, which is essential for the activity of several enzymes implicated in DNA damage response such as PARPs and SIRTs (Bai, 2015; Mei et al., 2016). Tumor cells required high amounts of NAD+ to ensure increased activity of these enzymes. Therefore, cancer cells, which are associated with PARP-1 overactivation, are vulnerable to NAD+ levels and reduction of NAD+ availability can be considered to affect both DNA repair efficiency and tumor progression. Thus NAD+ reduction for example by inhibiting the NAD+ -synthetic enzymes (e.g. such NMNAT and NAMPT) has been proposed as an antitumor strategy, too (Bajrami et al., 2012).

ii. mTor Inhibitors for Secondary Skin-Cancer Chemoprevention

Because of the high prevalence of cSCC in solid organ transplant recipients (STORs) in the context of immunodepression, another way to prevent the development of cSCC is to change the immunosuppressant. Indeed, the introduction of an inhibitor of the mTor pathway, sirolimus, instead of calcineurin inhibitors, has already been shown to reduce the occurrence of secondary skin cancers (Asgari, Ray, Quesenberry, Katz, & Silverberg, 2017; Euvrard et al., 2012). But the limitations of mTOR inhibitors are adverse effects and higher risk of death through infectious or cardio-vascular causes (Dantal et al., 2018).

In order to avoid these side effects, and to act directly on the skin, another way to intervene is to use topical sirolimus as it has previously been studied in tuberous sclerosis disease (Malissen et al., 2017; Wataya-Kaneda et al., 2017). Chong et al, has recently shown in a pilot study the efficacy of topical sirolimus with a 3-fold decrease in intra-epithelial carcinomas at 24 months (81% reduction as per protocol analysis) in SOTRs patients, without serious adverse events, (Chong et al., 2022), encouraging longer trials.

iii. DHODH Inhibition for Skin-Cancer Chemoprevention

Our data argues for the use of leflunomide in skin cancer chemoprevention (Hosseini et al., 2019). This protective effect has been demonstrated in hairless mice under UVB exposure by the systemic route, but the development of a topical form could be proposed to high-risk patients for multiple subsequent skin cancers. Leflunomide tablets were crushed and dissolved in 1.5% carboxymethylcellulose (CMC), with a syrupy consistency. Developing a topical gel form seems feasible by increasing the percentage of CMC.

4. The Era of Precision Cancer Medicine

Many metabolic enzymes have been studied as targets for cancer therapy, but vulnerabilities of specific tumour types to specific inhibitors either as single agents or in combination with chemotherapy, radiation, targeted therapy (such as kinase inhibitors) and/or immunotherapy remain to be decoded. Of note, metabolic plasticity is a challenge when targeting specific metabolic enzymes (Table 9 and Figure 35).

Table 9. Small molecules that target cancer metabolism. Adapted from Stine et al, 2022. Many anti-metabolite drugs, particularly those targeting nucleotide metabolism, have been approved and used in the clinic. To note that epacadostat (IDO1) did not improve in a phase 3 trial, the progression free survival of patients with metastatic melanoma (Long et al., 2019).

Agent	Target	Function	Indications
Approved cancer metabolic drugs			
Pemetrexed	TYMS, DHFR	dUMP to dTMP conversion; folate to THF conversion	NSCLC
5-Fluorouracil	TYMS	dUMP to dTMP conversion	CRC, gastric and breast cancer
Hydroxyurea	RNR	Ribonucleotide to deoxyribonucleotide conversion	CML, HNSCC
Gemcitabine	DNA incorporation	Nucleotide analogues	Pancreatic, ovarian and breast cancer; NSCLC
Fludarabine	DNA incorporation	Nucleotide analogues	CLL
6-Mercaptopurine	PPAT	Purine synthesis	ALL
Methotrexate	DHFR	Folate to THF conversion	Breast, HNSCC, lung, non-Hodgkin lymphomas
Enasidenib	Mutant IDH2	2-Hydroxyglutarate synthesis	AML
Ivosidenib	Mutant IDH1	2-Hydroxyglutarate synthesis	AML
Approved metabolic drugs for non-cancer indications			
Metformin	Complex I	Oxidative metabolism	Type 2 diabetes mellitus
Leflunomide	DHODH	Pyrimidine metabolism	Rheumatoid arthritis
Bempedoic acid	ACLY	Lipid synthesis	Heterozygous familial hypercholesterolaemia, established atherosclerotic cardiovascular disease
Hydroxychlorquine	Autophagy	Removal of damaged cellular components	Rheumatoid arthritis
Sulfasalazine	SLC7A11/xCT	Cystine/glutamate exchange	Ulcerative colitis
Small-molecule metabolic inhibitors in cancer clinical trials			
CPI-613	Mitochondria	Oxidative metabolism	Pancreatic cancer, AML, solid tumours, lymphoma
IM156	Mitochondria	Complex I	Solid tumours, lymphoma
IACS-010759	Mitochondria	Complex I	AML, advanced solid tumours
CB-839	Glutaminase	Glutamine to glutamate conversion	Leukaemia, CRC, breast cancer, RCC
IPN60090	Glutaminase	Glutamine to glutamate conversion	Advanced solid tumours
DRP-104	Glutamine-utilizing enzymes	Glutamine-dependent enzymes	NSCLC, NHSCC, advanced solid tumours
AZD-3965	MCT1	Lactate symporter	Advanced cancers
TVB-2640	FASN	Fatty acid synthesis	NSCLC, CRC, breast cancer, astrocytoma
AG-270	MAT2A	Production of S-adenosylmethionine	Advanced solid tumours or lymphoma
SM-88	Tyrosine metabolism	Oxidative stress	Sarcoma, prostate, breast and pancreatic cancer
Indoximod	IDO1	Kynurenine synthesis	Melanoma, breast and pancreatic cancer
Epacadostat	IDO1	Kynurenine synthesis	Breast cancer, HNSCC, NSCLC, melanoma, RCC

ACLY, ATP-citrate synthase; ALL, acute lymphatic leukaemia; AML, acute myeloid leukaemia; CLL, chronic lymphocytic leukaemia; CML, chronic myeloid leukaemia; CRC, colorectal cancer; DHFR, dihydrofolate reductase; DHODH, dihydroorotate dehydrogenase; FASN, fatty acid synthase; HNSCC, head and neck squamous cell carcinoma; IDH, isocitrate dehydrogenase; IDO1, indoleamine 2,3-dioxygenase 1; MAT2, S-adenosylmethionine synthase isoform type 2; MCT1, monocarboxylate transporter 1; NSCLC, non-small-cell lung cancer; PPAT, phosphoribosyl pyrophosphate amidotransferase; RCC, renal cell carcinoma; RNR, ribonucleotide reductase; THF, tetrahydrofolate; TYMS, thymidylate synthase.

A key question remains if we have exhausted nearly all metabolic axis as therapeutic targets. To fully understand carcinogenesis, it is necessary to focus not only on malignant cells and subclones (immature subpopulations and multiple lineages of differentiated cells) but also on

tumor microenvironments including various infiltrating immune populations (lymphocytes, myeloid cells, dendritic cells ...) as well as other stromal populations (Figure 35)(Kouidhi, Ayed, & Elgaaied, 2018).

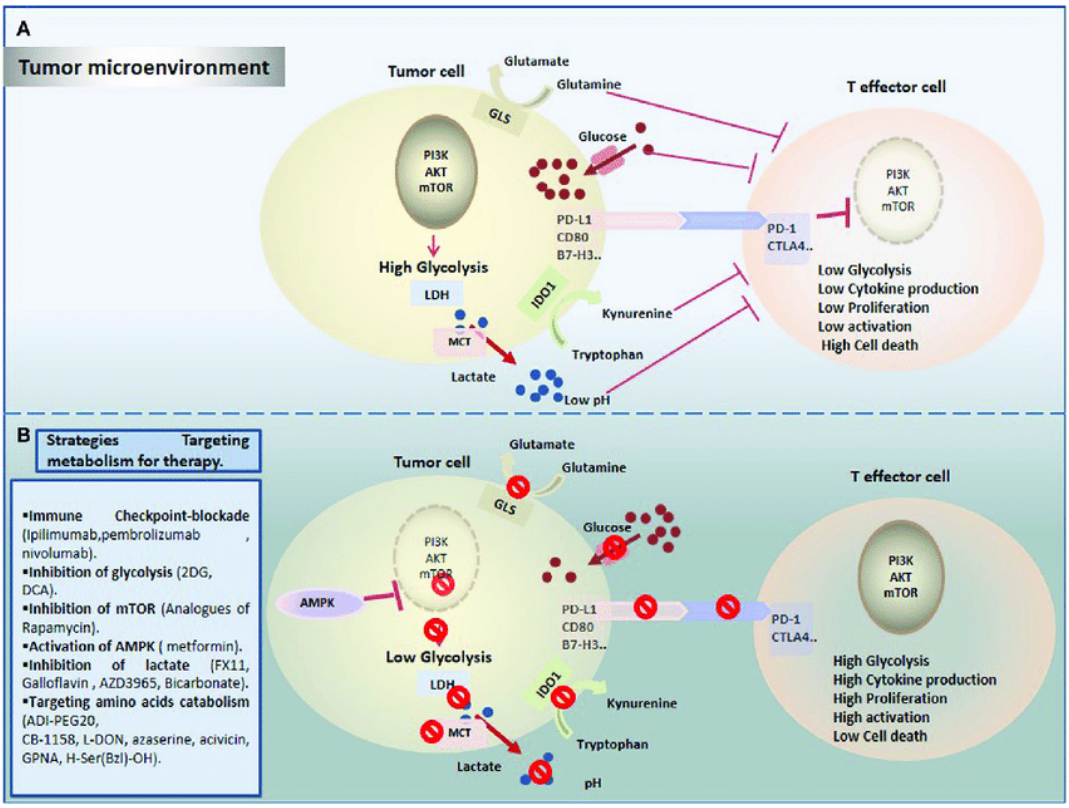

Figure 36. Targeting of Immune Cells by Bioenergetic Therapies. Adapted from Kouidhi et al, 2020. This figure summarizes the basics of intrinsic and extrinsic metabolic remodeling and metabolic checkpoints underlying the competition between cancer and infiltrating immune cells for nutrients and metabolites **(A)** Tumor cells create a hostile TME that affects metabolic fitness of T cells through multiple ways. T cells are challenged by different immunologic and metabolic checkpoints: Glucose and amino acid depletion, high acidity and lactate, and upregulation of immune checkpoints influence T cell metabolism to suppress glycolysis thereby reducing their activation and proliferation. **(B)** Currently, several novel promising approaches are proposed to rewire metabolic fitness of T cells in the TME and to boost existing immunotherapies.

Thus, the best therapeutic effect of a drug targeting metabolism for cancer may be to affect not only cancer cells but also to favor antitumour immunity. As we have shown the interpatient tumor heterogeneity must be considered for the bioenergetic profiling of tumor in clinical setting. Thus, patient stratification combining several techniques may be proposed for targeted metabolic inhibitors (Figure 36). For example, in cSCC patients, a metabolic score based on several metabolic key regulators combined with DHODH expression level may allow the stratification and identification of responders to DHODH inhibitors.

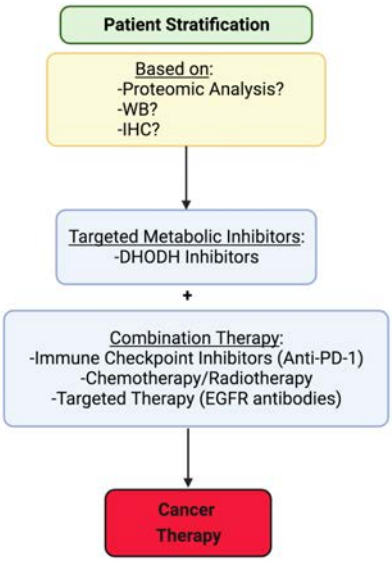

Figure 37. Rational Design for Metabolic Cancer Therapy.
Our work highlights the importance of metabolic profiling for precision medicine-based metabolic therapy of cSCC. For advanced cSCC, a patient stratification may be proposed in order to identify eligible patients for DHODH inhibition.

CONCLUSION

Overall, this work contributed to the knowledge about metabolic and immune features of cutaneous squamous cell carcinoma (cSCC) at different stages of carcinogenesis, which is of utmost importance for cSCC therapy and proper patient support care.

First, our data indicate that metabolic profiles of cSCCs have pivotal effects on tumor growth, metastatic potency and, response to treatment. Therefore, we propose metabolism scoring of cSCC, especially in the case of clinically/histologically aggressive (invasive/metastatic) behavior, as a key step in a precision medicine approach.

This work also contributed at a single cell resolution to the knowledge of immunometabolism during progression of advanced cSCC. Further characterization of patient's immune cells and interactors may allow the elaboration of new anti-immune strategies.

References

Asgari, M. M., Ray, G. T., Quesenberry, C. P., Katz, K. A., & Silverberg, M. J. (2017). Association of Multiple Primary Skin Cancers With Human Immunodeficiency Virus Infection, CD4 Count, and Viral Load. *JAMA Dermatology*, *153*(9), 892–896. https://doi.org/10.1001/JAMADERMATOL.2017.1716

Baenke, F., Chaneton, B., Smith, M., Van Den Broek, N., Hogan, K., Tang, H., … Marais, R. (2016). Resistance to BRAF inhibitors induces glutamine dependency in melanoma cells. *Molecular Oncology*, *10*(1), 73–84. https://doi.org/10.1016/J.MOLONC.2015.08.003

Bai, P. (2015). Biology of Poly(ADP-Ribose) Polymerases: The Factotums of Cell Maintenance. *Molecular Cell*, *58*(6), 947–958. https://doi.org/10.1016/J.MOLCEL.2015.01.034

Bajrami, I., Kigozi, A., Van Weverwijk, A., Brough, R., Frankum, J., Lord, C. J., & Ashworth, A. (2012). Synthetic lethality of PARP and NAMPT inhibition in triple-negative breast cancer cells. *EMBO Molecular Medicine*, *4*(10), 1087–1096. https://doi.org/10.1002/EMMM.201201250

Bajzikova, M., Kovarova, J., Coelho, A. R., Boukalova, S., Oh, S., Rohlenova, K., … Neuzil, J. (2019). Reactivation of Dihydroorotate Dehydrogenase-Driven Pyrimidine Biosynthesis Restores Tumor Growth of Respiration-Deficient Cancer Cells. *Cell Metabolism*, *29*(2), 399-416.e10. https://doi.org/10.1016/J.CMET.2018.10.014

Baumgartner, R., Walloschek, M., Kralik, M., Gotschlich, A., Tasler, S., Mies, J., & Leban, J. (2006). Dual binding mode of a novel series of DHODH inhibitors. *Journal of Medicinal Chemistry*, *49*(4), 1239–1247. https://doi.org/10.1021/JM0506975

Bensaad, K., & Vousden, K. H. (2007). p53: new roles in metabolism. *Trends in Cell Biology*, *17*(6), 286–291. https://doi.org/10.1016/J.TCB.2007.04.004

Boukalova, S., Hubackova, S., Milosevic, M., Ezrova, Z., Neuzil, J., & Rohlena, J. (2020). Dihydroorotate dehydrogenase in oxidative phosphorylation and cancer. *Biochimica et Biophysica Acta. Molecular Basis of Disease*, *1866*(6). https://doi.org/10.1016/J.BBADIS.2020.165759

Braakhuis, B. J. M., van Dongen, G. A. M. S., Peters, G. J., van Walsum, M., & Snow, G. B. (1990). Antitumor activity of brequinar sodium (Dup-785) against human head and neck squanmous cell carcinoma xenografts. *Cancer Letters*. https://doi.org/10.1016/0304-

3835(90)90149-R

Brown, K. K., Spinelli, J. B., Asara, J. M., & Toker, A. (2017). Adaptive Reprogramming of De Novo Pyrimidine Synthesis Is a Metabolic Vulnerability in Triple-Negative Breast Cancer. *Cancer Discovery*, *7*(4), 391–399. https://doi.org/10.1158/2159-8290.CD-16-0611

Chakravarty, E. F., Michaud, K., & Wolfe, F. (2005). Skin cancer, rheumatoid arthritis, and tumor necrosis factor inhibitors. *The Journal of Rheumatology*, *32*(11), 2130–2135. https://doi.org/10.1016/s0093-3619(08)70053-4

Chang, M. S., Hartman, R. I., Xue, J., Giovannucci, E. L., Nan, H., & Yang, K. (2021). Risk of Skin Cancer Associated with Metformin Use: A Meta-Analysis of Randomized Controlled Trials and Observational Studies. *Cancer Prevention Research (Philadelphia, Pa.)*, *14*(1), 77–84. https://doi.org/10.1158/1940-6207.CAPR-20-0376

Checkley, L. A., Rho, O., Angel, J. M., Cho, J., Blando, J., Beltran, L., … DiGiovanni, J. (2014). Metformin inhibits skin tumor promotion in overweight and obese mice. *Cancer Prevention Research (Philadelphia, Pa.)*, *7*(1), 54–64. https://doi.org/10.1158/1940-6207.CAPR-13-0110

Chen, A. C., Martin, A. J., Choy, B., Fernández-Peñas, P., Dalziell, R. A., McKenzie, C. A., … Damian, D. L. (2015). A Phase 3 Randomized Trial of Nicotinamide for Skin-Cancer Chemoprevention. *The New England Journal of Medicine*, *373*(17), 1618–1626. https://doi.org/10.1056/NEJMOA1506197

Chong, S., Wong, H. Y., Althabteh, A., Cox, C., Stevenson, P. H., Brown, S., … Khosrotehrani, K. (2022). Chemoprevention of cutaneous squamous cell carcinoma and its precursors in solid organ transplant recipients using topical sirolimus: A randomized, double-blind, placebo-controlled pilot trial. *Journal of the American Academy of Dermatology*, *87*(5). https://doi.org/10.1016/J.JAAD.2022.02.039

Dantal, J., Morelon, E., Rostaing, L., Goffin, E., Brocard, A., Tromme, I., … Serra, A. J. (2018). Sirolimus for Secondary Prevention of Skin Cancer in Kidney Transplant Recipients: 5-Year Results. *Journal of Clinical Oncology : Official Journal of the American Society of Clinical Oncology*, *36*(25), 2612–2620. https://doi.org/10.1200/JCO.2017.76.6691

Dolladille, C., Chrétien, B., Peyro-Saint-Paul, L., Alexandre, J., Dejardin, O., Fedrizzi, S., & Defer, G. (2021). Association Between Disease-Modifying Therapies Prescribed to Persons with Multiple Sclerosis and Cancer: a WHO Pharmacovigilance Database Analysis. *Neurotherapeutics : The Journal of the American Society for Experimental*

NeuroTherapeutics, *18*(3), 1657–1664. https://doi.org/10.1007/S13311-021-01073-Y

Euvrard, S., Morelon, E., Rostaing, L., Goffin, E., Brocard, A., Tromme, I., … Dantal, J. (2012). Sirolimus and secondary skin-cancer prevention in kidney transplantation. *The New England Journal of Medicine*, *367*(4), 329–339. https://doi.org/10.1056/NEJMOA1204166

Gil-Bernal, R., González-Caballero, J. L., Espinosa-Rosso, R., & Gómez-Gómez, C. (2021). Potential risk of disease modifying therapies on neoplasm development and coadjutant factors in multiple sclerosis outpatients. *Scientific Reports*, *11*(1). https://doi.org/10.1038/S41598-021-91912-X

Gronich, N., & Rennert, G. (2013). Beyond aspirin-cancer prevention with statins, metformin and bisphosphonates. *Nature Reviews. Clinical Oncology*, *10*(11), 625–642. https://doi.org/10.1038/NRCLINONC.2013.169

Haq, R., Shoag, J., Andreu-Perez, P., Yokoyama, S., Edelman, H., Rowe, G. C., … Widlund, H. R. (2013). Oncogenic BRAF regulates oxidative metabolism via PGC1α and MITF. *Cancer Cell*, *23*(3), 302–315. https://doi.org/10.1016/J.CCR.2013.02.003

Hosseini, M., Dousset, L., Mahfouf, W., Serrano-Sanchez, M., Redonnet-Vernhet, I., Mesli, S., … Rezvani, H. R. (2018). Energy Metabolism Rewiring Precedes UVB-Induced Primary Skin Tumor Formation. *Cell Reports*, *23*(12), 3621–3634. https://doi.org/10.1016/j.celrep.2018.05.060

Hosseini, M., Dousset, L., Michon, P., Mahfouf, W., Muzotte, E., Bergeron, V., … Rezvani, H. R. (2019). UVB-induced DHODH upregulation, which is driven by STAT3, is a promising target for chemoprevention and combination therapy of photocarcinogenesis. *Oncogenesis*, *8*(10). https://doi.org/10.1038/s41389-019-0161-z

Hu, S., Balakrishnan, A., Bok, R. A., Anderton, B., Larson, P. E. Z., Nelson, S. J., … Goga, A. (2011). 13C-pyruvate imaging reveals alterations in glycolysis that precede c-Myc-induced tumor formation and regression. *Cell Metabolism*, *14*(1), 131–142. https://doi.org/10.1016/J.CMET.2011.04.012

Hubackova, S., Davidova, E., Boukalova, S., Kovarova, J., Bajzikova, M., Coelho, A., … Neuzil, J. (2020). Replication and ribosomal stress induced by targeting pyrimidine synthesis and cellular checkpoints suppress p53-deficient tumors. *Cell Death & Disease*, *11*(2). https://doi.org/10.1038/S41419-020-2224-7

Jiang, L., Zhang, W., Li, W., Ling, C., & Jiang, M. (2018). Anti-inflammatory drug, leflunomide and its metabolite teriflunomide inhibit NSCLC proliferation in vivo and in vitro. *Toxicology Letters*, *282*, 154–165. https://doi.org/10.1016/J.TOXLET.2017.10.013

Khandekar, M. J., Cohen, P., & Spiegelman, B. M. (2011). Molecular mechanisms of cancer development in obesity. *Nature Reviews. Cancer*, *11*(12), 886–895. https://doi.org/10.1038/NRC3174

Kouidhi, S., Ayed, F. Ben, & Elgaaied, A. B. (2018). Targeting Tumor Metabolism: A New Challenge to Improve Immunotherapy. *Frontiers in Immunology*, *9*(FEB). https://doi.org/10.3389/FIMMU.2018.00353

Koundinya, M., Sudhalter, J., Courjaud, A., Lionne, B., Touyer, G., Bonnet, L., … Morris, A. (2018). Dependence on the Pyrimidine Biosynthetic Enzyme DHODH Is a Synthetic Lethal Vulnerability in Mutant KRAS-Driven Cancers. *Cell Chemical Biology*, *25*(6), 705-717.e11. https://doi.org/10.1016/J.CHEMBIOL.2018.03.005

Ladds, M. J. G. W., Van Leeuwen, I. M. M., Drummond, C. J., Chu, S., Healy, A. R., Popova, G., … Laín, S. (2018). A DHODH inhibitor increases p53 synthesis and enhances tumor cell killing by p53 degradation blockage. *Nature Communications*, *9*(1). https://doi.org/10.1038/S41467-018-03441-3

Long, G. V., Dummer, R., Hamid, O., Gajewski, T. F., Caglevic, C., Dalle, S., … Mitchell, T. C. (2019). Epacadostat plus pembrolizumab versus placebo plus pembrolizumab in patients with unresectable or metastatic melanoma (ECHO-301/KEYNOTE-252): a phase 3, randomised, double-blind study. *The Lancet. Oncology*, *20*(8), 1083–1097. https://doi.org/10.1016/S1470-2045(19)30274-8

Malissen, N., Vergely, L., Simon, M., Roubertie, A., Malinge, M. C., & Bessis, D. (2017). Long-term treatment of cutaneous manifestations of tuberous sclerosis complex with topical 1% sirolimus cream: A prospective study of 25 patients. *Journal of the American Academy of Dermatology*, *77*(3), 464-472.e3. https://doi.org/10.1016/J.JAAD.2017.04.005

Maroun, J., Ruckdeschel, J., Natale, R., Morgan, R., Dallaire, B., Sisk, R., & Gyves, J. (1993). Multicenter phase II study of brequinar sodium in patients with advanced lung cancer. *Cancer Chemotherapy and Pharmacology*, *32*(1), 64–66. https://doi.org/10.1007/BF00685878

Mei, Z., Zhang, X., Yi, J., Huang, J., He, J., & Tao, Y. (2016). Sirtuins in metabolism, DNA repair and cancer. *Journal of Experimental & Clinical Cancer Research : CR*, *35*(1). https://doi.org/10.1186/S13046-016-0461-5

Miret-Casals, L., Sebastián, D., Brea, J., Rico-Leo, E. M., Palacín, M., Fernández-Salguero, P. M., … Zorzano, A. (2018). Identification of New Activators of Mitochondrial Fusion Reveals a Link between Mitochondrial Morphology and Pyrimidine Metabolism. *Cell*

Chemical Biology, *25*(3), 268-278.e4. https://doi.org/10.1016/J.CHEMBIOL.2017.12.001

Natale, R., Wheeler, R., Moore, M., Dallaire, B., Lynch, W., Carlson, R., … Gyves, L. (1992). Multicenter phase II trial of brequinar sodium in patients with advanced melanoma. *Annals of Oncology : Official Journal of the European Society for Medical Oncology*, *3*(8), 659–660. https://doi.org/10.1093/OXFORDJOURNALS.ANNONC.A058298

Pollak, M. (2012). The insulin and insulin-like growth factor receptor family in neoplasia: an update. *Nature Reviews. Cancer*, *12*(3), 159–169. https://doi.org/10.1038/NRC3215

Rezvani, H. R., Kim, A. L., Rossignol, R., Ali, N., Daly, M., Mahfouf, W., … Bickers, D. R. (2011). XPC silencing in normal human keratinocytes triggers metabolic alterations that drive the formation of squamous cell carcinomas. *The Journal of Clinical Investigation*, *121*(1), 195–211. https://doi.org/10.1172/JCI40087

Sainas, S., Giorgis, M., Circosta, P., Poli, G., Alberti, M., Passoni, A., … Lolli, M. L. (2022). Targeting Acute Myelogenous Leukemia Using Potent Human Dihydroorotate Dehydrogenase Inhibitors Based on the 2-Hydroxypyrazolo[1,5- a]pyridine Scaffold: SAR of the Aryloxyaryl Moiety. *Journal of Medicinal Chemistry*. https://doi.org/10.1021/ACS.JMEDCHEM.2C00496

Shi, D. D., Savani, M. R., Levitt, M. M., Wang, A. C., Endress, J. E., Bird, C. E., … McBrayer, S. K. (2022). De novo pyrimidine synthesis is a targetable vulnerability in IDH mutant glioma. *Cancer Cell*, *0*(0), 14. https://doi.org/10.1016/J.CCELL.2022.07.011

Sykes, D. B., Kfoury, Y. S., Mercier, F. E., Wawer, M. J., Law, J. M., Haynes, M. K., … Scadden, D. T. (2016). Inhibition of Dihydroorotate Dehydrogenase Overcomes Differentiation Blockade in Acute Myeloid Leukemia. *Cell*. https://doi.org/10.1016/j.cell.2016.08.057

Tomic, T., Botton, T., Cerezo, M., Robert, G., Luciano, F., Puissant, A., … Rocchi, S. (2011). Metformin inhibits melanoma development through autophagy and apoptosis mechanisms. *Cell Death & Disease*, *2*(9). https://doi.org/10.1038/CDDIS.2011.86

Urba, S., Doroshow, J., Cripps, C., Robert, F., Velez-Garcia, E., Dallaire, B., … Gyves, J. (1992). Multicenter phase II trial of brequinar sodium in patients with advanced squamous-cell carcinoma of the head and neck. *Cancer Chemotherapy and Pharmacology*, *31*(2), 167–169. https://doi.org/10.1007/BF00685106

Wang, X., Yang, K., Wu, Q., Kim, L. J. Y., Morton, A. R., Gimple, R. C., … Rich, J. N.

(2019). Targeting pyrimidine synthesis accentuates molecular therapy response in glioblastoma stem cells. *Science Translational Medicine*, *11*(504). https://doi.org/10.1126/scitranslmed.aau4972

Ward, P. S., & Thompson, C. B. (2012). Metabolic reprogramming: a cancer hallmark even warburg did not anticipate. *Cancer Cell*, *21*(3), 297–308. https://doi.org/10.1016/J.CCR.2012.02.014

Wataya-Kaneda, M., Nakamura, A., Tanaka, M., Hayashi, M., Matsumoto, S., Yamamoto, K., & Katayama, I. (2017). Efficacy and Safety of Topical Sirolimus Therapy for Facial Angiofibromas in the Tuberous Sclerosis Complex : A Randomized Clinical Trial. *JAMA Dermatology*, *153*(1), 39–48. https://doi.org/10.1001/JAMADERMATOL.2016.3545

White, R. M., Cech, J., Ratanasirintrawoot, S., Lin, C. Y., Rahl, P. B., Burke, C. J., … Zon, L. I. (2011). DHODH modulates transcriptional elongation in the neural crest and melanoma. *Nature*, *471*(7339), 518–522. https://doi.org/10.1038/nature09882

Wu, C. L., Qiang, L., Han, W., Ming, M., Viollet, B., & He, Y. Y. (2013). Role of AMPK in UVB-induced DNA damage repair and growth control. *Oncogene*, *32*(21), 2682–2689. https://doi.org/10.1038/ONC.2012.279

Zhang, L., Zhang, J., Wang, J., Ren, C., Tang, P., Ouyang, L., & Wang, Y. (2022). Recent advances of human dihydroorotate dehydrogenase inhibitors for cancer therapy: Current development and future perspectives. *European Journal of Medicinal Chemistry*, *232*. https://doi.org/10.1016/J.EJMECH.2022.114176

ANNEXES

PUBLICATION

▪ During my Master 2 link to my thesis

-Energy metabolism rewiring precedes UVB-induced primary skin tumor formation.
Hosseini M, **Dousset L**, Mahfouf W, Serrano-Sanchez M, Redonnet-Vernhet I, Mesli S, Kasraian Z, Obre E, Bonneu M, Claverol S, Vlaski M, Ivanovic Z, Rachidi W, Douki T, Taïeb A, Bouzier-Sore AK, Rossignol R, Rezvani HR.
Cell Rep. 2018 Jun 19;(12):3621-3634.

▪ During my thesis

-UVB-induced DHODH Upregulation, which is driven by STAT3, is a promising target for chemoprevention and combination therapy of photocarcinogenesis.
Hosseini M, **Dousset L**, Michon P, Mahfouf W, Muzotte E, Bergeron V, Bortolotto D, Rossignol R, Moisan F, Taïeb A, Bouzier-Sore AK, Rezvani HR.
Oncogenesis. 2019 Sep 8 (10), 52.

- Loss of HIF-1a blocks UVB-transduced tumorigenesis by affecting DNA repair capacity and oxidative stress.
Mahfouf W, Hosseini M, Muzotte E, Serrano-Sanchez M, **Dousset L**, Moisan F, Rachidi W, Taïeb A, Rudolf J, Rezvani HR.
J Invest Dermatol. 2019 Sep;139(9)2016-2028

▪ During my thesis linked to my clinical activities

-Analysis of tumor response and clinical factors associated with vitiligo in patients receiving anti-programmed death-1 therapies for melanoma: a cross sectional study.
L.Dousset, A.Pacaud, T.Barnetche, M.Kostine, C.Dutriaux, A.Pham-ledard, M.Beylot-Barry, E.Gérard, S.Prey, N.Andreu, K.Boniface, J.Seneschal. **JAAD international**. 2021 19;5:112-120.

-Positive association between location of melanoma, UV-signature, tumor mutational burden and response to PD-1 therapy.
L.Dousset, F.Poizeau, C.Robert, (…), M.Beylot-Barry, L.Boussemart. **JCO Precis Oncol**. 2021 16;5:PO.2100084.

-Complete response in a patient with advanced melanoma following anti-PD-1 therapy is associated with high frequency of melanoma-infiltrating CXCR3+ resident memory CD8+ T cells and multiple chemokine pathways.
L. Dousset, C Martins, C Jacquemin, S Amico, T Schatton, K Boniface, J Seneschal.
Br J Dermatol. 2021. doi : 10.1111/bjd.20405.

-Non-acral skin manifestations during the COVID-19 epidemic: COVIDSKIN study by the French Society of Dermatology.
Guelimi R, Salle R, **Dousset** L, Assier H (…), Wolkenstein P, Le Cleach L, Beylot-Barry M.
J Eur Acad Dermatol Venereol. 2021; 35(9)e539-e541.

-Most childblains observed during the COVID-19 outbreak occur in patients who are negative for COVID-19 on polymerase chain reaction and serology testing.
Le cleach L, **Dousset L**, Assier H, Barbarot S, Boulard C, Bourseau-Quetier C, Cambon L, Cazanave C, Colin A, Kostrewa E, Lesort C, Levy Roy A, (…), Wolkenstein P, Sbidian E, Beylot-Barry M; French Society of Dermatology.
Br J Dermatol. 2020 Jul 6:10.1111/bjd.19377.

-Predictive Factors of Non-Response to Vismodegib in Locally Advanced Basal-Cell Carcinoma.
Marescassier H, **Dousset L**, Beylot-Barry M, Célérier P, Vaillant L, Bedane C, Leclère F, Wierzbicka-Hainaut E, Masson Regnault M.
Dermatology. 2021. 20 :1-6. doi: 10.1159/000512889.

GRANTS ACQUIRED DURING THE THESIS

For research work

- **From Fondation SILAB-Jean Paufique (2021-2023)**

-Grant for research work to Léa Dousset (60000 euros for 3 years 2021-2023)

- **From the French Skin Cancer Association (2022)**

-Grant for research work to Léa Dousset (20000 euros)

- **From the French Society of Dermatology (SFD):**

-Appel à projet exceptionnel, to Hamid Rezvani/Léa Dousset (150000 euros for 3 years)

Award or travel grant

- **From the European Society of Research in Dermatology**

-Travel Grant for ESDR 2022 in Amsterdam
-Travel grant for ESDR 2021
-Selected for the "ESDR Future Leader Academy" in 2021.

- **From the French Society of Dermatology (SFD):**

-Winner of the dermatopathology trophy in 2020
- Prix du meilleur cas clinique de carcinome basocellulaire des images en Dermatologie in 2021

- **From the European Academy of Dermatology and Venereology**

-Health Care Professional Scholarship registration to attend the 31st EADV Congress

SCIENTIFIC COMMUNICATIONS

▪ Oral communications in local, national and international congress meetings

-Journées de Dermatologie de Paris Décembre 2022, Paris
« Le profilage métabolique permet d'identifier un groupe de patients atteint de carcinome épidermoïde cutané sensible au traitement par leflunomide »
Léa Dousset, Pauline Michon, Walid Mahfouf, Elodie Muzotte, Giulia Guzzo, Marie Beylot-Barry, Hamid-Reza Revani

-European Society for Dermatological Research (ESDR) 2021, online
"Metabolic and immune features as predictive biomarkers of risk stratification of skin carcinoma"
L. Dousset, P. Michon, J. Giraud, D. Chalopin, B. Rousseau, M. Hosseini, W. Mahfouf, E. Muzotte, M. Beylot-Barry, M. Saleh, H. Rezvani

-Metaboslim and Cancer 2021, online
"Metabolic and immune features as predictive biomarkers of risk stratification of skin carcinoma"
L. Dousset, P. Michon, J. Giraud, D. Chalopin, B. Rousseau, M. Hosseini, W. Mahfouf, E. Muzotte, M. Saleh, M. Beylot-Barry, H. Rezvani.

-Congrès Annuel de Recherche en Dermatologie (JDP) 2020, online
« Profilage métabolique durant la photocarcinogenèse : identification des vulnérabilités métaboliques au stade précoce et au stade avancé comme cible thérapeutique »
L. Dousset*, P. Michon, M. Hosseini, W. Mahfouf, E. Muzotte, A. Taïeb, H. Rezvani. CO29.

-16èmes Journées Annuelles du Canéropôles GSO, Carcassonne, Novembre 2020
DHODH chemoprevention and combination therapy of UVB-induced skin cancers.
L Dousset, Pauline Michon, Walid Mahfouf, Elodie Muzotte, Giulia Guzzo, Marie Beylot-Barry, Hamid-Reza Rezvani

▪ Poster presentation

-European Society for Dermatological Research (ESDR), 2022, Amsterdam
"Inhibition of DHODH efficiently reduces tumor growth in a subgroup of cutaneous squamous cell carcinoma with a particular metabolic profile "
Léa Dousset, Pauline Michon, Walid Mahfouf, Elodie Muzott1, Giulia Guzzo, Marie Beylot-Barry, Hamid-Reza Revani

-4th Metabolism and Cancer Symposium 2021, online
Metabolic and immune features as predictive biomarkers of risk of stratification of skin carcinoma.
L. Dousset, P. Michon, J. Giraud, D. Chalopin, B. Rousseau, M. Hosseini, W. Mahfouf, E. Muzotte, M. Beylot-Barry, M. Saleh, H. Rezvani

-15èmes Journées Annuelles du Canéropôles GSO, Arcachon, Novembre 2019
DHODH chemoprevention and combination therapy of UVB-induced skin cancers.
L.Dousset, M.Hosseini, W.Mahfouf, A.Taïeb, HR Rezvani.
Prix du Poster « Silab Jean-Paufique ».

-European Society for Dermatological Research (ESDR), 2019
DHODH inhibition for chemoprevention and combination therapy of UVB-induced epithelial oncogenesis. **L. Dousset,** M. Hosseini, W. Mahfouf, E. Muzotte, A. Taïeb, H. Rezvani.
Selected for Poster Walk. **P462.**

OTHER ARTICLES DURING THESIS

ARTICLE 4

Energy metabolism rewiring following acute UVB irradiation is largely dependent on nuclear DNA damage

Article in preparation.

Energy metabolism rewiring following acute UVB irradiation is largely dependent on nuclear DNA damage

Pauline Michon[1], Walid Mahfouf[1], Léa Dousset[1,2], Corinne Faucheux[1], Elodie Muzotte[1], Giulia Guzzo[1], Alain Taieb[1,7], Rodrigue Rossignol[3,4], Stéphane Claverol[5], Laure Favot-Laforge[6], Muriel Cario[1;7], Anni I. Nieminen[8], Sepo Vainio[9,10,11,12], Nsrein Ali[9], Hamid-Reza Rezvani[1,7*]

[1] Univ. Bordeaux, Inserm, BRIC, UMR 1312, F-33076 Bordeaux, France.

[2] Dermatology Department, Hôpital Saint-André, Bordeaux, France

[3] Univ. Bordeaux, Inserm, MRGM, U1211, Bordeaux, France

[4] CELLOMET, Centre de Génomique Fonctionnelle de Bordeaux, Univ. Bordeaux, Bordeaux, France.

[5] Plateforme de protéomique, Centre de Génomique Fonctionnelle de Bordeaux, Univ. Bordeaux, Bordeaux, France.

[6] LITEC EA 4331, Poitier, France

[7] Aquiderm, University of Bordeaux, Bordeaux, France

[8] FIMM Metabolomics Unit, Institute for Molecular Medicine Finland, University of Helsinki, 00014, Finland

[9] Laboratory of Developmental Biology, Faculty of Biochemistry and Molecular Medicine, University of Oulu and Biocenter Oulu, Aapistie 5A, 90220, Oulu, Finland.

[10] Infotech Oulu, University of Oulu, Oulu, Finland

[11] Kvantum Institute, University of Oulu, Oulu, Finland

[12] Flagship GeneCellNano, University of Oulu, Oulu, Finland

*** Corresponding Author**
Postal address: INSERM U1312, Bordeaux, F-33000 France
Email address: hamid-reza.rezvani@u-bordeaux.fr
Phone: +33-557-575-683 Fax: +33-557-571-374

Abstract

Solar ultraviolet B (UVB) radiation-induced DNA damage is a well-known initiator of skin carcinomas. UVB-induced DNA damage response (DDR) is a series of signaling cascades that are activated for maintaining cell integrity. Among different biological processes, little is known about the role of energy metabolism in DDR.

We sought to identify whether the UVB-induced nuclear and/or mitochondrial cyclobutane pyrimidine dimers (CPD) alter cellular energy metabolism. To gain insight into this question, we took advantage of keratinocytes expressing nuclear or mitochondrial CPD photolyase. By applying a quantitative proteomic approach and targeted metabolomics, we found a biphasic alteration in metabolism, which was largely dependent on the presence of genomic CPD. The increased oxygen consumption rate at 24h after irradiation as well as the mitochondrial structural rearrangements were dependent on both mitochondrial and nuclear CPDs.

Understanding the influence of the nuclear and mitochondrial DNA damage on keratinocyte responses to UVB could enhance current knowledge regarding skin cancer prevention, initiation, and therapy.

Introduction

Solar ultraviolet radiation (UV) is the main risk factor for the induction of non-melanoma skin cancers (NMSCs), the most common types of human malignancies worldwide. The rate of NMSC including basal cell carcinomas and cutaneous squamous cell carcinomas (cSCCs) is increasing by 5-7% per year and its mainly due to UV exposure and ageing of population[1]. In 2012, 3.3 million patients in the USA were affected[2].

Solar radiation affects skin homeostasis through induction of well-defined structural alterations in DNA, which in turn, trigger the DNA damage response (DDR) network. DDR involves sensing the damage and subsequently signaling to downstream effectors. The balance between different activated signaling pathways, which is dependent on the type and extent of the damage and DNA repair capacity, would ultimately determine whether a cell remains quiescent, proliferates, differentiates, or undergoes apoptosis[3,4]. The major DNA damage, which are induced by UVB irradiation, are cyclobutane pyrimidine dimers (CPDs) and 6–4 photoproducts (6-4PPs). Those lesions are mainly repaired by the nucleotide excision repair (NER) DNA system through the release of a 24-mer to 32-mer oligonucleotide containing the damage and its replacement by a newly synthesized DNA fragment[5].

Characterizing and understanding the molecular basis underpinning the cross-talk among different programs forming part of DDR network are currently the subject of intense investigation. A growing literature suggests that there may be a crosstalk between DDR network and energy metabolism. Therefore, the main aim of this study is to determine whether reprogramming of metabolic pathways also occurs after acute UVB irradiation. If so, the two following scenarios should be taken in account. First, reprogramming of metabolic pathways is an adaptive response and, so, it could be considered as a sub-program of the DDR network supporting homeostasis of stressed cells. Second, energy metabolism alteration occurs prior DDR activation and, therefore, it plays decisive roles in launching and orchestrating the DDR network. The former scenario is supported by evidence showing that sensors (e.g. PARP1), transducers (e.g. ATM) and effectors (e.g. p53, CDK) of DDR network activate numerous enzymes involved in energy metabolism [6–9]. Evidence for the second scenario comes from data showing that different genotoxic-induced DNA damages result in the early activation of numerous enzymes involved in energy metabolism (such as AMPK, HIF-1 and TIGAR). These metabolic enzymes function as important

regulators of diverse cellular processes including transcriptional regulation, cell cycle, senescence, apoptosis and autophagy[9–11] Moreover, we and others have shown that modulation of the master regulators of energy metabolism (such as HIF-1α and Tfam) could affect the repair efficiency of UVB-induced DNA damage[12–14] epidermal differentiation and hair growth[15–20], suggesting that energy metabolism could affect diverse skin cellular processes.

To unravel the role of metabolism in keratinocyte responses to acute UVB irradiation, we took advantage of keratinocytes expressing nuclear or mitochondrial CPD photolyase (Nu-PL and Mt-PL, respectively). We show here that exposure of keratinocytes to acute UVB light leads to biphasic alterations in numerous metabolic pathways, which is largely dependent on nuclear CPDs and independent on mitochondrial CPDs. The abundance of numerous metabolites in keratinocytes exposed to UVB irradiation was also changed in a biphasic manner, which was partially restored in Nu-PL cells. The presence of nuclear and mitochondrial CPDs also affect the structure of the mitochondrial network.

Altogether, the current data provide substantial insights into the links between UVB-induced DNA damage and metabolic alterations in orchestrating DDR network.

Results

UVB irradiation induces biphasic variations in the metabolic pathways involved in energy metabolism

To study the cross-talk between different programs of DDR network and metabolism following acute UVB irradiation, we used immortalized human keratinocytes called KHAT. Even though they are immortal, they still retain their ability to form a fully stratified epidermis when used in an organotypic culture (**Figure S1**). These keratinocytes were irradiated with a single dose of UVB (15 $mJ.cm^{-2}$). The quantity of CPD was first analyzed at different time points after irradiation using immune-dot blotting (**Figure 1A**). Results showed a gradual removal of CPD with a peak at 9h. Besides the DNA repair machinery, other DDR signaling pathways such as autophagy (LC3 expression) and apoptosis (activated caspase 3 expression) were also triggered in these cells as shown by western blotting (**Figure 1B**). Metabolic sensor such as AMPK was also activated at 10h and 24h after acute UVB irradiation (**Figure 1B**). To obtain a global overview of signaling pathways triggered by a single exposure to UVB irradiation, we performed a quantitative label-free differential proteomic analysis of samples at different time points after UVB irradiation (**Figure 1C**). Ingenuity Computational Pathway Analysis (IPA®) software (www.ingenuity.com) was used to elucidate the global implications of differentially expressed proteins as well as the potentially modified molecular pathways at different time points after irradiation. The top canonical pathways from the IPA are shown in **Figure 1C**. In this list, as expected, there were numerous well-known signaling pathways that classically contribute to the DDR programs, such as EIF2 signaling, integrin signaling, senescence pathway, death receptor signaling, cell cycle control and ATM signaling pathways. Of note, the majority of these signaling pathways were modified in a biphasic manner with an early downregulation which was followed with a late upregulation. Besides those pathways, we found that the metabolic pathways involved in energy metabolism, such as oxidative phosphorylation (OXPHOS), glycolysis, TCA cycle and fatty acid β-oxidation, were also modified in a time dependent manner (**Figure 1C**).

Focusing on the expression levels of proteins involved in glycolysis, TCA cycle, and OXPHOS, the relative expression of the majority of these proteins were significantly decreased at 2h after irradiation. Those early downregulations were followed with their

gradual increases in the following hours (**Figure 2 A-C**), suggesting that reprogramming of metabolic pathways is an adaptive response and could be considered as a sub-program of the DDR network. Finally, proteins differentially expressed 2h after irradiation were categorized to related diseases and biological functions by the IPA enrichment analysis. Top enriched gene ontology terms for diseases and biological functions with a p-value less than 10^{-15} are listed in **Figure 2D**. Metabolic diseases were found among this list with a p-value less than 10^{-30} (**Figure 2D**).

Experiments were also performed on the HaCat keratinocyte cell line. Results indicated biphasic alterations of the majority of canonical pathways and biphasic expression levels of proteins involved in OXPHOS, similar to what we found in KHAT cells but with different kinetics (**Figure S2**). Hereinafter only the results obtained with KHAT InhNOX1 are shown.

Biphasic variations in the relative abundance of metabolites following acute UVB irradiation

To further examine the effects of acute UVB irradiation on metabolic signatures, keratinocytes harvested at different time points after UVB irradiation were subjected to metabolomics. Results revealed alterations in the abundance of metabolites that can be divided in three categories (**Figures 3A-B**). The abundance of the first group was decreased at 5h and increased at 48h after irradiation. Glutamine, glutamate, aspartate and malate were among these metabolites (**Figure 3C-F**). In the second group, the abundance of metabolites varied in an inverse manner compared to the first group, i.e. they were upregulated at 5h after irradiation and decreased in the following hours (**Figure 3A**). Saturated fatty acids (palmitate and myristic acids,) (**Figure 3G-H**), alpha-ketoglutarate, NADP, uracil, fructose 6 phosphate and phosphoenolpyruvate were among the metabolites of this group (**Figure 3A**). The third group was composed of the metabolites, such as pyruvate and nicotinamide (NAM), not quantitatively modified following UVB irradiation (**Figure 3I-J**).

Altogether, our results indicate that keratinocytes respond to UVB exposure via altering their metabolic patterns as an adaptive mechanism.

OXPHOS is upregulated as a late keratinocyte response to UVB irradiation

To further investigate the effects of acute UVB irradiation on energy metabolism, biochemical functional analyses were performed. Results showed lower glucose uptake in irradiated cells at 5h post-irradiation (**Figure 4A**). No significant difference in lactate production levels was detected between irradiated cells at both time points (5, and 24h) and non-irradiated cells, although a moderate decrease was noted. (**Figure 4B**). Similarly, the kinetics of extracellular acidification rates (ECAR) was not significantly changed after irradiation (**Figure 4C**). However glycolytic capacity was higher in irradiated cells compared to non-irradiated keratinocytes **(Figure 4C and figure S3)**. To evaluate OXPHOS activity following irradiation, basal oxygen consumption rate (OCR) was measured. By comparing non-irradiated to irradiated cells at different time-points, we found that that basal OCR increased significantly only 24h after irradiation **(Figure 4D).** To further examine the effect of acute UVB irradiation on OXPHOS activity, maximal respiration via different mitochondrial complexes was evaluated. The CI- and CII-dependent respirations were modified following UVB irradiation in a biphasic manner **(Figure 4E-F).** While no significant modification in the CIII-linked OCR was observed over time (**Figure 4G**), a significant increase in the CIV-dependent OCR was detected at 24h post-irradiation (**Figure 4G**). In agreement, the expression levels of nuclear-encoded mitochondrial complex I's subunit NDUFB8, II's subunit SDHB, III's subunit UQCRC2, IV's subunit COX II and V's subunit ATP5A were upregulated in cells at 24h post-irradiation compared to non-irradiated keratinocytes.

Altogether, our data reveal that OXPHOS is upregulated as a late response to UVB irradiation.

Mitochondrial network undergoes continuous morphological and structural remodeling following UVB irradiation

Mitochondrial network morphology is critically linked to bioenergetics, and consequently undergoes changes upon metabolic or environmental stresses[21–24].The morphology of mitochondrial network is mainly dependent on the balance between mitochondrial fusion and fission. Generally, while mitochondrial fission allows

exclusion of damaged mitochondria, mitochondrial fusion enables the exchange between functional mitochondria[25].

To examine the effect of UVB irradiation on the mitochondrial network features, we first wondered whether the mitochondrial DNA content is modified following irradiation. Results indicated that the levels of mtDNA (mtDNA to genomic DNA ratio) in irradiated cells were not significantly different from non-irradiated samples (**Figure 5A**). We then examined the morphological and structural remodeling of mitochondrial network at different time points after UVB irradiation. To this end, the MitoSegNet model was generated with a training set of 40 1024 x 1024-pixel confocal microscopy images, depicting mitochondria in body wall of keratinocytes (**Figure 5B** and methods). As observed in **Figure 5C**, dynamic rearrangement of mitochondrial network was observed at different time points after irradiation. Principal component analysis (PCA) indicated that the mitochondrial network features in cells at 9h after irradiation were farthest from other groups (**Figure 5D-E, and Figure S4**). Quantification analysis indicated that the average major axis, minor axis, perimeter and eccentricity of mitochondria were increased 9h after irradiation. On the contrary, the average solidity, number of branches and total brunch length were diminished in these cells (**Figure 5F**), suggesting an increased fission process at 9h after irradiation. In agreement, the expression of mitochondrial fission 1 protein (Fis-1) was rapidly upregulated following irradiation. This increased expression was followed by a decrease 24h post-irradiation (**Figure 5G**).

Overall, ours results indicates that mitochondrial network features are modified dynamically at different time points after UVB exposure with molecular and morphological evidence of fission.

Nuclear and mitochondrial DNA damage are key regulators of energy metabolism rewiring following acute UVB irradiation

To unravel whether the presence of nuclear and/or mitochondrial CPDs plays a decisive role in launching the UVB-induced metabolic alteration, keratinocytes were transduced with lentiviral vectors expressing nuclear or mitochondrial CPD photolyase (Nu-PL and Mt-PL, respectively) **(Figure S5).** Of note, CPD photolyases are DNA repair enzymes that efficiently remove the CPD lesions from DNA. These enzymes

require near-UV-blue light (300-500nm) as source of energy to repair efficiently CPD lesion [26,27]. Quantification of CPDs indicated that the majority of CPD were removed from genomic DNA within 30 min after irradiation in Nu-PL cells, while repair kinetics of CPD in Mt-PL cells were very similar to their control counterparts (**Figure 6A**). Focusing on proteomic data, we found that biphasic modifications in canonical pathways observed in control KHAT were largely restored in Nu-PL cells and no significant alterations were detected in these cells (**Figure 1C**). On the contrary, biphasic modulations in the activity of the canonical pathways (i.e. a decrease between 5-9h after acute UVB exposure followed with a late increase) were still observed in Mt-PL cells (**Figure 1C**). The expression profiles of proteins involved in glycolysis, TCA cycle, and OXPHOS were also restored in Nu-PL compared to their control counterparts (**Figure 2A-C**).

Analysis of metabolomics data indicated that the modification in the abundance of metabolites were partially restored in Nu-PL cells exposed to UVB (**Figure 3A**). Of note, the major effect of Nu-PL expression was on the first group of metabolites, which showed marked early downregulation followed with later significant upregulation in both control and Mt-PL cells. No significant downregulation was detected for the majority of these metabolites in Nu-PL cells 5h after irradiation, whereas a tendency in decreased levels of these metabolites was still noticed (**Figure 3A, C-F**). The late upregulation in the abundances of these metabolites were similar among control, Mt-PL and Nu-PL cells (**Figure 3A, C-F**).

Biochemical functional analyses revealed that, like control cells, ECAR and glycolytic capacity in Nu-PL cells at 24h after irradiation were higher than non-irradiated keratinocytes (**Figure S6A**). While not significant, an increased tendency of ECAR was detected in Mt-Pl cells at 24h after irradiation (**Figure S6B**). Measuring oxygen consumption in Nu-PL or Mt-PL cells at 24h after irradiation indicated that, on the contrary of the control cells, neither basal nor uncoupled OCR levels were significantly different from the levels found in their respective non-irradiated counterpart cells (**Figure 6C, D**). However, like control cells, the CI- and CIV-dependent respirations in Nu-PL cells at 24h after irradiation were higher than in non-irradiated cells (**Figure S6 C-F**). In agreement, the protein expression levels of mitochondrial subunits were increased 24h after irradiation in these cells (**Figure S6G**). No significant modifications

were detected in CI-, CII-, CII-, CIII and CIV-linked respiration rates between irradiated Mt-PL and their respective non-irradiated counterparts (**Figure S6 H-K**).

Mitochondrial network features at different time points after UVB irradiation were finally evaluated in Nu-PL and Mt-PL cells and compared with control cells. PCA indicated that mitochondrial network features in irradiated cells at any time point after irradiation were very close to each other and could not be discriminated from each other in both Nu-PL and Mt-PL cells. However, there were several differences between irradiated and non-irradiated cells in both conditions (**Figure 6E, F**). Quantification analyses on cells 9h after irradiation indicated that the average major axis, minor axis, and perimeter of mitochondria were decreased compared to non-irradiated cells. On the contrary, the average solidity was increased in both cells compared to their non-irradiated counterpart cells (**Figure 6G, H**), suggesting an increased mitochondrial fusion process after irradiation in these cells.

Collectively, our findings show that both nuclear and mitochondrial CPDs are key regulators of keratinocyte responses to UVB, influencing mitochondria features (morphology and function) via controlling/synchronizing metabolic proteins expression patterns.

Discussion

Overwhelming evidence indicate that DDR network activation alters the metabolic functions of its host organism and, vice versa, the metabolic profiling of the host regulates DDR[5,28,29]. Considering such bidirectional relationship, we aimed to study the effect of UVB-induced nuclear and mitochondrial CPDs on metabolic signatures of keratinocytes. Overall, our results indicated that rapid removal of CPD in Nu-PL cells restored the early downregulation of canonical pathways, the expression levels of proteins involved in glycolysis, TCA cycle and OXPHOS, and the early decreased abundance of the majority of metabolites. Furthermore, rapid removal of nuclear CPD blocked the UVB-induced mitochondrial fission process observed in UVB-irradiated control cells. Rapid removal of CPDs from mtDNA in Mt-PL cells leads to the modified patterns of canonical pathways activations, the increase of some metabolite levels, alterations of mitochondrial-dependent metabolism and mitochondrial network features compared to UVB-irradiated control cells.

Metabolism reprogramming upon UVB irradiation

DDR programs are highly energy demanding processes[28,30]. Moreover, several DDR components (such as ATM, p53 and CDK) have been shown to modulate the activities of several enzymes involved in energy metabolism[6–9,28]. Therefore, it is not surprising that genotoxic stress-induced DDR network triggers metabolic alterations. It has been shown that exposure of HaCat cells to acute UVB irradiation leads to upregulation of glycolysis, mitochondrial respiration and fatty acid β-oxidation 24h post-irradiation[31,32]. Our results showed that most metabolic pathways were altered in a biphasic manner with an early downregulation followed with a significant upregulation in both examined keratinocyte cell lines **(Figure 1-3 and S2).** Therefore, examining the cell response kinetics is key to better understanding the essence of the crosstalk between DDR activation and metabolism (i.e. maintenance cell survival and homeostasis). In agreement, several studies found that acute exogenous genotoxic stress-induced DDR repressed the expression of enzymes involved in TCA cycle and OXPHOS at the transcriptional level typically 1-2h after exposure [33,34]. However, examining at longer time points has been shown significant increase in OCR rate and in the expression levels of genes involved in mitochondrial respiration[35]. It is likely that the late metabolic modifications occur to compensate cellular ATP, NAD+ and other metabolites depleted throughout repairing DNA damage[31,32,36–38]. In accordance, the biphasic modulations

in metabolic pathways, and upregulated mitochondrial respiration 24h after irradiation were abolished in cells expressing Nu-PL **(Figures 1C and 6C)**. Moreover, a modified metabolism has also been demonstrated in several models of DNA repair deficient diseases. For example, cells from xeroderma pigmentosum (XP) patients (such as XPC, XPD and XPA) and Cockayne syndrome (CS) have shown intrinsically altered metabolism such as increased glycolysis and decreased mitochondrial metabolism[5], indicating that cells in which DNA damage persistently accumulate need to change their metabolism to ensure their homeostasis.

Functional mitochondria in cell responses to UVB irradiation

Owing to its central function in numerous cellular processes including cell cycle progression, apoptosis/senescence and autophagy, energy metabolism plays a crucial role in cellular homeostasis upon stress condition. It is now widely accepted that OXPHOS and glycolysis cooperate to sustain the variable energy demands and anabolic (biosynthetic) needs of cells during their responses to stressors[39,40] and that human cells achieve those needs through various regulatory mechanisms referred to as metabolic reprogramming[41–43]. Besides energy demands, functional mitochondria are also crucial to support cellular biosynthetic fluxes, which are necessary for providing cellular building blocks such as nucleic acids, proteins and membranes, but also for redox resetting to acquire a new redox balance upon stress[39,40,44]. Therefore, it is not surprising that cellular responses to UVB with the capacity to remove rapidly CPDs from mtDNA (i.e. Mt-PL cells) are different from control cells. Indeed, our data indicated that activation profiles of canonical pathways and mitochondrial network features after irradiation are significantly different between Mt-PL and control cells **(Figures 1, 2, 5 and 6).** One explanation could be that mtDNA damages persist longer than nuclear DNA damages[45]. Mitochondrial dysfunction when mtDNA damages persist can be responsible for mitochondrial ROS production[46,47] and may cause the observed modifications.

A better understanding of what role metabolism plays in keratinocyte responses to UVB is crucial for developing adapted metabolic therapies both for prevention and therapy of skin cancers, as proposed for isocitrate dehydrogenase (IDH) 1 and 2 mutant tumors[48,49]or for oxidative human lung adenocarcinomas[50].

Material & methods

KHAT cell line and culture media

Human keratinocytes were isolated from normal human skin in patients undergoing plastic surgery and grown in Keratinocyte serum free media (KSFM) supplemented with 50 µg/mL of bovine pituitary extract and 0,5ng/mL of epidermal growth factor (Gibco; Thermo Fisher Scientific) in a humidified atmosphere of 5% CO_2 at 37°C. KHAT cell line was obtained through immortalization of human primary keratinocytes following their transduction with lentiviral vector expressing hTERT and the large tumor antigen (also called large T-antigen). Transduced keratinocytes were cultivated in parallel with the non-transduced cells in KSFM. Immortalization has been considered to be occurred when KHAT cells grew for 50 population doublings beyond the life span of the parental keratinocytes. These immortalized cells formed a normally stratified epidermis when used in organotypic culture (**Figure S1A**). KHAT cells are also capable to form pigmented epidermis when human primary melanocytes were incorporated in skin equivalents (**Figure S1B**).

UVB irradiation procedure

KHAT were irradiated at a dose of 15 mJ.cm-2 using a Biotronic device (Vilber Lourmat, Marne la Vallée, France), equipped with a dosimeter, in which the UVB lamp emitted a continuous spectrum between 280 and 380 nm (major peak at 312 nm), as already described[51]. To select this dose, the propidium iodide (PI) exclusion assay was initially performed to evaluate viability of keratinocytes following irradiation with different doses. The viability of irradiated keratinocytes was around 70 % compared with non-irradiated controls 24 h after irradiation at the dose of 15 $mJ.cm^{-2}$ (**Figure S1**). This dose was selected for further experiments. For photoactivation of CPD photolyase after irradiation, cells were incubated for 30 min under 450 nm blue light in 37°C 5% CO2 incubator.

Quantification of CPDs by immunodot blot analysis

CPDs were quantified as described previously[12,52]. Briefly, dry pellets were incubated 3h at 65 °C in DirectPCR Lysis Reagent (Euromedex, Souffelweyersheim, France) and 2% proteinase K (Sigma-Aldrich). DNA was extracted by using sodium acetate/ethanol

precipitation and quantified on a Nanodrop spectrophotometer (Thermo Fisher Scientific, Waltham, MA). Next, 500 ng of genomic DNA was mixed with 1% SYBR Green (Brilliant III Ultra-Fast SYBR; Agilent Technologies, Les Ulis, France), dot-blotted onto a Hybond N+ nitrocellulose membrane (Amersham, Little Chalfont, UK). Membranes were blocked for 30 minutes (20 mmol/L Tris-buffered saline, 5% nonfat dry milk, 0.5% Tween 20, pH 7.6) and incubated with anti-CPD monoclonal antibody (1:1,000, CosmoBio) overnight at 4 °C. Membranes were washed in Tris-buffered saline and incubated for 1 hour with a horseradish peroxidase-conjugated secondary antibody (1:2,000, Vector Laboratories). Blots were developed with an enhanced chemiluminescence reagent (BioRad, Hercules, CA). Chemiluminescence signals were quantified and normalized against SYBR green fluorescence.

Lentiviral Vector Constructs and Keratinocyte Transduction

Lentivural vector expressing nuclear photolyase-mcherry was a generous gift from Dr. Jurgen A Marteijn (University Medical Center Rotterdam, Rotterdam, Netherlands)[53]. This vector used for constructing CPD photolyase targeted into mitochondria by inserting the mitochondria targeting signal (MTS) taken from human Tfam gene (atggcgtttctccgaagcatgtggggcgtgctgagtgccctgggaaggtctggagcagagctgtgcaccggctgtgg aagtcgactgcgctccccttcagttttgtgtatttaccgaggtggttt) into N-terminal of photolyase-mcherry.

Lentiviral particles were produced by transient transfection of 293T cells using a calcium phosphate transfection technique as previously described[14,51]. Determination of the titer of each viral supernatant was performed by assessing TOMATO protein expression by flow cytometry.

For transduction, keratinocytes (5 x 10^5 cells/T25 flask) were incubated for 24 h in complete medium. Prior to infection, medium was removed, and cells were incubated with viral supernatants for 24 h at 37 °C. After 5 days, the percentage of Tomato fluorescent protein-positive cells was determined by immunohistochemistry (**Figure S5**) and flow cytometry.

Proteomic analysis:

Sample preparation for proteomic analysis

Dry pellet of KHAT cell lines were subjected to proteomic analysis, as previously described[52]. Of note, each sample was taken from a distinct petri dishes which was irradiated or not (nIr). Samples were lysed in RIPA buffer containing a protease inhibitor cocktail (Sigma). Ten µg of each protein sample were solubilized in Laemlli buffer and were deposited onto SDS-PAGE gel for concentration and cleaning purposes. Separation was stopped after proteins had entered the resolving gel. After colloidal blue staining, bands were cut out from the SDS-PAGE gel and subsequently cut into 1 mm x 1 mm gel pieces. Gel pieces were destained in 25 mM ammonium bicarbonate 50% ACN, rinsed twice in ultrapure water and shrunk in ACN for 10 min. After ACN removal, gel pieces were dried at room temperature, covered with the trypsin solution (10 ng/µl in 40 mM NH_4HCO_3 and 10% ACN), rehydrated at 4 °C for 10 min, and finally incubated overnight at 37 °C. Spots were then incubated for 15 min in 40 mM NH_4HCO_3 and 10% ACN at room temperature with rotary shaking. The supernatant was collected, and an H_2O/ACN/HCOOH (47.5:47.5:5) extraction solution was added onto gel slices for 15 min. The extraction step was repeated twice. Supernatants were pooled and concentrated in a vacuum centrifuge to a final volume of 40 µL. Digests were finally acidified by addition of 2.4 µL of formic acid (5%, v/v) and stored at -20 °C.

nLC-MS/MS analysis

Peptide mixture was analyzed on an Ultimate 3000 nanoLC system (Dionex, Amsterdam, The Netherlands) coupled with a Q-Exactive quadrupole Orbitrap benchtop mass spectrometer (Thermo Fisher Scientific, San Jose, CA). Ten microliters of peptide digests were loaded onto a 300-µm-inner diameter x 5-mm C_{18} PepMap™ trap column (LC Packings) at a flow rate of 30 µL/min. The peptides were eluted from the trap column onto an analytical 75-mm id x 15-cm C18 Pep-Map column (LC Packings) with a 4–40% linear gradient of solvent B in 108 min (solvent A was 0.1% formic acid in 5% ACN, and solvent B was 0.1% formic acid in 80% ACN). The separation flow rate was set at 300 nL/min. The mass spectrometer operated in positive ion mode at a 1.8-kV needle voltage. Data were acquired in a data-dependent mode. MS scans (*m/z* 300-2000) were recorded at a resolution of R = 70 000 (@ m/z 200) and an AGC target of 1 x 10^6 ions collected within 100 ms. Dynamic exclusion was set to 30 s and the top 15 ions were selected from

fragmentation in HCD mode. MS/MS scans with a target value of 1 x 10^5 ions were collected with a maximum fill time of 120 ms and a resolution of R = 35 000. Additionally, only +2 and +3 charged ions were selected for fragmentation. Other settings were as follows: spray voltage, 1.8 kV, no sheath nor auxiliary gas flow, heated capillary temperature, 200 °C; normalized HCD collision energy of 25% and an isolation width of 3 m/z.

Database search and results processing

Data were searched by SEQUEST through Proteome Discoverer 1.4 (Thermo Fisher Scientific Inc.) against a subset of the 2013.08 version of the UniProt database restricted to the Mus musculus Reference Proteome Set (42,882 entries). Spectra from peptides higher than 5000 Da or lower than 350 Da were rejected. The search parameters were as follows: mass accuracy of the monoisotopic peptide precursor and peptide fragments was set to 10 ppm and 0.02 Da respectively. Only b- and y-ions were considered for mass calculation. Oxidation of methionines (+16 Da) was considered as variable modification and carabamidomethylation of cysteines (+57 Da) as fixed modification. Two missed trypsin cleavages were allowed. Peptide validation was performed using the Percolator algorithm[54] and only "high confidence" peptides were retained corresponding to a 1% False Positive Rate at peptide level.

Label-Free Quantitative Data Analysis

Raw LC-MS/MS data were imported in Progenesis LC-MS 4.1 (Nonlinear Dynamics Ltd, Newcastle, U.K). Data processing included the following steps: (i) Feature detection, (ii) Feature alignment across the samples (100 human samples and 60 mouse samples), (iii) Automatic peak picking and quantitation of ion abundance (+2 to +6 charge-state ions)[55], (iv) Normalization on total protein abundance, (v) Import of sequence information, (vi) ANOVA test at peptide level and filtering for features $p < 0.05$, (vii) Calculation of protein abundance (sum of the volume of corresponding peptides), (viii) calculation of fold change (the fold change for each protein was calculated by dividing the average intensity value of a protein in each skin lesion group by the average intensity value of the same protein in normal skin samples), (ix) ANOVA test at protein level and filtering for features $p < 0.05$. Noticeably, only non-conflicting features and unique peptides were considered for calculation at

protein level. Quantitative data were considered for proteins quantified by a minimum of 2 peptides.

Targeted LC-MS metabolomics profiling analysis

Dry pellet of KHAT cell lines collected each from 10 cm petri dishes and subjected to metabolomic analysis. Of note, each sample was taken from a distinct petri dish, which was irradiated or not (nIr). Metabolites were extracted from cells using 400µL of cold extraction solvent (Acetonitrile:Methanol:MQ; 40:40:20) and subsequently, samples were vortexed for 2 minutes and sonicated for 1 minutes (settings: sweep mode, frequency 37, power 60, no heating), followed by centrifugation at 14000rpm at 4°C for 5 minutes. Supernatants were transferred into polypropylene tubes and placed into Nitrogen gas evaporator and dried samples were suspended with 40µL of extraction solvent (Acetonitrile:Methanol:MQ; 40:40:20) and vortexed for 2 minutes and transfer into HPLC glass auto sampler vials. 2µL of sample injected with Thermo Vanquish UHPLC coupled with Q-Exactive Orbitrap quadrupole mass spectrometer equipped with a heated electrospray ionization (H-ESI) source probe (Thermo Fischer Scientific). A SeQuant ZIC-pHILIC (2.1×100 mm, 5-µm particle) column (Merck) was used for chromatographic separation. The gradient elution was carried out with a flow rate of 0.100 ml/minutes with using 20mM ammonium hydrogen carbonate, adjusted to pH 9.4 with ammonium solution (25%) as mobile phase A and acetonitrile as mobile phase B. The gradient elution was initiated from 20% Mobile phase A and 80% of mobile phase B and maintain till 2min., followed by 20% Mobile phase A gradually increasing up to 80% till 17 min., then 80% to 20% Mobile phase A decrease in 17.1 min. and maintained up to 24 minutes. The column oven and auto-sampler temperatures were set to 40 ± 3 °C and 5 ± 3 °C, respectively. MS was equipped with a heated electrospray ionization (HESI) source using polarity switching and following setting: resolution of 35,000, the spray voltages: 4250 V for positive and 3250 V for negative mode, the sheath gas: 25 arbitrary units (AU), and the auxiliary gas: 15 AU, sweep gas flow 0, Capillary temperature: 275°C, S-lens RF level: 50.0. Instrument control operated with the Xcalibur 4.1.31.9 software (Thermo Fischer Scientific). The peak integration was done with the TraceFinder 4.1 software (Thermo Fischer Scientific) using confirmed retention times for 58 metabolites standardized with library kit MSMLS-1EA (Merck). The data quality was monitored throughout the run using pooled

QC sample prepared by pooling 5µL from each suspended samples and interspersed throughout the run as every 10th sample. The metabolite data was checked for peak quality (poor chromatograph), % RSD (20% cutoff) and carryover (20% cutoff).

Metabolomics data analysis

The data was analysed with Metaboanalyst 5.0 (https://www.metaboanalyst.ca). Missing variables were imputated using KNN_VAR. The values were normalised to Total Ion Count for combined positive + negative polarity (0.0 to 17 min, range 55-825 m/z), log-transformed and auto-scaled. Following statistical analysis were performed: Multivariate clustering analysis was computed for heatmap with distance measure using euclidean, and clustering algorithm using ward.D.

Measurement of lactate production and glucose consumption

To measure lactate production and glucose consumption, we used YSI 2950 Biochemistry Analyzer (YSI Life Sciences) which applies immobilized enzymes to catalyze the corresponding chemical reactions to measure the concentration of a specific metabolite. Briefly, cells were irradiated in 6 wells plates. Once irradiated 1mL of KSFM complete medium was added in each the well. At 5h and 24h, 200 µl of medium was taken and put in duplicate in a 96-well plate. The concentration of glucose, and lactate was evaluated in collected medium by YSI analyzer using fresh corresponding medium as a reference. Results were normalized with total protein level.

Oxygen consumption, extracellular acidification and mitochondrial complex-dependent respiration

A Seahorse XF94 Extracellular Flux Analyzer (Seahorse Bioscience) was used. Results were normalized with total protein level. The assay medium for measurement of glycolytic capacity was XF Base medium (Agilent) supplemented with penicillin (100 IU/mL) and streptomycin (100 mg/mL) adjusted to pH 7.4. The assay medium for respiration via each mitochondrial complex consisted in XF Base medium supplemented with D-glucose (10 mM), sodium pyruvate (1 mM), penicillin (100 IU/mL), and streptomycin (100 mg/mL) adjusted to pH 7.4. Four wells contained no cells to control for temperature-sensitive fluctuations in O_2 fluorophore emission. One

hour before monitoring, plates were incubated in a CO_2-free incubator at 37°C for 1 hour to allow temperature and pH equilibration. Microplates were then put into XF96 and allowed to equilibrate for 15 min prior to first measurement. XF assays consisted of 3 min mix, 3 min wait, and 2 min measurement cycles and were performed at 37°C as described elsewhere [56]. Using this protocol, it was possible to calculate an O_2 consumption rate every 8 min. Drugs of interest prepared in the requisite assay medium were preloaded into reagent delivery chambers A, B, C, and D at 10X,11X,12X, and 13X the final working concentration, respectively, and injected sequentially at intervals of 24 min as indicated. The substrates were added as indicated in the figures at the following final working concentrations for glycolytic capacity and OXPHOS capacity: oligomycin (10µM), glucose (20g/L), 2-DG (50mM), rotenone (10µM), antimycin A (10µM), digitonin (4 mM), succinate (25 mM), DNP (50µM). In each 96-well plate, each cell lines were put in 4 or 6 wells.

Respiration via each mitochondrial complex was also evaluated using digitonin-permeabilised cells in the presence of the proper substrates and inhibitors of the other complexes. CI-, CII, CIII and CIV-linked respirations were measured by evaluation of oxygen consumption rate after consecutive addition of following substrates: rotenone (1µM), succinate (100mM), antimycin A (10 µM), ascorbate (10mM) and TMPD (100 µM).

Western Blot procedure

Western blotting was performed as previously described[24]. Briefly, equal amounts of total protein were resolved by SDS–polyacrylamide gel electrophoresis (SDS–PAGE) and electrophoretically transferred to Nitocellulose membrane for AMPK and p-AMPK and PDVF membrane for OXPHOS. The membranes were then incubated overnight at 4 °C with primary antibodies (**Table 1**). After additional incubation with a 1:1000 dilution of an anti-immunoglobulin horseradish peroxidase-linked antibody (Vector Laboratories, Biovalley S.A., Marne la Vallée, France) for 1 h, blots were developed using the chemiluminescence ECL reagent (Biorad).

Number of mitochondria

The mtDNA/gDNA ratio was assessed by performing a real-time PCR using qRT-PCR Brilliant III SYBR Master Mix (Agilent) on a Bio-Rad Real-Time PCR equipment (Bio-Rad CFX 96 wells). Specific primers were used to amplify fragment of mtDNA and gDNA were as followed: mtDNA, forward primer (GATTTGGGTACCACCCAAGTATTG) and reverse primer (ATTATTCAATGGTGGCTGGCAGTA); gDNA, forward primer (AAGAGGAGAGTGGGAGTGATGA) and reverse primer (ACTGCTTGAAGAGCTTGAGCAT). The PCR reactions program was: 95°C for 10min; 40 cycles at 95°C for 15sec and 60°C for 30sec. The duplicate Cq was averaged. The mtDNA/gDNA ratio was calculated with the following ratio: mtCq/gCq.

Cell staining and confocal microscopy

Cells were plated in 12 wells plates on glass coverslip (thickness:1,5mm) and cultured in medium until they reach 60% confluency at the time of irradiation. After a 10 minutes fixation with 3,4% formaldehyde and a 10 minutes permeabilization with 0,1% Triton X-100, cells were saturated 30 minutes in a 5% Bovine Serum Albumin solution. TOM20 antibody (**Table 1**) was incubated overnight at 4°C. After washing three time with PBS buffer, cells were incubated with phalloidin-Atto 647N antibody for 1h, and DAPI. Images were acquired on a Leica DMI6000 TCS SP8X confocal inverted microscope with a 63X oil objective. Hardware and image acquisition were controlled with LAS X Life Science software. A z stack of seven images was collected and subjected to 2-D deconvolution to obtain a single in-focus field with out-of-focus information removed.

Mitochondrial Morphology analysis

Mitochondrial Morphology was assessed by Machine Deep learning (Mitosegnet) as described elsewhere[57]. Briefly, forty 3D confocal images of mitochondrial network were preprocessed for segmentation for each irradiation time point and each cell type condition. Pictures size was 1024*1024 with a pixel size between 80-83 nm. Data analysis was done with the associated MitoA software. We used Graphpad Prism with PCA analysis with each morphological parameter analysed for determine the most

relevant irradiation time for which mitochondrial network can be affected. The 2 largest eigenvalues were chosen for principal component.

Statistics

Comparisons between two groups were calculated using Student's t-test (two tailed) and a p-value < 0.05 (*) was considered significant. Results are presented as means +/- SEM. Comparisons between more than two groups were calculated with a one-way analysis of variance (ANOVA) followed by Bonferroni's multiple comparison tests if values followed the normality (Shapiro and Wilk test). If the normality wasn't followed, a non-parametric Krustal-Wallis test associated with a Dunn's multiple comparison tests were done. If two independent variables needed to be tested, a two-way ANOVA analysis of variance followed by a post hoc Bonferroni's tests were used. If the distribution didn't follow the normality, a Mixed-effect model followed by Bonferroni's test for multiple comparison were calculated. p-value < 0.05 was considered significant. Results are presented as means +/- SEM. PCA analyses were done using the GraphPad Prism software

Data availability

The authors declare that the data supporting the findings of this study are available within the paper and its Supplementary Information files. Additional data are available from the corresponding author upon reasonable request.

Acknowledgments

The authors wish to thank Véronique Guyonnet-Duperat (TBMCore, Plateforme de Vectorologie, University of Bordeaux), **Funding:** H.R.R gratefully acknowledges support from the Institut National du Cancer "INCa_2021-105", and "Société Française de Dermatologie (SFD). PM was supported by grant from "Aquitaine region" and "La Ligue contre le cancer". FIMM metabolomics unit was supported by HiLIFE and Biocenter Finland. **Competing interests:** The authors declare that they have no financial or non-financial conflict of interest.

References

1. Donaldson, M. R. & Coldiron, B. M. No End in Sight: The Skin Cancer Epidemic Continues. *Seminars in Cutaneous Medicine and Surgery* (2011) doi:10.1016/j.sder.2011.01.002.
2. Rogers, H. W., Weinstock, M. A., Feldman, S. R. & Coldiron, B. M. Incidence estimate of nonmelanoma skin cancer (keratinocyte carcinomas) in the us population, 2012. *JAMA Dermatology* (2015) doi:10.1001/jamadermatol.2015.1187.
3. Bouafia, A. *et al.* p53 Requires the Stress Sensor USF1 to Direct Appropriate Cell Fate Decision. *PLoS Genet.* (2014) doi:10.1371/journal.pgen.1004309.
4. Surova, O. & Zhivotovsky, B. Various modes of cell death induced by DNA damage. *Oncogene* (2013) doi:10.1038/onc.2012.556.
5. Hosseini, M., Ezzedine, K., Taieb, A. & Rezvani, H. R. Oxidative and energy metabolism as potential clues for clinical heterogeneity in nucleotide excision repair disorders. *Journal of Investigative Dermatology* (2015) doi:10.1038/jid.2014.365.
6. Alexander, A., Kim, J. & Walker, C. L. ATM engages the TSC2/mTORC1 signaling node to regulate autophagy. *Autophagy* (2010) doi:10.4161/auto.6.5.12509.
7. Fang, E. F. *et al.* Nuclear DNA damage signalling to mitochondria in ageing. *Nature Reviews Molecular Cell Biology* (2016) doi:10.1038/nrm.2016.14.
8. Liu, J., Zhang, C., Hu, W. & Feng, Z. Tumor suppressor p53 and its mutants in cancer metabolism. *Cancer Letters* (2015) doi:10.1016/j.canlet.2013.12.025.
9. Sanli, T., Steinberg, G. R., Singh, G. & Tsakiridis, T. AMP-activated protein kinase (AMPK) beyond metabolism: A novel genomic stress sensor participating in the DNA damage response pathway. *Cancer Biology and Therapy* (2014) doi:10.4161/cbt.26726.
10. Ji, C. *et al.* Exogenous cell-permeable C6 ceramide sensitizes multiple cancer cell lines to Doxorubicin-induced apoptosis by promoting AMPK activation and mTORC1 inhibition. *Oncogene* (2010) doi:10.1038/onc.2010.379.
11. Obacz, J., Pastorekova, S., Vojtesek, B. & Hrstka, R. Cross-talk between HIF and p53 as mediators of molecular responses to physiological and genotoxic stresses. *Molecular Cancer* (2013) doi:10.1186/1476-4598-12-93.
12. Mahfouf, W. *et al.* Loss of Epidermal HIF-1α Blocks UVB-Induced Tumorigenesis by Affecting DNA Repair Capacity and Oxidative Stress. *J. Invest. Dermatol.* **139**, 2016-2028.e7 (2019).
13. Rezvani, H. R. *et al.* Hypoxia-inducible factor-1α regulates the expression of nucleotide excision repair proteins in keratinocytes. *Nucleic Acids Res.* **38**, 797–809 (2010).
14. Rezvani, H. R. *et al.* Hypoxia-inducible factor-1α, a key factor in the keratinocyte response to UVB exposure. *J. Biol. Chem.* **282**, 16413–16422 (2007).
15. Hamanaka, R. B. & Chandel, N. S. Mitochondrial metabolism as a regulator of keratinocyte differentiation. *Cell. Logist.* (2013) doi:10.4161/cl.25456.
16. Hamanaka, R. B. *et al.* Mitochondrial reactive oxygen species promote epidermal differentiation and hair follicle development. *Sci. Signal.* (2013) doi:10.1126/scisignal.2003638.
17. Wong, W. J., Richardson, T., Seykora, J. T., Cotsarelis, G. & Simon, M. C. Hypoxia-inducible factors regulate filaggrin expression and epidermal barrier function. *J. Invest. Dermatol.* (2015) doi:10.1038/jid.2014.283.
18. Kloepper, J. E. *et al.* Mitochondrial function in murine skin epithelium is crucial for hair follicle morphogenesis and epithelial-mesenchymal interactions. *J. Invest. Dermatol.* (2015) doi:10.1038/jid.2014.475.
19. Baris, O. R. *et al.* The mitochondrial electron transport chain is dispensable for proliferation and differentiation of epidermal progenitor cells. *Stem Cells* (2011) doi:10.1002/stem.695.
20. Rezvani, H. R. *et al.* Loss of epidermal hypoxia-inducible factor-1α accelerates epidermal aging and affects re-epithelialization in human and mouse. *J. Cell Sci.*

(2011) doi:10.1242/jcs.082370.
21. Tondera, D. *et al.* SLP-2 is required for stress-induced mitochondrial hyperfusion. *EMBO J.* **28**, 1589–1600 (2009).
22. Rolland, S. G. *et al.* Impaired complex IV activity in response to loss of LRPPRC function can be compensated by mitochondrial hyperfusion. *Proc. Natl. Acad. Sci. U. S. A.* (2013) doi:10.1073/pnas.1303872110.
23. Wai, T. & Langer, T. Mitochondrial Dynamics and Metabolic Regulation. *Trends in Endocrinology and Metabolism* (2016) doi:10.1016/j.tem.2015.12.001.
24. Rezvani, H. R. *et al.* XPC silencing in normal human keratinocytes triggers metabolic alterations that drive the formation of squamous cell carcinomas. *J. Clin. Invest.* (2011) doi:10.1172/JCI40087.
25. Pernas, L. & Scorrano, L. Mito-Morphosis: Mitochondrial Fusion, Fission, and Cristae Remodeling as Key Mediators of Cellular Function. *Annual Review of Physiology* (2016) doi:10.1146/annurev-physiol-021115-105011.
26. Essen, L. O. & Klar, T. Light-driven DNA repair by photolyases. *Cellular and Molecular Life Sciences* (2006) doi:10.1007/s00018-005-5447-y.
27. Sancar, G. B. & Sancar, A. Purification and Characterization of DNA Photolyases. *Methods in Enzymology* (2006) doi:10.1016/S0076-6879(06)08009-8.
28. Cucchi, D., Gibson, A. & Martin, S. a. The emerging relationship between metabolism and DNA repair. *Cell Cycle* (2021) doi:10.1080/15384101.2021.1912889.
29. Hosseini, M., Kasraian, Z. & Rezvani, H. R. Energy metabolism in skin cancers: A therapeutic perspective. *Biochim. Biophys. Acta - Bioenerg.* **1858**, 712–722 (2017).
30. Kaniak-Golik, A. & Skoneczna, A. Mitochondria-nucleus network for genome stability. *Free Radical Biology and Medicine* (2015) doi:10.1016/j.freeradbiomed.2015.01.013.
31. Hegedűs, C. *et al.* Cyclobutane pyrimidine dimers from UVB exposure induce a hypermetabolic state in keratinocytes via mitochondrial oxidative stress. *Redox Biol.* **38**, 101808 (2021).
32. Hegedűs, C. *et al.* PARP1 inhibition augments UVB-mediated mitochondrial changes—implications for UV-induced DNA repair and photocarcinogenesis. *Cancers (Basel).* (2020) doi:10.3390/cancers12010005.
33. Gasch, A. P. *et al.* Genomic expression responses to DNA-damaging agents and the regulatory role of the yeast ATR Homolog Mec1p. *Mol. Biol. Cell* (2001) doi:10.1091/mbc.12.10.2987.
34. Jaehnig, E. J., Kuo, D., Hombauer, H., Ideker, T. G. & Kolodner, R. D. Checkpoint Kinases Regulate a Global Network of Transcription Factors in Response to DNA Damage. *Cell Rep.* (2013) doi:10.1016/j.celrep.2013.05.041.
35. Bu, P. *et al.* DNA damage response activates respiration and thereby enlarges dNTP pools to promote cell survival in budding yeast. *J. Biol. Chem.* (2019) doi:10.1074/jbc.RA118.007266.
36. Qin, L. *et al.* CDK1 Enhances Mitochondrial Bioenergetics for Radiation-Induced DNA Repair. *Cell Rep.* (2015) doi:10.1016/j.celrep.2015.11.015.
37. Bai, P., Nagy, L., Fodor, T., Liaudet, L. & Pacher, P. Poly(ADP-ribose) polymerases as modulators of mitochondrial activity. *Trends in Endocrinology and Metabolism* (2015) doi:10.1016/j.tem.2014.11.003.
38. Dawson, T. M. & Dawson, V. L. Mitochondrial mechanisms of neuronal cell death: Potential the rapeutics. *Annu. Rev. Pharmacol. Toxicol.* **57**, 437–454 (2017).
39. Smolková, K. *et al.* Waves of gene regulation suppress and then restore oxidative phosphorylation in cancer cells. *Int. J. Biochem. Cell Biol.* (2011) doi:10.1016/j.biocel.2010.05.003.
40. Ward, P. S. & Thompson, C. B. Metabolic Reprogramming: A Cancer Hallmark Even Warburg Did Not Anticipate. *Cancer Cell* (2012) doi:10.1016/j.ccr.2012.02.014.
41. Wise, D. R. *et al.* Myc regulates a transcriptional program that stimulates mitochondrial glutaminolysis and leads to glutamine addiction. *Proc. Natl. Acad. Sci. U. S. A.* (2008) doi:10.1073/pnas.0810199105.
42. DeBerardinis, R. J. *et al.* Beyond aerobic glycolysis: Transformed cells can engage in

glutamine metabolism that exceeds the requirement for protein and nucleotide synthesis. *Proc. Natl. Acad. Sci. U. S. A.* (2007) doi:10.1073/pnas.0709747104.
43. Jose, C., Bellance, N. & Rossignol, R. Choosing between glycolysis and oxidative phosphorylation: A tumor's dilemma? *Biochimica et Biophysica Acta - Bioenergetics* (2011) doi:10.1016/j.bbabio.2010.10.012.
44. Galluzzi, L., Kepp, O., Heiden, M. G. V. & Kroemer, G. Metabolic targets for cancer therapy. *Nat. Rev. Drug Discov.* **12**, 829–846 (2013).
45. Yakes, F. M. & Van Houten, B. Mitochondrial DNA damage is more extensive and persists longer than nuclear DNA damage in human cells following oxidative stress. *Proc. Natl. Acad. Sci. U. S. A.* (1997) doi:10.1073/pnas.94.2.514.
46. Kawamura, K., Qi, F. & Kobayashi, J. Potential relationship between the biological effects of low-dose irradiation and mitochondrial ROS production. *Journal of Radiation Research* (2018) doi:10.1093/jrr/rrx091.
47. Shiga, M. *et al.* Characteristic phenotype of immortalized periodontal cells isolated from a Marfan syndrome type I patient\rAssessing ageing of individual T lymphocytes: Mission impossible?\rFacile Synthesis of Naphthoquinone Spiroketals by Diastereoselective Oxidative [3. *Cell Tissue Res* (2007).
48. Emadi, A. *et al.* Inhibition of glutaminase selectively suppresses the growth of primary acute myeloid leukemia cells with IDH mutations. *Exp. Hematol.* (2014) doi:10.1016/j.exphem.2013.12.001.
49. Seltzer, M. J. *et al.* Inhibition of glutaminase preferentially slows growth of glioma cells with mutant IDH1. *Cancer Res.* (2010) doi:10.1158/0008-5472.CAN-10-1666.
50. Amoedo, N. D. *et al.* Targeting the mitochondrial trifunctional protein restrains tumor growth in oxidative lung carcinomas. *J. Clin. Invest.* (2021) doi:10.1172/JCI133081.
51. Rezvani, H. R. *et al.* Protective effects of catalase overexpression on UVB-induced apoptosis in normal human keratinocytes. *J. Biol. Chem.* (2006) doi:10.1074/jbc.M600536200.
52. Hosseini, M. *et al.* Energy Metabolism Rewiring Precedes UVB-Induced Primary Skin Tumor Formation. *Cell Rep.* **23**, 3621–3634 (2018).
53. Steurer, B. *et al.* Fluorescently-labelled CPD and 6-4PP photolyases: New tools for live-cell DNA damage quantification and laser-assisted repair. *Nucleic Acids Res.* (2019) doi:10.1093/nar/gkz035.
54. Käll, L., Canterbury, J. D., Weston, J., Noble, W. S. & MacCoss, M. J. Semi-supervised learning for peptide identification from shotgun proteomics datasets. *Nat. Methods* (2007) doi:10.1038/nmeth1113.
55. Chelius, D. & Bondarenko, P. V. Quantitative profiling of proteins in complex mixtures using liquid chromatography and mass spectrometry. *J. Proteome Res.* (2002) doi:10.1021/pr025517j.
56. Wu, M. *et al.* Multiparameter metabolic analysis reveals a close link between attenuated mitochondrial bioenergetic function and enhanced glycolysis dependency in human tumor cells. *Am. J. Physiol. - Cell Physiol.* (2007) doi:10.1152/ajpcell.00247.2006.
57. Fischer, C. A. *et al.* MitoSegNet: Easy-to-use Deep Learning Segmentation for Analyzing Mitochondrial Morphology. *iScience* (2020) doi:10.1016/j.isci.2020.101601.

Table 1. List of antibodies used in this study.

Protein	Reference	Dilution
B-Actine	**A2228 - Sigma**	**1/5000**
Tubulin	**ab7291**	**1/5000**
OXPHOS tot	**ab110411**	**1/500**
Fis-1	**Sc-376469**	**1/500**
p-AMPK	**Sc101630**	**1/1000**
AMPK	**Sc25792**	**1/1000**
LC3B	**Cell-Signaling - 38685**	**1/1000**
Cleaved Caspase-3	**Cell-Signaling- 9664L**	**1/1000**
TOM20	**Sc-17764**	**1/100**
ATTO 647N	**Invitrogen- 50135**	**1/500**

Figure legends

Figure 1. Quantitative proteomic analyses reveal biphasic variations in the activities of several signaling pathways following UVB irradiation.

A) Cyclopyrimidine dimer (CPD) levels were quantified in KHAT cell line by immuno-dot blot analysis at different time points after irradiation

B) AMPK, cleaved caspase-3 and LC3 expression levels were analyzed by western blot. β-actin was used as a loading control.

C) Ctrl, Nu-PL and Mt-PL keratinocytes were exposed to acute UVB irradiation. Cells were then harvested at indicated time points after UV treatment and subjected to label free quantitative proteome analysis. Heatmap of z-score for activated canonical pathways at different hours after acute irradiation, n=3 per condition. The color indicates canonical pathway activation z-score values; blue: downregulation and red: upregulation.

Nu-PL: keratinocytes expressing nuclear CPD photolyase, Mt-PL: keratinocytes expressing mitochondrial CPD photolyase.

Figure 2. Rapid repair of nuclear and mitochondrial CPDs affects critically the expression patterns of proteins involved in glycolysis, TCA cycle and OXPHOS

A-C) Proteomic analysis was used to investigate the effects of acute UVB irradiation on profile expressions of proteins involved in energy metabolism. Heatmap show fold change expression levels of proteins involved glycolysis (**A**), TCA cycle (**B**) and OXPHOS (**C**) at indicated time points after acute irradiation for Ctrl, Nu-PL and Mt-PL cells. n=3 per condition. The color indicates fold change expression level; green: low expression, red: high expression, blue: predicted downregulation, brown: predicted upregulation.

D) Analysis of Gene Set Enrichment comparing 2h-postirradiated cells with non-irradiated cells showed that the metabolic disease are among the top 16 enriched Gene Ontology (GO) terms for diseases and biological functions.

Figure 3. UVB irradiation triggers a biphasic variation in the abundances of metabolites, which is partially dependent on nuclear CPDs

A) Ctrl, Nu-PL and Mt-PL keratinocytes were exposed to acute UVB irradiation. Cells were then harvested at indicated time points after UV treatment and subjected to

metabolomics. Heatmap showing the differential abundances of indicated metabolites at different time points after acute UVB irradiation in Ctrl, Nu-PL and Mt-PL cells. n=3 per condition. The colors indicate lwo (blue) and high (red) metabolite abundance.
B) PCA plot show differential variation patterns of metabolites following irradiations.
C-J) Relative abundances of palmitate (**C**), mystiric acid (**D**), glutamine (**E**), glutamate (**F**), malate (**G**), fumarate (**H**), pyruvate (**I**) and nicotinamide (NAM) (**J**) were compared at different time points after UVB irradiation in control, Nu-PL and Mt-PL cells.
*P< 0.05, **<0.01 and **** p<0.0001 for irradiated versus respective non-irradiated cells.

Figure 4. OXPHOS is upregulated at 24h after acute UVB irradiation
A-B) The glucose uptake and lactate production by irradiated (Ir) and nonirradaited (nIr) keratinocytes were measured. Ir cells exhibit lower glucose consumption than nIr cells at 5h and 24h after irradiation. P-values were obtained by t-test for 5h and Wilcoxon test for 24h. n=3 (**A**). No difference was observed in lactate production between nIr and Ir at 5h and 24h. P-values were obtained by t-test. n=3 (**B**).
C-H) Extracellular acidification (ECAR), Oxygen consumption rate (OCR) and mitochondrial complex-linked respiration were measured. $3 \leq n \leq 7$ [C-H] and significant P-values (< 0.05) from Mixed-effect model [**C-D**], ANOVA-One way [**E-G**], and Krustal Wallis test with $3 \leq n \leq 7$ [**H**].
I) Representative western blot showing the five proteins involved in OXPHOS (ATP5A, ATP synthase alpha subunit; UQCR2, ubiquinol-cytochrome c reductase core protein II; SDHB, succinate dehydrogenase complex iron sulfur subunit B; COXII, cytochrome c oxidase II; NDUFB8, NADH:ubiquinone oxidoreductase subunit B8. β-Actin was used as a loading control.

Figure 5. Dynamic modifications in mitochondrial morphology features after UVB irradiation
A) ADNmt/ADNg ratio was assessed by qPCR. p-value from ANOVA-One way. n=3.
B) Schematic representation of image processing by MitoSegNet for quantitative analyses with MitoA software. Mitochondria imaged by confocal microscopy were subjected to image processing that involved 2D deconvolution, morphological transformation, intensity thresholding, and object quantification. Phalloidin labeled in green was used to determine the thresholding boundaries for each individual cell.

C) Representative images showing mitochondrial network features at indicated time points after irradiation.

D) PCA plot comparing mitochondrial morphology features (including solidity, eccentricity, major and minor axis length, area and perimeter) among non-irradiated (nIr) and irradiated (Ir) cells at 5h, 9h and 24h post-irradiation.

E) Mitochondrial morphology features were compared between non-irradiated and 9h post-irradiation conditions.

F) Representative western blot showing Fis-1 expression levels at indicated time points after UVB irradiation. Tubulin was used as a loading control.

Figure 6. The effects of increased nuclear and mitochondrial CPD on the patterns of OCR level variations and dynamic of mitochondrial morphology modifications following UVB irradiation

A-B) CPD levels were quantified in Nu-PL and Mt-PL cells at indicated time points after irradiation by immuno-dot blot analysis. SYBR green was used as loading control.

C-D) OCR was measured in Nu-PL (**C**) and Mt-PL (**D**) cells at different time points after irradiation. p-values were calculated by Mixed-effect model. n=4.

E-F) PCA plot comparing mitochondrial morphology features (including solidity, eccentricity, major and minor axis length, area and perimeter) among non-irradiated (nIr) and irradiated cells at 5h, 9h and 24h post-irradiation in both Nu-PL (**E**) and Mt-PL (**F**) cells.

G-H) Mitochondrial morphology features were compared between non-irradiated and 9h post-irradiation conditions in Nu-PL (**G**) and Mt-PL (**H**) cells.

Supplemental Data

Figure S1. KHAT cells are able to form a fully stratified epidermis

A-B) Epidermis reconstructed with KHAT (**A**) and KHAT+melanocyte (**B**). Architectures of epidermis were evaluated with H&E staining. Differentiation status of epidermis were assessed using immunofluorescence staining of K10. The nuclei were marked in blue with DAPI. Proper positioning of melanocytes in basal layer was evaluated with melan-A and TRP1 staining.

C) KHAT were irradiated with various doses of UVB light. Cell viability was determined using the propidium iodide (PI) exclusion assay 24h after irradiation. Data are mean±SD of three independent experiments.

Figure S2. Quantitative proteomic analyses reveal biphasic variations in the activities of several signaling pathways following UVB irradiation in HaCat cell line.

A) Cyclopyrimidine dimer (CPD) levels were quantified in HaCat cell line by immuno-dot blot analysis at different time points after irradiation.

B) HaCat cells were exposed to acute UVB irradiation, harvested at indicated time points after UV treatment and subjected to label free quantitative proteome analysis. Heatmap of z-score for activated canonical pathways at different hours after acute irradiation, n=3 per condition. The color indicates canonical pathway activation z-score values; blue: downregulation and red: upregulation.

C) Heatmap show fold change expression levels of proteins involved in OXPHOS at indicated time points after acute irradiation. n=3 per condition. The color indicates fold change expression level; green: low expression, red: high expression, blue: predicted downregulation, brown: predicted upregulation.

D) Representative western blot showing the five proteins involved in OXPHOS (ATP5A, ATP synthase alpha subunit; UQCR2, ubiquinol-cytochrome c reductase core protein II; SDHB, succinate dehydrogenase complex iron sulfur subunit B; COXII, cytochrome c oxidase II; NDUFB8, NADH:ubiquinone oxidoreductase subunit B8. GAPDH was used as a loading control.

E) Oxygen consumption rate (OCR) were measured at indicated time points after irradiation in HaCat cells.

Figure S3. Increased glycolytic capacity of KHAT at 24h after irradiation

A) Schematic representation of ECAR kinetics in cell response to glucose, oligomycin and 2-DG.

B-E) Basal OCR (**B**), glycolysis (**C**), glycolytic capacity (**D**) and glycolytic reserves (**E**) of KHAT at different times after irradiation were measured. One way ANOVA was used as statistic test and p-values < 0.05 were considred as significant. $3 \leq n \leq 6$.

Figure S4. Morphological features of mitochondrial network in irradiated keratinocytes are prominently different from non-irradiated cells

Plots show the mutual correlation between two features.

Figure S5. Keratinocytes were transduced efficiently with Nu-PL and Mt-PL

KHAT were transduced with lentiviral vectors expression either nuclear or mitochondrial photolyases coupled with a mCherry (Nu-PL and Mt-PL, respectively). Immunofluorescence analyses showed efficiency of transduction and their appropriate localization.

Figure S6. CPD removal from mtDNA abolishes UVB-induced upregulation of mitochondrial respiration.

Keratinocytes expressing Nu-PL and Mt-PL were exposed to acute UVB irradiation. (**A-B**) ECAR levels were measured in Nu-PL (**A**) and Mt-PL (**B**) cells in non-irradiated and 24h postirradiation conditions. Mixed-effect model was used and p-values < 0.05 were considered as significant. n=4

(**C-F**) Mitochondrial complex-linked respirations were measured in non-irradiated and 24h postirradiation conditions. t-test was used as statistical test and p-values < 0.05 were considered as significant. n=4

G) Representative western blot showing the five OXPHOS proteins. β-actin was used as loading control.

H-K) Mitochondrial complex-linked respirations were measured in Mt-PL cells. No significant difference was observed in complexes activities. t-test was used as statistical test and p-values < 0.05 were considered as significant. n=4

Figure 1.

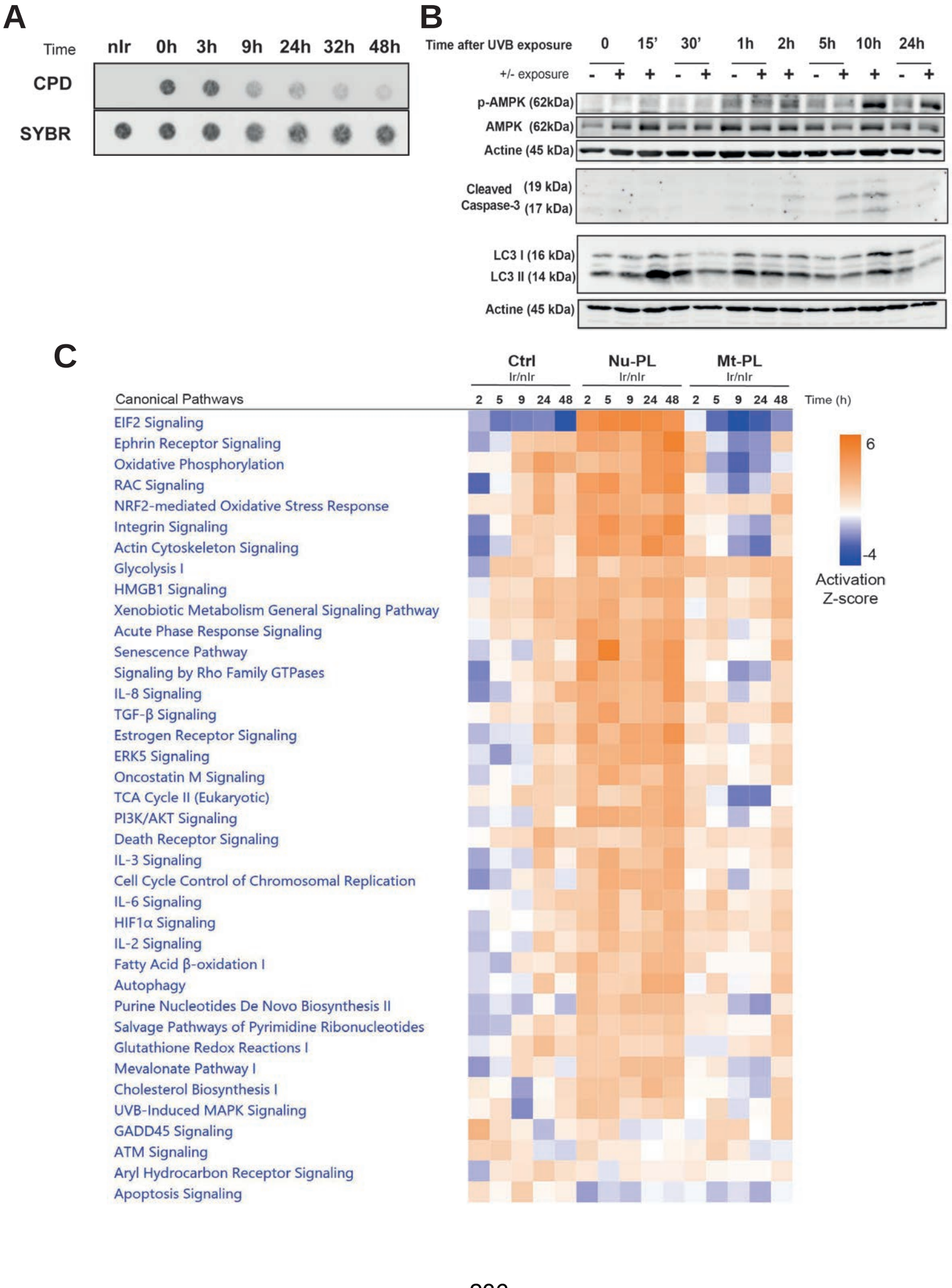
A
Time
nIr
0h
3h
9h
24h
32h
48h
CPD
SYBR
B
Time after UVB exposure
0
15'
30'
1h
2h
5h
10h
24h
+/- exposure
p-AMPK (62kDa)
AMPK (62kDa)
Actine (45 kDa)
Cleaved Caspase-3
(19 kDa)
(17 kDa)
LC3 I (16 kDa)
LC3 II (14 kDa)
Actine (45 kDa)
C
Ctrl
Ir/nIr
Nu-PL
Ir/nIr
Mt-PL
Ir/nIr
Canonical Pathways
2 5 9 24 48 2 5 9 24 48 2 5 9 24 48
Time (h)
EIF2 Signaling
Ephrin Receptor Signaling
Oxidative Phosphorylation
RAC Signaling
NRF2-mediated Oxidative Stress Response
Integrin Signaling
Actin Cytoskeleton Signaling
Glycolysis I
HMGB1 Signaling
Xenobiotic Metabolism General Signaling Pathway
Acute Phase Response Signaling
Senescence Pathway
Signaling by Rho Family GTPases
IL-8 Signaling
TGF-β Signaling
Estrogen Receptor Signaling
ERK5 Signaling
Oncostatin M Signaling
TCA Cycle II (Eukaryotic)
PI3K/AKT Signaling
Death Receptor Signaling
IL-3 Signaling
Cell Cycle Control of Chromosomal Replication
IL-6 Signaling
HIF1α Signaling
IL-2 Signaling
Fatty Acid β-oxidation I
Autophagy
Purine Nucleotides De Novo Biosynthesis II
Salvage Pathways of Pyrimidine Ribonucleotides
Glutathione Redox Reactions I
Mevalonate Pathway I
Cholesterol Biosynthesis I
UVB-Induced MAPK Signaling
GADD45 Signaling
ATM Signaling
Aryl Hydrocarbon Receptor Signaling
Apoptosis Signaling
6
-4
Activation Z-score

Figure 2.

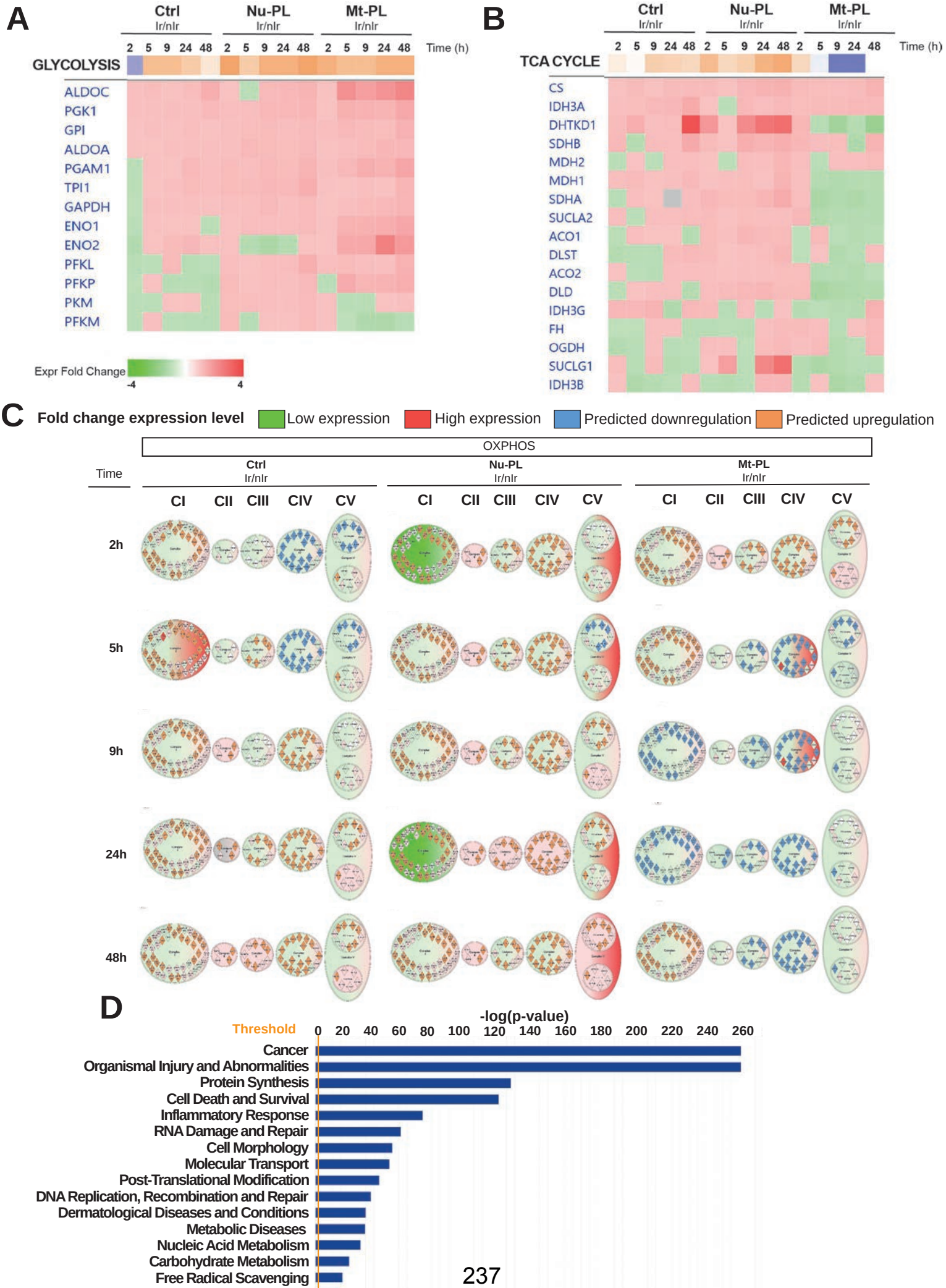
A
Ctrl
lr/nlr
Nu-PL
lr/nlr
Mt-PL
lr/nlr
2 5 9 24 48 2 5 9 24 48 2 5 9 24 48
Time (h)
GLYCOLYSIS
ALDOC
PGK1
GPI
ALDOA
PGAM1
TPI1
GAPDH
ENO1
ENO2
PFKL
PFKP
PKM
PFKM
Expr Fold Change
-4
4
B
Ctrl
lr/nlr
Nu-PL
lr/nlr
Mt-PL
lr/nlr
2 5 9 24 48 2 5 9 24 48 2 5 9 24 48
Time (h)
TCA CYCLE
CS
IDH3A
DHTKD1
SDHB
MDH2
MDH1
SDHA
SUCLA2
ACO1
DLST
ACO2
DLD
IDH3G
FH
OGDH
SUCLG1
IDH3B
C
Fold change expression level
Low expression
High expression
Predicted downregulation
Predicted upregulation
OXPHOS
Time
Ctrl
lr/nlr
Nu-PL
lr/nlr
Mt-PL
lr/nlr
CI CII CIII CIV CV
2h
5h
9h
24h
48h
D
-log(p-value)
Threshold
0 20 40 60 80 100 120 140 160 180 200 220 240 260
Cancer
Organismal Injury and Abnormalities
Protein Synthesis
Cell Death and Survival
Inflammatory Response
RNA Damage and Repair
Cell Morphology
Molecular Transport
Post-Translational Modification
DNA Replication, Recombination and Repair
Dermatological Diseases and Conditions
Metabolic Diseases
Nucleic Acid Metabolism
Carbohydrate Metabolism
Free Radical Scavenging
Lipid Metabolism

Figure 3.

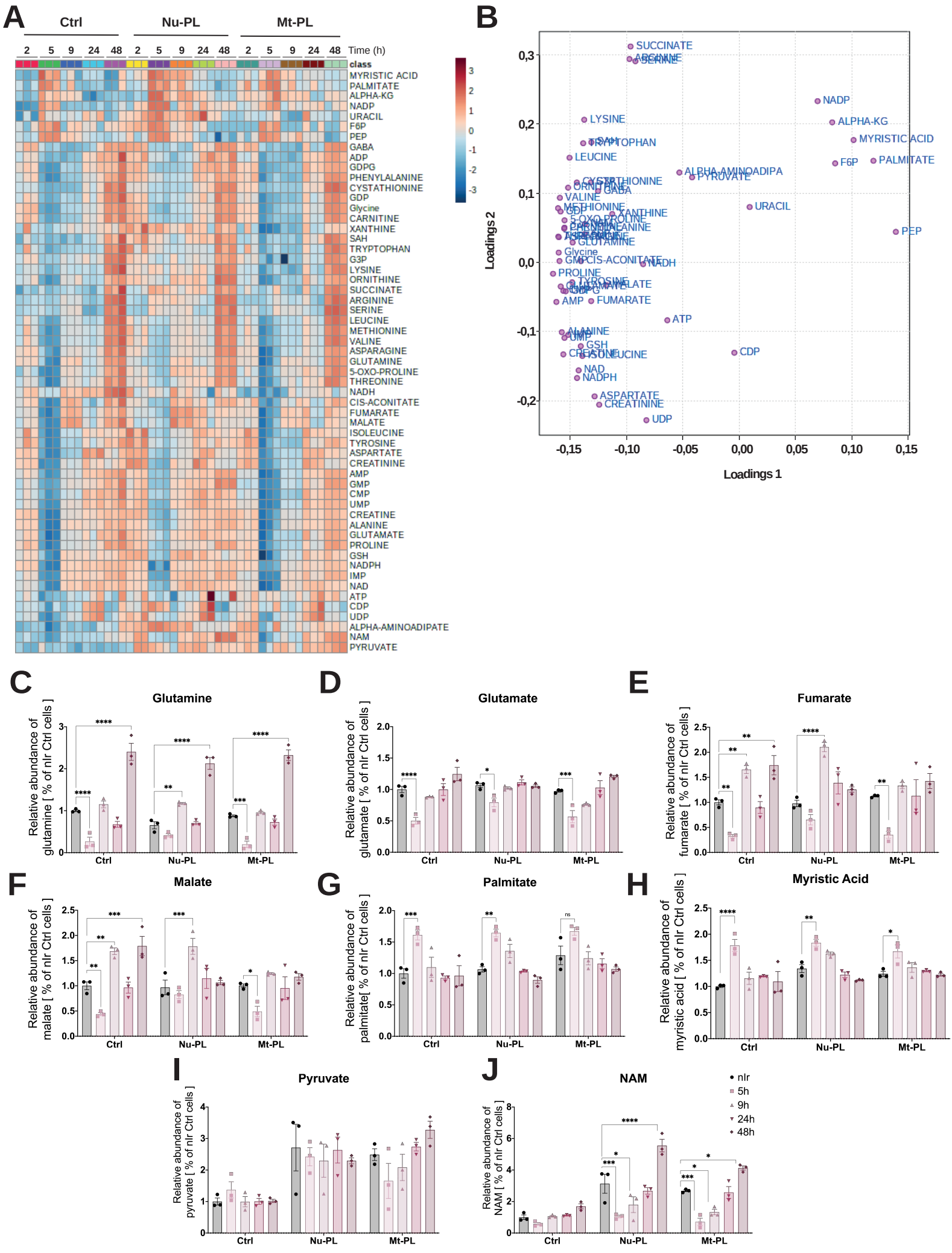
A
Ctrl
Nu-PL
Mt-PL
Time (h)
class
MYRISTIC ACID
PALMITATE
ALPHA-KG
NADP
URACIL
F6P
PEP
GABA
ADP
GDPG
PHENYLALANINE
CYSTATHIONINE
GDP
Glycine
CARNITINE
XANTHINE
SAH
TRYPTOPHAN
G3P
LYSINE
ORNITHINE
SUCCINATE
ARGININE
SERINE
LEUCINE
METHIONINE
VALINE
ASPARAGINE
GLUTAMINE
5-OXO-PROLINE
THREONINE
NADH
CIS-ACONITATE
FUMARATE
MALATE
ISOLEUCINE
TYROSINE
ASPARTATE
CREATININE
AMP
GMP
CMP
UMP
CREATINE
ALANINE
GLUTAMATE
PROLINE
GSH
NADPH
IMP
NAD
ATP
CDP
UDP
ALPHA-AMINOADIPATE
NAM
PYRUVATE
B
Loadings 2
Loadings 1
SUCCINATE
NADP
LYSINE
ALPHA-KG
MYRISTIC ACID
TRYPTOPHAN
LEUCINE
F6P
PALMITATE
ALPHA-AMINOADIPA
PYRUVATE
VALINE
URACIL
METHIONINE
PEP
Glycine
NADH
PROLINE
AMP
FUMARATE
ATP
CDP
NAD
NADPH
ASPARTATE
CREATININE
UDP
C
Glutamine
Relative abundance of glutamine [% of nlr Ctrl cells]
D
Glutamate
Relative abundance of glutamate [% of nlr Ctrl cells]
E
Fumarate
Relative abundance of fumarate [% of nlr Ctrl cells]
F
Malate
Relative abundance of malate [% of nlr Ctrl cells]
G
Palmitate
Relative abundance of palmitate[% of nlr Ctrl cells]
H
Myristic Acid
Relative abundance of myristic acid [% of nlr Ctrl cells]
I
Pyruvate
Relative abundance of pyruvate [% of nlr Ctrl cells]
J
NAM
Relative abundance of NAM [% of nlr Ctrl cells]
nlr
5h
9h
24h
48h
Ctrl
Nu-PL
Mt-PL

Figure 4.

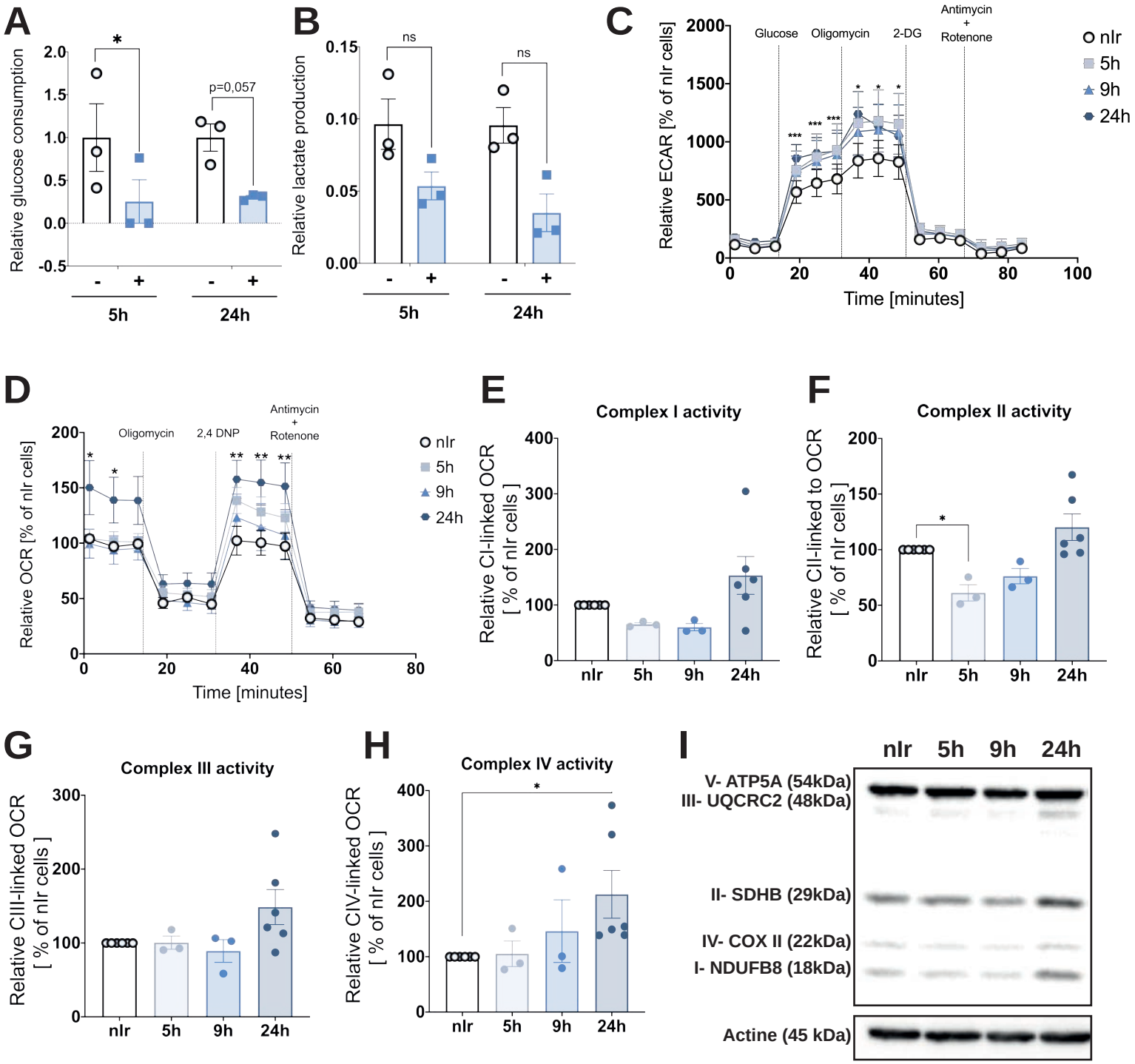
A
Relative glucose consumption
p=0,057
5h
24h
B
Relative lactate production
ns
ns
5h
24h
C
Relative ECAR [% of nlr cells]
Glucose
Oligomycin
2-DG
Antimycin + Rotenone
Time [minutes]
nlr
5h
9h
24h
D
Relative OCR [% of nlr cells]
Oligomycin
2,4 DNP
Antimycin + Rotenone
Time [minutes]
E
Complex I activity
Relative CI-linked OCR [% of nlr cells]
F
Complex II activity
Relative CII-linked to OCR [% of nlr cells]
G
Complex III activity
Relative CIII-linked OCR [% of nlr cells]
H
Complex IV activity
Relative CIV-linked OCR [% of nlr cells]
I
nlr
5h
9h
24h
V- ATP5A (54kDa)
III- UQCRC2 (48kDa)
II- SDHB (29kDa)
IV- COX II (22kDa)
I- NDUFB8 (18kDa)
Actine (45 kDa)

Figure 5.

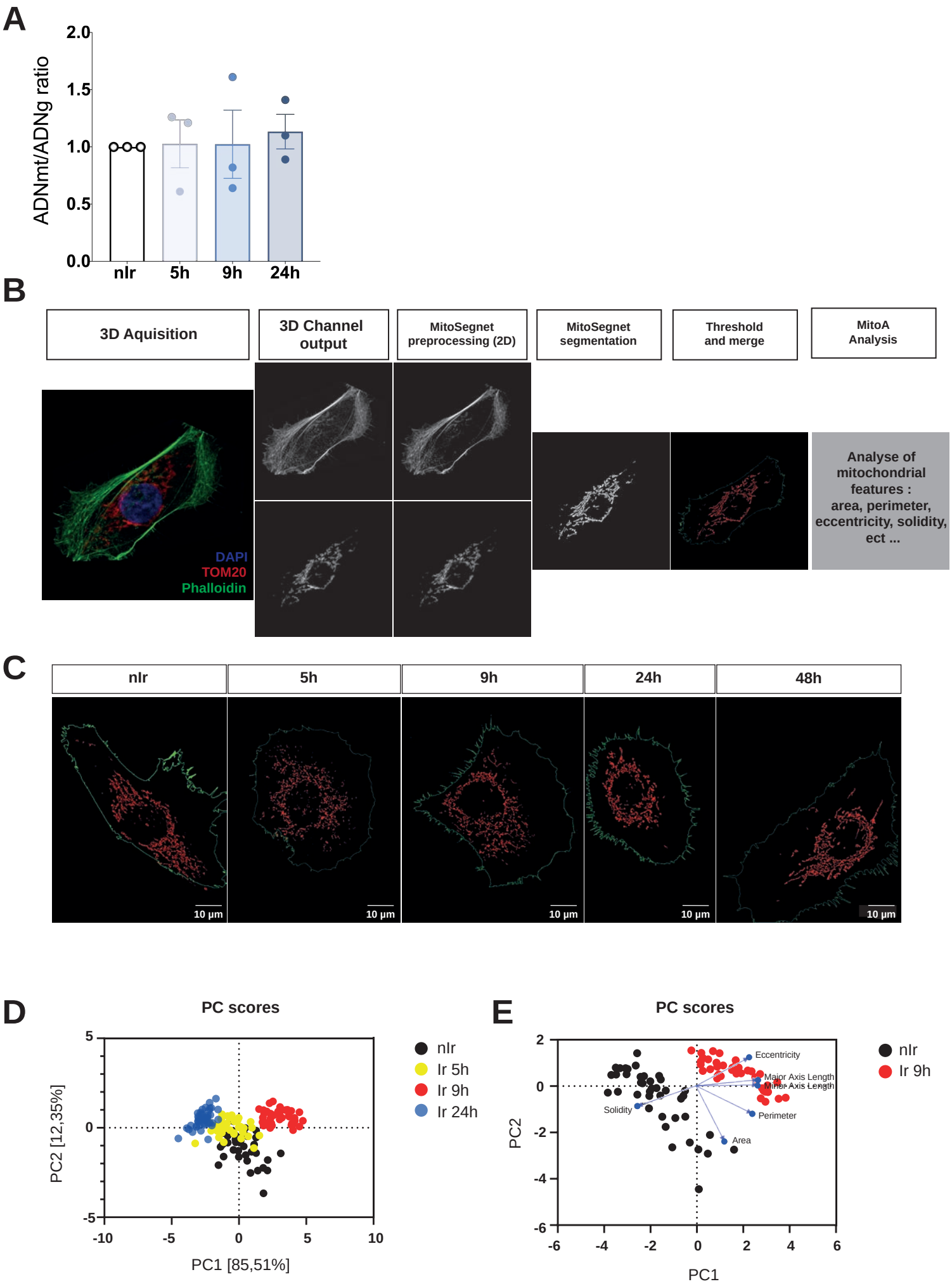
A
ADNmt/ADNg ratio
2.0
1.5
1.0
0.5
0.0
nlr
5h
9h
24h
B
3D Aquisition
3D Channel output
MitoSegnet preprocessing (2D)
MitoSegnet segmentation
Threshold and merge
MitoA Analysis
DAPI
TOM20
Phalloidin
Analyse of mitochondrial features : area, perimeter, eccentricity, solidity, ect ...
C
nlr
5h
9h
24h
48h
10 µm
D
PC scores
PC2 [12,35%]
PC1 [85,51%]
nlr
Ir 5h
Ir 9h
Ir 24h
E
PC scores
PC2
PC1
Eccentricity
Major Axis Length
Minor Axis Length
Solidity
Perimeter
Area
nlr
Ir 9h

0,85

Figure 5.

F

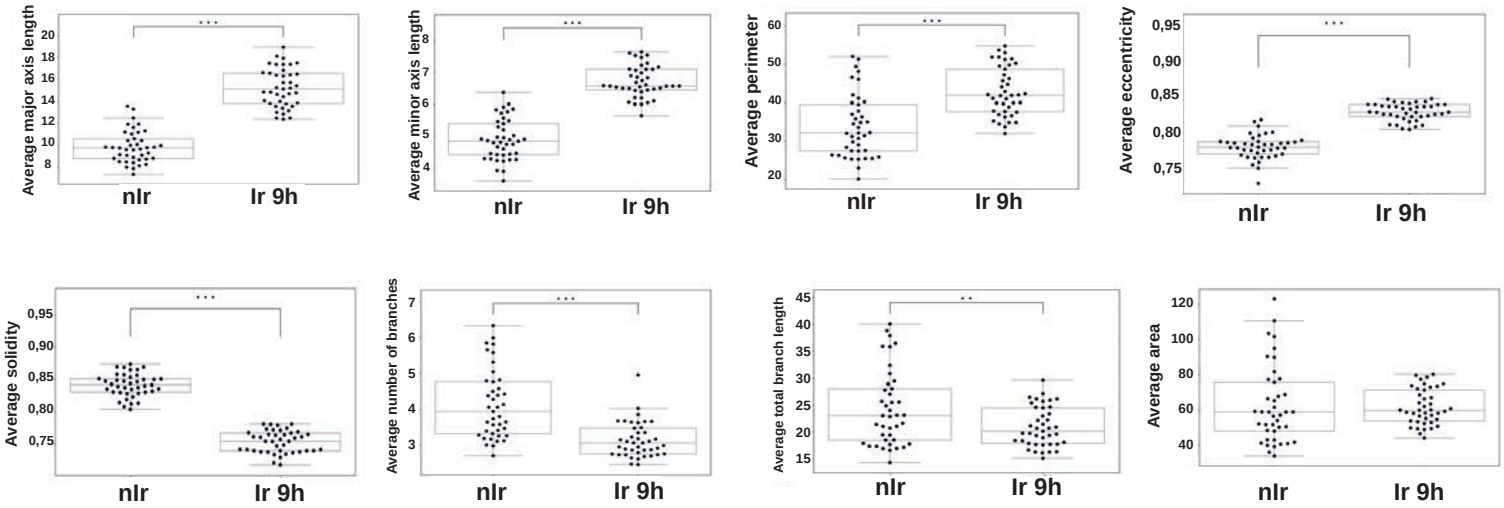

G

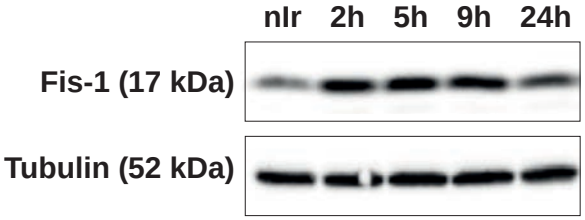

Figure 6.

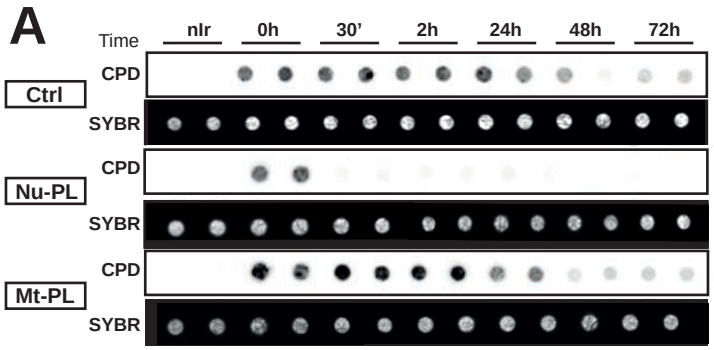

B

CPD immuno-dot blot in Mt-PL cells

in progress

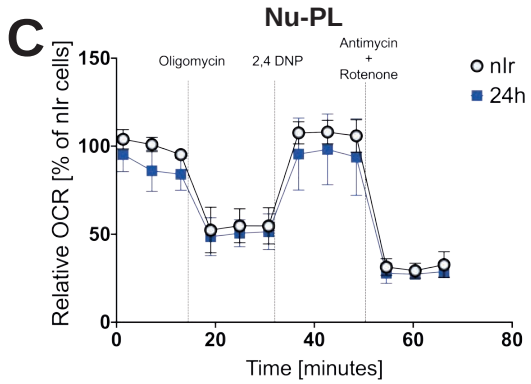

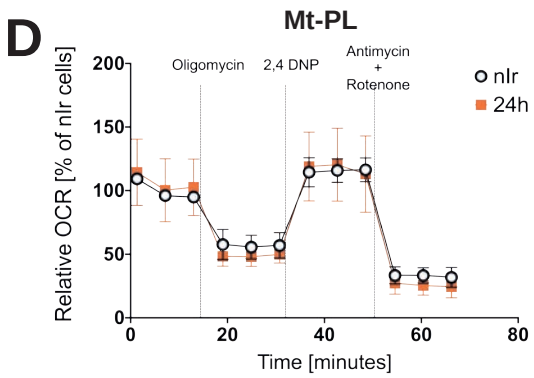

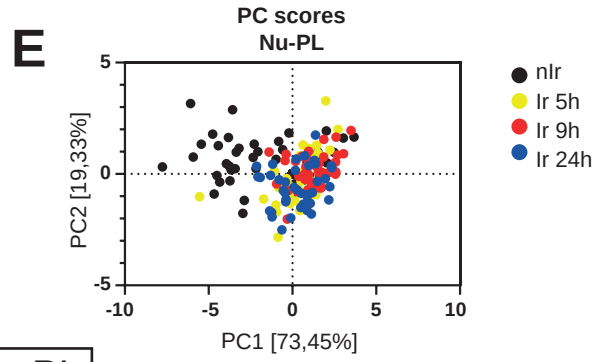

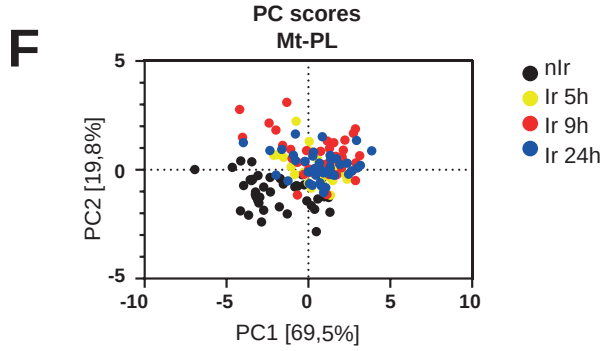

G Nu-PL

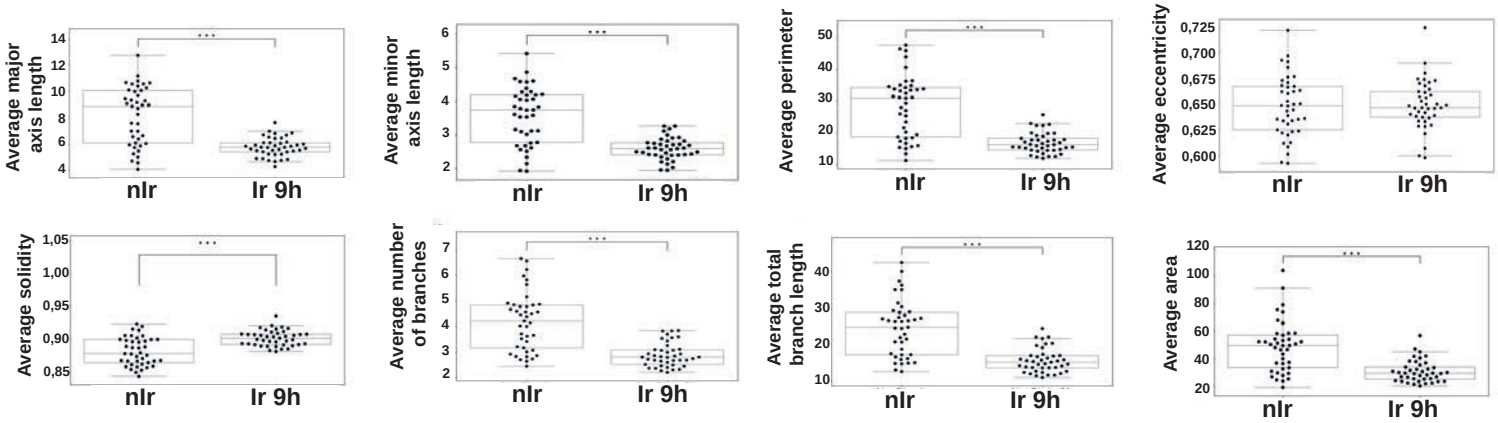

H Mt-PL

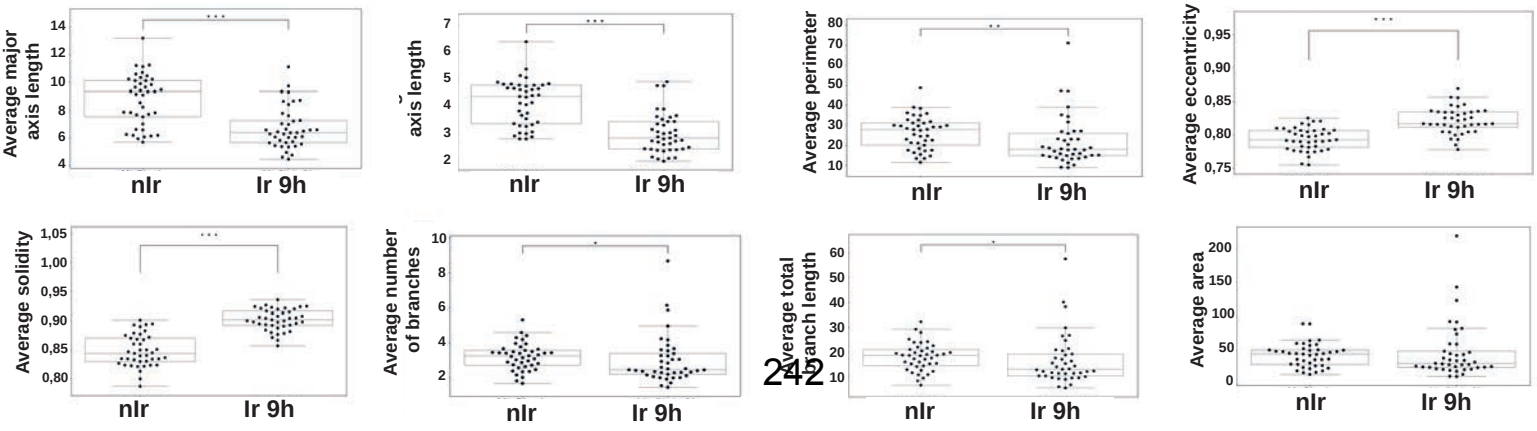

Supplemental Data

Figure S1.

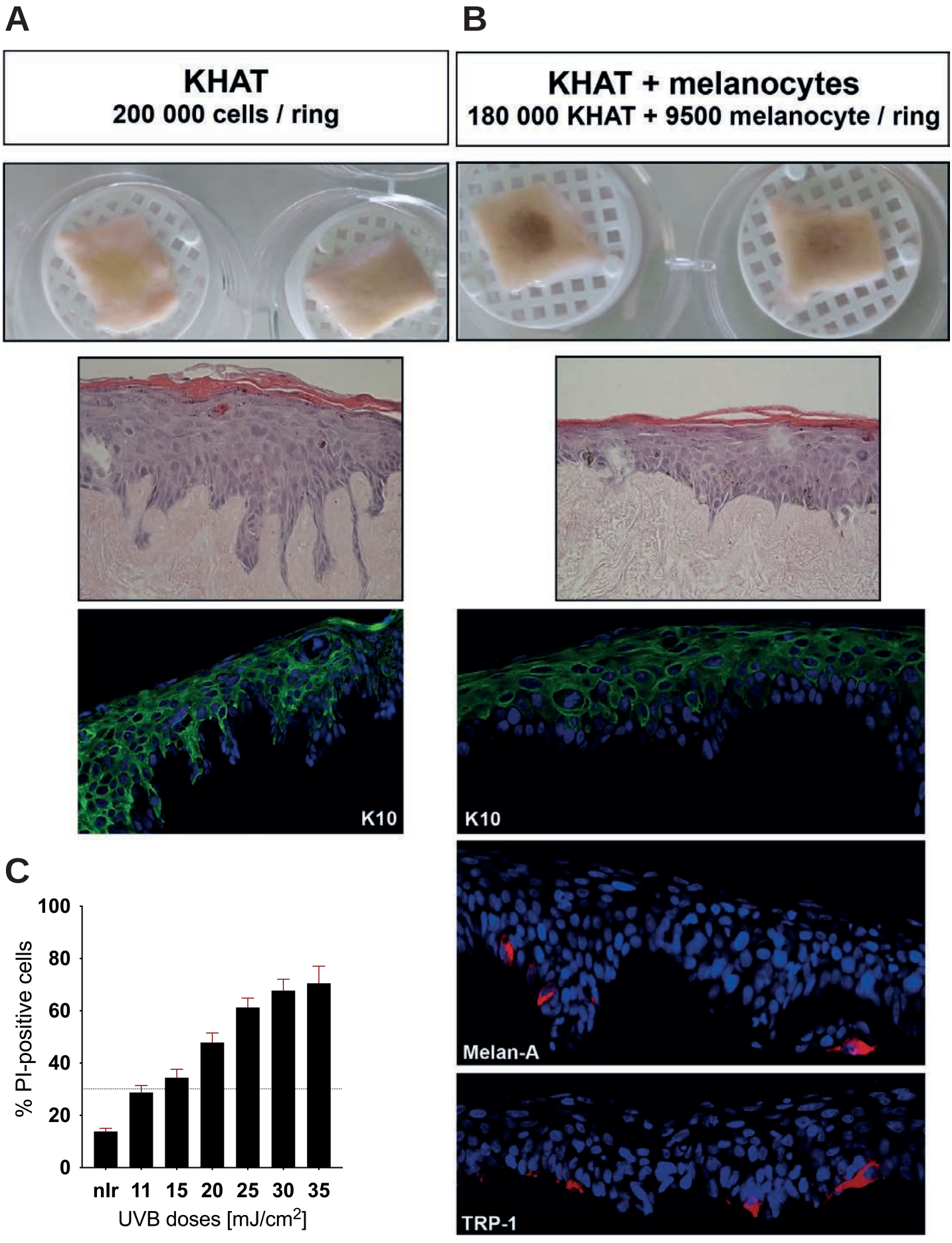

Figure S2.

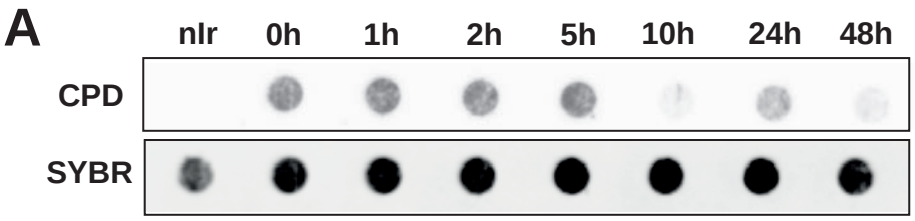
A
nIr
0h
1h
2h
5h
10h
24h
48h
CPD
SYBR

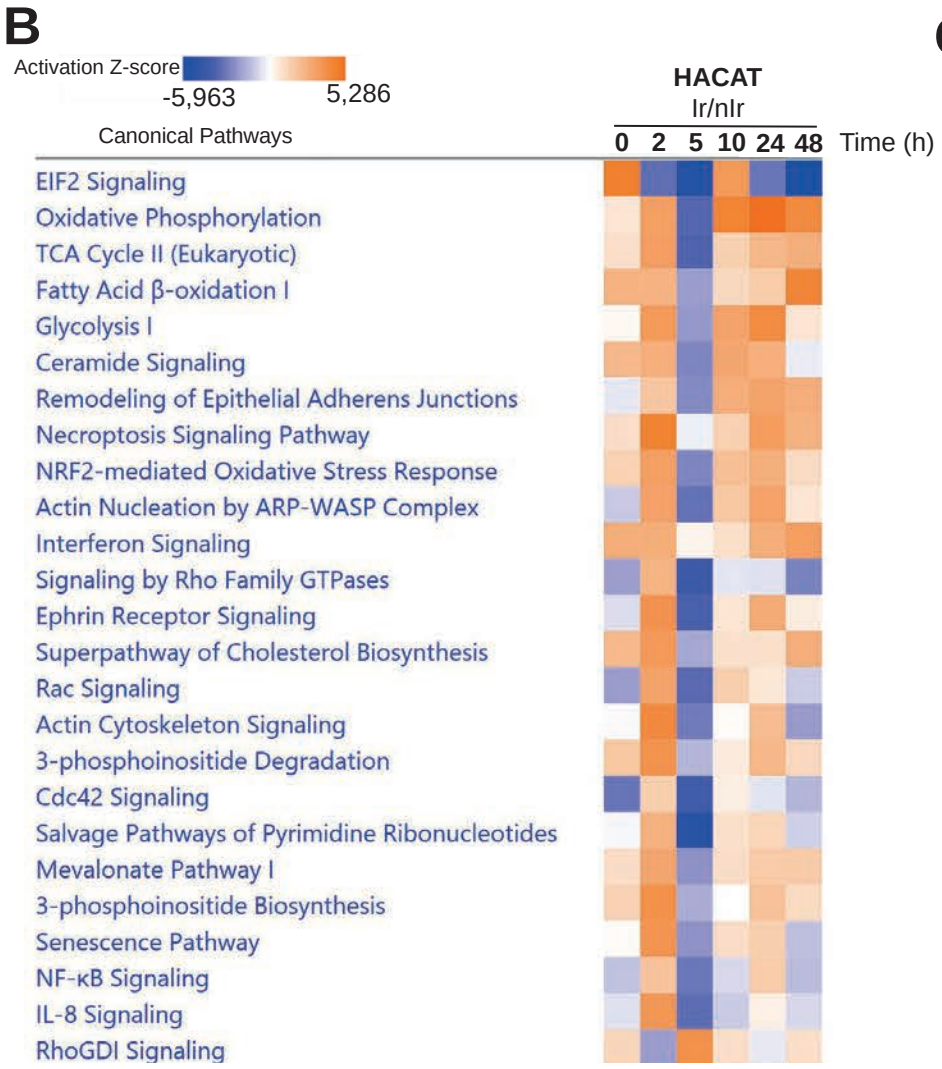
B
Activation Z-score
-5,963
5,286
Canonical Pathways
HACAT
Ir/nIr
0 2 5 10 24 48 Time (h)
EIF2 Signaling
Oxidative Phosphorylation
TCA Cycle II (Eukaryotic)
Fatty Acid β-oxidation I
Glycolysis I
Ceramide Signaling
Remodeling of Epithelial Adherens Junctions
Necroptosis Signaling Pathway
NRF2-mediated Oxidative Stress Response
Actin Nucleation by ARP-WASP Complex
Interferon Signaling
Signaling by Rho Family GTPases
Ephrin Receptor Signaling
Superpathway of Cholesterol Biosynthesis
Rac Signaling
Actin Cytoskeleton Signaling
3-phosphoinositide Degradation
Cdc42 Signaling
Salvage Pathways of Pyrimidine Ribonucleotides
Mevalonate Pathway I
3-phosphoinositide Biosynthesis
Senescence Pathway
NF-κB Signaling
IL-8 Signaling
RhoGDI Signaling

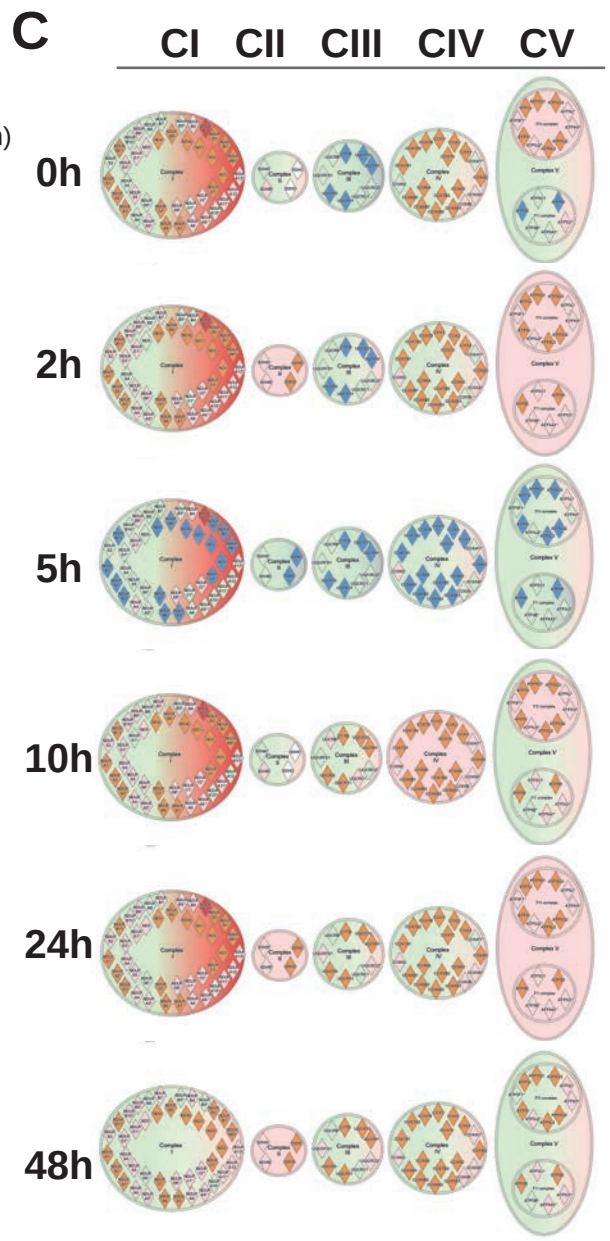
C
CI CII CIII CIV CV
0h
2h
5h
10h
24h
48h

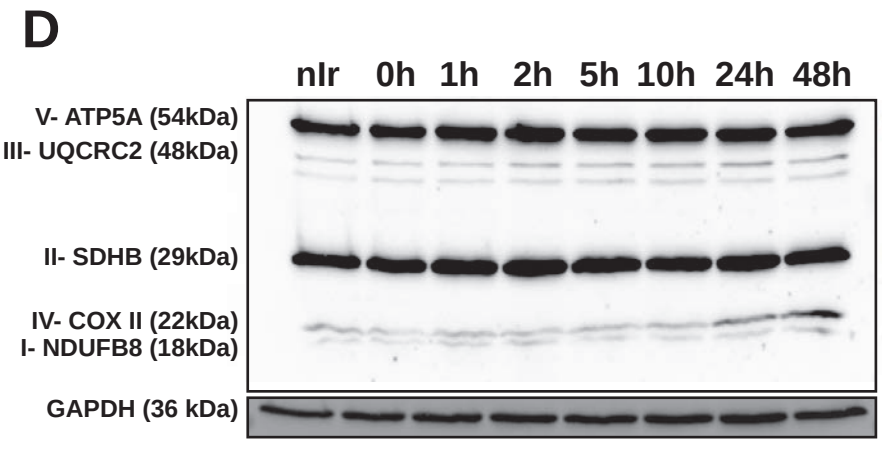
D
nIr 0h 1h 2h 5h 10h 24h 48h
V- ATP5A (54kDa)
III- UQCRC2 (48kDa)
II- SDHB (29kDa)
IV- COX II (22kDa)
I- NDUFB8 (18kDa)
GAPDH (36 kDa)

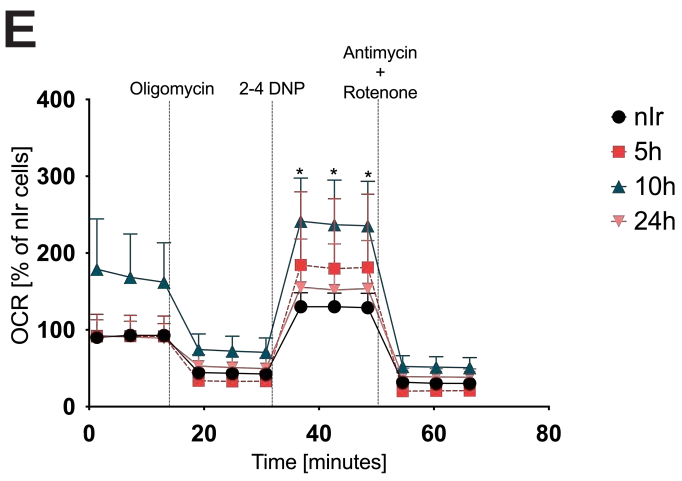
E
Oligomycin
2-4 DNP
Antimycin
+
Rotenone
OCR [% of nIr cells]
400
300
200
100
0
0
20
40
60
80
Time [minutes]
nIr
5h
10h
24h

Figure S3.

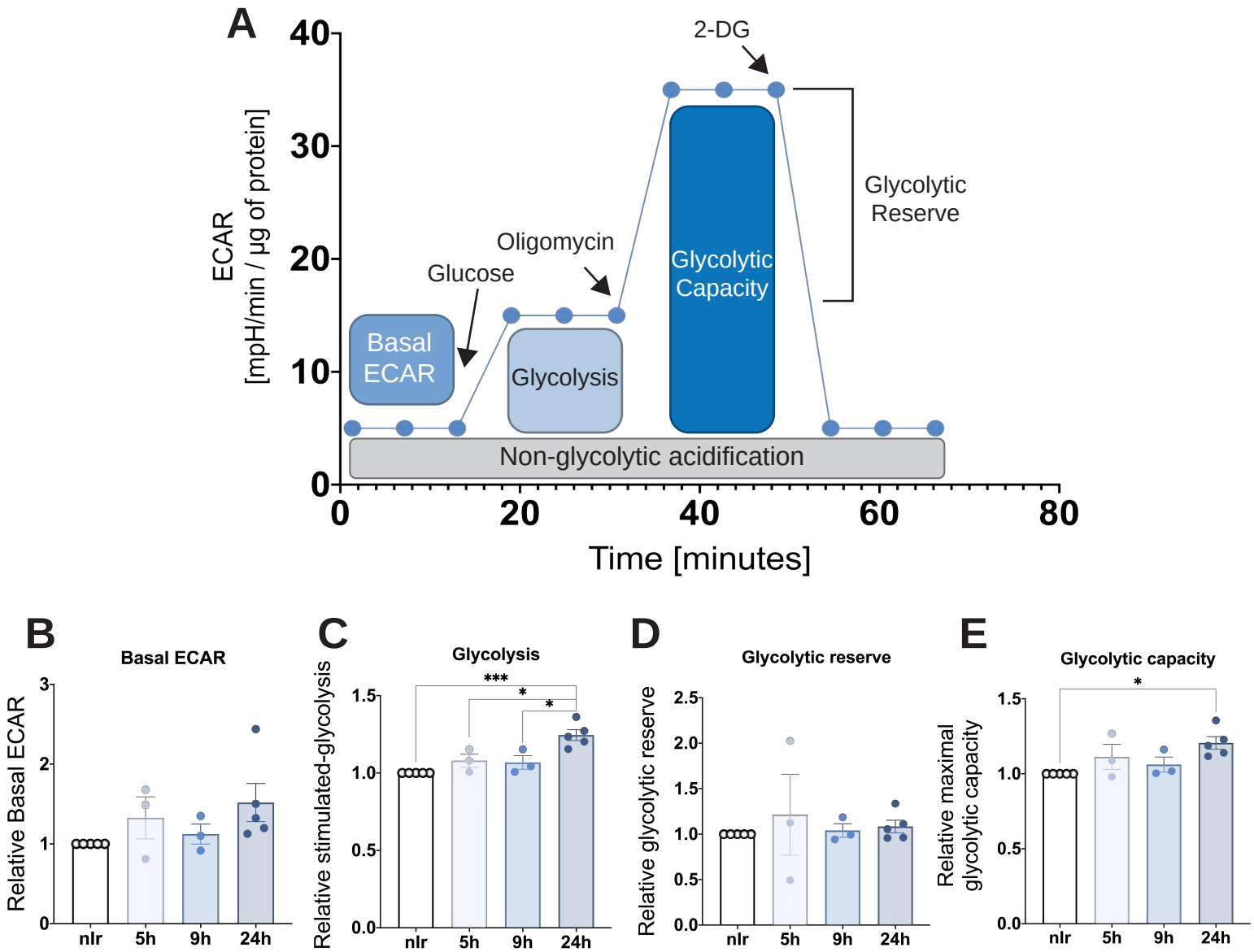
A
ECAR
[mpH/min / µg of protein]
40
30
20
10
0
0
20
40
60
80
Time [minutes]
2-DG
Glycolytic
Reserve
Oligomycin
Glucose
Glycolytic
Capacity
Basal
ECAR
Glycolysis
Non-glycolytic acidification
B
Basal ECAR
Relative Basal ECAR
nlr
5h
9h
24h
C
Glycolysis
Relative stimulated-glycolysis
***
*
*
D
Glycolytic reserve
Relative glycolytic reserve
E
Glycolytic capacity
Relative maximal
glycolytic capacity
*

Figure S4.

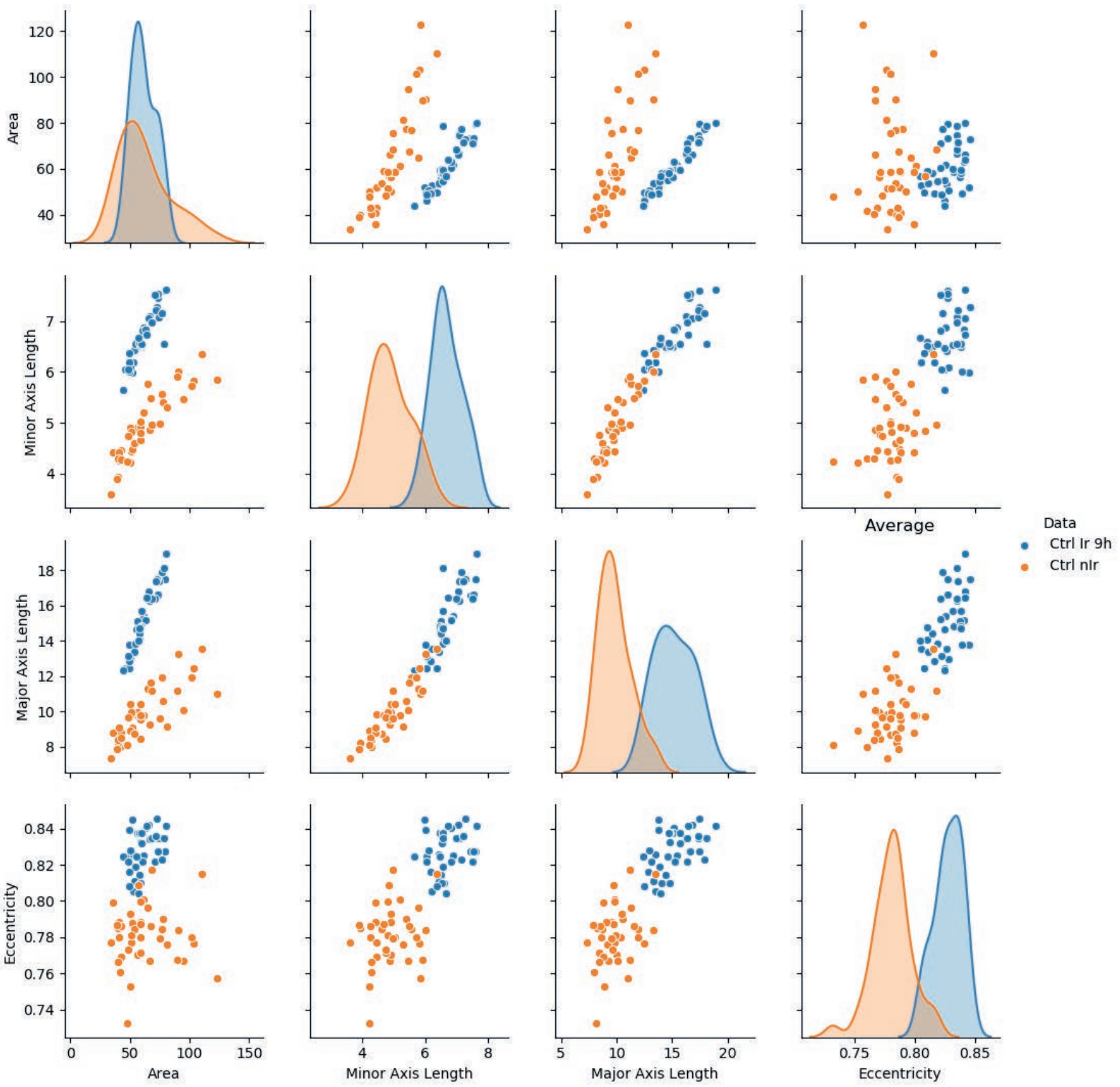
Area
Minor Axis Length
Major Axis Length
Eccentricity
Average
Data
Ctrl Ir 9h
Ctrl nIr

Figure S5.

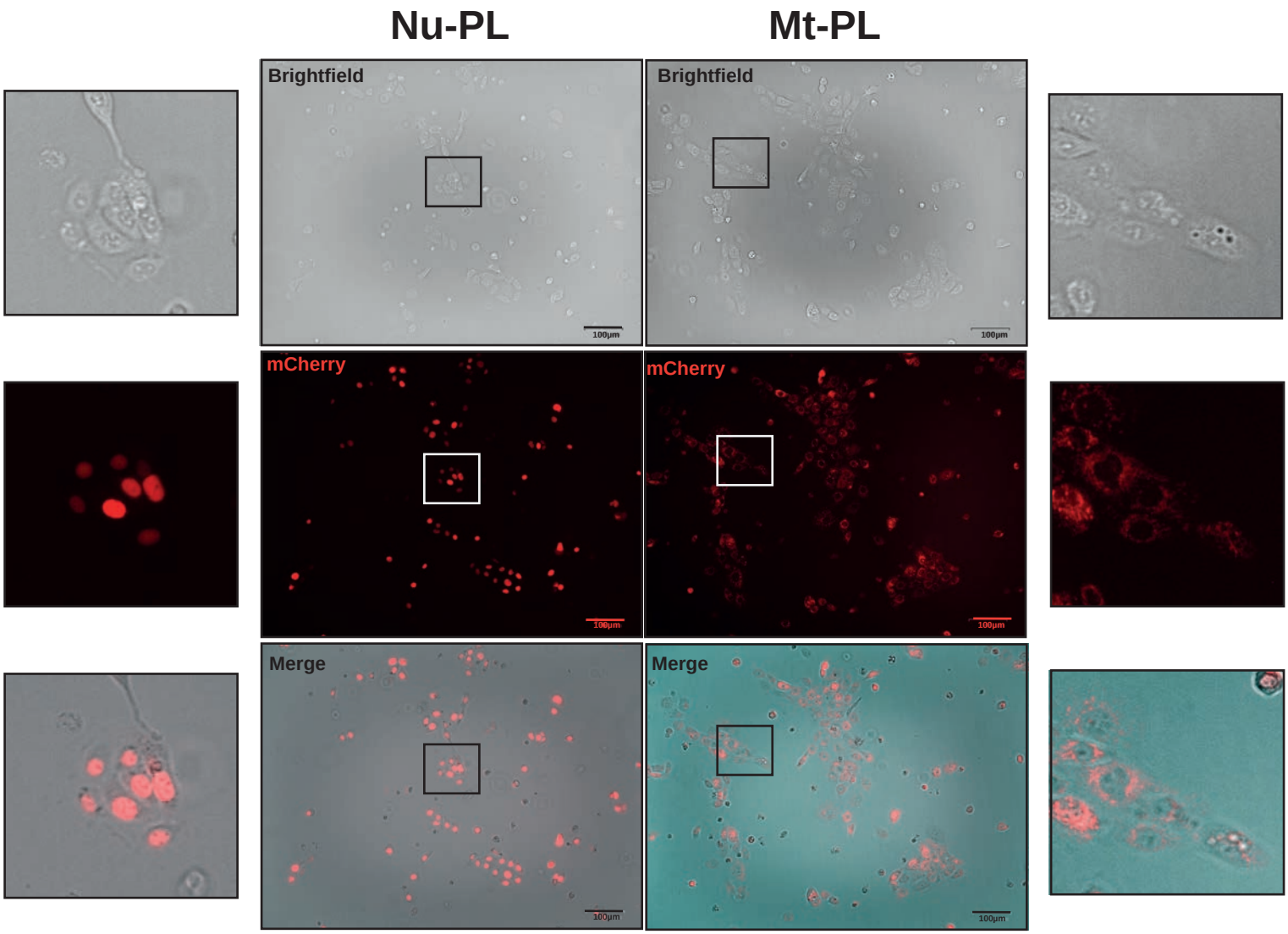
Nu-PL
Mt-PL
Brightfield
Brightfield
mCherry
mCherry
Merge
Merge
100µm

Figure S6.

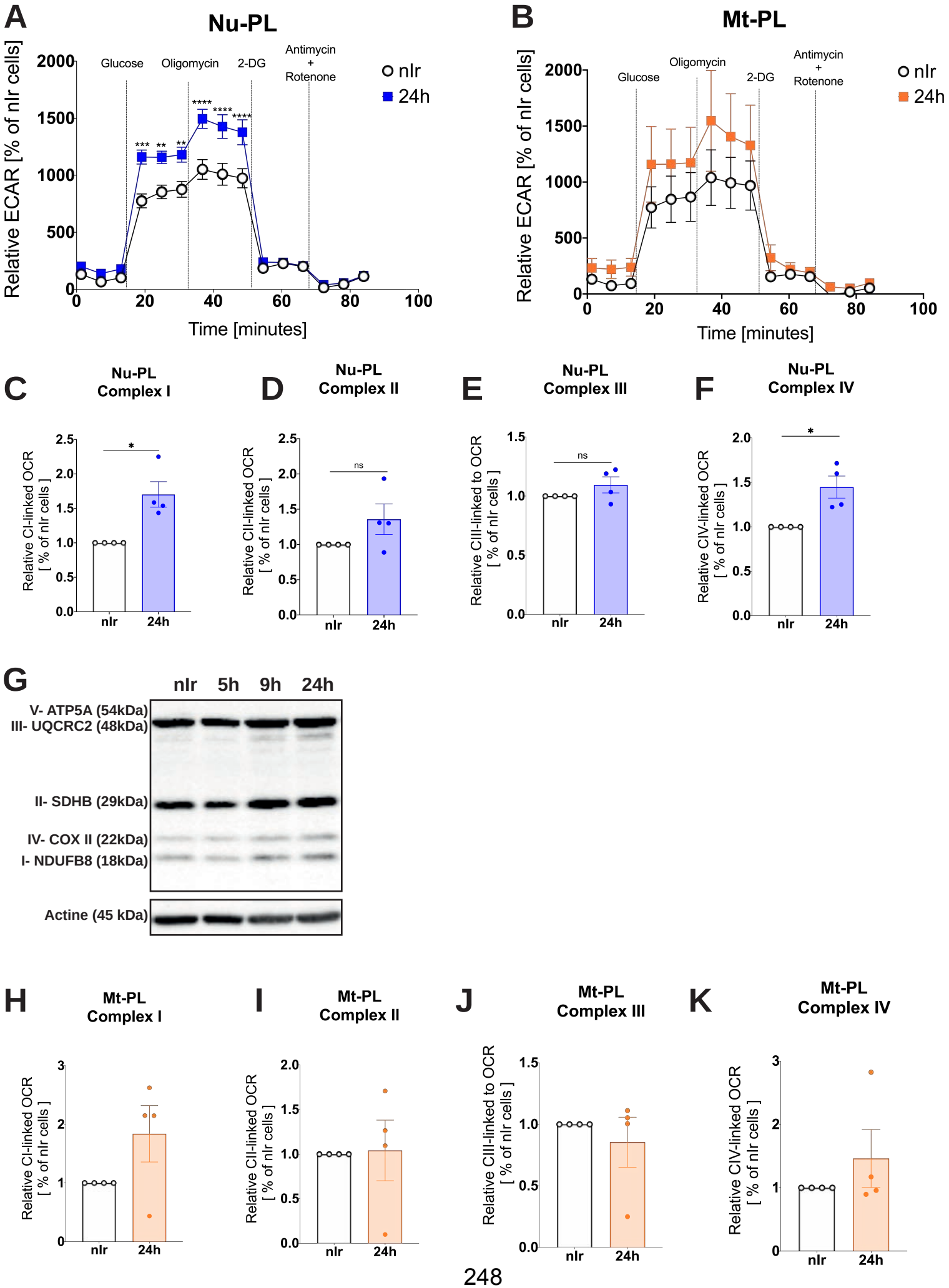
A
Nu-PL
Relative ECAR [% of nlr cells]
Glucose
Oligomycin
2-DG
Antimycin + Rotenone
nlr
24h
Time [minutes]
B
Mt-PL
C
Nu-PL Complex I
Relative CI-linked OCR [% of nlr cells]
D
Nu-PL Complex II
Relative CII-linked OCR [% of nlr cells]
E
Nu-PL Complex III
Relative CIII-linked to OCR [% of nlr cells]
F
Nu-PL Complex IV
Relative CIV-linked OCR [% of nlr cells]
G
nlr 5h 9h 24h
V- ATP5A (54kDa)
III- UQCRC2 (48kDa)
II- SDHB (29kDa)
IV- COX II (22kDa)
I- NDUFB8 (18kDa)
Actine (45 kDa)
H
Mt-PL Complex I
I
Mt-PL Complex II
J
Mt-PL Complex III
K
Mt-PL Complex IV

ClinicalTrials.gov Search Results 09/13/2022

	Title	Status	Study Results	Conditions	Interventions	Locations
1	Study to Evaluate the Safety, Pharmacokinetics and Clinical Activity of RP7214 in Combination With Azacitidine in Patients With Myelodysplastic Syndrome, Chronic Myelomonocytic Leukemia and Acute Myeloid Leukemia	Not yet recruiting	No Results Available	•Myelodysplastic Syndromes •Chronic Myelomonocytic Leukemia •Acute Myeloid Leukemia	•Drug: RP7214	
2	Study to Evaluate the Efficacy, Safety and Tolerability of IMU-838 in Patients With Relapsing Multiple Sclerosis	Recruiting	No Results Available	•Multiple Sclerosis, Relapsing-Remitting	•Drug: IMU-838 tablets •Drug: Placebo matching IMU-838 tablets	•Neuro of Central Florida, Altamonte Springs, Florida, United States •Healthcare Innovations, Coral Springs, Florida, United States •Homestead Associates, Miami, Florida, United States •Premier Clinical Research, Miami, Florida, United States •Boston Clinical Trials, Boston, Massachusetts, United States •Cantonal Hospital Bihac Dr. Irfan Ljubijankic, Biha#, Bosnia and Herzegovina •University Clinical Center of Sarajevo, Sarajevo, Bosnia and Herzegovina •University Clinical Center Sarajevo, Sarajevo, Bosnia and Herzegovina •University Clinical Center Tuzla, Tuzla, Bosnia and Herzegovina •Astra Clinic, Tallinn, Estonia •and 19 more
3	Therapeutic Monitoring of Drugs Used in the Treatment of Multiple Sclerosis	Not yet recruiting	No Results Available	•Multiple Sclerosis	•Diagnostic Test: Measurement of concentrations of orally-used DMDs •Diagnostic Test: Genetic testing •Diagnostic Test: Parameters for routine use of DMDs •Other: Side effects of orally used DMDs	•University of Ostrava, Ostrava, Moravian-Silesian Region, Czechia •University Hospital Ostrava, Ostrava, Moravian-Silesian Region, Czechia
4	A Study of JNJ-74856665 in Participants With Acute Myeloid Leukemia (AML) or Myelodysplastic Syndrome (MDS)	Active, not recruiting	No Results Available	•Acute Myeloid Leukemia •Myelodysplastic Syndromes •Chronic Myelomonocytic Leukemia	•Drug: JNJ-74856665 •Drug: AZA •Drug: VEN	•The University of Alabama at Birmingham, Birmingham, Alabama, United States •NYU Langone Health Laura and Isaac Perlmutter Cancer Center, New York, New York, United States •The Ohio State University, Columbus, Ohio, United States •CHU de Nice Hopital de l Archet, Nice, France •Hopital Saint-Louis, Paris, France •Centre Hospitalier Universitaire (CHU) de Bordeaux Hopital HautLeveque Centre Francois Magendie, Pessac, France •Institut Universitaire du Cancer Toulouse Oncopole, Toulouse cedex 09, France •CHRU Tours Hôpital Bretonneau, Tours, France •Severance Hospital, Yonsei University Health System, Seoul, Korea, Republic of •Asan Medical Center, Seoul, Korea, Republic of •and 13 more

	Title	Status	Study Results	Conditions	Interventions	Locations
5	MRI Trial to exPlore the efficAcy and Safety of IMU-838 in Relapsing Remitting Multiple Sclerosis (EMPhASIS)	Active, not recruiting	Has Results	•Relapsing-Remitting Multiple Sclerosis (RRMS)	•Drug: IMU-838 (30 mg/day) •Drug: IMU-838 (45 mg/day) •Drug: Placebo •Drug: IMU-838 (10 mg/day)	•MHAT Pulse AD, Department of Neurology Diseases, Blagoevgrad, Bulgaria •UMHAT "Dr.Georgi Stranski" EAD Pleven Department of Professional Diseases, Pleven, Bulgaria •MHAT "Heart and brain" EAD Pleven Department of Neurology Diseases, Pleven, Bulgaria •UMHAT " Kaspela" EOOD, Department of Neurology Diseases, Plovdiv, Bulgaria •UMHAT "Kanev Ruse", Department of General and Vascular Neurology, Ruse, Bulgaria •MHATNP "Sveti Naum" EAD, Neurology Clinic for Movement Disorders, First Department of Neurology Diseases, Sofia, Bulgaria •MHATNPsy "Sveti Naum" EAD, Intensive Therapy Clinic Of Neurology Diseases, Sofia, Bulgaria •DCC "Neoclinic" EAD, Cabinet Neurology Diseases, Sofia, Bulgaria •UMHAT "Alexandrovska" EAD, Clinic of Neurology Diseases, Department of Inherited Degenerative and Immunoinflamatori Diseases at Peripheral Nervous System, Sofia, Bulgaria •UMHAT "Sveti Ivan Rilski" EAD Sofia Clinic of Neurological Diseases, Sofia, Bulgaria •and 28 more
6	A Study of AG-636 in the Treatment of Subjects With Advanced Lymphoma	Terminated	No Results Available	•Lymphoma	•Drug: AG-636	•Yale Cancer Center, New Haven, Connecticut, United States •Moffitt Cancer Center, Tampa, Florida, United States •University of Nebraska Medical Center, Omaha, Nebraska, United States •Memorial Sloan Kettering Cancer Center, New York, New York, United States •Weill Cornell Medical Center, New York, New York, United States •Seattle Cancer Care Alliance, Seattle, Washington, United States
7	Study of PTC299 (Emvododstat) in Relapsed/Refractory Acute Leukemias	Terminated	No Results Available	•Leukemia, Myeloid, Acute •AML	•Drug: PTC299	•Rocky Mountain Cancer Center, Aurora, Colorado, United States •Yale University, New Haven, Connecticut, United States •Henry Ford Health System, Detroit, Michigan, United States •Rutgers, Cancer Institute of NJ, New Brunswick, New Jersey, United States •Columbia, New York, New York, United States •University of Rochester MC, Rochester, New York, United States •Duke Cancer Center, Durham, North Carolina, United States •Gabrail Cancer Center, Canton, Ohio, United States •Oncology Hematology Care, Inc., Cincinnati, Ohio, United States •Cleveland Clinic Foundation, Cleveland, Ohio, United States •and 7 more

	Title	Status	Study Results	Conditions	Interventions	Locations
8	A Study of Brequinar in Subjects With Relapsed/Refractory Acute Myeloid Leukemia	Terminated	Has Results	•Acute Myeloid Leukemia	•Drug: Brequinar/Brequinar + Ribavirin	•City of Hope, Duarte, California, United States •Massachusetts General Hospital, Boston, Massachusetts, United States •Beth-Israel Deaconess Medical Center, Boston, Massachusetts, United States •Dana Farber Cancer Institute, Boston, Massachusetts, United States •Cleveland Clinic Lerner College of Medicine, Cleveland, Ohio, United States •The University of Texas MD Anderson Cancer Center, Houston, Texas, United States
9	Vidofludimus Calcium for Primary Sclerosing Cholangitis	Completed	Has Results	•Primary Sclerosing Cholangitis	•Drug: Vidofludimus calcium	•Mayo Clinic in Arizona, Phoenix, Arizona, United States •Arizona State University, Tempe, Arizona, United States •Mayo Clinic in Rochester, Rochester, Minnesota, United States
10	Leflunomide in Previously Treated Metastatic Triple Negative Cancers	Recruiting	No Results Available	•Breast Neoplasms •Breast Diseases •Metastatic Triple Negative Breast Cancer	•Drug: Leflunomide	•Mt Sinai Chelesa, New York, New York, United States •Mt Sinai West, New York, New York, United States •Icahn School of Medicine at Mount Sinai, New York, New York, United States
11	Mechanistic Studies of Teriflunomide in RRMS	Active, not recruiting	No Results Available	•Relapsing Remitting Multiple Sclerosis	•Drug: Teriflunomide	•University of Michigan, Ann Arbor, Michigan, United States
12	A Dose Optimisation Study of ASLAN003 in Acute Myeloid Leukemia	Completed	Has Results	•Acute Myeloid Leukemia	•Drug: ASLAN003	•1 Site, Louisville, Kentucky, United States •1 Site, Albury, New South Wales, Australia •3 Sites, Darlinghurst, New South Wales, Australia •1 Site, Waratah, New South Wales, Australia •1 Site, Douglas, Queensland, Australia •1 Site, Adelaide, South Australia, Australia •3 Sites, Melbourne, Victoria, Australia •3 Sites, Singapore, Singapore
13	A Study to Investigate BAY2402234, a Dihydroorotate Dehydrogenase (DHODH) Inhibitor, in Myeloid Malignancies	Terminated	No Results Available	•Leukemia	•Drug: BAY2402234	•Montefiore Medical Center, Bronx, New York, United States •Memorial Sloan-Kettering Cancer Center, New York, New York, United States •Thomas Jefferson University, Philadelphia, Pennsylvania, United States •Vanderbilt University Medical Center, Nashville, Tennessee, United States •Institut Gustave Roussy, Villejuif Cedex, France
14	Leflunomide in Treating Patients With Relapsed or Refractory Multiple Myeloma	Active, not recruiting	No Results Available	•Recurrent Plasma Cell Myeloma •Refractory Plasma Cell Myeloma	•Other: Laboratory Biomarker Analysis •Drug: Leflunomide •Other: Pharmacological Study	•City of Hope Medical Center, Duarte, California, United States